THE MEASUREMENT, MODELING AND IMPROVEMENT OF PRODUCT FLOW EVENNESS OFF OF METER ROLLERS

A Thesis Submitted to the College of

Graduate Studies and Research

In Partial Fulfillment of the Requirements

For the Degree of Master of Science

In the Department of Chemical and Biological Engineering

University of Saskatchewan

Saskatoon

By

Joel Gervais

PERMISSION TO USE

In presenting this thesis in partial fulfilment of the requirements for a Postgraduate degree from the University of Saskatchewan, I agree that the Libraries of this University may make it freely available for inspection. I further agree that permission for copying of this thesis in any manner, in whole or in part, for scholarly purposes may be granted by the professor or professors who supervised my thesis work or, in their absence, by the Head of the Department or the Dean of the College in which my thesis work was done. It is understood that any copying or publication or use of this thesis or parts thereof for financial gain shall not be allowed without my written permission. It is also understood that due recognition shall be given to me and to the University of Saskatchewan in any scholarly use which may be made of any material in my thesis.

Requests for permission to copy or to make other use of material in this thesis in whole or part should be addressed to:

Head of the Department of Chemical and Biological Engineering

University of Saskatchewan

57 Campus Drive

Saskatoon, Saskatchewan

S7N 5A9

ABSTRACT

In agricultural seeding operations the metering system, typically containing a meter roller, is the heart of the operation as it dispenses product into an airstream where it is distributed across a seeding implement and placed in the soil. Accurate and even metering of product into the airstream translates into better distribution and increased benefits for the farmer. Development of a test method and design tool (empirical model) for meter roller optimization is the main goal of this study.

A test method, called the continuous test method, to measure the metering performance was developed using an imaging apparatus to capture data of the product flow coming off of a meter roller by a measure called the product flow coefficient of variation (CV). The lower the product flow CV is the more even the product flow is. There are three main settings to note; first, defining a frame-per-flute (fPFL) ratio of 10 or more must be used to ensure the camera is capturing at or above a minimum rate. Second, a constant frame height captured by the camera must be maintained throughout all testing. Third, there was minimal to no effect due to oversampling of particles and occlusion from product overlap in the range of meter speeds used (<65 RPM).

Parameterization of a meter roller in such a way that the overall design parameters can be controlled and utilized in a model for optimization is required. Two minor parameters and four major parameters define a meter roller. With these parameters, a test set of meter rollers was designed and prototyped to be tested using the continuous test method.

Analysis of the data showed that pitch ratio (PR), the number of flutes (F), and meter roller speed (ω_m) were the most significant explanatory variables for predicting product flow CV. Applying a stepwise regression technique in Matlab and a polynomial expansion of the variables, the general model form was determined. Training and testing of the raw data yielded a model fit

with a RMSE of 1.94. This model predicted a meter roller with 6 flutes, a PR of 1.25, and a speed of 53 RPM to yield a predicted CV of 4.30.

ACKNOWLEDGMENTS

First off, I would like to thank my parents for encouraging me to pursue my passion for engineering and aiding me through University to help reach my goals, for that I will be forever grateful. Growing up on a family farm there were plenty of opportunities to learn and grow through experience. Whether it was hands on practical experience or theoretical problem solving, my parents and the family farm allowed me to grow and make my own career path leading to Agricultural Engineering.

I would also like to extend a huge thanks to Professor Scott Noble, whose patience over this extended period towards my M.Sc. and excellent guidance in tough times along the way has allowed me get to the point I am at while pursuing a career in engineering. The engineering career has extended my M.Sc. by about 3 years, so again, his patience and understanding has played a large role in getting to this point. Thank you as well to Mr. Jim Henry, the Senior Project Engineer for Seeding Innovation , CNH Industrial, for all in kind support to design and build the testing equipment as well as the financial support of the first 2 years. Jim Henry also provided a lot of valuable feedback over the years and has acted as a mentor to myself, for that I am also grateful. Mr. John Posselius was my other CNH Industrial contact and became my manager when I started working. His patience and mentorship throughout this program is what has allowed me to both work in industry and pursue a graduate degree in agricultural engineering, this type of experience taught me a lot and I cannot thank him enough for giving me the opportunity.

Over the course of the program there have been a number of colleagues at the University of Saskatchewan that I would like to thank as well. Mr. Bill Crerar, Tavis Karnes, and Blair MacDonald helped immensely in collecting a portion of the data in the lab when I was unable to and their advice and suggestions improved the overall flow of the test procedure. Mr. David Pastl

contributed vastly to the development of the LabVIEW test program as I would not have brought it as far along without his experience in that field. Devon Schollar, a design group partner and friend, was a big part in getting the whole idea of improving metering accuracy and how to go about testing it very early on in the project so his knack for generating ideas helped early on.

Lastly, thank you to my very understanding and lovely wife, Amanda. Your support and sacrifice for me over this time to complete my M.Sc was unwavering, even though tough at times, I would not have gotten to this point without you.

TABLE OF CONTENTS

PERMISSION TO USE i

ABSTRACT ii

ACKNOWLEDGMENTS iv

TABLE OF CONTENTS vi

LIST OF TABLES viii

LIST OF FIGURES xi

LIST OF SYMBOLS AND ABBREVIATIONS xvi

CHAPTER 1. INTRODUCTION 1

CHAPTER 2. LITERATURE REVIEW 5

2.1 Conventional Air Seeding 5
2.2 Metering Mechanisms 6
2.3 Meter Roller Design 11
2.4 Material Flow Properties and Characteristics 18

CHAPTER 3. OBJECTIVES 21

3.1 Specific Goals 21

CHAPTER 4. TEST METHOD DEVELOPMENT AND VALIDATION 23

4.1 Background of Test Methods for Measuring Flow Continuity 23
4.2 Validation of Experimental Test Method 30
4.2.1 Test Apparatus for Test Method Validation 31
4.2.2 Imaging Apparatus 33
4.2.3 Control and Analysis Software 34
4.2.4 Illumination 35
4.3 Sampling Limits 36
4.3.1 Test to Establish Lower Sampling Limits 37
4.3.2 Results of Test to Establish Lower Sampling Limits 40
4.4 Significance of Image Frame Height 46
4.4.1 Frame Height Test 47
4.4.2 Frame Height Test Results 48

4.5 Product Oversampling and Occlusion 50
4.5.1 Test for Product Oversampling and Occlusion 52
4.5.2 Results for Product Oversampling and Occlusion 53
4.6 Summary 61
CHAPTER 5. EMPIRICAL MODEL DEVELOPMENT OF FLUTED METER ROLLERS WITH EXPERIMENTAL DATA COLLECTED USING THE CONTINUOUS TEST METHOD 65
5.1 Meter Roller Performance 65
5.2 Meter Roller Parameterization 67
5.2.1 Meter Roller Parameters 68
5.2.2 Roller Parameter Boundary Conditions 74
5.2.3 Roller 3D Model Template 82
5.3 Experimental Apparatus Design and Procedure Development 85
5.4 Results and Analysis 90
5.4.2 Model Development 108
5.4.3 Model Validation 113
CHAPTER 6. SUMMARY AND CONCLUSIONS 121
LIST OF REFERENCES 125
APPENDIX A . METER ROLLER DESIGN AND TESTING SPECIFICATIONS 128
APPENDIX B . STANDARD OPERATING PROCEDURES 136
B.1. Changing Meter Rollers on the Air Cart Simulator 136
B.2. Running a Test to Measure Meter Roller Performance on the Air Cart Simulator 141
APPENDIX C . METER TESTING AND STATISTICAL ANALYSIS RESULTS 152

LIST OF TABLES

Table Page

Table 4-1: List of equipment used in the experiment. 32

Table 4-2: Light intensity for the frame height test. 35

Table 4-3: Establishing sampling limits test conditions for wheat and canola. 39

Table 4-4: Estimated projected area of wheat and canola. 43

Table 4-5: Average CV from three frame height test replicates for wheat and canola flow from a meter roller and the maximum change in CV (ΔCV) as the camera frame rate changes to achieve the desired fPFL ratio. 49

Table 4-6: Product overlap data for a 6 and 15-flute roller in wheat (fPFL ratio of 11) and canola (fPFL ratio of 176.5) with the Tukey test results for each roller in the speed corrected data showing the significance in the difference of means on a 95% confidence interval where one test is two roller rotations. 58

Table 5-1: Levels and range of variation for meter roller parameters. 82

Table 5-2: Individual flute volumes of the meter rollers to be tested. 84

Table 5-4: Test statistic output from the ANOVA with Tukey HSD comparison. 94

Table 5-5: Results of the summary for the general linear model with wheat at a 95% level of confidence. 95

Table 5-6: Results of the ANOVA for the GLM's of each parameter versus the summary model GLM of wheat (CV is the response variable) at a 95% level of confidence showing the explanatory variable order of significance. 96

Table 5-7: Model form optimization results and coefficients from the stepwise regression with the extra pitch roller data split into three different training/testing sets as shown by Tr.1, Tr.2, and Tr.3. 111

Table 5-8: Fitted model coefficients yielding the new optimal model form from training and testing the 11 (T1a – T3a) and 15 (T1b – T3b) coefficient models with a 70/30 split of the raw data. 115

Table 5-9: Predicted optimal meter roller parameters to give the most even product flow. 120

Table A-1: Meter roller labels, testing order, and testing speeds. 128

Table A-2: Critical meter roller speed. 130

Table B-1: Components that make up the air cart simulator. 142

Table C-1: Canola tested with an extra coarse roller at increasing frame rates to locate a lower sampling limit for the continuous test method. The extra coarse roller with canola showed one anomaly at 12 fps that was discussed in the body of the thesis. 153

Table C-2: Canola tested with a fine roller at increasing frame rates to locate a lower sampling limit for the continuous test method. The fine roller with canola showed very consistent data all the way through with an apparent lower sampling limit around 6 fps (7.2 fPFL) but was eventually chosen to be 15 fPFL (greater than 12 fps in this table). 154

Table C-3: Wheat tested with an extra coarse roller at increasing frame rates to locate a lower sampling limit for the continuous test method. The extra coarse roller with wheat showed very consistent data all the way through with an apparent lower sampling limit around 6 fps (7.2 fPFL). 155

Table C-4: Wheat tested with a fine roller at increasing frame rates to locate a lower sampling limit for the continuous test method. The fine roller with wheat showed very consistent data all the way through with an apparent lower sampling limit around 6 fps (7.2 fPFL). 156

Table C-5: Test statistic output from the Tukey HSD comparison for the product overlap significance with a 6-flute meter roller in wheat. 157

Table C-6: Test statistic output from the Tukey HSD comparison for the product overlap significance with a 15-flute meter roller in wheat. 158

Table C-7: Results of the ANOVA for the GLM's of each parameter versus the summary model GLM of wheat. 162

Table C-8: Individual GLM summary output for the number of flutes vs the product flow evenness. 162

Table C-9: Individual GLM summary output of the R_2 design parameter vs the product flow evenness. 162

Table C-10: Individual GLM summary output of the PHI design parameter vs the product flow evenness. 163

Table C-11: Individual GLM summary output of the Pitch Ratio (PR) design parameter vs the product flow evenness. 163

Table C-12: Individual GLM summary output of the Roller Speed parameter vs the product flow evenness. 163

Table C-13: Model coefficients of the final empirical model form (10-coefficients model). 174

Table C-14: Model coefficients of the final empirical model form (12-coefficients model). 175

Table C-15: Model coefficients of the final empirical model form (11-coefficients model). 176

Table C-16: Predicted optimal meter roller parameters to give the most even product flow 177

LIST OF FIGURES

Figure Page

Figure 1-1: Cross-sectional view of a downdraft metering system with a fluted meter roller in operation (Flexi-Coil Ltd., 2001). 2

Figure 1-2: Typical air seeding system including a tractor pulling the seeding implement in conjunction with an air cart; where the air cart includes a metering system under the tanks and an air mover (fan or blower) to push the product out to the implement to be placed in the soil. 3

Figure 2-1: Metering, Tank, and Air Flow Assembly (Flexi-Coil Ltd., 2001) 5

Figure 2-2: Fluted meter roller segments offered by CNH (CNH, 2008) used with permission from CNH. 8

Figure 2-3: Extra-fine meter roller (Flexi-Coil Ltd., 2001) 9

Figure 2-4: Fine meter roller (Flexi-Coil Ltd., 2001) 9

Figure 2-5: Coarse meter roller (Flexi-Coil Ltd., 2001) 10

Figure 2-6: Curved and straight angle roller groove adapted from Kim and Ryu (1998). 12

Figure 2-7: Typical relationship between volumetric flow rate and rotor speed for a rotary valve as adapted from Kessel (1985). 14

Figure 2-8: Top feed metering mechanism (A) that Jotaki and Tomaki (Kessel, 1985) and Reed (Kessel, 1985) used in their rotary valve study and the offset feed metering mechanism (B) used in this study (Flexi-Coil Ltd., 2001). 17

Figure 2-9: The straight bladed flute (A) and curved bladed flute (B) design from the Finkbeiner study adapted from Kessel (1985). 19

Figure 4-1: General setup of a seed spacing measurement test stand with sticky belt and high-speed camera system. 27

Figure 4-2: General test setup for the Discrete and Continuous test method developed by Gervais and Schollar (2008) and Gervais and Noble (2010) respectively. 29

Figure 4-3: Experimental test apparatus for method validation testing. Labels referenced in Table 4-1. 32

Figure 4-4: Locations of light intensity readings on testing apparatus. 36

Figure 4-5: Standard deviation (SD) of product flow as fPFL ratio is varied for wheat with error bars at each data point indicating the variation between the three repetitions. 40

Figure 4-6: Standard deviation (SD) of product as the fPFL ratio is varied for canola with error bars at each data point indicating the variation between the three repetitions.....42

Figure 4-7: Repetition 1 of the raw data (shown in Table C-1) for the sampling limits test for canola (extra-coarse roller) with its corresponding product flow CV (%) measure displayed on the right.....44

Figure 4-8: Percent area of product per image vs roller speed with a 6 flute prototyped roller in wheat showing roller-speed corrected data “Applied” and raw “Not Applied” data. .54

Figure 4-9: Percent area of product per image vs roller speed with a 15 flute prototyped roller in wheat showing roller-speed corrected data “Applied” and raw “Not Applied” data. .56

Figure 5-1: Schematic of a single flute of a roller showing angular distance of flute edges β, fillet circle angular distance φ, fillet radius R_1, and fillet circle center distance R_2 parameters of a meter roller. 69

Figure 5-2: Meter roller comparison of a straight flute meter roller (left) vs a meter roller with a flute pitch (θ_p) of 54° (right) where θ_F defines the center-center angle between flute ridges (note: the front view is comparing the front face to the rear face (lines not drawn as 2D face), top view shows angular variables labelled as if they were linear measures, the color dots should match for each roller in both views). 73

Figure 5-3: Curved profile created by one fillet circle when φ is equal to zero. 76

Figure 5-4: Schematic of a flute profile showing the flute wall angle.....79

Figure 5-5: Meter roller labelling nomenclature for 10 flute rollers. 83

Figure 5-6: Experimental setup configuration. 86

Figure 5-7: Flow chart of the LabVIEW program for the seed flow monitoring test setup. 87

Figure 5-8: Visual check for homogeneity of the data between repetitions (15F_medR2_medPHI_24deg shown).....91

Figure 5-9: Tukey HSD test results on meter roller data showing the overall mean of the data (blue line), the median of the data in each rep, and the outliers of each repetition (Wheat1-4) that correlate to all the zero pitch rollers. 93

Figure 5-10: Variation of product flow (CV_PercentArea) versus pitch ratio (PR) showing the general linear trend as pitch ratio is increased as well as the total linear trend of the 6, 10, and 15 flute roller data combined together. 97

Figure 5-11: Results of the extra pitch rollers tested to fill the missing gap between 0 and 1 pitch ratio. Note that the x-axis is categorical and therefore not scaled by PR value.....99

Figure 5-12: Variation of product flow (CV_PercentArea) versus the number of flutes (F) and the general linear trend of the product flow variation as the number of flutes on a roller is increased (note: not including the extra pitch rollers). 101

Figure 5-13: Variation of product flow (CV_PercentArea) versus the meter roller speed showing the general linear trend across the entire dataset as meter roller speed is increased..103

Figure 5-14: Data spread showing the effect of product flow evenness as meter roller speed and pitch ratio was varied. 104

Figure 5-15: Variation of product flow (CV_PercentArea) versus the center distance to fillets (R_2) and the general linear trend in the product flow variation as R_2 increases (effective flute depth decreases as R_2 increases).....106

Figure 5-16: Flute profile shape (PHI) versus the variation of product flow (CV_PercentArea) coming off the roller. 107

Figure 5-17: Meter roller product flow evenness as a function of pitch ratio with the extra pitch rollers and a trend line fitted for each group of meter rollers showing the overall relationship.....108

Figure 5-18: Model fit summary of measured CV versus predicted CV output using testing data from the three optimized models Tr.1, Tr.2, and Tr.3 of the general form in equation 5-10. 112

Figure 5-19: Coefficients of the 10-coefficient empirical model after fitting the raw data to the 11-coefficient base model form showing the dominant interactions. 116

Figure 5-20: Coefficients of the 12-coefficient empirical model after fitting the raw data to the 15-coefficient base model form showing the dominant interactions. 117

Figure 5-21: Overall correlation model fit of the 11-coefficient empirical model form (CV_{11c}) of the 6, 10, and 15-flute rollers displayed as product flow CV versus pitch ratio with a trend line fitted to show the general trend. 119

Figure A-1: Model template of the flute design on the rollers (*10F_minR2_maxPHI* shown). ..132

Figure A-2: Meter roller profile template with a flute pitch assigned (*10F_minR2_maxPHI_36deg* roller shown).....133

Figure A-3: Meter roller profile template with a curved flute profile (*6F_medR2_minPHI* shown).....134

Figure B-1: Air cart simulator.....136

Figure B-2: Breakdown of meter roller parts (rubber end caps not shown). 137

Figure B-3: Metering assembly clamps. 138

Figure B-4: Coupling and uncoupling the lovejoy coupler from the stepper motor drive when removing and installing a meter roller in the metering assembly. 138

Figure B-5: Bottom view of opened metering assembly with the meter roller pulled out. 139

Figure B-6: Disassembling the meter roller to replace the meter roller profile segment on the meter roller shaft. 140

Figure B-7: Air cart simulator test stand.....141

Figure B-8: Platform ladder for adding product to the storage tank. 143

Figure B-9: LabVIEW test program home screen. 144

Figure B-10: Schematic of the parameters that describe a flute on a meter roller.....146

Figure B-11: 10-flute roller with a medium pitch (PR of 1). 147

Figure B-12: Home screen when the "Stepper" tab is selected. 148

Figure B-13: Home screen when the "Camera" tab is selected. 149

Figure B-14: View of product being metered into the hopper and down the slide into the product catchment during step11. 150

Figure C-1: Tukey HSD test result graphical representation for a 6-flute meter roller in wheat to compare the significance of product overlap as roller speed is increased. 157

Figure C-5: Individual GLM summary output graph from R of the entire dataset.....165

Figure C-6: Normal distribution of the roller data (15F_medR2_medPHI_0deg). 166

Figure C-7: Normal distribution of the roller data (15F_medR2_medPHI_24deg). 167

Figure C-8: Normal distribution of the roller data (15F_medR2_medPHI_36deg). 167

Figure C-9: Matlab output from stepwise regression analysis for training set 1 with extra pitch roller data. 168

Figure C-10: Residuals comparison of testing model 1 from the model form optimization exercise. 169

Figure C-11: Model fit with the testing data (30%) on the 10-coefficient empirical model. 170

Figure C-12: Residuals from the 10-coefficient empirical model tests showing random error...170

Figure C-13: Coefficients of the 10-coefficient empirical model.....171

Figure C-14: Correlation fit for 6, 10, and 15-flute rollers with the 10-coefficient model. 171

Figure C-15: Model fit with the testing data (30%) on the 12-coefficient empirical model. 172

Figure C-17: Coefficients of the 12-coefficient empirical model.....173

Figure C-18: Correlation fit for 6, 10, and 15-flute rollers with the 12-coefficient model. 173

LIST OF SYMBOLS AND ABBREVIATIONS

Symbol	Quantity	Units
D_1	Linear distance between fillet circles	mm
D_2	Linear flute width	mm
D_3	Linear fin width	mm
D_4	Flute depth	mm
d_r	diameter of rotor	m
F	Number of flutes	-
f_f	filling factor coefficient	-
FW_{min}	Minimum flute wall angle	°
g	Gravitational constant	m/s^2
l	length of inlet port	m
$\dot{m}_S$	Mass flow rate	kg/s
n	Rotor speed	rev/min
n_{crit}	Critical rotor speed	rev/min
V_S	Volumetric feed rate	m^3/rev
V_0	Volumetric capacity	m^3/rev
PR	Pitch ratio	-
R_0	Outer radius of meter roller	mm
R_1	Fillet circle radius	mm
R_2	Center distance to fillet circle	mm
U_c	Coefficient of uniformity	-
w	Width of inlet port	m

Greek Symbol	Quantity	Units
α	Angular flute width	rads
β	Angular fin width	rads
θ	Angular distance between fillet circles	rads
θ_F	Center-center angle between flute ridges	°
θ_P	Flute pitch	°
ρ_b	Bulk density	kg/m^3
φ	Angular distance of fillet circles	rads
ω_m	meter roller speed	rev/min

Abbreviations	Quantity	Units
3D	Three dimensional	-
ANOVA	Analysis of variance	-
CAD	Computer-aided design	-
CV	Coefficient of Variation	%
SD	Standard Deviation	-
FLps	Flutes-per-second	-
fPFL	Frame-per-flute	-
fps	Frames-per-second	-
RPM	Revolutions-per-minute	-

CHAPTER 1. INTRODUCTION

A meter roller is a component in many bulk material conveying systems, whether it is on an agriculture seeding machine where metering precision is required or in a plant facility where bulk granular products have to be conveyed from one point to the next. Meter rollers are commonly referred to as fluted rollers, fluted feed rolls, or rotary airlocks. They are typically utilized in mass flow seed metering devices and also referred to as volumetric style metering mechanisms. Figure 1-1 show a cross-sectional view of a volumetric style metering system that is commonly used in seeding operations. The meter roller is located below the product so that it is in a position where the rate of product being dispensed from the hopper can be easily controlled based on the speed the meter roller is rotated. Around the periphery of a meter roller are a number of flutes that fill with product as the roller is rotated and dispense product at the desired drop point. One of the acknowledged problems of fluted meter rollers is the uneven or pulsating flow that can result as product is periodically dumped into an airstream which is accentuated at lower metering speeds.

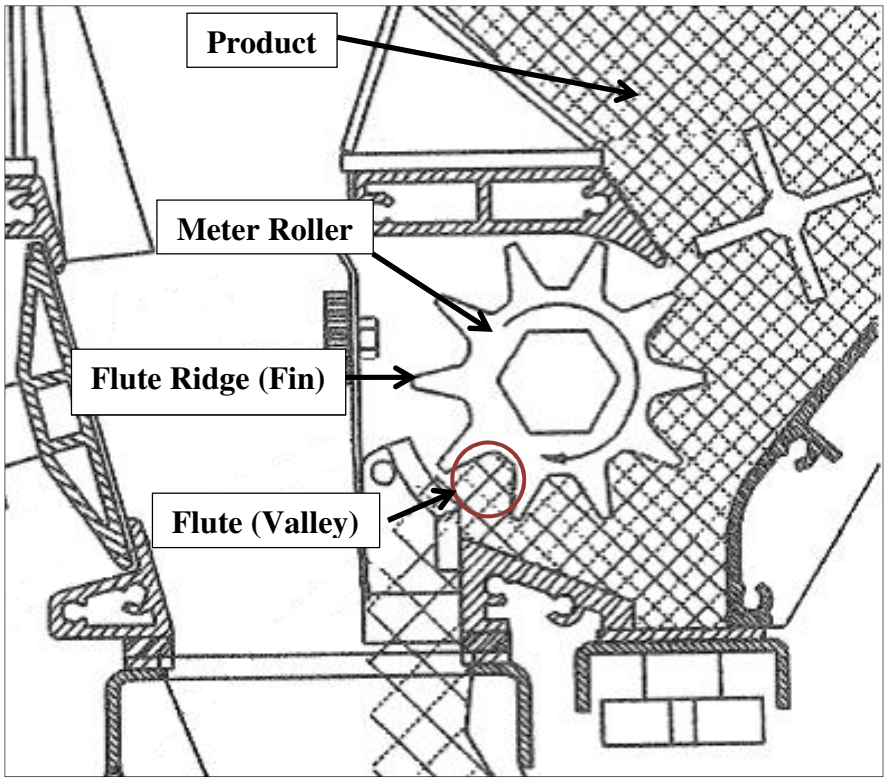

Figure 1-1: Cross-sectional view of a downdraft metering system with a fluted meter roller in operation (Flexi-Coil Ltd., 2001).

The main context for this research is in the seeding industry where air seeders are utilized to cover large areas of land to place seed and fertilizer in the ground for crop production. Figure 1-2 shows a typical air seeder configuration. These air seeders, manufactured by many companies, utilize a volumetric-style metering mechanism to drop product into an airstream which then conveys the product to furrow openers and into the soil for crop production. Air seeders, and thus meter rollers, must be able to handle a large number of cereal, pulse, and grass seeds as well as any kind of granular fertilizer that farmers wish to seed. The large variety of granular products an air seeder must handle means the metering mechanism must handle a wide range of product dimensions and seeding rates depending on what is being seeded.

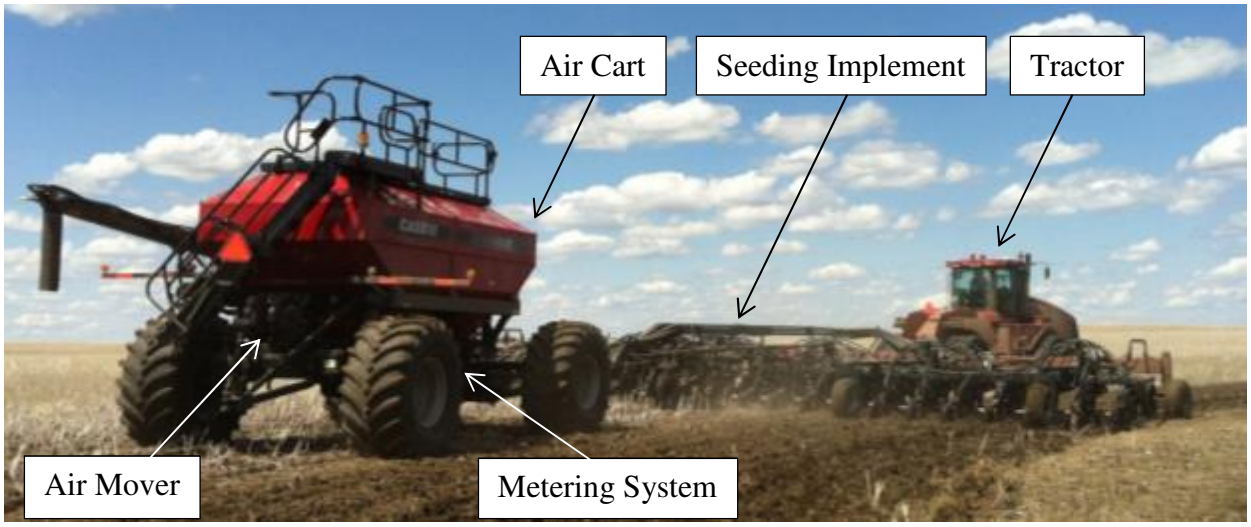

Figure 1-2: Typical air seeding system including a tractor pulling the seeding implement in conjunction with an air cart; where the air cart includes a metering system under the tanks and an air mover (fan or blower) to push the product out to the implement to be placed in the soil.

Currently, Case New-Holland (CNH) meter roller designs utilize four roller styles to accommodate different products and rates. Within these designs there is some level of non-uniformity apparent in product release rates which are thought to mainly be caused by the straight flutes of the meter rollers combined with the slower roller speeds required for metering certain products. No model relating product flow characteristics with roller design parameters is currently known. Having access to and understanding this type of model would greatly improve the design of metering systems, specifically the meter roller, in industry.

The objective of this project is to develop an empirical model that will predict the metering uniformity performance of the roller which in turn could be used to predict the design of a metering system with optimal uniformity. To reach this ultimate objective there needs to be a reliable and statistically sound test method for data collection and a full definition of the design parameters that make up the meter roller. With a valid test method and design parameters, clear relationships between each of the design parameters and how they affect product flow evenness

can be deduced and used to build the form of the model. Once an empirical model is actually developed then the data from the test method can be used to check the model's performance and eventually predict the meter roller design parameters that would result in the most even product flow discharge.

CHAPTER 2. LITERATURE REVIEW

2.1 **Conventional Air Seeding**

Using a meter roller as a method of metering product to the air delivery system is not a new technology. Air carts are commonly towed in sequence with the tillage equipment to place fertilizer and seed or a combination of both in the soil. Air carts are generally comprised of a metering system along with a pneumatic distribution system as seen in Figure 2-1. The metering system releases a fixed volume of seed per unit of linear distance while the air delivery system carries product from the tank to the ground (Mayerle, 2006).

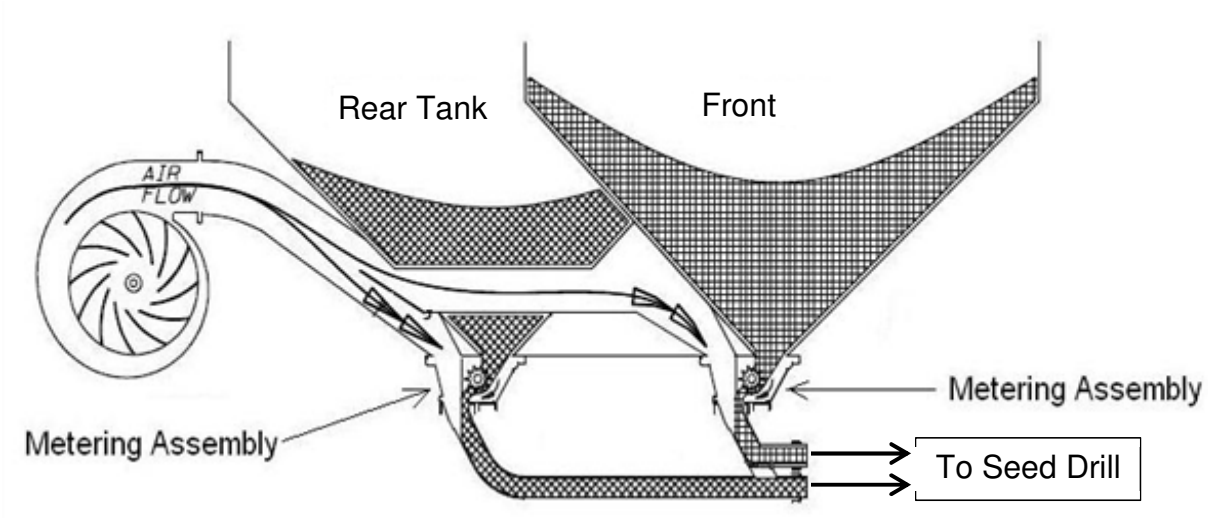

Figure 2-1: Metering, Tank, and Air Flow Assembly (Flexi-Coil Ltd., 2001)

The product is usually metered by augers or fluted rollers into an air stream that is typically created by a centrifugal fan. This type of air system is defined as a positive pressure material-into-air-stream-system by Kraus (1980). These systems are able to handle a wide range of products for a wide range of air velocities with minimal product damage and blockage (Kraus, 1980). This air stream carries the product through the distribution system of hoses to secondary distribution manifolds that lead to the seed boots where the seed is placed into the soil directly

behind the ground openers of the tillage equipment (Ernst and Gregor, 1999). The more evenly distributed the flow is at the secondary distribution system; the more evenly it will be distributed across the ground openers (Mayerle, 2006). Current conventional air seeders have trouble rationing the product evenly into the secondary manifolds across the width of the seeding implement as a function of time. Therefore, if a metering system can be devised to provide continuous evenly distributed flow into the secondary system, a more consistent and efficient placement of seed in the ground can be achieved (Mayerle, 2006).

2.2 **Metering Mechanisms**

Metering mechanisms must be designed specifically to be able to handle pressure effects caused by the airstream in pneumatic conveying. Basnet et al. (2006) state that there are three specific mechanisms by which you can load an airstream with seed. The first is the pressurized box system which allows the pressure in the tank above the meter roller to be equal to the pressure in the distribution lines, essentially eliminating blowback issues which can hinder meter performance. Blowback is caused by a pressure difference between the tank and lines, causing seed to either be sucked past the meter or restricted from flowing out of meter. This system employs gravity to move the product into the airstream. The second system suggested by Basnet et al. (2006) is the venturi system, in which a venturi is used to create a low-pressure zone below the tank, eliminating blowback and promoting free falling of seeds. The third method discussed by Basnet et al. (2006) is the airlock or rotary valve system that is typically used in industrial pneumatic conveying systems or grain vacuums. Ideally, the rotary valve must be completely sealed from the pressurized airstream for optimal operation so that product flow may not be restricted. This need for tight seals on the roller can result in seeds getting crushed. The first two systems proposed are best for conventional air seeding operation because of the minimal damage done to the product and lower maintenance (Basnet et al., 2006).

Buckmaster et al. (2006) state that seed metering is split into two categories, seed metering by volume and by individual seeds. The oldest method of metering seeds is by variable orifice mechanism. It is also the least accurate of all methods because the metering rate is not directly linked to the travel speed of the seeder, but rather by adjustments of the orifice size by the operator. Buckmaster et al. (2006) also included the fluted wheel and the internal double-run (semi-positive displacement metering device that uses variable sized fins rather than flutes) as volumetric metering mechanisms, both of which are placed at the bottom of the seed hopper and gravity fed. Each mechanism has an adjustable feed gate to match seed sizes and regulate flow rate along with rotational speed. Both of these mechanisms allow for the seed rate to be more accurately controlled than the variable orifice because their rotation rate is directly connected to the travel speed. Therefore accurate rates can be calculated for any variety of seed through calibration of the mechanism. In actual field operation the average seeding rate may be accurate, however the precision of each seed along the row is decreased because it is deposited into the distribution stream in stages as each meter flute rotates by (Buckmaster et al., 2006). The straight flutes and distinct ridges separating each flute make the product flow dump in distinct pulses.

Many of the major manufacturers of seeding equipment utilize a volumetric metering system by fluted, studded, or auger rollers for a wide range of products. The rollers come in various sizes and shape to best suit the type of product being metered. CNH currently uses four different meter rollers; extra-fine, fine, coarse, and extra coarse (CNH, 2008).

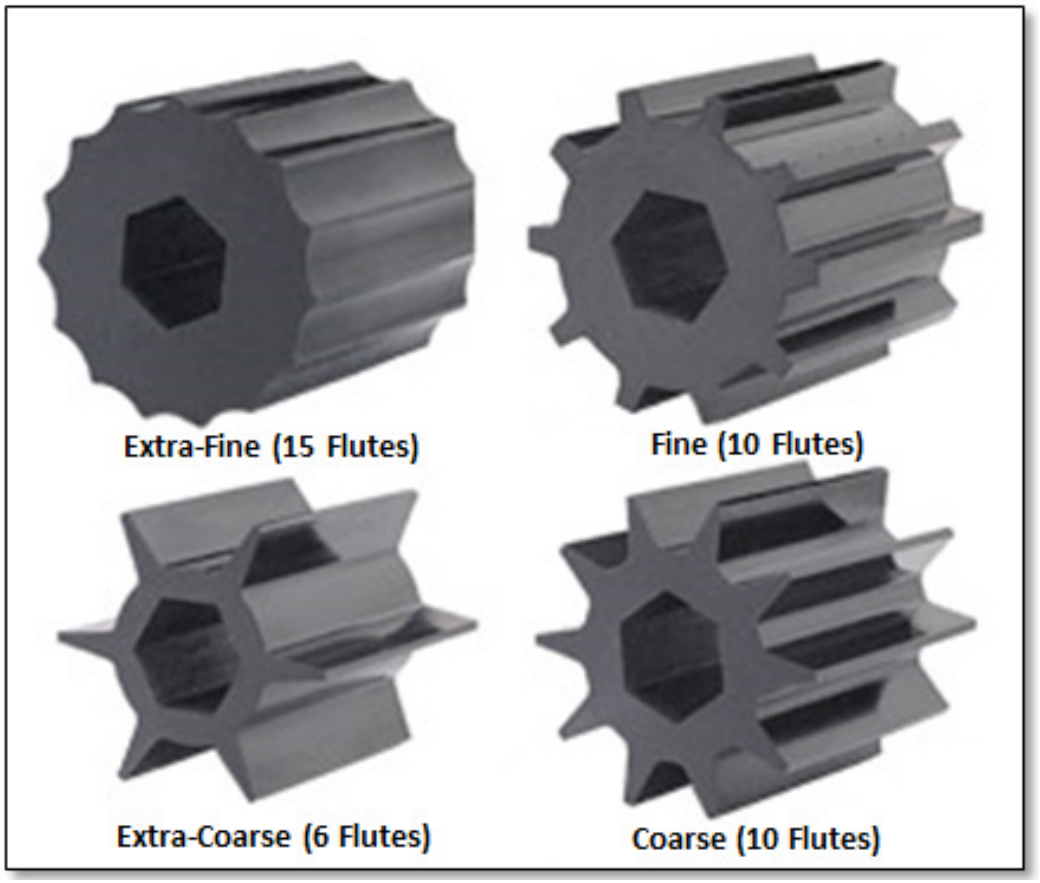

Figure 2-2: Fluted meter roller segments offered by CNH (CNH, 2008) used with permission from CNH.

Extra-fine metering rollers are used most commonly for alfalfa, grass, canola or anything with a seed diameter of less than 3.2 mm (1/8”), as seen in Figure 2-3. This roller has 15 flutes with a flute depth of 3.2 mm and a void width (distance between top of each flute) of 14.3 mm. Due to the small size of product being metered, low metering rates are typically required. The higher number of flutes allows for better accuracy at low rates compared to the fine roller. In canola, the extra fine meter roller can meter at a rate anywhere from 1.7 to 35.1 kg/ha (Flexi-Coil Ltd., 2001).

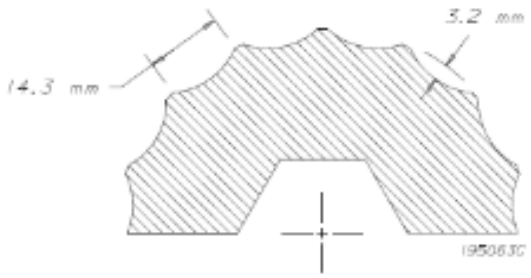

Figure 2-3: Extra-fine meter roller (Flexi-Coil Ltd., 2001)

The fine roller (Figure 2-4) is used to meter such products as wheat, barley, oats, soybeans, or anything with a seed diameter of 6.35mm (¼") or less. This metering wheel is considered to be accurate, with 10 flutes at a depth of 6.4 mm and a void width of 19.1 mm. In wheat, the fine roller can meter out at rates from 10.7 to 202.4 kg/ha (Flexi-Coil Ltd., 2001).

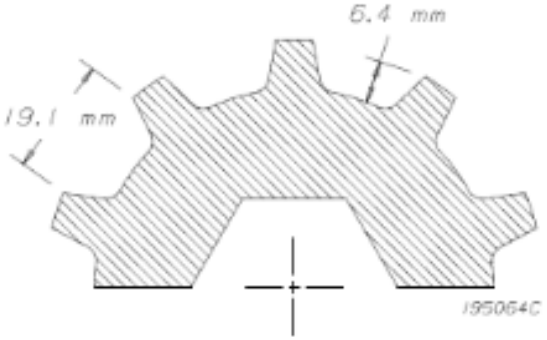

Figure 2-4: Fine meter roller (Flexi-Coil Ltd., 2001)

Coarse metering rollers (Figure 2-5) are used for larger product, which includes peas, smaller beans, and products of up to 9.4mm (3/8") seed diameter. The coarse roller also has 10 flutes with a depth of 12.7 mm and a void width of 22.2 mm. Typical application rates required for peas can vary from 34.5 to 314.1 kg/ha (Flexi-Coil Ltd., 2001).

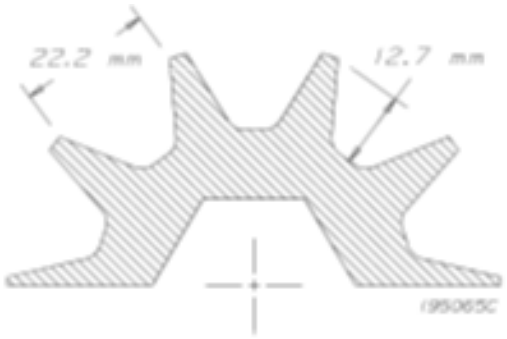

Figure 2-5: Coarse meter roller (Flexi-Coil Ltd., 2001)

Finally, the extra-coarse meter roller is used for product such as large fragile seeds like peas, and for higher fertilizer rates. It has 6 flutes that can meter at rates from 15 to 339 kg/ha in fertilizer and peas (Flexi-Coil Ltd., 2001).

Seed Hawk (Langbank, Saskatchewan) has introduced a newly designed spiral-shaped roller that is believed to improve overall seeding rate efficiency by five to six percent (Hart, 2008). The new style of roller allows for one roller to do the job of a fine-medium and coarse roller. The new roller reportedly does a better job distributing seed across the drill. The straight fluted roller that was previously used caused momentary interruptions of seed in the air stream. A spiral flute profile reportedly eliminates this delay and provides a more even flow to the secondary towers. Seed Hawk has eight secondary towers; half the towers have seven runs and the other half have eight runs. With the straight roller, the product distributed to each tower was the same no matter how many runs used. This caused an over-seeding effect of 11% at the seven run towers. To maximize efficiency, they created a spiral roller with three sections. The two outside sections distribute a rate 11.2 % less than the center section to account for the seven run towers as well as providing a constant feed into the air stream (Hart, 2008).

2.3 **Meter Roller Design**

The design of fluted meter rollers has been studied by a few researchers but not at the extensive level desired for the current study. Previous studies looked at specific characteristics of the fluted roller as they affect the flow of specific products but on a smaller scale. Guler (2005) looked specifically at alfalfa seed flow and how flute diameter, length, and speed affected the evenness of flow. The flute diameter is the diameter of a circle that would fit inside the profile of the flute void, therefore defining the curvature of the flute shape. Guler (2005) concluded that flow evenness increased (coefficient of variation, CV decreased) as flute diameter and roller speed was increased. Flow evenness was the lowest at the smallest flute diameter and roller speed with a CV well above 20% (Guler, 2005). An increase in flute roller length was also attributed to a more even flow off the meter roller (Guler, 2005).

Kim and Ryu (1998) evaluated a special type of fluted roller for precision hill planting. It was slightly different in functionality because they wanted specific gaps between dumping the product, and for the product to fall off the roller as quickly as possible when it was time. Kim and Ryu (1998)realized that the shape of the flute or groove was the most important factor affecting how product was released. They observed that when product was released from the curved surface of the flute, there were actually two separate dumping phases from a single flute. The first occurred as the angle increased above the repose angle of the seeds then the second occurred as the seed weight overcame the frictional force between the product and surface of the roller (Kim and Ryu, 1998). Kim and Ryu (1998) found that a roller groove with a straight angle rather than curved would release the product in one quick step with no delay, no matter how small that time between dumps may be. Figure 2-6 illustrates the curved roller groove and straight angle groove observed by Kim and Ryu (1998).

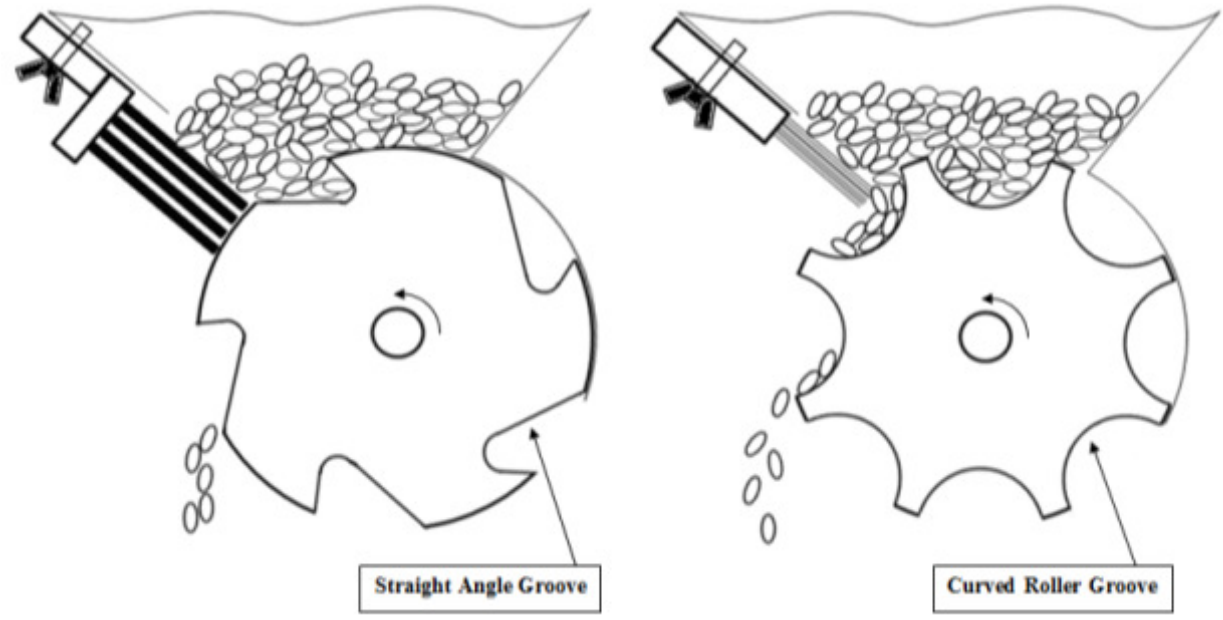

Figure 2-6: Curved and straight angle roller groove adapted from Kim and Ryu (1998).

Agricultural seeding machine manufacturers such as CNH Industrial, John Deere, Seed Hawk, and Morris Industries, just to name a few, all seem to incorporate the theory that Kim and Ryu (1998) presented in their paper where a straight angle groove can give one even dumping of product compared to the curved roller groove. Although each of these companies has a variation of a straight angle groove roller and a curved roller groove, each has been manufacturing meter rollers well before this paper was published. The idea of using meter rollers to meter product, not only for seeding, is not a new concept so each company has developed its own versions based on experience, space constraints on the machines, and type of material being metered. In the agriculture industry especially, where metering of the product is the heart of the seeding system, it may be very beneficial to take a more systematic approach to designing a meter roller while incorporating practical aspects that need to be considered (ie. product types, size constraints, roller material, etc.).

Maleki et al. (2006a) evaluated seed distribution uniformity for an auger or screw type meter roller. The auger design is essentially a fluted meter roller with a very large pitch angle on each flute. In designing rollers for testing they stated that the flute width and depth should be at least greater than the maximum length of the largest seed to be metered (Maleki et al., 2006a). If possible, to prevent any sort of blockage it was suggested that the flute dimension be larger than the seed diameter and length summed together (Maleki et al., 2006a). The results of experimentation were much the same as Guler (2005) where increased auger diameter, increasing the depth and width, and increased auger speed of grooves led to improved discharge uniformity. The results also showed equivalent results to a fluted roller system with similar characteristics, both of which showed the best discharge uniformity with seven flutes (Maleki et al., 2006a). This study was conducted using only wheat.

Another concept of roller design is looking at the speeds at which a roller can actually dispense product and how it is actually positioned in a system for metering. A study by Kessel (1985) thoroughly looked at roller design in terms of roller speed and orientation. Kessel discussed the concept of critical roller speed as it pertained to rotary valves (a form of meter roller) and two studies on mathematical models describing the relationship between throughput and roller speed. The two studies reported by Kessel (1985) showed a positive linear relationship up to a certain roller speed and then a negative relationship for the product throughput versus roller speed.

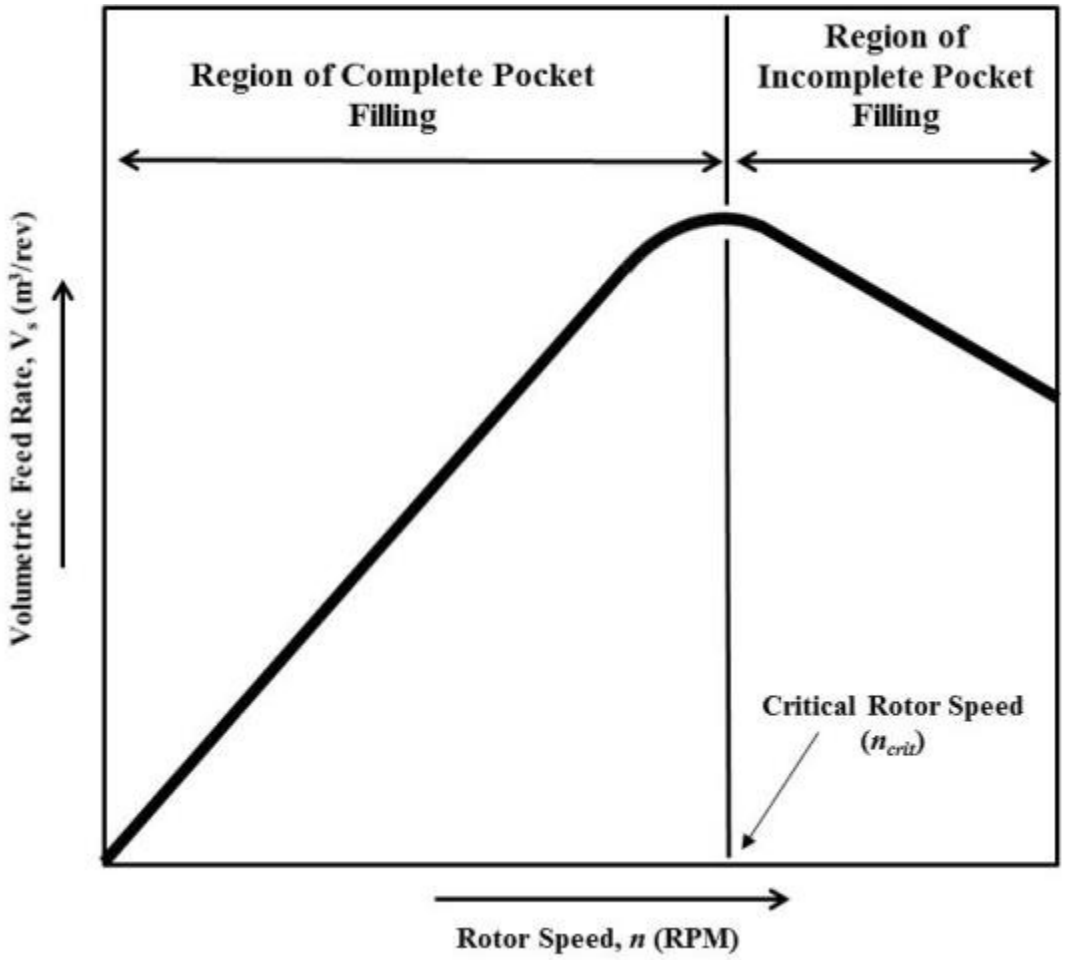

Figure 2-7: Typical relationship between volumetric flow rate and rotor speed for a rotary valve as adapted from Kessel (1985).

Jotaki and Tomita (1970) and Reed (1978) separately argued that the relationship in Figure 2-7 was due to incomplete filling of the flutes on the roller due to the decreased time available for product to fall into the void from the tank and fill the flute completely. Therefore, both researchers separately proposed a mathematical expression to show the region of complete and incomplete filling and realized that a critical roller speed was apparent with rotary valves. At lower speeds below the critical rotor speed it was assumed that the pockets completely fill, therefore the mass flow rate through a roller was easily calculated as a product of roller speed,

volumetric displacement of the flutes per revolution, and the bulk density of the material as shown by equation 2-1 (Kessel, 1985).

$$\dot{m}_s = \frac{n}{60} V_0 \rho_b \qquad 2\text{-}1$$

where, $\dot{m}_s$ is the mass flow rate going through the roller [kg/s],

n is the rotor speed [RPM],

V_0 is the volumetric capacity of the rotor [m^3/rev], and

ρ_b is the bulk density of the material [kg/m^3].

When determining the mass flow rate in the region of incomplete filling both studies incorporated the equation of motion for a particle in free fall to calculate the amount of material that can enter a flute during the specific amount of time that it is open to allow product in. At this point Reed's equations became more widely accepted because his did not rely on the flute width and inlet port width and pitch to be equal as Jotaki and Tomita's equations did. Therefore, the equation of Reed (Kessel, 1985) for mass flow rate in the incomplete pocket filling region (Equation 2-2) and the critical rotor speed could be more generally applied for sizing rotors (Kessel, 1985).

$$\dot{m}_s = \frac{30}{n} \rho_b \frac{g w l^2}{\pi d_r} \ , \qquad 2\text{-}2$$

where, g is the gravitational acceleration [9.81 m/s^2],

w is the width of the inlet port [m],

l is the length of the inlet port [m], and

d_r is the diameter of the rotor [m].

The critical roller speed (n_{crit}) is expressed by solving equations 2-1 and 2-2 simultaneously to get equation 2-3.

$$n_{crit} = \left(\frac{1800 g w l^2}{\pi d_r V_0} \right)^{\frac{1}{2}} \qquad 2\text{-}3$$

This does not mean the rollers cannot be operated over the critical rotor speed, but for testing purposes and keeping the mass flow rate relatively linear this could be an upper limit to be imposed. It is important to note that the critical rotor speed is very dependent on the geometry of the metering assembly. Equations 2-1, 2-2, and 2-3 predict parameters well if the inlet is directly above the meter roller (ie. centerline of inlet is in line with centerline of roller, roller A in Figure 2-8). However, if the inlet is offset towards the direction of rotation (roller B in Figure 2-8) then the throughput and critical roller speed increases by as much as 30% with an inlet offset of 30° (Kessel, 1985). In fact, equation 2-1 by itself will overestimate the actual feed rate because it assumes that product completely fills all voids. This is where a coefficient called the filling factor (f_f) will have to be considered and introduced in equation 2-1 to give the most accurate estimate of throughput. The filling factor is a measure of volumetric efficiency and will vary with the roller speed and type of material being metered (Kessel, 1985). The equations laid out here regarding the throughput and critical roller speed provide a good overview of what to expect out of the roller and at what point the linear relationship between roller throughput and roller speed becomes invalid.

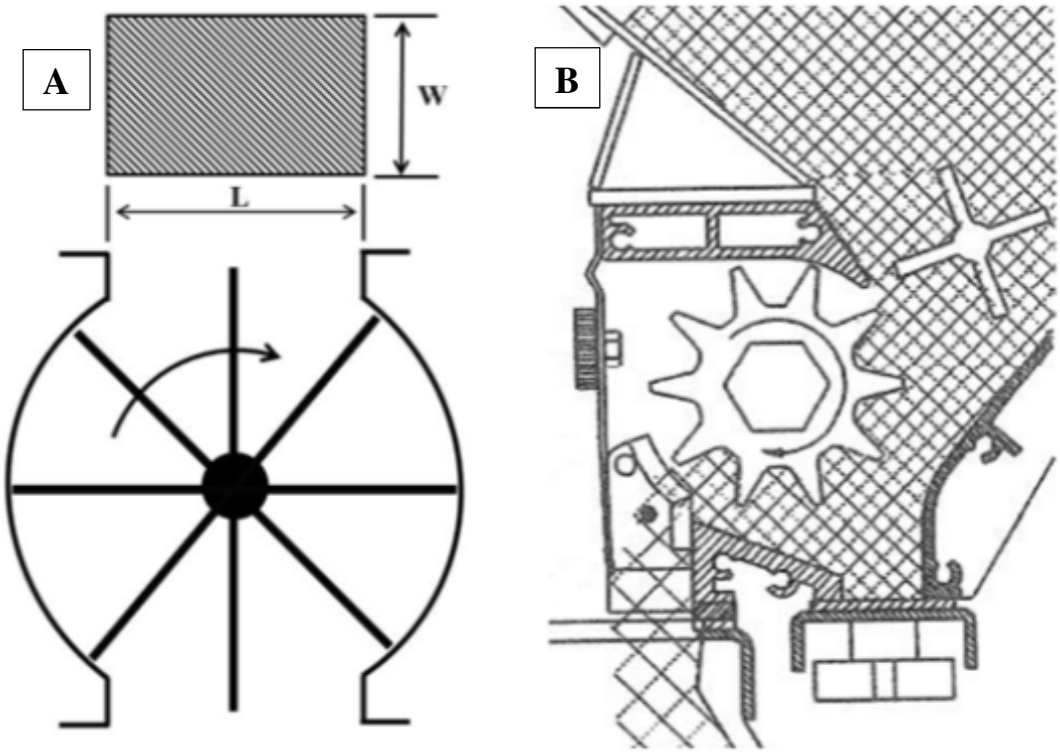

Figure 2-8: Top feed metering mechanism (A) that Jotaki and Tomaki (Kessel, 1985) and Reed (Kessel, 1985) used in their rotary valve study and the offset feed metering mechanism (B) used in this study (Flexi-Coil Ltd., 2001).

In Figure 2-8, roller A is a the typical orientation of a rotary valve setup where there is a very tight tolerance between the flutes and walls of the assembly in order to give an almost complete seal from the pressurized air stream. Roller A assembly is also the setup that Kessel (1985) utilized in his study. Roller B in Figure 2-8 is the orientation of the setup for the present study where a tight seal between the assembly walls is not required because the holding compartment above the roller is pressurized to the same level as the air stream below. Roller B also displays the offset style of metering described in Kessel (1985). Most of Kessel's work involved an airstream, but for the purpose of the current study air flow has been eliminated to solely focus on the profile shape of the roller.

2.4 **Material Flow Properties and Characteristics**

The physical properties of the product being metered and how these characteristics may affect the product flow are important to consider in this study. In a study by Jayan and Kumar (2004), the relation between physical properties of seeds and planter design was studied. It was known previously and further evaluated that product flow through distribution lines is dependent on the physical properties of the seeds, namely size, shape, sphericity, true density, and angle of repose (Jayan and Kumar, 2004). These properties seem to have larger effect when flowing through the distribution lines to the seedbed via an airstream, but are expected to have a slight effect on how they are metered. For example, irregularities in shape will cause uneven packing in the hopper and as they pass through the metering mechanism. Also, products of different and varying sizes will have changing bulk densities and angle of repose and may therefore fall off the meter roller differently as discussed by Kim and Ryu (1998). Looking at the angle of repose further, it is the minimum angle that a surface needs to be when the product on top begins to slide. Thus, the angle of repose is a good indication of the flowability of a product. Generally, the lower the angle of repose the easier the product will flow (Boumans, 1985). According to Boumans (1985), products with an angle of repose of 25 to 30 degrees are considered very free flowing, 30 to 38 degrees is considered free flowing and 38 to 45 degrees is considered fair flowing. Considering the findings of Kim and Ryu (1998) where a straight angle groove on a flute released product more evenly than a curved groove on a flute and the range of angles of repose for the products used in seeding, it is very possible that each product (or group of products with similar characteristics) may require a specific roller design for optimal metering performance. Kessel (1985) reviewed research on the topic of optimizing a roller design to achieve better flute filling efficiencies which would equate to a higher throughput. In Kessel's

thesis he found research from 1974 by Finkbeiner showing that a curved flute design could maximize the filling of each flute by mathematically analyzing the path that an individual particle would follow which was then validated (Kessel, 1985). The curved flute shape he proposed was specifically related to the profile shape as seen in Figure 2-9 and not related to the flute pitch discussed in this paper.

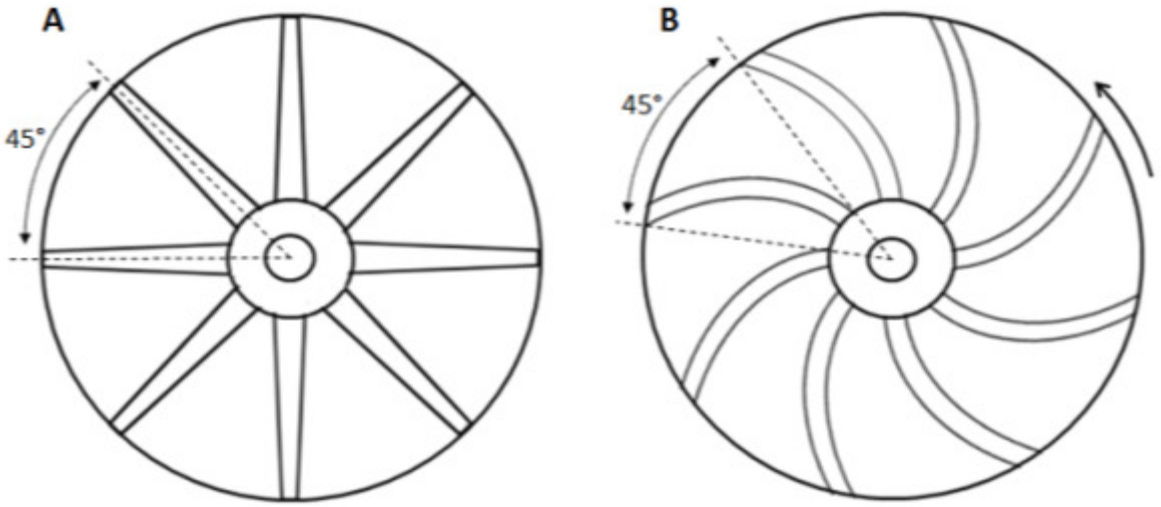

Figure 2-9: The straight bladed flute (A) and curved bladed flute (B) design from the Finkbeiner study adapted from Kessel (1985).

The curved profile shape worked well in the rotary air lock configuration he was working on where the product was being fed into the roller directly above the centerline of the roller, but Kessel (1985) presented further work showing that if this geometry is changed then the benefits of the optimized profile shape were cancelled. Changing the geometry of how product is fed into the roller combined with the material characteristics (ie. angle of repose) of the product will ultimately affect the shape of the optimal flute profile of the roller.

Moisture content influences the physical properties of seeds, and is another variable that should be acknowledged. Igozulike and Aremu (2009) investigated the effects of moisture on

seed dimensions, seed weight, true density, bulk density, porosity, seed volume, static coefficient of friction, and angle of repose and clearly found that all had a linear relationship with variations of moisture content in kola seeds. Mohsenin (1986) investigated some important criterion for describing the shape and size of all agricultural products and how to conduct standard tests for these measurements. The mass of the product, specifically its 1000-grain weight is a good indicator of the relative size of the seed which will vary relative to the growing conditions (Chakraverty et al., 2003). Bulk and true density give a good idea of how much space is needed to move a certain amount of seed, and are therefore important in calculating product rates. Because this study involves the development of a test method to evaluate meter roller performance and a model that will aid in the optimal design of a meter roller, the interaction with a specific product should be considered.

When referring to the physical size of a product the average projected area should also be considered. The average projected area is related to the dimensions of the seed and the geometric shapes that a seed may resemble when it is rotated about its major or minor axis. Mohsenin (1986) describes the prolate spheroid, oblate spheroid, and right circular cone as the three geometric shapes that represent the body of the desired product. Each shape has a developed equation for its volume and surface area. Based on the theory of convex bodies, it was found that the average projected area is one-fourth the surface area of the product calculated from its geometric shape (Mohsenin, 1986). Therefore, having an idea of a product's average projected area may be a good indication of its size.

CHAPTER 3. OBJECTIVES

Building on methods previously developed for evaluating product flow (Gervais and Noble, 2010), the objective of this project is to develop an empirical model for predicting the effects of roller characteristics. The effect of roller characteristics such as flute pitch and flute depth on product flow uniformity will be developed and evaluated. Using this model to explore the design space, roller designs with the potential to have uniform flow over a wider range of products and rates could be tested in future work.

3.1 **Specific Goals**

1) Validate that the previously developed continuous test method is an acceptable approach for evaluating meter roller performance.

2) Develop an appropriate nomenclature and design parameterization of the meter rollers to facilitate analysis and interpretation of the design components involved and the data collected.

3) Use the continuous test method to collect experimental data relating roller design parameters to flow uniformity. Wheat will be used as the test product.

4) Determine the interactions between the meter roller parameters and product flow uniformity (CV) to determine what parameters have the most significant effect of product flow evenness.

5) Using the roller design characteristics and the flow uniformity data, an empirical model will be developed.

6) Using the developed model, optimal roller design characteristics will be predicted. These characteristics would be used to design the optimal meter roller(s) for testing and verification of the model's performance. Design and testing the optimal roller are not part of the study but validating the model with the collected data and predicting the optimal characteristics are.

The specific goals listed here will be addressed in two separate chapters. Chapter 4 will specifically focus on the first goal of validating the continuous test method to ensure that all data gathered for the study are statistically sound and provide an acceptable measurement of the meter roller performance. Chapter 5 will then focus on goals 2 through 6 where the parameterization of the meter roller, experimental procedure and data analysis are discussed. Significant interactions

will be determined and used to develop the form of the model to predict meter roller performance. The variables of the model will be specific design parameters of a meter roller so the empirical model can be a direct tool to design an optimal meter roller.

CHAPTER 4. TEST METHOD DEVELOPMENT AND VALIDATION

Metering systems are utilized to control the feed rate of a range of bulk materials. Some applications require large amounts of product to be metered into a containment structure or a bulk product pneumatic conveying system. Other systems require more precision over the amount and rate of product being dispensed, such as in agricultural seeding and planting applications. Within these metering systems a rotating roller or auger is typically employed to dispense the product. A classic meter roller (or rotary airlock) design includes a number of straight flutes or grooves around the circumference of the roller, with large enough spaces between them to safely meter product with minimal damage. Most of the literature regarding the design and testing of metering system performance is related to the effect of the air system or overall throughput of the roller. In precision applications such as agricultural seeders it becomes important to understand what meter roller designs dispense the most accurate and even flow into the air stream to give the user the most control over system inputs and the best chance of optimal seed placement in the soil. Therefore, the product flow evenness coming out of the metering system becomes the important metric to measure and quantify metering performance. With a metric defined, a reliable test method for comparing different metering systems and understanding what design parameters are most influential on product flow evenness must be developed to quantify the metering performance. Both the measurement metric and test method will be developed and validated in this chapter.

4.1 **Background of Test Methods for Measuring Flow Continuity**

The sticky belt test stand has been used as the standard for evaluating meter roller performance in agricultural seeding applications. The sticky belt test stand utilizes a conveyor-type belt passing directly under the meter roller to catch the seeds as they fall. The belt is coated in sticky oil so the belt captures the seed with minimal bouncing and rolling. The meter roller

and sticky belt are operated by the same motor and gear system so that the seeding rate and belt velocity directly correspond with each other. The product captured by the sticky belt can be directly measured to correspond to the continuity of product flow coming from the meter roller. The sticky belt method is quite effective. However, it requires a lot of maintenance, the oil makes it impossible to re-use the product, and it requires a lot of time for testing.

The sticky belt method is also commonly used in conjunction with new testing methods as a baseline to test against. Maleki et al. (2006b) used the sticky belt method to evaluate the performance of different fluted auger designs. They split the belt up into individual frames then counted individual seeds in each frame. The typical method to quantify metering performance would be to calculate the standard deviation and mean number of the seeds in each frame and corresponding coefficient of variation (CV). Coefficient of variation could then be used as the measurement of performance. They went on to propose a method called the coefficient of uniformity, U_c, based on the least absolute deviations so it has the tendency to be less sensitive to outlying data and variations around the mean (Maleki et al., 2006b). The coefficient of uniformity caters very well to the sticky belt method because every kernel must be counted in the measured frames, providing the most accurate measure of performance. It appears to be a very robust method of testing metering systems but the sticky belt method is also a very tedious method which really can only be used for short segments of laboratory testing.

Using a different approach, Guler (2005) used a precision balance to continuously measure the cumulative mass of product coming off the meter roller under test. From the data collected by the balance a coefficient of variation (CV) could be calculated for each roller to quantify its performance. This method worked very well in his study on how different roller characteristics affect the product flow evenness coming off the roller for alfalfa. However, the

amount of data gathered was limited by the precision balance. The discrete test method in Gervais and Schollar (2008) built on the continuous mass method used by Guler (2005). Realizing that the continuous mass method was limited by the rated mass of the precision balance, the discrete method broke the roller motion down into discrete incremental steps of 2.5 to 4 degrees of motion with a precision stepper motor. In this test method (Gervais and Schollar, 2008; Henry et al., 2012), a meter roller would rotate incrementally (2.5-to-4 degree increments) over one full revolution while a precision balance gathered and recorded the data from each increment. At the end of one revolution the coefficient of variation was calculated as a measure of the meter roller performance where a CV of zero would indicate perfectly uniform flow off the roller. The limitation of the discrete test method is that it does not account for dynamic effects of roller speed on flow rate or uniformity.

To address the limitations of sticky belt and the precision mass measurement method, methods based on machine vision have been explored. Image processing has the advantage of being non-intrusive to the nominal operation of the metering system and very flexible in the amount of data collected. Incorporating image processing into the evaluation of metering systems is relatively new compared to the standard sticky belt test method. Alchanatis et al. (2002) and Karayel et al. (2006) are some of the more recent successes in determining if an image processing based system could replace the sticky belt system typically used in evaluating seed spacing uniformity from metering systems. Before Alchanatis et al. (2002) mostly opto-electronic sensors were being developed to replace the sticky belt method and measure the spacing distribution of seeds. These opto-electronic sensors had a few major limitations. They were unreliable at measuring small seeds (4 mm or less) due to poor spatial resolution and could not pick up clusters of seeds (an important measure for planters because seed singulation is

desired and clusters are unwanted) (Alchanatis et al., 2002). This limitation pushed Alchanatis et al. (2002) to develop a high-resolution optical system for evaluating the performance of planters specifically for smaller, irregular shaped particles. Using a line scan camera (4,000 – 15,000 frames-per-second (fps)) they developed image processing algorithms that were able to acquire data for average seed spacing, coefficient of variation (CV) of seed intervals, feeding index, and doubles that were equivalent to the sticky belt method (Alchanatis et al., 2002).

Karayel et al. (2006) built on the previous work and developed a high-speed camera method aimed more specifically at volumetric style metering systems where it is more likely to see random clusters of seed compared to a seed-singulating planter. The high-speed method was conducted in conjunction with the standard sticky belt test to directly compare results. The test stand had a fluted meter roller metering wheat or soybeans at typical seeding rates, and incorporated both the sticky belt and a high-speed camera (750 fps) capturing images of seeds falling onto the belt. Seed spacing was determined by calculating the time difference between seeds from the capture images. The CV was calculated for each test. An analysis of variance (ANOVA) of the data had showed no major differences at all roller speeds tested. Thus the high-speed camera system can be adapted as an acceptable method of evaluating seed spacing uniformity coming off of seed drills and replace the sticky belt test method. This approach also has the advantage of using larger sample sizes without wasting product, and the ability to determine the velocity of the particles (Karayel et al., 2006). A general test setup that would have been used by Karayel and others to follow can be seen in Figure 4-1.

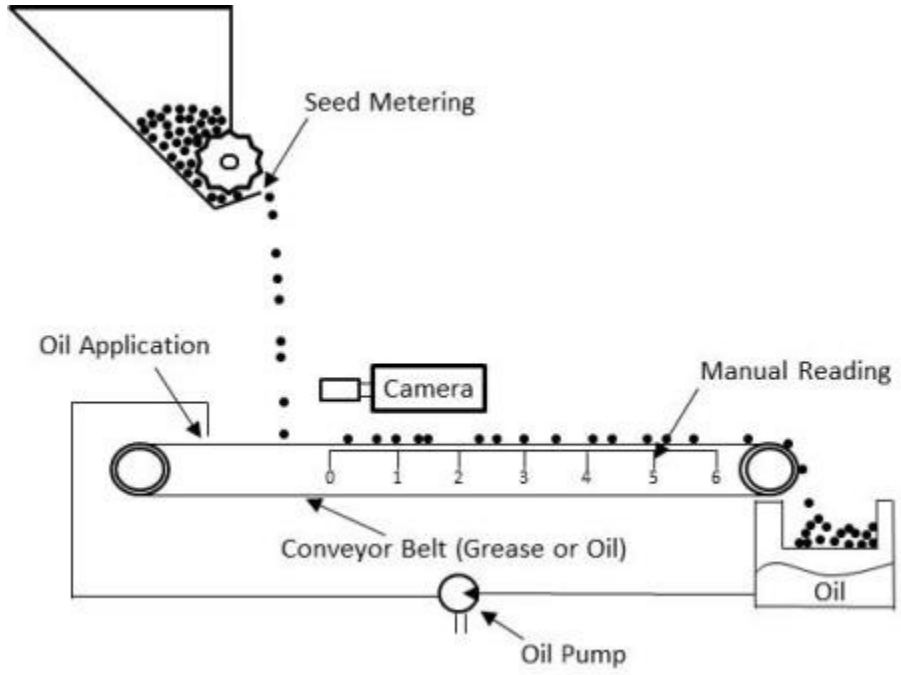

Figure 4-1: General setup of a seed spacing measurement test stand with sticky belt and high-speed camera system.

Navid et al. (2011) also set out to evaluate the performance of a seed metering device, but with a consumer-grade digital camera. The seed metering device they chose to evaluate was a vertical seed disc-type roller from a row-crop planter with individual slots for a particle to sit in which in turn will drop each particle one at a time as the roller rotates. Similar to Karayel et al. (2006) they also compared imaging-determined seed spacing against the standard sticky belt method to validate their test method. Navid et al. (2011) came to the same conclusion that image processing was a powerful tool for evaluating the performance of metering systems. Although their results were not as well correlated as Karayel et al. (2006), it was made apparent that a camera able to achieve a faster frame rate (or more consecutive images) combined with a shorter distance between the camera and the metering system would give better results in their case (Navid et al., 2011).

A version of the high-speed camera system was used in a study by Gervais and Noble (2010) and called the "continuous method" for evaluating flow continuity from meter rollers. The continuous method utilized a machine-vision camera to capture the product flow from the meter roller as it is metered out at typical roller velocities. The image frames captured by the camera are fed into an image analysis program where the projected area occupied by the product per image can be calculated. The data indicate the variation of product projected area in each image and therefore give insight to the performance of the meter roller being utilized. This variation of projected area over time is expressed as the coefficient of variation (CV), and is used as the flow uniformity metric. The performance referred to here is solely based on the evenness and consistency of the product coming off the roller. The continuous method was compared against the discrete test method of Gervais and Schollar (2008). Like the continuous method, the discrete method also tests the evenness of product coming off the roller. Product being dispensed from a meter roller typically falls off the roller with a slight pulsing motion because the straight flutes on the roller act as separate drop points. Therefore the continuous method can detect this pulsing as product is dispensed, and with the addition of an illumination source to contrast the product in the images, individual particles are easily distinguishable. While the discrete method measures the mass of the product from set discrete motions of the roller there in an inherent pulsing of product measured but some of it may be induced by the "starting and stopping" of each discrete increment. The potential measurement uncertainty added by the discrete method was one of the main drawbacks of the test method as well as the longer testing time required (up to 40 times longer than the continuous method). Both methods were found to be acceptable measurements of product flow continuity off of meter rollers, but could not be directly compared with each other because of the different units in which the data were collected (Gervais and

Noble, 2010). It soon became apparent that the continuous test method could evaluate meter rollers faster than the discrete method, and on a continuous basis. The continuous nature of the test method was a desired characteristic based on feedback from people in industry and academia who were interested in its applications because it better replicated the intended use of a meter roller. Figure 4-2 give a general representation of both the discrete and continuous test methods developed previously.

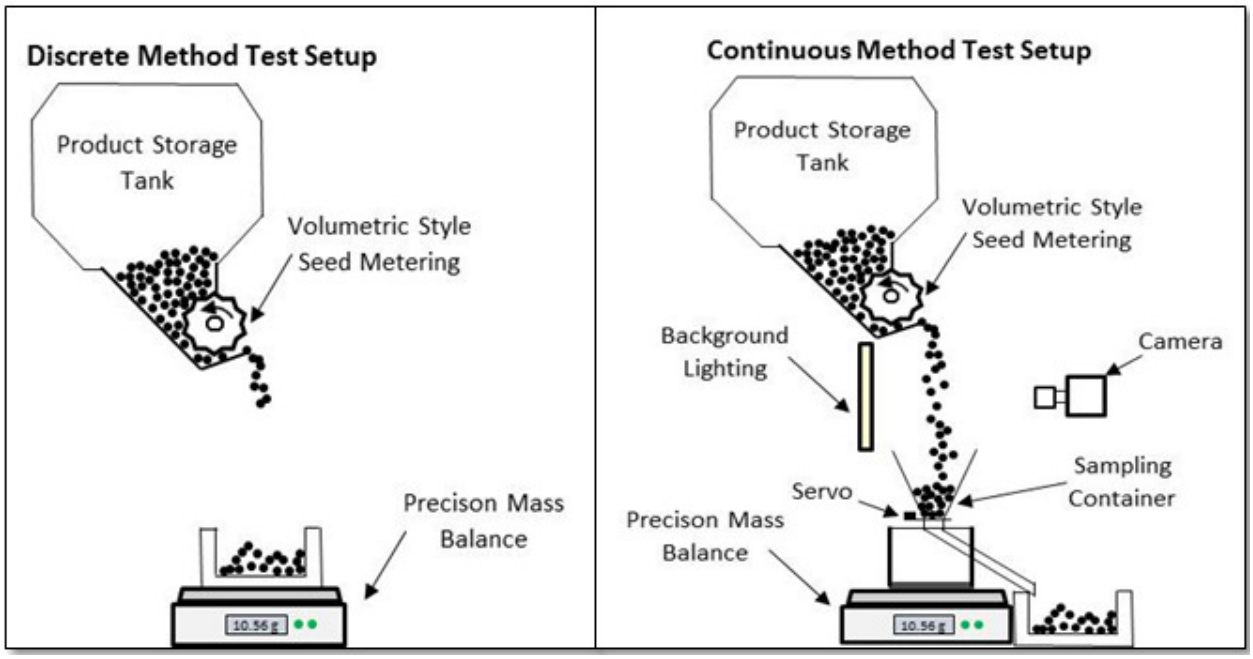

Figure 4-2: General test setup for the Discrete and Continuous test method developed by Gervais and Schollar (2008) and Gervais and Noble (2010) respectively.

In reviewing the literature it is apparent that there needs to be some standardization and control within these test methods so that the results from one test can be accurately compared with the results of another test no matter what metering system or product is utilized. Using an imaging-based apparatus to conduct the tests typically means there are more factors to control because of the added flexibility the imaging methods add. For instance, camera frame rate selection, lighting, and data processing are some of the factors that will affect the meter

evaluation results in some way. Determining what the key factors are and their importance is a first step to developing a sound test method for the imaging approach. Once the important factors or parameters are known then a set of boundary conditions could be established to ensure the most reliable and repeatable test method is developed. The next section will look at the continuous test method and introduce the parameters of importance for validating the test method.

4.2 **Validation of Experimental Test Method**

Validation of the continuous test method is a critical step to ensure the data collected are repeatable and comparable between different roller designs and test conditions. There are certain characteristics of the continuous method that must be evaluated to not only ensure the most meaningful results, but to also establish any boundary conditions. For example, a boundary condition that may arise is the camera frame rate being a limiting factor for the roller speeds that can be tested. The characteristics to be evaluated in this section are a test for any aliasing between the camera and roller speed signals to establish sampling limits, a test to determine the extent to which particle occlusion occurs at higher roller speeds, and understanding the effects of frame height and frame-per-flute (fPFL) ratio on the resulting data. The experiment was divided into three components: one to test and establish the lower bound for sampling rate, one to test the combined effects of oversampling and occlusion, and one to test the significance of the image frame height.

The first important step of the experimental validation would be to locate the lower sample limit boundary at which results are meaningful. Below this boundary the product flow signal will not be representative of the actual product flow.

Occlusion is a phenomenon that would occur mostly at very high roller speeds where a very large mass of product would be coming off the roller. There would be a point where the

projected area of the individual particles would overlap making them indistinguishable from one another and thus making the total estimated measurement of the projected area smaller than it actually is. Because the main characteristic of the product being measured is the projected area, it is important to collect clear representative images. It is possible to process the images to smooth out blurry effects but the trouble comes when individual particles need to be traced. As it is desired to consistently collect data in the region where the projected areas of particles have minimal overlap, the point of occlusion would act as a boundary condition for the maximum roller speed for testing.

The last characteristics deal with the sampling effects of varying the frame height for image processing and the number of times each particle is imaged as it falls. Results from the last characteristic test will give insight on what parameters can be varied without affecting data, and which parameters must be held constant.

4.2.1 Test Apparatus for Test Method Validation

The test apparatus consisted of an air cart simulator for metering product at varying rates and with different meter rollers and the seed flow analyzer. The seed flow analyzer consisted of imaging, data acquisition, and control components.

Table 4-1 lists the equipment used for the test, and the experimental apparatus configuration is presented in Figure 4-3.

Table 4-1: List of equipment used in the experiment.

Main Setup (Air Cart Simulator)	1. Product Tank 2. Metering Assembly 3. Meter Roller 4. Meter Drive 5. Product Catchment
Imaging Setup	6. Camera a. Point Grey Research Inc. Dragonfly b. Fastec Imaging TroubleShooter RS Camera c. Allied Vision Technologies Prosilica GE680 7. Whiteboard Background 8. Additional Lighting
Data Acquisition System (DAQ)	9. Computer and LabVIEW8.6

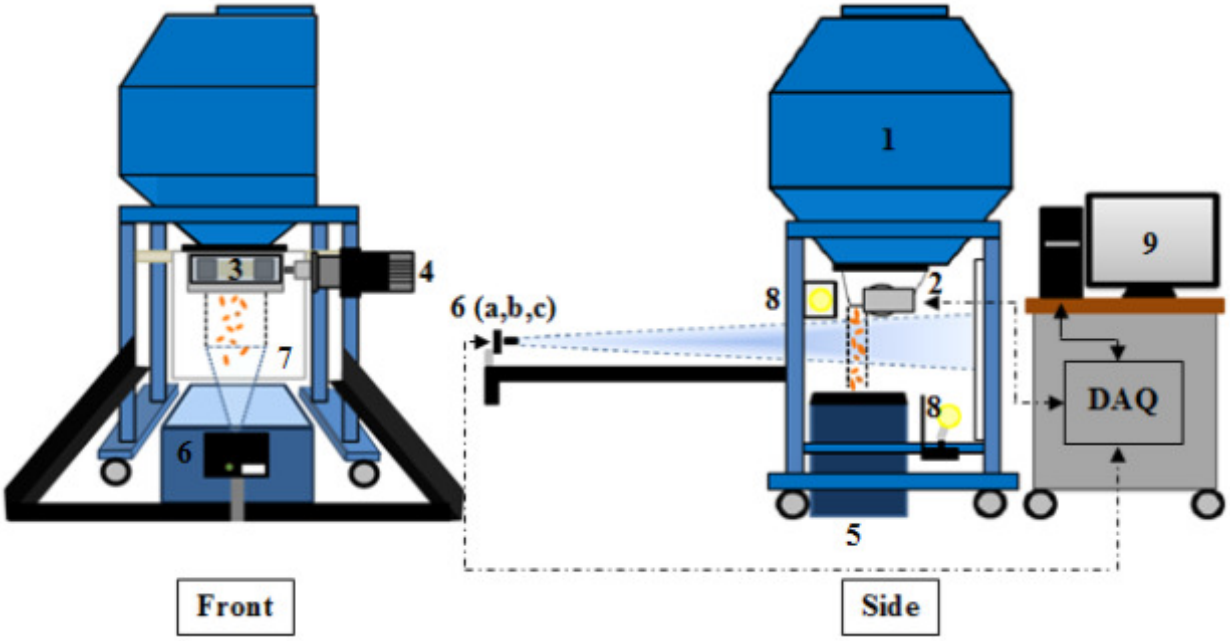

Figure 4-3: Experimental test apparatus for method validation testing. Labels referenced in Table 4-1.

The apparatus (Figure 4-3) consisted of a metering assembly (2) mounted under a product tank (1). Within the metering assembly is a meter roller (3) that is driven by a stepper motor

(MDrive 42, Motor+Driver AC plus2 by Schneider Electric Motion USA, Marlborough, CT) equipped with a 10-to-1 reducing gearhead so the meter can be rotated between 0.5 and 100 revolutions-per-minute (RPM) in an appropriate torque range. This drive unit was coupled to the meter roller shaft via an interlocking-jaw coupler. This coupler allowed easy removal of the meter roller from the assembly so the meter roller could be changed according to what product is to be metered. The meter roller profiles chosen for testing were the fine roller and extra coarse roller (Figure 2-2, Figure 2-4, and Figure 2-5). Details of the standard operating procedures to change a meter roller (remove the meter roller profile from the shaft, and place it back in the metering assembly for testing) are contained in Appendix B.

The product tank can hold any agricultural product necessary for testing and is large enough to hold 0.4 m^3 of product. The meter roller meters product out of the tank and into the product catchment (5). As product is metered out it passes through the field of view of a camera (6) that captures the product flow at specific camera rates. Three different cameras were used through the course of the project based on the requirements of the test and cameras available at the time of testing. The product being imaged was back-lighted by an illuminated white panel (7) with extra lighting (8) providing the necessary lighting required for each camera. The image data captured by the cameras was transferred back to the computer (9) for image processing and logging. The computer processes the images through a vision acquisition software driver via the LabVIEW (National Instruments, Austin TX) control system and recorded those into a comma delimited file format.

4.2.2 Imaging Apparatus

The imaging required to validate the test method needed to cover a wide range of metering properties which means that a very versatile camera would be required. Different camera characteristics were required for each test. In this case, it was most appropriate to use a

different camera for each. Minimum frame-rate tests were performed with a monochrome camera capable of 30 fps at a resolution of 640x480 pixels (Dragonfly DR2-HIBW-CS, Point Grey Research Inc., Richmond BC). Frame height testing required much higher frame rates and a Troubleshooter RS camera capable of capturing up to 1,000 fps at 640x480 pixels was used (Fastec Imaging, San Diego, CA). Additional lighting was also added for imaging at higher frame rates due to shorter exposure times. The disadvantage of the Troubleshooter camera was that it could not be interfaced directly to the control computer. Based on results of the aliasing and frame height tests, a third camera was specified for the final tests and roller testing. The Prosilica GE680 was capable of a 205 fps image capture rate at a resolution of 640x480 pixels (Allied Vision Technologies GmbH, Statroda Germany).

4.2.3 Control and Analysis Software

The user interface for controlling the imaging portion of the air cart simulator for test method validation was developed using LabVIEW software. The imaging system layout for each camera was slightly different in LabVIEW depending on what test was underway. For the two machine vision cameras (Dragonfly and GE680) they were easily controlled through LabVIEW via the NI-IMAQdx programming interface which was part of the vision acquisition software within LabVIEW. The high-speed camera from Fastec Imaging was a standalone system that collected data to an onboard memory card. The images on the memory were then fed into the vision analysis program developed in LabVIEW for analysis. The LabVIEW vision analysis takes the captured images and look at them pixel by pixel. To distinguish the product from the background a threshold limit must be set to ensure the white background and black (appear dark because of lighting) are separated for analysing the area of product in each image.

4.2.4 Illumination

The way the test apparatus was set up for canola required approximately three times as much light as for wheat, as seen in Table 4-2, and a shorter exposure time for the Fastec camera to clearly distinguish the small canola kernels. For analysis of the data from the Fastec camera, the images had to be processed at a lower threshold limit for appropriate separation of the product from the background. The difference in light intensity and threshold limits for processing will change the properties of the test conditions, therefore the wheat and canola cannot be directly compared in this case. The concept that varying the frame height has an effect on product flow CV can still be tested individually on each product, as long as the test conditions remain constant between repetitions of a single product.

Table 4-2: Light intensity for the frame height test.

		Light Intensity (lux)		
Product	**Rep**	**At Lens**	**Halfway**	**At Meter**
Wheat	**1**	157.0	268.0	1243.5
	2	145.1	251.5	1140.1
	3	148.5	256.5	1344.1
Canola	**1**	327.9	659.9	3948.0
	2	323.8	600.1	3667.0
	3	322.1	613.8	3413.0

The light intensity was measured with a LI-250A light meter (LI-250 by LI-COR Environmental, Lincoln NB) at three different locations before each test repetition began. The light intensity measurement was taken to ensure that the repetitions of wheat and canola were in an appropriate range so that image thresholding during processing for wheat and canola could be maintained at 75 and 65 respectively (approximately 3 times more light for canola) and not so

much to achieve a specific light intensity. The three locations, at the lens, at the meter, and at the background are outlined in Figure 4-4.

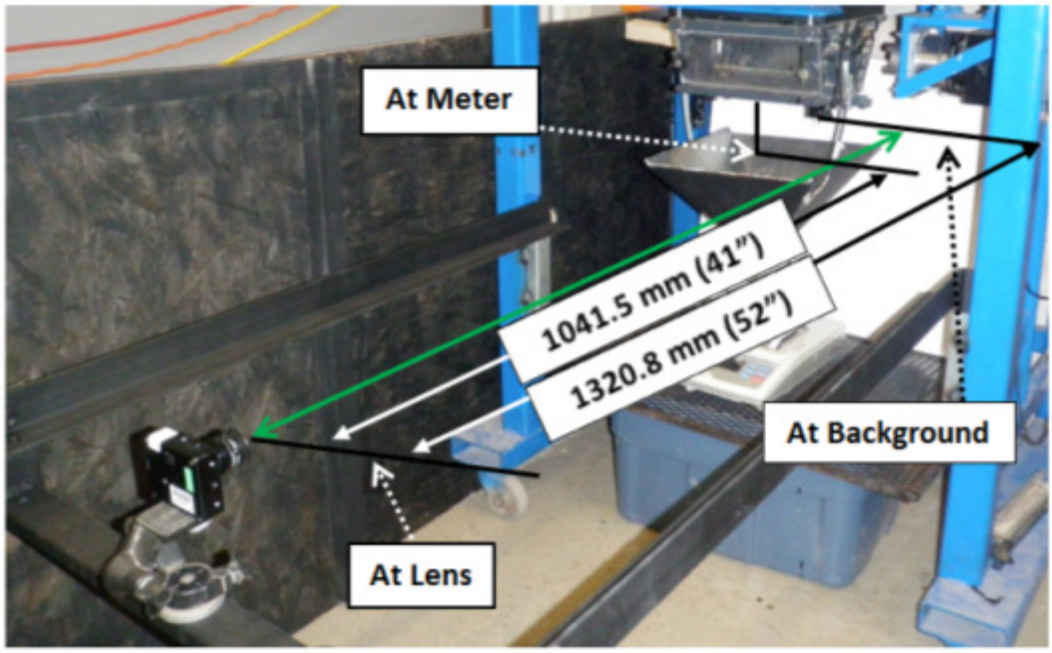

Figure 4-4: Locations of light intensity readings on testing apparatus.

The different light intensities required for wheat and canola show the importance of having a camera with automatic exposure adjustments and a means to consistently set it to streamline the testing process and produce more consistent images if the illumination is changed. This will eliminate the need to set up extra lighting and fine tune the camera every time a test is conducted.

4.3 **Sampling Limits**

Establishing if there are sampling limit boundaries to be maintained is a critical aspect of the continuous test method to ensure the sampling rate is high enough to accurately reflect the variation in the data. As discussed in the literature review, the data being sampled is the

projected area of product coming off the meter roller. The non-uniform nature of the flow is a result of the geometrical design of fluted meter rollers, as discussed in the literature review, made up of valleys (flutes) and peaks (flute ridges that separate each flute) placed circumferentially to dispense the product in each valley as the roller is rotated. Because the product will be metered at varying roller speeds with varying numbers of flutes, this will create a range of product projected-area pulse frequencies. The sampling rate is the camera rate in frames-per-second (fps) that is capturing the projected area of the product coming from the roller. To facilitate the comparison between meter rollers with a different number of flutes, the flute frequency measured in flutes-per-second (FLps) was used instead of meter roller speed (RPM). The flute frequency determines how much product is released and measured by the camera. If the sampling rate of the camera is too low with respect to the flute frequency then the signal of the product flow (projected area with respect to time) coming off the roller cannot be accurately captured because of under sampling. Therefore, determining the allowable possible sampling rates is an important boundary condition to define for any test method involving an imaging methodology.

4.3.1 Test to Establish Lower Sampling Limits

In order to establish the lower sampling limit, a test procedure was developed using the fine (10 flutes) and extra-coarse (6 flutes) rollers using canola and wheat as the products to be metered (See Figure 2-2 for rollers). These two rollers and products were chosen to give a representative sample across the range of rollers with two very different products. Little variation between rollers and products was expected because the test condition for detecting sampling limits relies on the interaction between camera rate and flute frequency. Aliasing or other artefacts due to under-sampling are more likely to occur when a low camera frame rate is used

relative to the flute frequency. The ratio between camera rate and flute frequency corresponds to the number of frames the camera captures per flute on the roller. Therefore this ratio, termed the frames-per-flute (fPFL) ratio; and provides a normalized measure of frame rate that is comparable between roller speeds and roller flute number.

In the preliminary stages of developing a testing procedure, all of the speeds that each meter roller must be tested at for each product to achieve its range of seeding rates were determined. The corresponding flute frequency at each roller speed could then be calculated. Because the Dragonfly camera had a maximum frame rate of 30 fps, the range of camera rates tested were between 30 and 1 fps. Therefore, knowing the roller speeds to be tested, roller used, and the range of camera rates, an expected range of fPFL ratios between camera rate and flute frequency was found to be between 1.09 and 342 by the following equation.

$$fPFL = \frac{fps \times 60}{RPM_{roller} \times Flutes} \qquad 4\text{-}1$$

The smallest fPFL ratio of 1.09 frames/flute comes from the largest expected roller speed of 103 RPM with field peas at 225 kg/ha, equivalent to a flute frequency of 25.75 FLps at a frame rate of 28 fps. The largest fPFL ratio of 342 frames/flute comes from the smallest expected roller speed of 0.82 RPM with canola at 3.4 kg/ha using a 6 flute roller, equivalent to a flute frequency of 0.082 FLps at a frame rate of 28 fps. The larger fPFL ratios are not of concern for this test because the number of images captured per flute is very large and under-sampling will not occur. Therefore the test for establishing sampling limits was focused on lower fPFL ratios between 1.2 and 33.6 fPFL (fPFL ratios are limited by camera frame rate which was a maximum of 28 fps).

To test for sampling limits, the flute frequency was held constant and the projected area of the metered product was imaged at various camera frame rates. To minimize the amount of

testing required, only three faster camera rates (28, 24, and 20 fps) were used in each of the replicates. Resulting data were sub-sampled to create other rates. When the data from the three rates were sub-sampled, data for eleven other camera rates became available from these three higher rates. All of the test conditions including flute frequency, camera rate, and the resulting fPFL ratio are found in Table 4-3 for the fine and extra coarse roller to be tested.

Table 4-3: Establishing sampling limits test conditions for wheat and canola.

Roller Type	# of Flutes	Roller Speed (RPM)	Flute Freq. (FLps)	Frame Rate (fps)													
				28	24	20	14	12	10	8	7	6	5	4	3	2	1
				fPFL Ratio (Frames/Flute)													
F	10	5.00	0.83	33.6	28.8	24	16.8	14.4	12	9.6	8.4	7.2	6	4.8	3.6	2.4	1.2
EC	6	8.33	0.83														

With the continuous method, meter roller performance is quantified by measuring the continuity of the product flow off the roller in terms of the coefficient of variation of the projected area of falling product over time. The coefficient of variation is calculated for each repetition in each test at every frame rate stated in Table 4-3. If enough data are collected to prevent under-sampling, the coefficient of variation should remain constant from test to test because the flute frequency is held constant throughout. If the coefficient of variation begins to taper off or suddenly increases, the minimum sampling point will have been detected.

Under-sampling effects could also occur at whole-numbered fPFL, where the camera would be catching the exact same point on each flute of the roller and could provide a biased representation of the roller's performance. However, if the fPFL ratio is high enough there will be no effect on the data.

4.3.2 Results of Test to Establish Lower Sampling Limits

Along with the standard deviation (SD) of the product flow on the primary y-axis, the average percent area of product occupying each image was calculated and graphed on the secondary y-axis versus the fPFL ratio in Figure 4-5 and Figure 4-6 for wheat and canola, respectively. Figure 4-5 and Figure 4-6 display how the SD of the product flow reacts as the fPFL ratio is decreased from 34 down to 1. As the fPFL ratio is decreased, the signal representing the product SD will start to fluctuate. It is at this point of fluctuation that under-sampling effects become present and therefore must be avoided when capturing data. The analyzed data can be found in Appendix C.

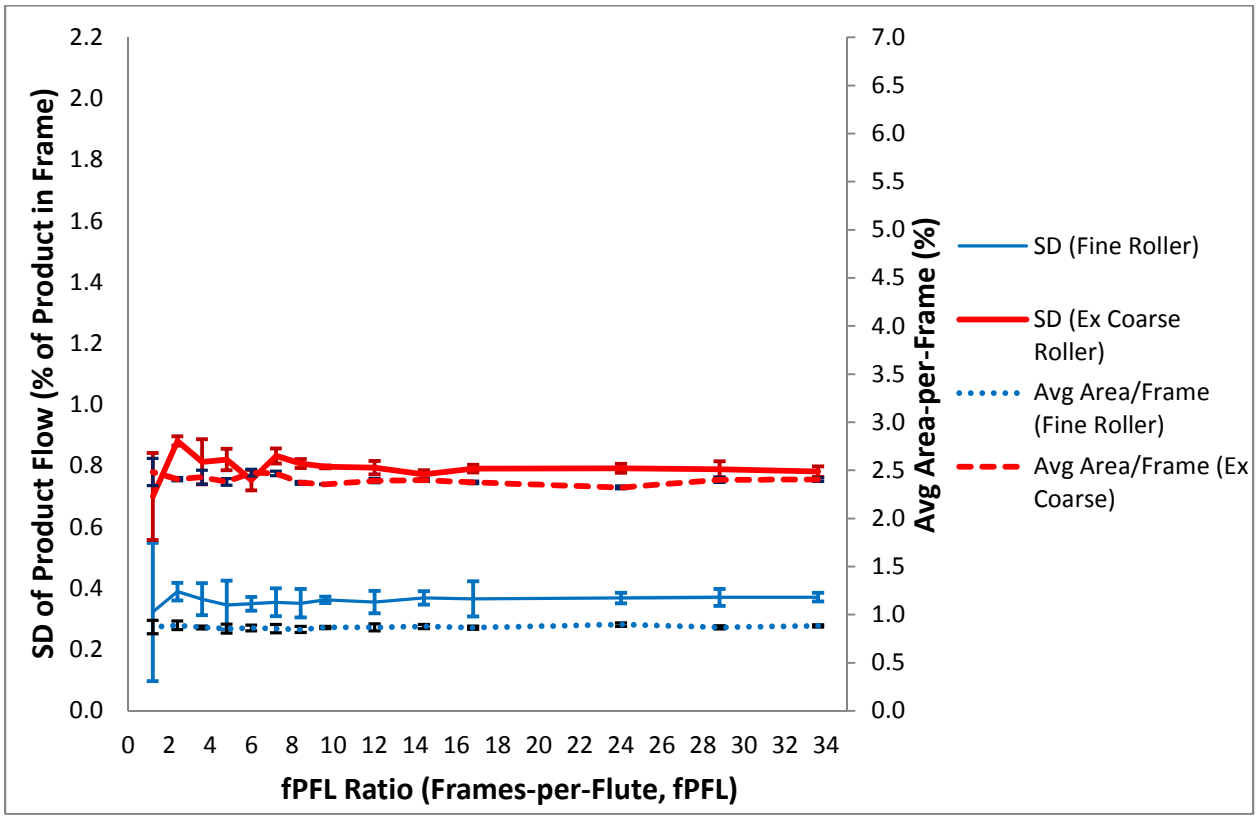

Figure 4-5: Standard deviation (SD) of product flow as fPFL ratio is varied for wheat with error bars at each data point indicating the variation between the three repetitions.

The graphical representation of the test for establishing sampling limits for wheat in Figure 4-5 shows a slight variation in product flow SD at higher fPFL ratios and more variation at the lower end starting at around 6 frames-per-flute (fPFL) with the extra coarse roller and 4 frames-per-flute with the fine roller. At 4 and 6 fPFL the camera frame rate is too low relative to the flute frequency to accurately capture the variation in product flow coming off the meter roller. The lines representing the average projected area of product per frame as captured by the camera show the difference between the amount of product released by the fine and extra coarse roller. Figure 4-5 shows about 2.5 times more product-per-image with the extra coarse roller which translates into a lower SD of product flow (see error bars in Figure 4-5) compared to the fine roller at the same flute frequency. The larger area of product per frame then translates into a lower sensitivity to detect smaller variations in the product flow for the higher volume extra coarse roller as compared to the fine roller. This explains why the SD line (solid lines) for the fine roller is lower than the extra coarse SD line and the average area-per-frame line is higher for the extra coarse roller than that of the fine roller.

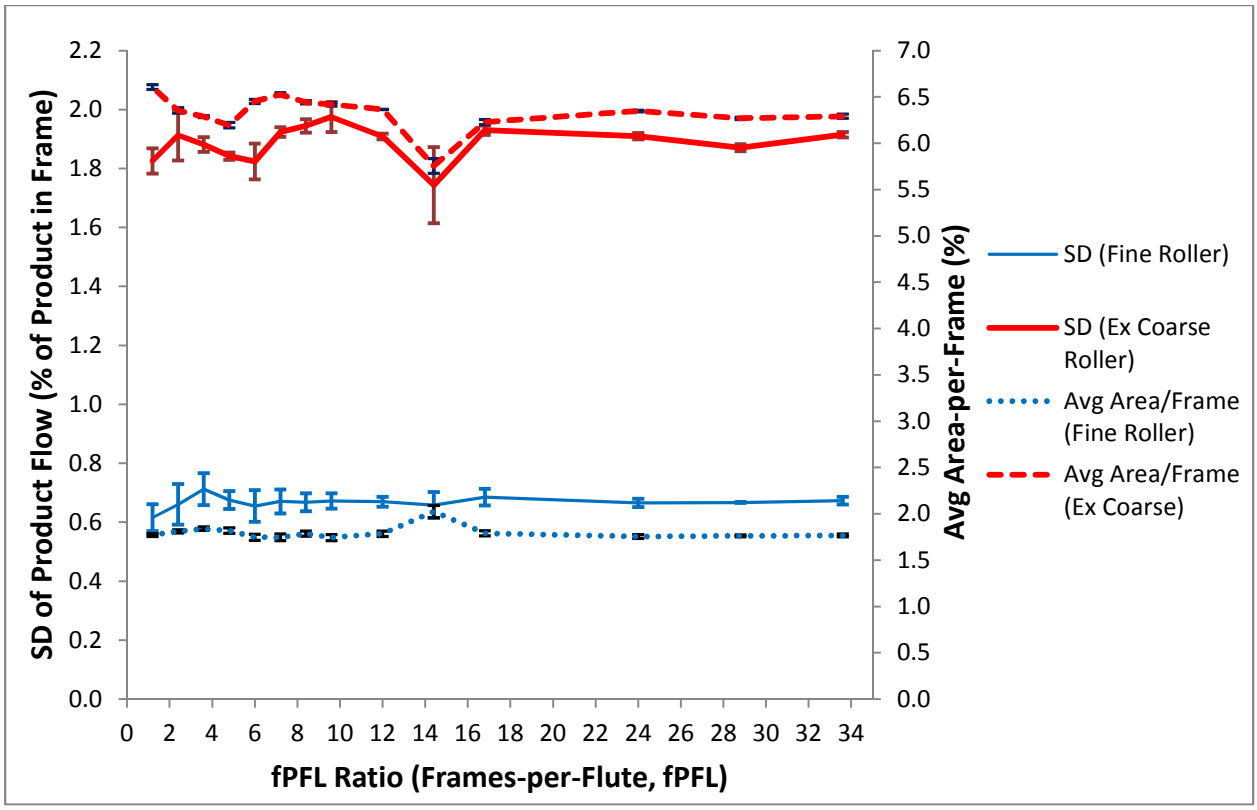

Figure 4-6: Standard deviation (SD) of product as the fPFL ratio is varied for canola with error bars at each data point indicating the variation between the three repetitions.

The graphical representation of the test for establishing sampling limits for canola in Figure 4-6 shows a similar trend compared to that of wheat but with smaller variations in the SD of product flow. The smaller variations are attributed to the smaller relative size of canola seeds along with the larger area being occupied per frame by canola as seen in Figure 4-6. Even though the wheat and canola are being metered at the same flute frequency with the same rollers, the smaller canola seeds occupy a larger area-per-frame (right axis of Figure 4-5 and 4-6). The larger occupied area is attributed to the fact that canola packs together more tightly, therefore more seeds are falling at any given point. Using equations from Mohsenin (1986) for estimating the projected area of an agricultural particle and the known volumes of the flutes on a fine and extra coarse roller will show why canola has a larger area-per-frame (Table 4-4).

Table 4-4: Estimated projected area of wheat and canola.

Roller	Product	Flute Volume (mm^3)	Average Projected Area (mm^2)	Seeds Per Flute	Total Projected Area Per Flute (mm^2)
F	Canola	9,404	11.47	1,691	19,396
	Wheat		58.76	185	10,871
EC	Canola	35,324	11.47	6,355	72,892
	Wheat		58.76	695	40,838

The estimated total projected area of canola and wheat in Table 4-4 shows that canola has almost twice as much projected area of product per flute. This correlates with the larger area-per-frame for canola observed in Figure 4-6 compared to the data for wheat in Figure 4-5 for both the fine and extra coarse meter rollers. To an extent the same trend described above between canola and wheat projected area can be used to explain the difference between the extra coarse and fine roller (Figure 4-6) where the fine roller has a higher SD of product flow and a lower average area-per-frame than the extra coarse roller which has a lower SD of product flow compared to the average area-per-frame. With less product being delivered with the fine roller, and therefore less projected area, it is more sensitive to changes in product flow than the extra coarse roller at the same roller speeds.

There is one anomaly apparent from the canola data at an fPFL ratio of 14.4 (sub-sampled from a camera frame rate of 24 fps to match 12 fps) for both the extra coarse and fine roller. The main contributing factor to this dip in the data comes from the fact that the data graphed are the average of 3 repetitions so any variation in one more of the repetitions will show. For the fine roller there was a spike in the average area per frame which contributes to a drop in the SD of product flow which also had a slightly higher error variation (both in SD and Avg Area/Frame data) at the 14.4 fPFL ratio data point. This slight spike with the fine roller is quite minor though compared to the dip in the data for the extra coarse roller. The large dip in Figure

4-6 for the extra-coarse roller is due to one repetition being way out of line and therefore skewing the average line. To help explain this anomaly further one repetition from most of the camera rates tested were stacked on top of each other in Figure 4-7 to show how the product flow signal varies with increasing camera rates.

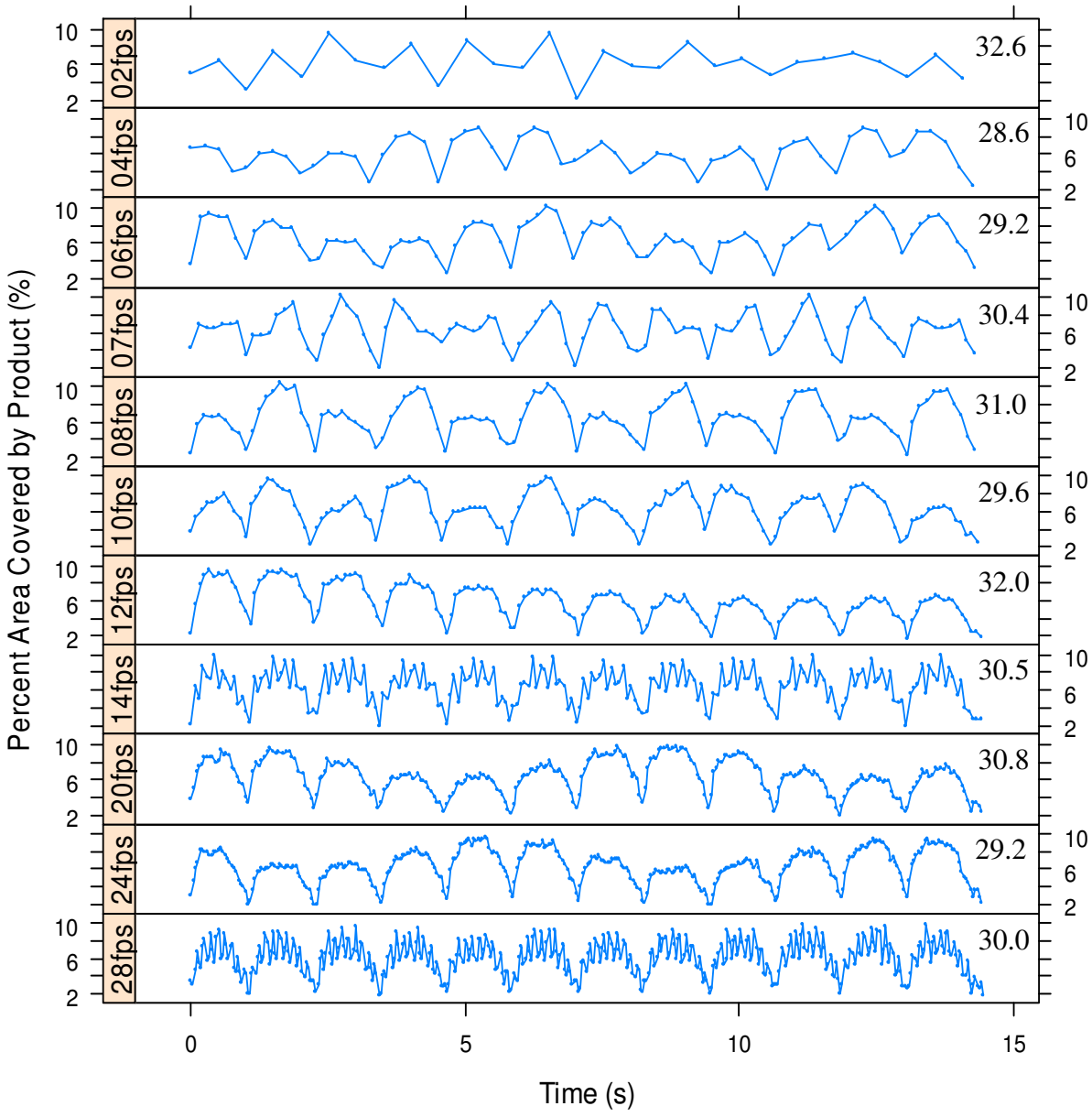

Figure 4-7: Repetition 1 of the raw data (shown in Table C-1) for the sampling limits test for canola (extra-coarse roller) with its corresponding product flow CV (%) measure displayed on the right.

The data in Figure 4-7 are from the experiments involving canola with the extra-coarse roller (6 Flutes over 2 revolutions) because that is where the anomaly was observed earlier. There is a large variation in the data especially at the lower camera rates below 12 fps where the anomaly occurred. The larger variation bars in Figure 4-6 for the lower camera rates (1-10 fps) are explained based on the product flow trends observed in Figure 4-7 but it almost appears to even out at 12 fps. Because this is only one repetition and it is a relatively random dispensing of product from the roller (random because of the bulk pile of product feeding into the flutes from above) that could easily be interrupted by an obstruction or foreign object passing through the product holding tank. The raw data are presented in Appendix C (Table C-1) for all 3 repetitions. Repetition 2 and 3 at 12 fps appeared to dispense slightly less material based on the area of product imaged per frame compared to every other setting. This could be due to an obstruction potentially affecting the feeding of the roller or it could be a result of the minimal data set length (only two revolutions of the roller) so the test could not reveal an underlying frequency that may be happening every two or more revolutions. In either case, this anomaly was not observed in any other instances at the same camera rate or higher for each product so the 14.4 fPFL ratio will be considered the start of the low end sampling limit. At least for canola it would be safest to stay above the 14.4 fPFL ratio. It should be noted that if the camera is the restricting factor then it may be possible to collect at a fPFL ratio between 6 and 14 because the data in Figure 4-6 showed promising results, but if possible it would be best to stay above 15 fPFL.

The test to establish lower sampling limits has revealed that a minimum fPFL ratio should be utilized for gathering product flow variability data using this test method. Wheat can be captured at an fPFL ratio as low as 6 but is recommended to stay above 10 unless absolutely needed. Canola can also be captured as low as 6 fPFL but there is a point between 14 and 15

fPFL that should be avoided. Therefore for canola it is recommended to capture data at 15 fPFL or higher. Further, it would be safe to assume that any product with a low 1000-seed weight, and more specifically the products with a low single-seed projected area, similar to that of canola could fall into the same range of fPFL ratios as canola as a precaution to ensure accurate data are collected. There does not appear to be a clear correlation between 1000-seed weight and fPFL ratio, but the data for wheat and canola suggest that the test has greater uncertainty at low fPFL ratios when seeds have a smaller projected area. This is thought to be related to the amount of seeds being released at a time because products with a larger projected area are essentially larger seeds. There are fewer of them seen per frame which also means there is less variation in the amount of seeds per frame as well. This can be seen from the data in Table 4-4.

4.4 **Significance of Image Frame Height**

Frame height refers to the vertical size of the object the camera captures, in this case the height of the area where the falling product is imaged by the camera. The number of times a particle falling through this frame is imaged by the camera will be determined by the frame rate of the camera, the height of the frame, and the velocity of the particle. If the particles all start falling from the same height above the imaging frame, the velocity profile is assumed to be consistent for all particles. For a constant frame rate (and resulting fPFL ratio), a single particle in free-fall will be imaged more than once before leaving the field of view as the frame height increases. It was hypothesized that this could have an averaging effect on the data because each kernel of grain is being captured in multiple images as it crosses the image frame. For instance, over a standard frame with a height of 480 pixels (or 136.5 mm [5.375”]), a single particle might be imaged four times with a camera frame rate of 50 fps, but 16 times at a camera frame rate of 200 fps. If the frame height decreases over a constant frame rate, there is a point when the frame height will get small enough that each particle may not be imaged at least once. One could argue

that both too large and too small of a frame height is not ideal, so understanding the implications of frame height versus frame rate is important. Therefore, a frame height test should give insight into what has more effect on the coefficient of variation of product flow, the frame height at which it is processed or the frame rate.

4.4.1 Frame Height Test

For an experiment to be conducted to test the significance of the frame height during analysis, a camera with the capability to reach high enough rates to keep the fPFL ratio in suitable ranges and a method of calculating the baseline frame height at specific camera rates are needed. The camera utilized was an HSI Fastec Imaging camera with the capability of capturing 1000 fps. Baseline frame height ranges (i.e. frame height at which each kernel is captured in only one camera frame) can be found by manipulating and applying the equations of motion, specifically that of a uniformly accelerated body in linear motion as in the equation below.

$$s = \sqrt{2as_i}\Delta t + \frac{1}{2}a\Delta t^2 \qquad 4\text{-}2$$

Where, s is the position of the kernel at the end of the interval, s_i the kernel's initial position, and Δt is the time interval (s) corresponding to the frame rate of the camera. Equation 4-2 also assumes that velocity equals zero when time equals zero (t_0) and s_i is measured with respect to position s when time equals zero (s_0)

The goal of this experiment is to determine whether the frame height at which the data are processed is more or less important than the fPFL ratio. Three replicates of each product, wheat (extra coarse roller) and canola (fine roller), were metered at 0.83 flutes-per-second and the falling product imaged at 250 fps. This resulted in a frame-per-flute ratio of 300 fPFL. These data were then sub-sampled to simulate imaging at a series of smaller fPFL ratios. In this experiment the data were sub-sampled into data sets for 150, 60, and 30 fPFL. Because flute

frequency was held constant these fPFL ratios are equivalent to camera frame rates of 125, 50, and 25 fps, respectively. Each camera rate had a frame height associated with it such that each seed is only processed once as found by Equation 4-2. Therefore, the raw data were processed at four different frame heights corresponding to 250 (0.004 s), 125 (0.008 s), 50 (0.020 s), and 25 (0.040 s) fps. Data were analyzed to show the effect frame height has on the CV of product flow from the roller.

The test was run using wheat with an extra-coarse roller, and with canola using a fine roller. Both cases were run with a flute frequency of 0.83 flutes-per-second. Three replicates were taken for each product. The camera was mounted on the apparatus at a fixed distance (41") from the metering assembly. The camera was zoomed in and focused on the plane of interest where product fell to give an initial frame height of 0.136 m (5.375") over the full 480 pixels. The initial frame height was needed to calculate the number of pixels in the region of interest for processing of the images from each replicate. The top of the frame began 0.078 m (3.06") below the metering assembly (the metering assembly being the assumed point of zero velocity) for wheat and 0.10 m (3.94") for canola. Both of these values were used as the kernel's initial position, s_i, in Equation 4-2 for calculating the optimal frame height. Wheat and canola had different points of zero velocity simply because the camera angle was nudged so that the top of the camera frame was slightly further away from the metering assembly for wheat.

4.4.2 Frame Height Test Results

With the roller metering product at a constant rate of 0.83 flutes-per-second, the imaged data from each product was then processed at the optimal frame height that corresponded to fPFL ratios of 300, 150, 60, and 30. For wheat the baseline frame heights were 6.8, 13.5, 35.0, and 72.5 mm and for canola the optimal frame heights were 7.1, 14.3, 37.0, and 75.4 mm

respectively. Table 4-5 shows the results of the coefficient of variation of product flow for wheat and canola at specific conditions.

Table 4-5: Average CV from three frame height test replicates for wheat and canola flow from a meter roller and the maximum change in CV (ΔCV) as the camera frame rate changes to achieve the desired fPFL ratio.

Product	Frame Rate (fps)	fPFL Ratio	**Frame Height (mm)**				Δ CV
			6.8 (24 pixels)	**13.5 (47 pixels)**	**35.0 (123 pixels)**	**72.5 (255 pixels)**	
Wheat	**250**	**300**	61.77	51.14	41.85	37.16	24.61
	125	**150**	61.71	51.10	42.13	37.18	24.53
	50	**60**	62.64	51.53	41.98	37.41	25.23
	25	**30**	62.03	51.70	41.97	37.88	24.15
Canola			**7.1 (25 pixels)**	**14.3 (50 pixels)**	**37.0 (130 pixels)**	**75.4(264 pixels)**	
	250	**300**	43.27	37.34	32.72	31.02	12.24
	125	**150**	43.12	37.37	32.78	31.02	12.10
	50	**60**	43.75	37.09	32.77	30.96	12.79
	25	**30**	43.49	37.03	32.58	31.01	12.48

The highlighted blocks show points at which the baseline frame height (i.e. seeds theoretically imaged only once) was used for processing the data with baseline frame height corresponding to a specific camera rate. Observation of the results horizontally across Table 4-5 indicate a steady decrease in the CV of product flow as the frame height is being increased to accommodate for lower frame rate. Looking at the columns, the CV of product flow remains relatively constant for a given frame height regardless of the frame rate. Looking at the rows, the CV decreases as frame height increases at a set camera rate because the ratio of product area over background area is decreasing which means it is harder to sense very small variations in the product flow. Because all tests were done at the same metering rate the CV of the product flow should be equal for every test. Therefore it is critical to maintain a constant frame height when processing all images from the data to ensure the results from each tests are comparable to the

next. The results also indicate that a wide range of frame rates can be used for testing in order to accommodate a wide range of seeding rates for various products and maintain consistency in the data. Data should not be collected at an fPFL ratio lower than 6 at the absolute lowest end if the camera is the limiting factor, but it is recommended to stay above 10 for wheat and 15 for canola as found from the sampling limits test earlier.

The results for canola follow a similar trend to that of wheat where the CV of the product flow decreases as frame height increases but remains relatively constant as the frame rate is varied. The ΔCV column shows that the variation in canola is slightly less pronounced which can be attributed to several factors. First, the smaller overall size of canola as well as the fact there are more individual kernels of canola per image compared to wheat means that the sensitivity to frame area changes would be lower. Second, the fact that more light was needed for imaging the canola with this camera meant that the threshold limit for image analysis was different than the wheat so the CV results of the two products cannot actually be directly compared a with this setup. However, the results across each product clearly point to the same conclusion.

The frame height test set out to answer the question of whether the frame height should be varied with camera rate or if maintaining a constant frame height while varying the frame rate was a better method. The data clearly points to maintaining one constant frame height across all products tested while the camera frame rate can be varied with roller speed to attain the desired fPFL ratio.

4.5 **Product Oversampling and Occlusion**

Occlusion happens when the particles block the view of other particles as they fall from the metering compartment, resulting in overlap in their projected areas. A minor amount of occlusion is happening all of the time to some extent with volumetric style metering systems.

Significant occlusion is more likely to happen at high product flow rates, potentially making the product flow signal becomes unrecognizable. The capacity of a meter roller is limited by its volume, its rotational speed, and the rate at which product can fill the flute volume. Based on past experience with the meter rollers utilized in this study they are not capable of metering product at a rate high enough to make the flow signal unrecognizable. What is unknown is the degree at which minor occlusion is happening and what affect it has on the product flow signal.

In the previous section it was determined that maintaining a constant frame height throughout the meter roller testing is required to maintain consistent and comparable results between repetitions and products. When testing meter rollers it is ideal to test over a range of roller speeds that relate to real life applications. Therefore, in testing where imaging of the particles is essential and the imaging must be done within a fixed frame size over a range of roller speeds, a degree of occlusion is expected because of the volumetric nature of the product being dispensed. The imaging interference effects expected can be broken into two categories during testing; minor occlusion and oversampling:

1) A particle falling partially or completely behind another particle as it is being imaged is referred to as *occlusion*. The chance of this type of minor occlusion happening increases as the flow rate off of the meter increases (roller speed). We know the meter dispenses a constant amount of product per revolution so this occlusion should be consistent but as meter roller speed increases the amount of product falling per unit of time increases. Because imaging is happening from one direction only, this kind of occlusion is inevitable to some extent. Since the total area the product occupies in each image is the main variable being measured and not individual particles, some amount of occlusion is allowed, as it is unlikely that any two particles will be fully overlapped.

2) The second effect related to high roller speeds that can occur relates to the amount of product in a given image frame as the meter roller speed increases. This will be referred to as *oversampling*. Because the frame height of the image is constant throughout the entire test, then as roller speed increases there will be more particles in any given image. The roller is not dispensing more particles per flute but because its rotational speed increases the mass flow rate is increased. As the camera rate is increased with roller speed to maintain a set fPFL ratio, each particle is being imaged

more frequently. The rate at which particles are being imaged more than once will also increase as camera rate increases.

The question to be answered now is what kind of an effect do minor occlusion and oversampling have on the results and how can it be measured. Previously it was discussed that maintaining a constant frame height was a critical for consistent and comparable results across different products at a set roller speed. It was also discovered that changing the fPFL ratio at a set roller speed yielded consistent CV results as well. Varying the fPFL ratio (changing camera rate) showed that minor occlusion and oversampling had no effect on the results at a set roller speed, but what about at varying meter roller speeds? That is what this section will address using results from meter roller testing done with the continuous test method.

4.5.1 Test for Product Oversampling and Occlusion

Minor occlusion is inevitable in this kind of testing and is expected to have a minimal effect based on roller geometry and operational roller speeds. Oversampling can be eliminated if the frame height is matched with the camera rate so that an image of each particle is recorded only once. However, because it was determined that the frame height must be held constant for every meter roller speed, hence camera rate, there will always be a certain amount of oversampling.

To analyse occlusion effects two sets of data from different roller speeds were used. For oversampling, the degree of variation in the product flow signal increases as more particles are being sampled multiple times per image. The raw data contain the portion of total projected product area per image, so as roller speed, and therefore camera rate, is increased the amount of product per image will also increase. The following section will discuss the impact that oversampling has on the final product flow results as it pertains to the continuous method to evaluate the performance of a meter roller.

4.5.2 Results for Product Oversampling and Occlusion

The data presented in this section come from some preliminary meter roller testing with a group of prototype rollers used to further validate the continuous test method. The roller data presented here are from two randomly selected rollers chosen to depict the trends observed. The tests were operated at roller speeds similar to actual rates used in field operation with a range of products typically metered in seeding operations. Therefore, the 6-flute roller (roller 79) operated at 20, 25, and 30 RPM should theoretically output the same product mass flow rate as the 15 flute roller (roller 45) operating at 39, 49, and 59 RPM based on the volume of the flutes. Therefore no calibration was conducted to ensure the same mass flow rate was being dispensed at each roller speed, and it was not critical to achieve identical rates. The same relationship was assumed for canola. The first repetition of all three speeds was collected followed immediately with the second repetition. All test conditions, fPFL ratio and frame heights were held constant to ensure comparable data were gathered. The best way to view the oversampling effect is to graph the percent area of product per image captured by the camera and grouped by meter roller speed in a box and whisker plot as seen in Figure 4-8.

The effect of oversampling was visually apparent for all meter rollers tested. Results for rollers 79 and 45 in wheat are presented and discussed. The remainder of the figures discussed in the oversampling test results section can be found in Appendix C whereas all the data are displayed in a table in this section for discussion.

At each roller speed for Figure 4-8, 4-9, 4-10, and 4-11 the percent area of product per image increases with increased roller speed. This trend is attributed to oversampling. Higher roller speeds equal higher camera rates so therefore more particles are being imaged more than once contributing to the oversampling referred to here. Investigating this trend further it was soon discovered that the oversampling could be filtered out by a correction factor. The correction

factor is a simple ratio of the reference speed (20 RPM is this case) and roller speed at which testing occurred. That ratio can then be multiplied by the percent area for each image. For example, applying the correction factor to the data of Figure 4-8, the reference speed would be 20 RPM and the roller speed would be 20, 25, or 30 RPM. The tables shown in this section use the logic above to present the correction "Applied" data (roller-speed corrected) for comparison with the un-corrected data (raw data) and graphically presented in the following figures.

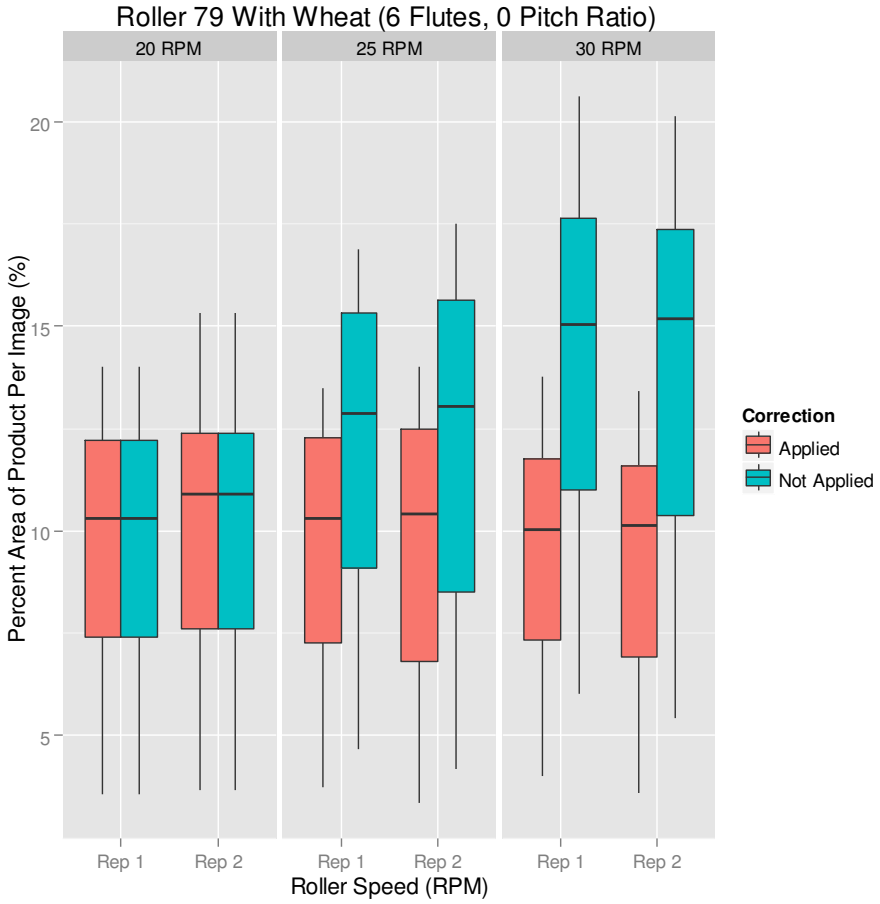

Figure 4-8: Percent area of product per image vs roller speed with a 6 flute prototyped roller in wheat showing roller-speed corrected data "Applied" and raw "Not Applied" data.

The box and whisker plot of Figure 4-8 shows the results of two repetitions for each of the three roller speeds for this roller, showing uncorrected and corrected data in each case. With

the correction factor applied the oversampling effect is essentially factored out with respect to the 20 RPM speed. By calculating the CV of product flow for the entire data set with and without the correction factor applied and comparing the two cases it can be shown how oversampling affects the data for the performance of a meter roller. Figure 4-8 shows that oversampling has no effect on the overall reading of the performance of a meter roller which is displayed in the column labelled "CV of Product Flow (%)". Even though the raw data for each image are slightly skewed from the incremental increase in meter roller speed causing the oversampling, it does not appear to affect the CV of product flow for this roller. However, a variety of rollers using different products still need to be looked at before a conclusion can be made. To evaluate the effect of oversampling further and ensure that the trends observed previously are comparable on completely different meter rollers, a second set of data was chosen from another meter roller. Roller 45 had zero pitch with 15 flutes and required roughly twice the speed to discharge an equivalent throughput as roller 79 containing 6 flutes at zero pitch.

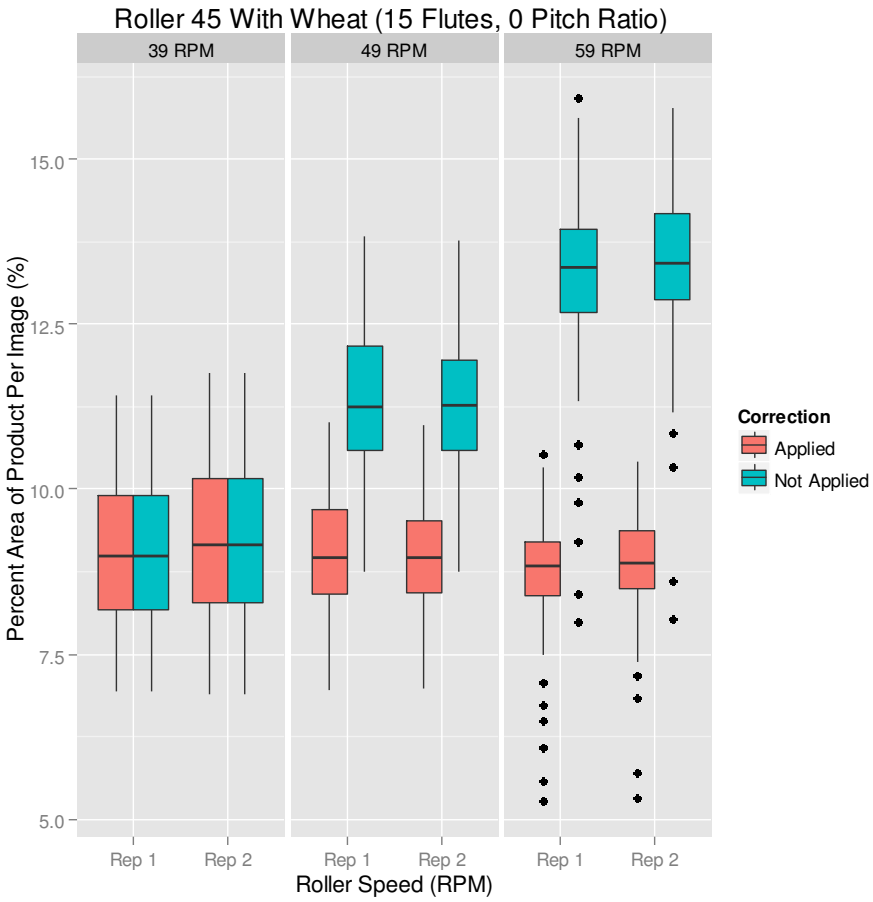

Figure 4-9: Percent area of product per image vs roller speed with a 15 flute prototyped roller in wheat showing roller-speed corrected data "Applied" and raw "Not Applied" data.

Figure 4-9 above shows the same trend as wheat with the 6-flute roller in Figure 4-8 where percent area of product per image increases as roller speed increases which again can be attributed to oversampling. One difference to note here compared to the 6-flute roller data of Figure 4-8 is that the 15-flute roller does not have as much spread in the data. This lower spread of the data are another attribute of a roller with more flutes, especially when each of those flutes has a lower volume (ie. 15-flute roller vs 6-flute roller). So the spread of the data in each block from Figure 4-8 and Figure 4-9 can give an indication of how even the product is actually coming off of the meter roller where a lower spread could actually mean a more even flow.

Visually looking at each block is not enough because outliers and other factors could skew it which is why numerical analysis is required. In the case here for Figure 4-9 the extreme points for both repetitions at 59 RPM are not outliers but extreme points caused by the variation of flow with straight flutes.

Table 4-6: Product overlap data for a 6 and 15-flute roller in wheat (fPFL ratio of 11) and canola (fPFL ratio of 176.5) with the Tukey test results for each roller in the speed corrected data showing the significance in the difference of means on a 95% confidence interval where one test is two roller rotations.

Test ID		Roller Speed (RPM)	Avg. Area Covered by Product Per Frame (%)	CV of Product Flow (%)	# of Particles Per Frame	Total Mass of Product Per Test (g)
Wheat Roller 79 - 6 Flutes	**Raw Data**	20	9.82	31.48	86	> 630*
		25	12.15	30.32	95	> 630*
		30	14.10	29.03	105	> 630*
	Speed Corrected	20	9.82 a	31.48	---	---
		25	9.72 a	30.32	---	---
		30	9.40 a	29.03	---	---
Wheat Roller 45 - 15 Flutes	**Raw Data**	39	9.12	11.85	86	293.1
		49	11.33	8.85	99	294.0
		59	13.38	7.60	109	294.1
	Speed Corrected	39	9.12 e	11.85	---	---
		49	9.01 e	8.85	---	---
		59	8.84 d	7.60	---	---
Canola Roller 79 - 6 Flutes	**Raw Data**	0.86	0.80	53.55	52	262.4
		1.26	1.14	47.95	74	259.9
		1.7	1.51	43.88	98	262.3
	Speed Corrected	0.86	0.80 h	53.55	---	---
		1.26	0.78 g	47.95	---	---
		1.7	0.77 g	43.88	---	---
Canola Roller 45 - 15 Flutes	**Raw Data**	1.78	0.86	23.87	49	112.6
		2.61	1.18	21.16	70	114.7
		3.5	1.52	21.27	89	118.2
	Speed Corrected	1.78	0.86 l	23.87	---	---
		2.61	0.80 k	21.16	---	---
		3.5	0.77 j	21.27	---	---

** 630 grams is the maximum measurable mass on the scale: (1100g [max rating]- 470g [catchment mass]) = 630 g*

Table 4-6 gives a summary of the raw data from Figure 4-8 and Figure 4-9 to show what effect oversampling and occlusion has on the CV of product flow with these specific rollers. The

raw data rows include the average percent area of product-per-frame, the CV of product flow, as well as the average number of particles per frame and mass of product per test over 3 repetitions. No mass data could actually be presented for wheat with roller 79-6 because the output of this roller was just out of range for the mass balance to measure. The other three rollers displayed a consistent amount of product discharged per test at less than 5% variation between repetitions. Taking a closer look at the data displayed in the table it shows that oversampling can be factored out by a simple ratio with respect to the reference speed, or lowest speed used for the specific roller. However, as the oversampling effect is factored out of the raw data to yield the speed corrected data, the average area of product per frame appears to decrease as roller speed is increased for each roller consistently. What this trend shows is a certain degree of occlusion that occurs during the measurement. During testing, as the frequency (roller speed) was increased and frame height remained constant there would be more product in each collected image (increase in the number of particles per frame shown in Table 4-6) as shown in the raw data. Because there are more particles per image there is a higher probability of occlusion occurring. So when oversampling is factored out due to roller speed increase one would expect the percent area of product-per-frame to be almost identical for each speed, but the downwards trend with increased roller speed observed in Table 4-6 reveals a degree of occlusion apparent in the measurement. Therefore, a Tukey test was done on the speed corrected data to see if the occlusion was statistically significant. The Tukey test revealed a statistically insignificant decrease in the average area of product for the 6 flute wheat data but the remainder of the data showed a statistically significant decrease in percent area of product-per-frame. When looking at the 15 flute wheat data versus the 6 flute wheat data, the difference between areas at each speed are consistent but the CV with the 15-flute roller is quite a bit lower. The lower CV means the data

are more sensitive to changes in product area so if the same amount of occlusion occurred in both tests it may show up as insignificant for the 6-flute roller and significant for the 15-flute-roller test. Therefore, one has to take a closer look at the data if the Tukey test reveals a significant decrease. Looking at the 15-flute wheat data closer shows a 3% decrease in area of product-per-frame at 59 RPM compared to 39 RPM, which on a practical scale would be considered acceptable. This 3% percent change is actually better than 4.3% decrease observed in the 6 flute wheat data which passed the Tukey test (ie. no significant difference). The Tukey test here is not a definitive measure of pass or fail but rather an indicator. In this case the Tukey test has shown that there is a small amount of occlusion apparent as roller speed is increased but it is on a small enough scale that it could be neglected for this study. The details of the Tukey tests and other corresponding figure to go along with the canola tests can be found in Appendix C.

It is reasonable to say that oversampling and occlusion do not have an effect across a range of different meter rollers based on the above results. Oversampling was shown as the difference between the average area of product-per-frame raw data versus the speed-corrected data. However, it is unnecessary to factor out oversampling due to roller speed because it does not affect the CV of product flow (shown in Table 4-6). Identifying the difference between oversampling and occlusion in the data was the important aspect in this results section. Once the oversampling trend was defined, the occlusion effect could be deduced as the slight downwards trend in area of product-per-frame as roller speed increases in the speed-corrected data. Even though the occlusion effect showed a statistically significant decrease in the average area covered by product-per-frame, it was shown that the deviation was relatively small (up to 4.3% decrease in corrected area of product-per-frame). In the canola data this deviation was even smaller than wheat mostly because of the particle size difference and throughput requirement.

Regardless of particle type, occlusion will always be a small part of any imaging setup. For the continuous test method the slight downwards trend with metering speed increase is a nature of the test setup in a 2D frame of view. Ensuring the data captured are in an allowable region is important to recognize.

Considering the test setup utilizes a constant frame size, as metering speed increases then the amount of product in the frame at one time will increase. An increased amount of product means an increase in occlusion is possible. The tests displayed here had minimal effect on product flow CV due to occlusion. There may be a situation when the metering speed gets so high that the CV of product flow would approach zero and no longer improve because individual particles could no longer be distinguished from each other. At this point oversampling no longer follows the same trend (function of speed increase) because the amount of product-per-frame would appear constant in the raw data so the speed corrected data would have a negative trend with speed increase. Understanding at what point occlusion may begin to have a detrimental effect on product flow measurement via imaging techniques would be an interesting study to pursue for future work.

4.6 **Summary**

The study to evaluate and validate the continuous test method are broken up into three components; one is a test to establish the lower sampling limits, one to test the significance of the image frame height, and one to test for the combined effects of oversampling and occlusion. For the validation two of the most common agricultural materials, wheat and canola, were chosen to cover both ends of the spectrum for meter roller geometries used in this section. In the test to establish the lower sampling limits of the test method it was found that product should be imaged at or above a minimum rate defined by the frame-per-flute (fPFL) ratio. This ratio determines how fast a camera should capture images of the product flow coming off a meter roller with

respect to the roller speed. It is found that maintaining a constant fPFL ratio is not required but ensuring that product flow is never sampled below the minimum fPFL ratio is the most important conclusion out of this test. Below the minimum fPFL ratio the product flow signal is not accurately represented. Therefore, a minimum of 10 fPFL is recommended for wheat and 15 fPFL as the minimum for canola. However, it is possible to go as low as 6 fPFL if the speed of the camera is limiting.

The next test was to determine the significance of the frame height and whether it was more important to vary the frame height during processing to match the camera speed and ensure that each particle is imaged only once, or if it was acceptable to maintain one common frame size. The result confirmed that maintaining one frame size for all processing ensured the most consistent and repeatable data were captured, regardless of the camera rate. In fact, changing the frame size to match the camera rate meant that the CV of product flow would decrease as the frame size decreases for the same roller and product rate. Thus it is critical to maintain a constant frame height size across every roller to be tested and compared against each other when using the continuous test method.

Based on the test parameters confirmed in the first two components of the test method validation it was next important to determine the combined effects of oversampling and occlusion imposed by maintaining a constant frame height. A constant frame height means that there will be some particles being imaged more than once over consecutive images (oversampling) as camera rate increases (as a result of increasing meter roller speed and maintaining a constant fPFL ratio). It was determined that the rollers being utilized were not going to be operated in ranges where major or complete occlusion (particle overlap) will occur. Therefore it was important to verify that the small amount of occlusion happening and

oversampling were not affecting the signal representing the product flow coming off each roller. On a frame-by-frame basis the oversampling could be observed graphically but could easily be factored out by a correction factor ratio of the roller speed being compared. It is not necessary to use the correction factor but the correction factor does allow the user a method to quantify the amount of occlusion (or product overlap) occurring due to increasing meter roller speed. However, the small amount of occlusion measured was considered negligible so it was concluded that oversampling did not affect the overall product flow CV. A future topic of study regarding product area decrease with increasing meter roller speed (maximum limits of occlusion) may be of interest as it pertains to advancing the study of meter roller performance.

It was therefore concluded that when using the continuous test method to evaluate the performance of meter rollers, a frame-per-flute (fPFL) ratio must be set as roller speed is varied. The test must be operated no lower than a ratio 6 fPFL for wheat but is recommended to stay above 10 fPFL with no maximum fPFL ratio. There may be a maximum meter roller speed (not found in this study) in which a meter roller can be tested at to maintain a set fPFL ratio but aside from meter roller speed there is no maximum fPFL ratio. Additionally, canola can also be tested as low as 6 fPFL but is recommended to stay above 15 fPFL. Operation of the continuous test method also requires that the frame height captured by the camera of the product coming off the roller is a constant height throughout all tests to ensure consistent results across a range of roller speeds. Lastly, the oversampling that will occur because of increasing roller speed while imaging over a constant frame size has a very minimal effect of the product flow CV being used as the meter roller performance. Occlusion will have a very small effect in the range of roller speed being used in this study but this occlusion effect has no detrimental effect on product flow CV. A certain degree of occlusion becomes a function of the 2D imaging test setup utilized for the

continuous test method. The top end speed at which meter rollers can be tested with the continuous test method was not evaluated because it was out of the range of flow rates required for the intended tests.

With all components of the test method validation confirmed it is important to note a few things for future work. It will be very important to have a constant light source set in a light chamber that ensures the light is evenly distributed so there are no hot spots in the background to give the most consistent imaging characteristics. This becomes particularly important if meter roller performance was to be benchmarked and compared to a range of different designs using the continuous test method. The constant light source should be paired with a high speed camera that adjusts its frame rate to meet the required frame rate to achieve a consistent image for post processing no matter what product is tested. For the purpose of validating the test method it was acceptable to use different cameras for each component of the experiment as it was required. However, for future meter roller testing where the continuous test method is employed for meter roller performance evaluation then one camera with a constant light source should be used.

CHAPTER 5. EMPIRICAL MODEL DEVELOPMENT OF FLUTED METER ROLLERS WITH EXPERIMENTAL DATA COLLECTED USING THE CONTINUOUS TEST METHOD

The main goal of this chapter is to present the development of an empirical model for flow uniformity from fluted meter rollers. Little has been done in the literature regarding the definition of design parameters that make up the meter roller. The first half of Chapter 5 will go through and build a parameterized meter roller to be utilized for the design of a set of meter rollers that cover a wide variation of parameters. A set of meter rollers were then prototyped according to the design from the parameterized meter roller definition and tested using the continuous test method. The last half of Chapter 5 will explore the resulting data and look at how each parameter of the meter roller affects the meter roller performance. A statistical analysis and observation of the data will indicate what parameters are most significant for explaining meter roller performance. These parameters will form the basis for developing the general form of the model. The last portion of this chapter will end off with the determination of the model form and a proposed set of coefficients for the model.

5.1 **Meter Roller Performance**

It is known that a more evenly distributed particle flow can lead to the product being more evenly placed in the soil, and thus decreasing row-to-row variation during seeding as seen in Ess et al. (2004) and discussed in Mayerle (2006). The yield potential of individual seeds can be maximized if they are evenly separated rather than in clusters because there is less competition when growing to their full potential. However specific types of seeds (eg. corn and sunflowers) are more sensitive to this than others and there are many environmental factors that also play into the yield potential of a seed (Hagney, 2009). A study conducted at Purdue University presented in Ess et al. (2004) looked at the improved row-to-row accuracy between a fluted metering system and a belt metering system for soybeans. Soybean is a crop that can

achieve a yield increase with more precise placement. In Ess et al. (2004) the belt metering system did show higher row-to-row accuracy but it did not contribute to a yield increase as expected. It is important to note that the benefits go beyond a potential yield increase. A more accurate metering system means that the seeder/planter could be calibrated more accurately and translates into cost savings of up to $3.00 per acre for the producer allowing better control over what product they are buying and seeding as described in this study (Ess et al., 2004).

The test method and validation discussed in chapter 4 and developed for this study addressed some of the issues to improve seed resolution as well as other parameters that must be controlled when evaluating the performance of meter rollers, especially when switching to different products for evaluation of the same meter roller. Some of the benefits of increasing the performance of metering systems were discussed, hinting at the importance of decreasing the seed spacing variability in metering systems and how it applies to the end user.

Meter rollers have generally been categorized by the number of flutes on the periphery of the roller, the shape of the flute, and the angle of the flute (flute pitch). The number of flutes is by far the most widely used parameter of the meter roller which directly relate to the volume of product held by each flute. There has been little research on topics relating the different parameters of a meter roller with its performance aside from output versus speed relationships presented by Kessel (1985). Individually, most of the meter roller parameters have been introduced or discussed in past literature. Buckmaster et al. (2006) discussed some of the earliest seed-metering methods with a fluted wheel. Some of these early fluted wheels would be one standard size but would have an adjustable orifice that would open or cover up more flutes to adjust the metering rate while maintaining a constant roller speed (based on ground speed). Basnet et al. (2006) presented a detailed history of farming practices that included metering

systems with and without air. Again, fluted meter rollers (or rotary airlocks with air) are by far the most common practice but nothing more was discussed or referenced as to why certain systems were utilized other than they were easy to implement and control. Kessel (1985), Kim and Ryu (1998), Guler (2005), and Maleki et al. (2006a and 2006b) all started asking the questions as to why this generic fluted meter roller was so widely accepted, how accurate it was, and how the performance could be optimized in certain applications. Kim and Ryu (1998) specifically looked at the shape of the grooves (or flutes) on the roller and how changing the flute shape would affect the release of product. The shapes of the flutes were not sufficiently parameterized to fully characterize the design, but insight was given into how small changes in flute shape can affect product flow evenness.

5.2 **Meter Roller Parameterization**

Parameterizing a meter roller is an important aspect of this study both because it is required to empirically model the roller performance and it has never been done in literature to this extent. The generic parameters such as flute depth, flute width, and flute pitch are all commonly referred to in literature but how a roller design may be fully described by these parameters has not been defined. Defining the parameters in such a way that they can easily be varied to change characteristics of the meter roller and in turn be applied to model and optimize roller performance would be very beneficial for future development. This section will define the parameters required to numerically describe a meter roller, discuss the boundary conditions to be considered when designing a meter roller, and apply the parameters and boundary conditions to develop a 3D CAD (computer-aided design) template to design meter rollers. The 3D CAD template will then be applied to develop the prototype rollers to be used for primary testing of meter roller performance.

5.2.1 Meter Roller Parameters

In order for the performance of meter rollers to be modelled and evaluated, there are some parameters of the roller that must be considered in the design and defined for clarification. The conventional descriptions of meter roller parameters from literature are generic and interactions between them are not formally defined. For instance, flute width is defined as the opening between the ridges around the periphery of a roller, but how the flute width is related to flute depth, shape, pitch, roller diameter, and roller length is not defined. By specifically defining each parameter mathematically and understanding relationships with each other, a greater range of control can be had across the design of a meter roller.

Six parameters are suggested that affect the physical characteristics of the roller and can be used to design any size and shape of fluted roller with a few boundary conditions (Figure 5-1). The six parameters can further be grouped into two separate categories for clarity. The first category is the minor characteristic category containing the angle between the flute edges, β [rads], and fillet circle radius R_1 [mm]. The minor characteristics have a relatively small effect on the overall roller shape but are still important to the overall description. Both minor characteristics are shown in Figure 5-1 where the angular distance of the flute edges describes the width of each fin between flutes in reference to the angle it creates with the center of the roller. The second category is the major flute shape parameters that have a much more noticeable impact on the overall shape of the meter roller. These major flute shape parameters are the number of flutes, F, the fillet circle center distance, R_2 [mm], the fillet circle angular distance, φ [rads], and roller pitch θ_p [°] (shown in Figure 5-2). These six parameters geometrically describe the shape and profile of a meter roller. By using the angular distance parameters rather than the linear distances the design is effectively normalized with respect to roller diameter. By varying these parameters, the continuity of product flow off of the roller may be optimized by finding the

appropriate combination of values for each parameter. Four of the parameters that describe the roller, specifically the shape of each flute, are shown in Figure 5-1.

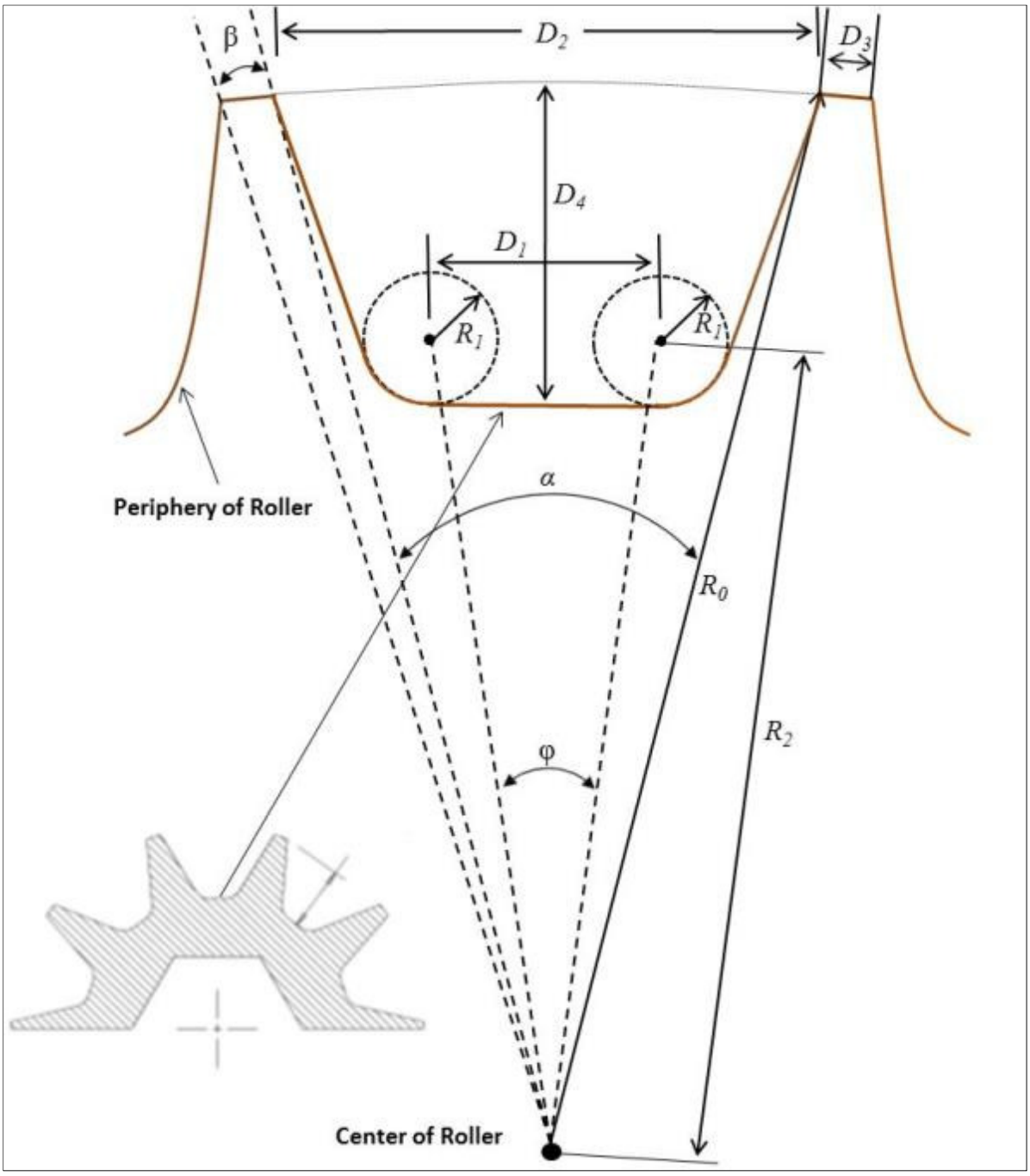

Figure 5-1: Schematic of a single flute of a roller showing angular distance of flute edges β, fillet circle angular distance φ, fillet radius R_1, and fillet circle center distance R_2 parameters of a meter roller.

The two minor parameters β and R_1 are the first characteristics to notice in Figure 5-1. The flute edge parameter, β, is a characteristic that will usually stay fairly constant in various meter roller shapes at this diameter. It is usually preferred to keep β relatively small to keep availability for the flute void to carry product. The fillet circle radius, R_1, is the second macro parameter that rarely makes a very noticeable change in typical meter roller dimensions. The value of R_1 depends on the shape of the flute profile desired and the flute shape is determined by the angular distance φ which falls into the main flute shape category. The actual dimensions of β and R_1 will be discussed further in the next section.

The fillet circle center distance, R_2, and fillet circle angular distance φ are the first two main flute shape parameters to notice in Figure 5-1. R_2 is closely related to flute depth (D_4 in Figure 5-1) which is the more common term referred to in industry when describing meter rollers characteristics. However, defining it as R_2, and relating it to φ, gives a lot more control over the overall flute shape as will be discussed in more detail in the next section about the parameter boundary conditions.

Other dimensions found in Figure 5-1 that relate to the main flute parameter shapes are the roller radius R_0, angular flute width α, distance between fillet circles D_1, flute width D_2, fin width D_3, and flute depth D_4. By defining these widths in angular terms, the design is normalized to the roller radius. The roller radius is one parameter that will be held constant for every roller evaluated as there is a size restriction in the metering assembly where it is placed, particularly as it pertains to the study state later. The angular flute width can be calculated from the number of flutes and the angular distance of the flute edge by the following equation.

$$\alpha = \frac{2\pi}{F} - \beta \qquad 5\text{-}1$$

Where α and β are in radians and F is the number of flutes.

The variables φ, α, and β (in radians) in angular form can be converted into linear form defined by D_1, D_2, and D_3 (in mm) respectively. The linear forms of the parameters are not necessary for the design of the roller here but will be useful in calculating the volume of seed that can be held in each flute. The linear forms of D_1 and D_2 are calculated from the geometry relationships of the imaginary triangles (not shown) present in the Figure 5-1 single flute profile and shown in equations 5-2 and 5-3.

$$D_1 = 2 * \left[R_2 \sin\left(\frac{\varphi}{2}\right) \right] \qquad 5\text{-}2$$

$$D_2 = 2 * \left[R_0 \sin\left(\frac{\alpha}{2}\right) \right] \qquad 5\text{-}3$$

Flute depth D_4 can be found from a simple relation between the radii R_1 and R_2 depending on the flute profile shape (straight flute or curved flute). These two profile shapes that define the flute depth are referred to as a straight flute ($\varphi > 0$ radians) and a curved flute ($\varphi = 0$ radians). Equation 5-4 and 5-5 respectively show both instances of calculating the flute depth.

$$D_4 = R_0 - \left(R_2 \cos\left(\frac{\varphi}{2}\right) - R_1 \right) \quad \text{, for } \varphi > 0 \text{ radians} \qquad 5\text{-}4$$

$$D_4 = R_0 - \left(R_2 - R_1\right) \quad \text{, for } \varphi = 0 \text{ radians} \qquad 5\text{-}5$$

The flute pitch, θ_F, and the number of flutes on a roller, F, are the last two parameters to be described. The flute pitch describes the number of degrees the profile of the roller is rotated over the length of the roller. For instance, in Figure 5-2, the front profile of the roller has twisted a specified amount by the time it reaches the entire length of the roller. The aim of the flute pitch is to have enough of an angle so that when one flute is done dumping, the next flute has started dumping, thus continually releasing product.

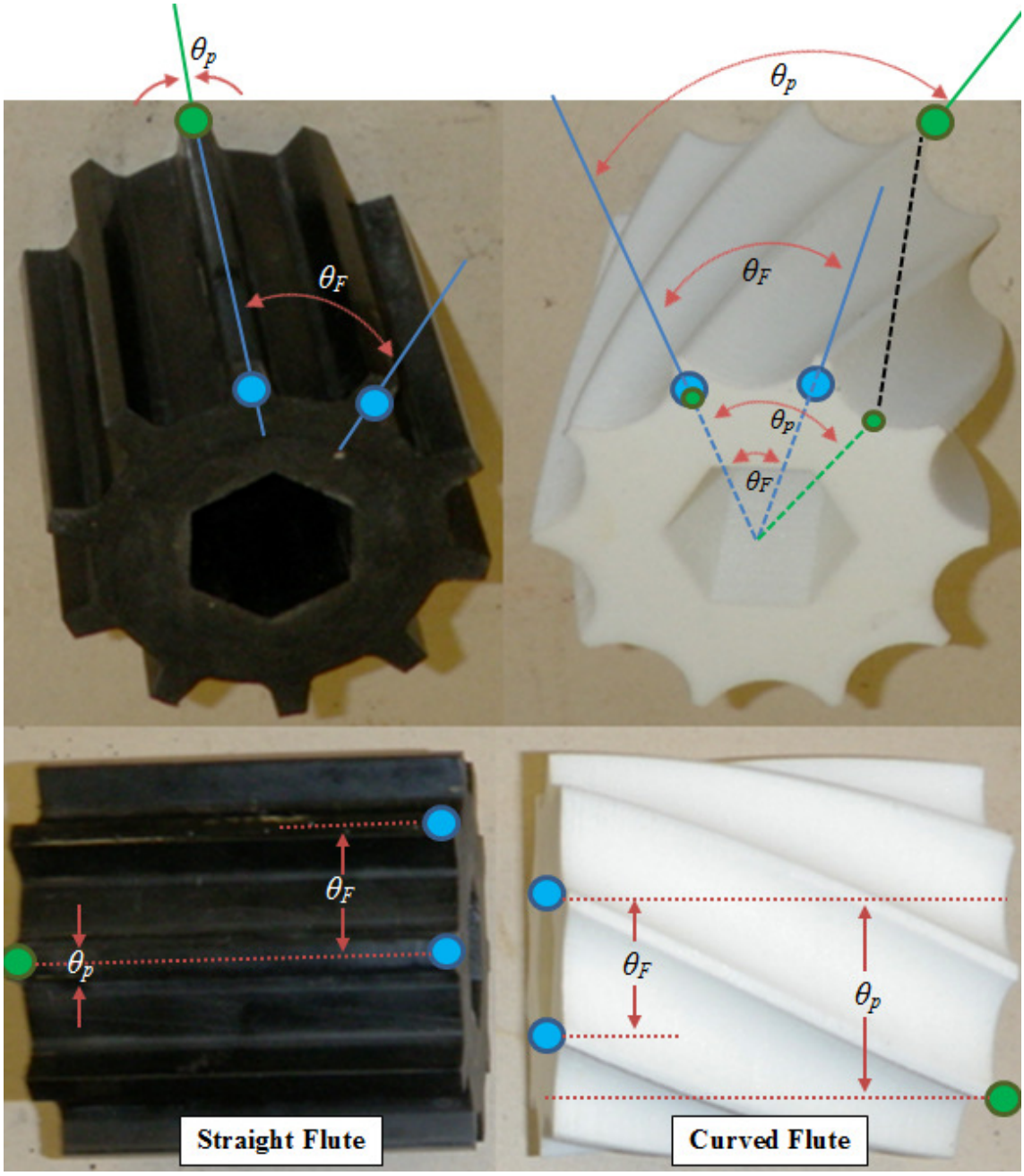

Figure 5-2: Meter roller comparison of a straight flute meter roller (left) vs a meter roller with a flute pitch (θ_p) of 54° (right) where θ_F defines the center-center angle between flute ridges (note: the front view is comparing the front face to the rear face (lines not drawn as 2D face), top view shows angular variables labelled as if they were linear measures, the color dots should match for each roller in both views).

In Figure 5-2, θ_F defines the center-center angle between the two ridges of a flute which will be constant around the periphery of the roller depending on the number of flutes. In this case a 10 flute roller would have a θ_F equal to 36° (0.63 radians) regardless of the flute pitch. The flute pitch is defined as θ_p for both rollers above. The straight flute roller would have a flute pitch of 0° and the curved flute roller shown has a pitch of 54°. The number of flutes will affect the flute pitch in each roller if at least one flute must be dumping at a time. Therefore adding more flutes will decrease the flute pitch to satisfy this condition. For instance, to satisfy the condition stated earlier where one flute should begin dumping product as the previous one is ending, the flute pitch for the 10 flute roller should equal the center-center angle between two flutes ($\theta_p = \theta_F$). Too large of a flute pitch may cause product and air flow problems as the flutes are unable to form a seal with the sides of the meter housing.

A better way to define flute pitch so that it is independent of roller length and the number of flutes is by defining a variable called pitch ratio (*PR*). The pitch ratio is a ratio of the flute pitch (θ_p) over the center-center angle between two ridges (θ_F).

$$PR = \frac{\theta_p}{\theta_F} \qquad 5\text{-}6$$

Where, θ_p, and, θ_F, are in radians. Pitch ratio (*PR*) will be the main variable to describe flute pitch when modelling the roller performance. The pitch ratio of the curved flute roller in Figure 5-2 for example, would then be 1.5 using equation 5-6.

5.2.2 Roller Parameter Boundary Conditions

Initially, the plan was to vary each parameter on three levels independently of each other. However, the number of rollers that could be developed for six parameters and three levels of each totalled 729 possible combinations. The six parameters were examined to estimate the importance of their contribution to the study and it was decided to minimize the levels tested on

two parameters, β and R_1, to one. Essentially, β and R_1 are being held constant in every combination of rollers tested, leaving a total of 81 combinations to be developed.

It was hypothesized that the effects caused by varying the angular fin width and fillet radius are much smaller than the other four parameters. Effects due to angular fin width β can be virtually cancelled out by increasing or decreasing the flute pitch on the roller. Currently, the fins are no wider than 5.8 mm and no smaller than 2.8 mm. Practically, narrower fins would have wear issues and thicker fins would be unnecessary on these rollers. Effects due to changes in the fillet radius R_1 are expected to be minimal because it is only changing a small characteristic of the roller and has no direct effect on the flute width and depth. The fillet radius (R_1) will then be held constant at 2.54 mm for all combinations where $\varphi > 0$. For all combination where φ is equal to zero, the fillet radius will be fitted so that it covers the designated flute width and depth as shown in equations 5-2 to 5-5, thus creating a curved profile. An example of this profile can be seen in Figure 5-3 where φ is equal to zero, leaving one fillet circle to fill the void creating a curved profile.

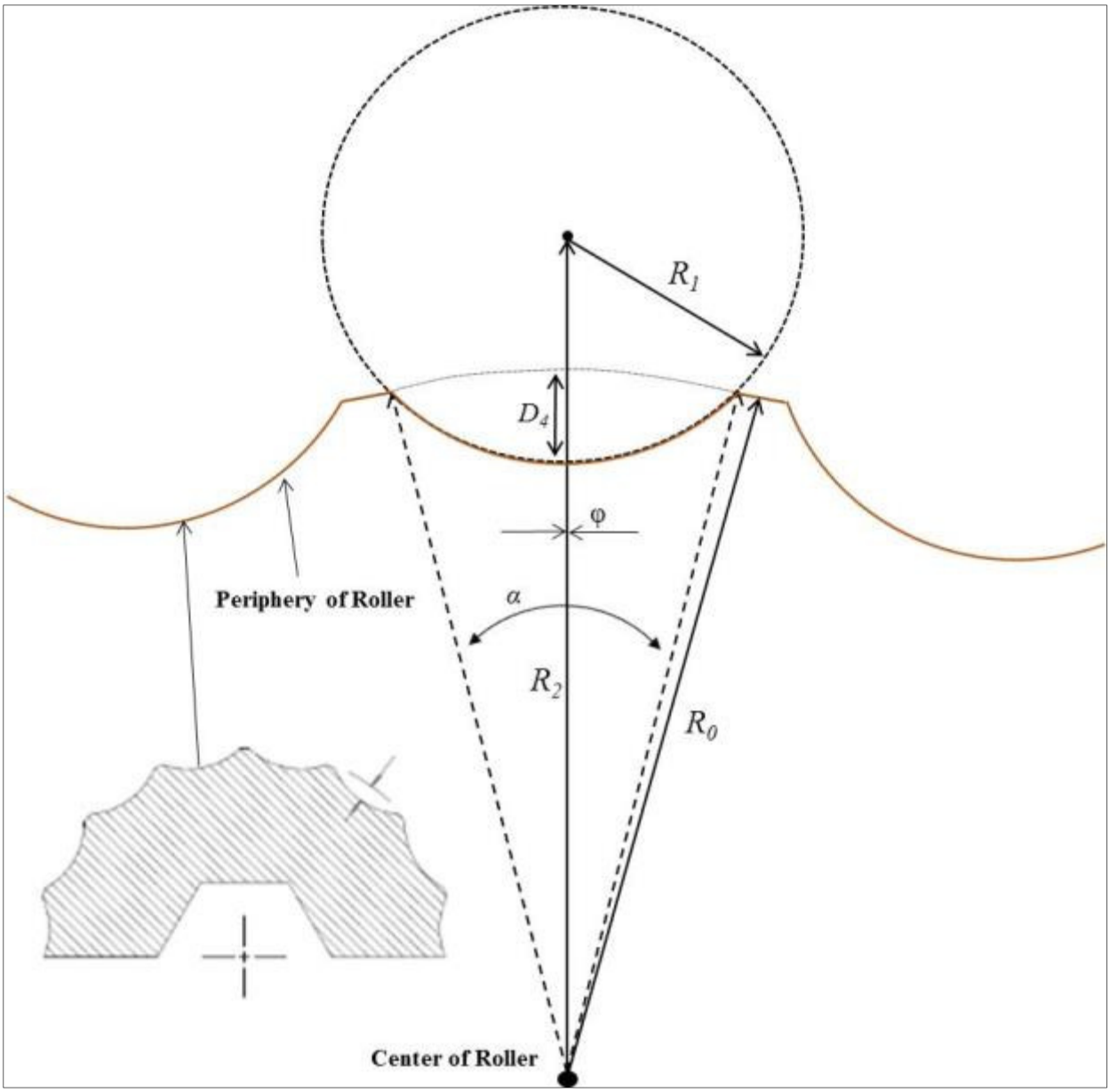

Figure 5-3: Curved profile created by one fillet circle when φ is equal to zero.

When the curved profile is forced onto the roller because φ is equal to zero, R_2 must be greater than or equal to R_0 to ensure that the walls of the flute do not start to form a cupped shape which would hinder an even release of product off the roller. Flute depth can still be calculated using equation 5-5 shown previously.

The number of flutes *F* is limited by the size of the product that can fit in the flute as well as the corresponding rate at which it must be metered. The more flutes on the periphery of a roller, the smaller each flute void becomes for a fixed roller diameter. The flute void may become so small that some products will not fit, thus causing damage to the product. Larger products also tend to be planted at a higher rate (mass/area); therefore the roller would have to be rotated at a much higher speed with smaller flutes. The high speed could potentially cause filling problems with the roller due to the critical roller speed (Kessel, 1985). Roller speed is obviously not physically related to the number of flutes on a roller, but it is related to the physical throughput of product flow metered by rollers. Therefore, roller speed acts as a boundary condition for each roller with different characteristics. The critical roller speed is this boundary condition that can be theoretically calculated for any meter roller design so it would be desired to operate any testing in the positive linear relationship zone (Figure 2-7). The critical roller speed would act as an upper limit for the meter rollers to be tested. A list of the critical roller speeds for each of the rollers used in this study can be found in Table A-2.

In the current meter systems used by agricultural manufacturers, specifically CNH Industrial, a roller with 15 flutes (*F*) has the largest number of flutes but it is mostly used for smaller seeds at typically lower seeding rates. Six flutes (*F*) is the smallest number on a roller and would primarily be used for fertilizers at very high rates or very large seeds such as peas. There are also two intermediate rollers with 10 flutes (*F*), each with differing volumes. Based on these three parameter settings on the current meter rollers, the three levels of the parameter *F* were evaluated at 6, 10, and 15 flutes. These levels allow for a wide range of products to be used and data to be gathered while keeping in mind that one of the goals is to minimize the number of rollers required to meter all products.

The angle created by the fillet circles (φ) directly affects the overall profile of the flute as well as the valley width in the bottom of the flute. The minimum value of φ will be zero radians, creating the curved profile illustrated in Figure 5-3. Each set of rollers with 6, 10, and 15 flutes will have a different maximum value of φ which correlates to a maximum linear distance D_1 between the centers of the fillet circles (in Figure 5-1 a maximum φ correlates to a maximum value of D_1). With a fillet radius R_1 already defined as 2.54 mm it was decided to set the maximum linear distance D_1 between the fillet circles at 5.08 mm. D_1 could be calculated by equation 5-2, but setting a specific range of linear fillet distances (D_1) was the best means of maintaining a constant flute profile. A maximum D_1 of 5.08 mm was chosen so the fillet circles did not overlap and to ensure the bottom width of the flute is sufficiently wide to fit most products. The actual values of φ vary while the linear distance is held constant because the rollers with different numbers of flutes will have their own value of R_2 while still having an angle of at least 10˚ on the flute wall. Because a 10˚ flute wall angle is a boundary condition of the flute dimension it will be referred to as FW_{min}. FW_{min} is an essential boundary condition when the minimum R_2 is being set for a specific flute. As R_2 is increased (flute depth decrease) and maximum D_1 (maximum φ) is maintained then the flute wall angle will begin to increase above the FW_{min}. The flute wall (FW) angle is measured at the moment dumping starts to occur so the angle must be measured relative to the center of the roller similar to what is shown in Figure 5-4. Using the same geometry relationships used to calculate the linear width of D_1 and D_2 for a flute, the maximum φ coordinate can be calculated by equation 5-7.

$$\varphi = 2 * \sin\left[\frac{D_1/2}{R_2}\right]^{-1} \qquad 5\text{-}7$$

Where φ is in radians, D_1 is equal to 5.08 mm, and R_2 is equal to R_{2min} in mm from Table 5-1 corresponding to the flutes on the roller.

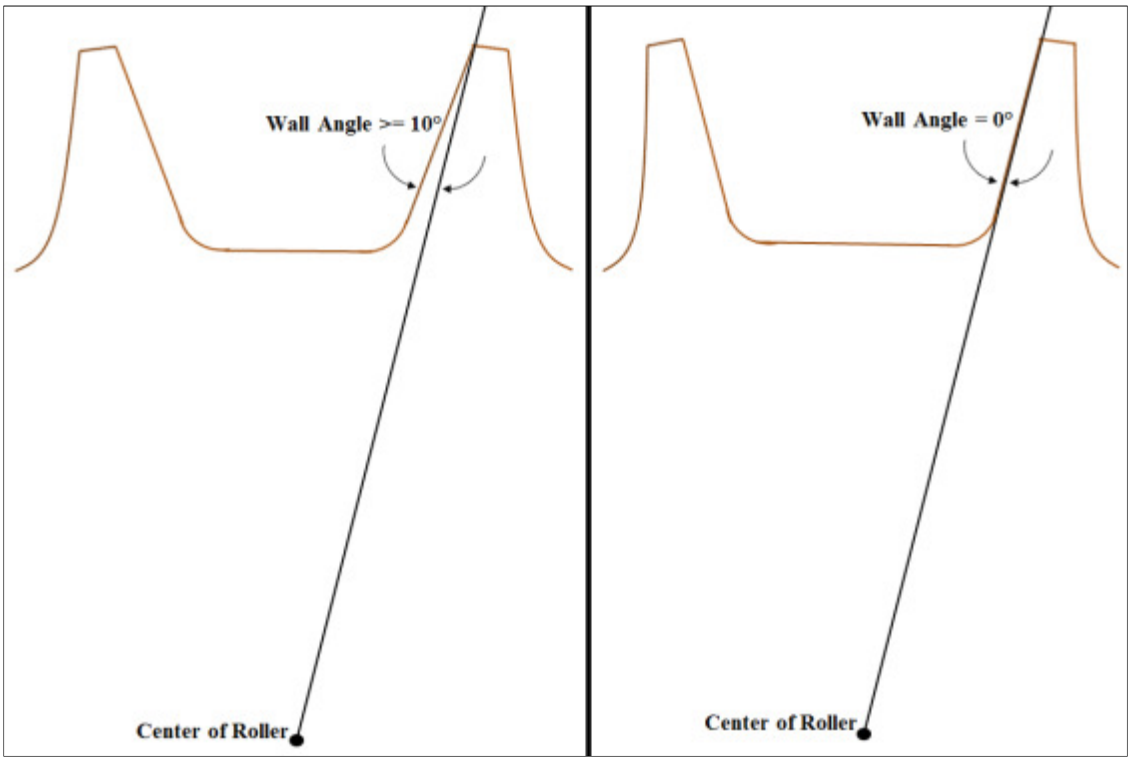

Figure 5-4: Schematic of a flute profile showing the flute wall angle.

The number of flutes on a roller directly affects the maximum flute depth, thus affecting the maximum angular distance between the fillet circles, φ_{max}. An angle of 0˚ on the flute wall refers to a straight vertical wall. Maintaining an angle of at least 10˚ will ensure that the product will not be scooped at any point causing recirculation of product. It is also the minimum wall

angle used in the current rollers. The middle value will be some value halfway between zero and φ_{max}.

The center distance to the fillet circles R_2 (referring to Figure 5-1 and Figure 5-3) ultimately define the depth of the flute, the lowest value of R_2 corresponding to the largest flute depth. The limits of this parameter must allow for all products to safely be metered while maintaining 3 levels of the parameter for a wide range of observation data. Currently, the minimum flute depth utilized is about 2.7 mm on the extra-fine roller. However, 2.7 mm is too small of a flute depth to safely meter peas which have a seed diameter of anywhere between 6.03 to 7.49 mm (Borowska et. al, 1996). Therefore, knowing that the flute depth of the fine meter roller (7.87 mm) is large enough to safely meter peas, this depth will be used to find the maximum R_2 value from equation 5-4.

With R_0 equal to 39.37 mm and R_1 equal to 2.54 mm, the maximum R_2 value will be 34.05 mm. The minimum R_2 value is specific to each set of rollers with different number of flutes, much like the parameter φ. The minimum R_2 value, or maximum flute depth, is found from the physical dimensions of the roller template drawings. It is found where a minimum flute wall angle of 10˚ and a maximum fillet circle distance (D_1) of 5.08 mm can simultaneously be achieved (maximum. and minimum values discussed previously). Because these two conditions could not be achieved, the R_2 limits for a 15-flute roller in Table 5-1 is different than that of the 6 and 10-flute rollers. Because the minimum and maximum R_2 value had to be decreased for a 15-flute roller, the flute depth of the roller is essentially decreased (5.83 mm by eqn. 5-4) which means that larger diameter product like field peas could not be metered by the 15-flute rollers. Initially it was thought that a minimum R_2 should be chosen to create a flute depth similar to the maximum flute depth on the current coarse meter roller of 16.35 mm (R_2 of 29.94 mm). It was

also found in the template drawings of the rollers that it was physically impossible to reach this value of R_2 for the 15-flute rollers. Thus, the condition of a minimum flute wall angle and a maximum linear distance between fillet circles (D_1) was used to define a minimum R_2 for each roller. The mid-range value comes from the average of the maximum and minimum value of R_2 as shown in Table 5-1. The values of R_2 for the rollers tested are from the 3D roller template model, but the mathematical value of R_2 for both scenarios when φ is equal to zero and when φ is greater than zero are shown in equations 5-8 and 5-9.

$$R_2 = R_0 + \left(R_1 - D_4\right) \text{ , for } \varphi = 0 \text{ radians} \qquad 5\text{-}8$$

$$R_2 = \frac{R_0 - \left(D_4 - R_1\right)}{\cos\left(\frac{\varphi}{2}\right)} \text{ , for } \varphi > 0 \text{ radians} \qquad 5\text{-}9$$

The mathematical expressions for R_2 in both scenarios of φ are just rearranged versions of equations 5-4 and 5-5 shown previously.

All six of the parameters discussed in this section plus the roller radius, R_0, and the range of variation to be applied in testing are summarized in Table 5-1

Table 5-1: Levels and range of variation for meter roller parameters.

Parameter	Description	Levels of Variation	Range of Variation
R_0 (mm)	Roller Radius	1, constant	39.37
F	Number of Flutes	3, {min, intermediate, max}	{6, 10, 15}
θ_p (°)	Flute Pitch	3, {0, θ_{max}/1.5, θ_{max}}	F=6, {0, 60, 90} F=10, {0, 36, 54} F=15, {0, 24, 36}
R_1 (mm)	Fillet Radius	2, forced constants	2.54 if φ>0,defined by largest inscribed circle if φ=0
R_2 (mm)	Center Distance to Fillet	3, {R_{2min}, (R_{2min}+R_{2max})/2, R_{2max}}	F=6, {19.92, 26.98, 34.05} F=10, {27.80, 30.92, 34.05} F=15, {35.08, 35.58, 36.08}
φ (rads)	Angular Distance of Fillets	3, {0, φ_{max}/2, φ_{max}}	F=6, {0, 0.1267, 0.2557} F=10, {0, 0.0915, 0.1831} F=15, {0, 0.0724, 0.1449}
β (rads)	Angular Fin Width	1, constant	0.07117

The range of each parameter in Table 5-1 will be necessary for both designing prototype meter rollers and determining meter roller speeds for testing to achieve the desired application rate. Meter roller speed was discussed in this section as a parameter to consider when designing a roller but it was not listed as a parameter to be varied because the speed will be determined based on the volume of the flutes after the above design parameters have been applied.

5.2.3 Roller 3D Model Template

Applying the parameters defined in the previous section and outlined in Table 5-1 to develop a practical tool for easy design and modification of the meter rollers to be prototyped for testing will be discussed in this section. Other benefits of the design tool such as its use as an analysis aid and an interactive way to visualize the rollers as parameters are altered will be discussed.

The 3D CAD package used for the meter roller design was SolidWorks (Dassault Systems, France). Based off of the four current meter roller designs from CNH Industrial and the

flute parameterization sketches in Figure 5-1 and Figure 5-3 a design template was developed. Details of the meter roller design template can be found in Appendix A.

A total of 81 individual meter rollers were developed by varying the design parameters as outlined in Table 5-1. A common nomenclature was used to distinguish each roller. Roller names were based on the four varying parameters forming the basis for written and symbolic identification codes. For instance, a 10-flute roller with the lowest center distance to the fillets (R_2), a maximum angular distance of the fillets (φ), and a 36° flute pitch (θ_p) would have the name 10F_minR2_maxPHI_36deg. The corresponding label scribed on this meter roller can be seen in Figure 5-5. In the labelling scribed on the roller there is no indication of the flute pitch other than a visual examination of the roller to observe the three variations of pitch on the flutes.

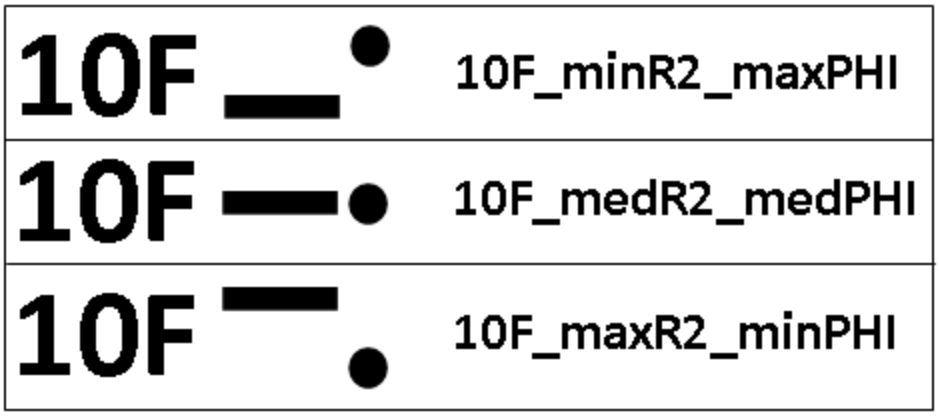

Figure 5-5: Meter roller labelling nomenclature for 10 flute rollers.

The complete list of rollers to be designed and tested can be found in Table A-1 in Appendix A. Included in this list are the roller speeds and fPFL that were tested.

With the rollers designed in SolidWorks, the software was used to gather useful information about each roller. Because the main purpose of meter rollers is to dispense precise amounts of product, knowing the volume of the flutes will be beneficial in determining the roller

speed to test at in order to maintain a constant metering rate with each roller. Determining the volume of each flute is a very easy process in SolidWorks. The cross-sectional area of the flute profile can be exported then the area can be multiplied by the roller length (80.5 mm) to get the flute volumes displayed in Table 5-2.

Table 5-2: Individual flute volumes of the meter rollers to be tested.

Flutes	**Flute Volume (mm^3)**			
	R2 Level	**PHI (φ)**		
		min	**med**	**max**
6F	min	40,155	38,443	40,509
	med	30,559	26,714	28,459
	max	14,971	14,822	15,700
10F	min	16,482	15,418	16,920
	med	13,550	11,991	13,273
	max	9,632	8,557	9,527
15F	min	5,481	5,144	5,964
	med	5,077	4,745	5,515
	max	4,653	4,347	5,065

It should be noted that there are only 27 flute volumes listed in Table 5-2 because flute pitch is not incorporated in the table as the flute volume remains constant as the pitch changes. As parameter R_2 goes from minimum to its maximum level the flute volume decreases because R_2 is the measure from the center of the roller to the center of the fillets so it essentially has an inverse relationship with the flute depth. As flute depth increases the R_2 parameter decreases. Parameter φ has a slightly different and inconsistent relationship as it goes from the minimum (φ=0) to the maximum level. The medium level of φ consistently has the lowest volume, but the minimum and maximum φ level is consistently the highest volume. Specifically, the minimum φ

parameter defines the curved flute profile which has slightly more variability as R_2 and the number of flutes change.

5.3 **Experimental Apparatus Design and Procedure Development**

The test setup developed for testing and evaluating the meter roller performance is a modified version of the air cart simulator used for validating the test method in Chapter 4. The air cart simulator test stand presented in Figure 5-6 was automated by integrating the meter roller control of the main setup with the imaging system and DAQ/control system together via LabVIEW through a computer. The equipment utilized in the air cart simulator test stand can be found in Table 5-3.

Table 5-3: List of equipment for meter roller performance experimental setup.

Main Setup (Air Cart Simulator)	1 Product Tank 2 Metering Assembly 3 Meter Roller 4 Meter Drive 5 Product Catchment System
Imaging Setup	6 Camera (Allied Vision Prosilica GE680) 7 Back-lighting source box
Data Acquisition System (DAQ) and Control	8 Computer and LabVIEW8.6 9 NI cDAQ-9172 Chassis 10 NI 9402 Digital I/O Module 11 DC Power Supplies (1 HP 6215A & 1 HP 6218A) 12 Precision Balance (A&D GX-1000) 13 Servo Motor (HS-322HD)/Hopper System

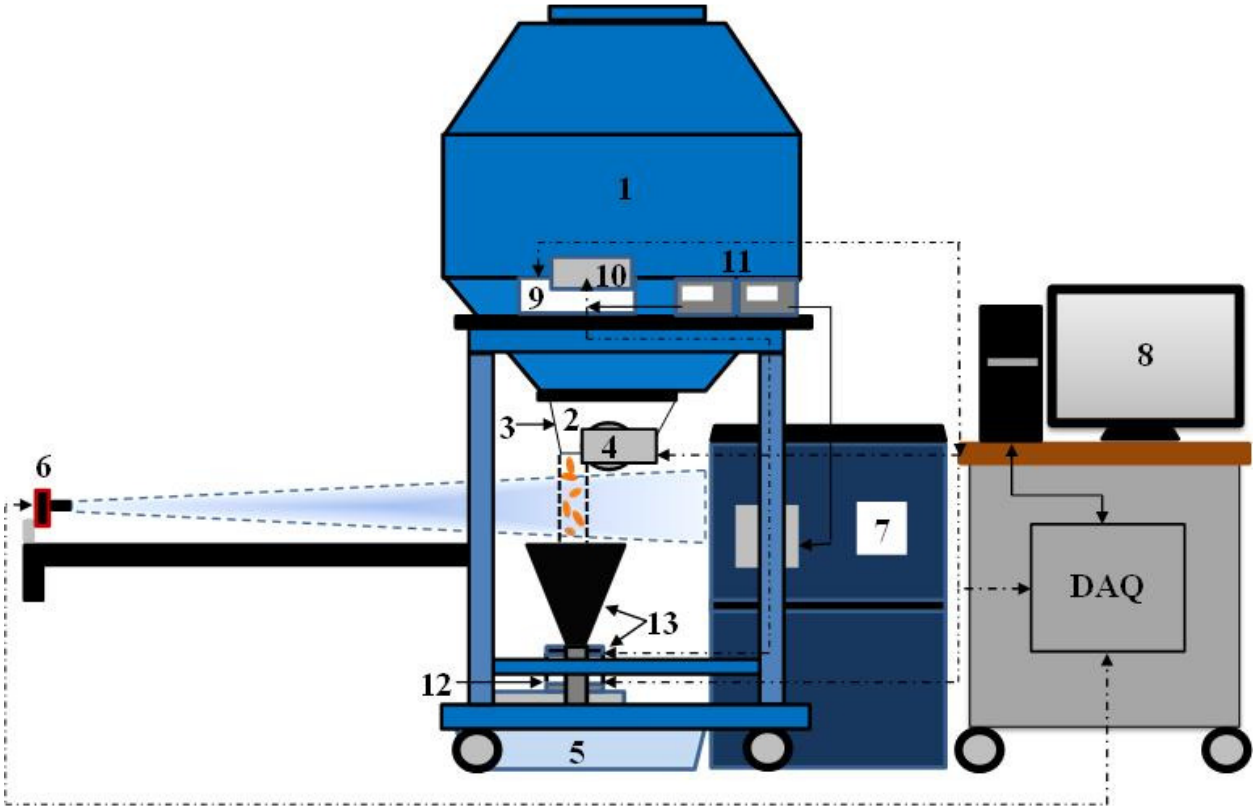

Figure 5-6: Experimental setup configuration.

A detailed step-by-step standard operating test procedure is given in Appendix B. To summarize the detailed test procedure, Figure 5-7 shows a flow chart overview of the operations that the experimental setup is required to pass through.

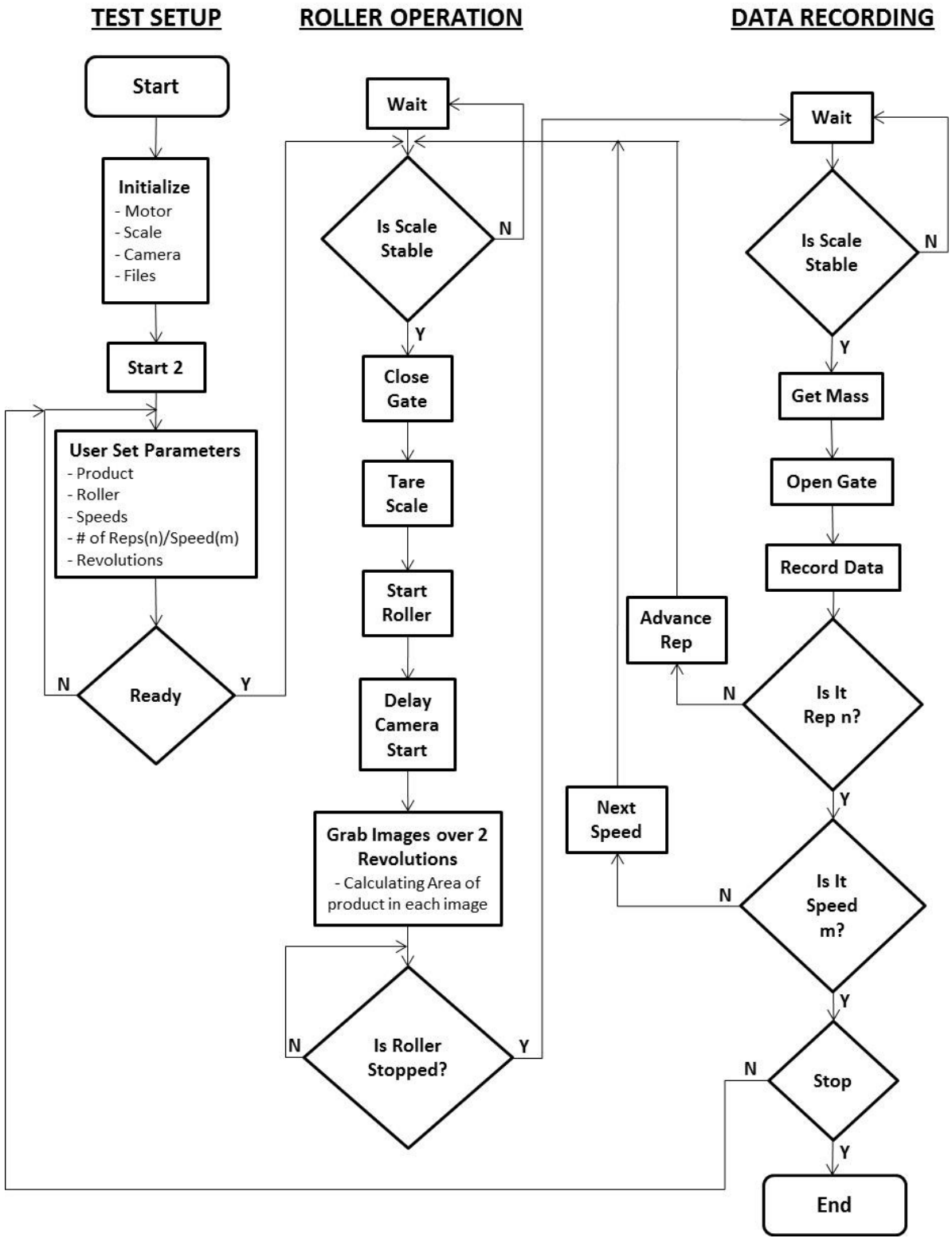

Figure 5-7: Flow chart of the LabVIEW program for the seed flow monitoring test setup.

In referring to Figure 5-7 the test procedure can generally be broken down into three categories; test setup, roller operation, and data recording. In the test setup a number of checks are first made to ensure all the instruments are connected and communicating with each other. When that passes there is a number of user-defined variables that need to be set to match the product and meter roller to be tested. The most critical variables are the type of roller, fPFL ratio, and roller speeds to be tested at because this determines what camera rate to collect data. Other variables such as the number of reps, number of revolutions to complete, and the type of product are not going to change the data being collected as they are used in labelling the output files. Taking the time to set the user parameters is the most important step because everything after this step is automated.

Once the test setup is finished the system moves into roller operation. A series of steps are required with set time delays and checks ensuring that the previous operation is completed. For instance, the roller does not start rotating until the scale has tare, then the camera will have a slight delay after the meter roller starts so that there are no data recording partial flow coming out of the roller. In this test procedure the standard number of revolutions was set at two so as to stay under the limit of the precision balance. As the camera is imaging over the two revolutions it is sending each image through the image analysis software tool in LabVIEW where the area of product in each image is calculated and stored in a buffer file. Once the roller has stopped then the data recording stage begins.

Data recording is pretty self-explanatory but it does occur in a separate step after the test has stopped so as to maximize computer resources for each step. The image data would immediately be sent to a spreadsheet to be saved with the user parameters entered at the beginning. As well, the image data are sent through some basic statistical calculations. If

multiple repetitions or roller speeds are requested by the user at the beginning during ‘test setup’, there is another series of logic operations to cycle through before the test operation stops. At this point the user can either add a new set of parameters or hit “End” to replace the meter roller or product to be tested.

5.4 **Results and Analysis**

Four complete repetitions of data were collected for every meter roller according to the experimental procedure. Repetitions 1 and 2 were done together first and then repetitions 3 and 4 were done together at a later date because of the time required and logistics of running the tests. These data were analyzed using the R statistical package (R Development Core Team, 2012) to check for outliers, check for homogeneity of the variance between tests, and test whether the data were normally distributed. This initial examination was a check of the data to ensure they were acceptable to use an analysis of variance (ANOVA) using a general linear model to evaluate the data further.

Examination of the data showed that results were consistent between replicates for each roller. Meter roller 15F_medR2_medPHI_24deg was chosen as a representative example. Figure 5-8 shows how the data are spread across each of the four repetitions. The response variable in Figure 5-8 is the percent area of the product occupying each image.

Figure 5-8 is a blocked box and whisker plot showing the three different tests split up as determined by the three different roller speeds to be tested within each repetition of the 15F_medR2_medPHI_24deg roller. There are 3 clusters in each repetition because they are grouped together at three different speeds. As roller speed increases the amount of product in each cluster increases as was discussed in chapter 4.

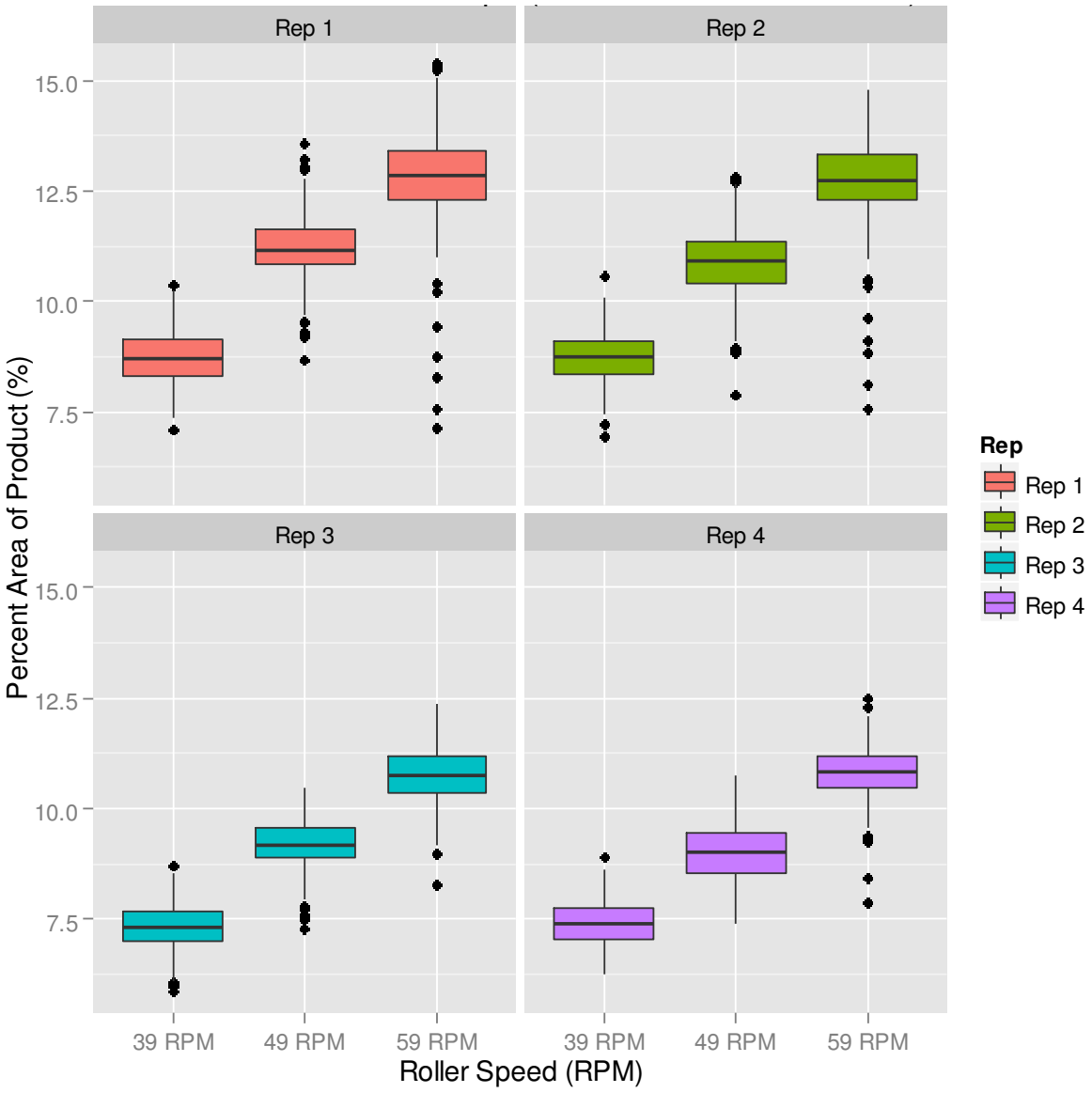

Figure 5-8: Visual check for homogeneity of the data between repetitions (15F_medR2_medPHI_24deg shown).

All of the rollers tested showed very similar trends to that observed in Figure 5-8. It is quite clear from Figure 5-8 that the data are homogeneous as the variance in each repetition is almost identical. This is an important check because repetitions 3 and 4 were collected eight months after repetition 1 and 2 then combined together. Because a strict testing protocol was followed it was assumed that variance in the data would be relatively consistent. The

homogeneity of the data can be viewed in Figure 5-8 and was further tested with a Levene (NIST/SEMATECH, 2012) test. A Levene test will evaluate if the variances are equal (null hypothesis), and if the p-value is less than the significance level of 0.05 the null hypothesis would be rejected. The Levene test computed in R (R development Core Team, 2012) revealed a p-value of 0.3004, so it was concluded that the entire dataset (repetitions 1, 2, 3, and 4) had equal variances which satisfied one of the main assumptions to be able to apply an ANOVA on the data. The output of the Levene test can be found in Appendix C.

The next evaluation was to perform an ANOVA on the total data set to ensure there were no significant differences between the means of each repetition. ANOVA was used in conjunction with a Tukey HSD (honest significant difference) function in R. The Tukey HSD test has a null hypothesis that all means tested are from the same population and if the p-value statistic is less than 0.05 (95% confidence interval) then the null hypothesis would be rejected. The graphical representation of the Tukey HSD test can be seen in Figure 5-9 with the test statistics displayed in Table 5-4. The four repetitions are labelled Wheat1 to Wheat4 in the figure.

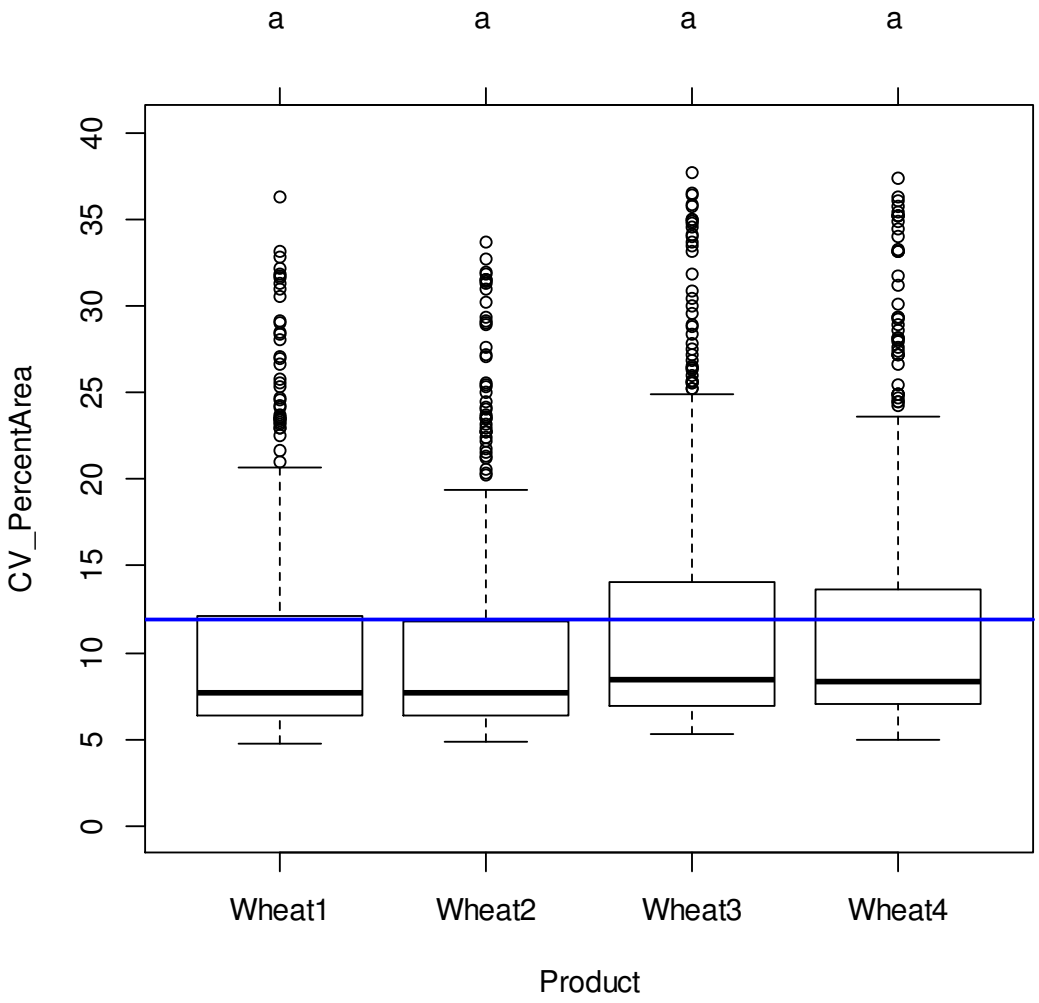

Figure 5-9: Tukey HSD test results on meter roller data showing the overall mean of the data (blue line), the median of the data in each rep, and the outliers of each repetition (Wheat1-4) that correlate to all the zero pitch rollers.

Each of the four repetitions is labelled along the x-axis with the CV of the percent area of product flow variation on the y-axis. Each repetition has a scatter of data points above the upper extremes that correlate to the zero pitch ratio rollers. These data points are not true outliers but extreme points of the data set that need to be considered in the final model. The median of each repetition is displayed in each box and the mean (11.92%) of the entire data set is represented by the blue line. Overall, Figure 5-9 shows that each repetition has relatively the same spread of data with repetition 3 and 4 having a slightly higher median. If the slight difference between each

repetition is significant it will show up in the Tukey HSD test which is doing a pairwise comparison between each of the population means. The test statistics are shown in Table 5-4.

Table 5-4: Test statistic output from the ANOVA with Tukey HSD comparison.

Mean Comparison	Estimate	Std. Error	t-value	Pr(>|t|)
Wheat2 - Wheat1 == 0	-0.12	0.74	-0.16	0.999
Wheat3 - Wheat1 == 0	1.39	0.74	1.88	0.238
Wheat4 - Wheat1 == 0	1.44	0.74	1.95	0.210
Wheat3 - Wheat2 == 0	1.51	0.74	2.04	0.175
Wheat4 - Wheat2 == 0	1.56	0.74	2.11	0.152
Wheat4 - Wheat3 == 0	0.05	0.74	0.07	1.000

The important value to take away form Table 5-4 is the Pr(>|t|) value (p-value) of each mean comparison. As stated earlier, the null hypothesis being tested was that the differences between the means are not significantly different from each other. Because each p-value was greater than 0.05 for each pairwise comparison the null hypothesis was accepted and it was established that further analysis could proceed using a general linear model approach.

A general linear model (glm) was used to explore the relationship between the product flow CV, the response variable, and the five explanatory variables: F, PR, R_2, PHI and meter roller speed. The main intent of using the glm was to give insight into the explanatory power of each variable and whether the variable was significant enough to keep in the model using the entire dataset from all four repetitions. The output of the complete glm with all five design parameters included can be seen in Table 5-5.

Table 5-5: Results of the summary for the general linear model with wheat at a 95% level of confidence.

GLM Summary (model_Wheat1234)				
	Estimate	**Std Error**	**t value**	**Pr(>|t|)**
(Intercept)	31.419196	1.067568	29.431	< 2.00E-16
Pitch_AL_per_FW	-9.282614	0.242588	-38.265	< 2.00E-16
Num_Flutes	-0.613451	0.058329	-10.517	< 2.00E-16
Speed_RPM	-0.145087	0.021838	-6.644	5.09E-11
PHI_rads	1.789298	1.849681	0.967	0.334
***R2*_mm**	-0.004118	0.052033	0.079	0.937

The most important value to pay attention to in Table 5-5 is the Pr(>|t|) value. This gives insight into the significance of that variable to the overall model and a Pr(>|t|) > 0.05 would suggest that the variable is insignificant to the model. The smaller the value the more explanatory power it has. From the overall glm summary the output shows that pitch ratio (Pitch_AL_per_FW), the number of flutes (Num_Flutes), and meter roller speed (Speed_RPM) have significant explanatory power to the overall model, but R_2 (R2_mm) and PHI (PHI_rads) have the lowest significance. The glm also suggests the number of flutes and the pitch ratio carry the highest explanation of the response. To quantify the design parameter significance further and the exact order each variable would be ranked and an individual glm was completed for each design parameter. Each individual glm would then be compared to the total glm (glm containing all 5 design parameters) via an ANOVA. From the results in Table 5-6 the residual deviance can be compared for each design parameter glm versus the total glm (model_Wheat1234). The lowest residual deviance from the total glm is the design parameter with the highest explanatory power.

Table 5-6: Results of the ANOVA for the GLM's of each parameter versus the summary model GLM of wheat (CV is the response variable) at a 95% level of confidence showing the explanatory variable order of significance.

Model	Explanatory Var.	DoF	Resid. Dev	Deviance	F	Pr(>F)
model_Wheat1234	all parameters (+)	966	21489			
model4_Pitch	Pitch_AL_per_FW	970	32673	-11184	125.7	2.2E-16
model1_Flutes	Num_Flutes	970	55612	-34124	383.5	2.2E-16
model5_Speed	Speed_RPM	970	57545	-36056	405.22	2.2E-16
model2_R2	R2_mm	970	58044	-36555	410.82	2.2E-16
model3_PHI	PHI_rads	970	64313	-42824	481.28	2.2E-16

The results of the ANOVA for each glm shows that pitch ratio (model4_Pitch) is the highest ranked explanatory variable with the number of flutes F (model1_Flutes), roller speed (model5_Speed), and flute depth R_2 (model2_R2) as the next most significant. The flute profile shape PHI (model3_PHI) and R_2 (model2_R2) came in as the lowest ranked explanatory variables as was expected from the total glm shown in Table 5-5. The data in Table 5-5 suggest that R_2 should have the lowest explanatory power. Therefore, from the results in Table 5-5 and Table 5-6 it is safe to conclude that R_2 and PHI are both insignificant to the model. Both of these insignificant parameters cannot be removed from further models yet until the data are viewed. The form of the general linear models can be found in appendix C.

This statistical analysis has verified the relative significance that each design parameter has in estimating the response variable which is the variation of the product flow. The pitch ratio (PR) appears to have the greatest effect on the overall statistical model with the next four parameters F, roller speed, R_2, and PHI coming next in the order of explanatory power. It is important to look at each parameter individually and view the observed trends and statistical significance closer as they relate to the overall glm and potential benefit to an empirical model of the meter roller. The glm summaries of each design parameter versus the variation in product flow evenness can be found in appendix C.

5.4.1.1 Pitch Ratio (*PR*)

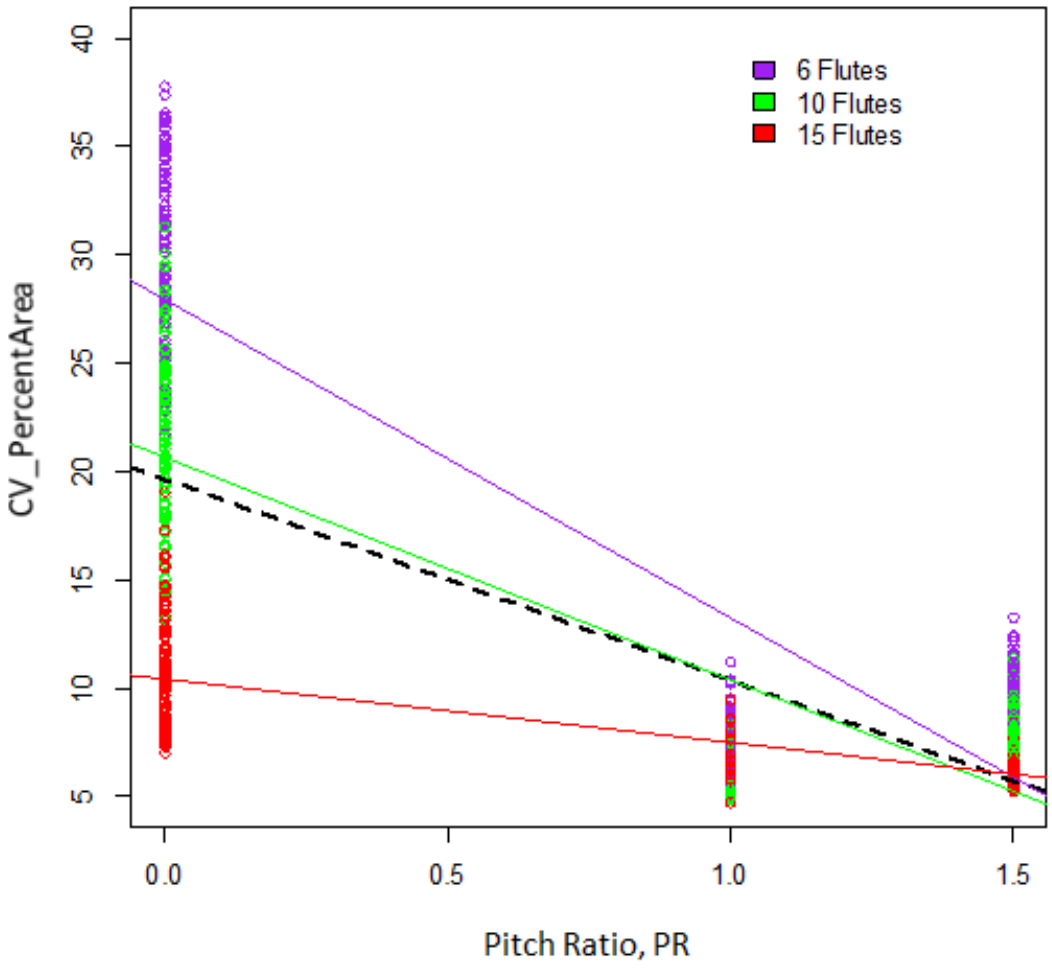

Figure 5-10: Variation of product flow (CV_PercentArea) versus pitch ratio (PR) showing the general linear trend as pitch ratio is increased as well as the total linear trend of the 6, 10, and 15 flute roller data combined together.

Figure 5-10 shows how the pitch ratio affects the product flow evenness with linear trend lines displayed on the graph color-coordinated with the number of flutes and also a dashed trend line showing the combined linear trend. The first trend apparent is an improvement in product flow evenness as the pitch ratio increases, with a larger improvement noticed on rollers with a lower number of flutes. This does make sense because rollers with a lower number of flutes typically move a larger amount of product per revolution so there is a higher chance to see

pulsating flow off the roller when the flutes are straight (i.e. PR = 0). The 15 flute roller, having anywhere from one third to one eighth the volume of a 6-flute roller, appears to remain almost level showing a minimal improvement in product flow evenness. In observing these trends it was apparent that the underlying trend may be non-linear where there is a fairly large improvement in product flow evenness (decrease in CV) up to a pitch ratio of 1 but some of that improvement is lost as the pitch ratio continues to increase. It was anticipated that the flow evenness would increase up to a pitch ratio of about 1 but the non-linear effect above a PR of 1 was something not expected when setting out to test and establish relationships between design parameters and meter roller performance. Because the total glm (Table 5-5) and the ANOVA comparison of the total and individual glm residuals (Table 5-6) both conclude that pitch ratio has the most significance to the response it is important to focus on and understand the relationship further.

Based on Figure 5-10 product flow CV appears to approach a minimum at a PR level within the range investigated. However, given the apparent non-linear trend and only three PR values investigated, there were not enough PR levels to anticipate exactly where that minimum may occur. As Figure 5-10 shows, a PR of 1 appears to be the minimum but that cannot be concluded with confidence. At this point it was decided to test a small set of rollers at a range of pitch ratios to fill in the gap between 0 and 1 to understand the shape of the correlation and make a better judgement. The point of the testing was not to test the full set of rollers but rather select a small set that would be representative. In doing so one must consider what design parameters are most critical. Given previous analysis showing that the number of flutes (F), meter roller speed, and pitch ratio were most significant, while R_2 and PHI contribute little to the overall effect, it was decided to choose a set of rollers where R_2 and PHI were held constant and only the most significant parameters were varied. The base roller chosen had a medR2_medPHI parameter at

the three different flute numbers and the three previous pitch ratios (0, 1, and 1.5) as well as the four new pitch ratios (0.125, 0.25, 0.5, and 0.75) to fill the gap in the data. Therefore, 12 new extra pitch rollers were designed and prototyped to be tested alongside the previous 9 rollers at the three levels of required meter roller speeds used during the primary testing. The extra pitch rollers were all tested according to the standard operating procedure to ensure comparable data over four repetitions giving a total of 252 additional data points. The results of the extra pitch roller testing can be observed in Figure 5-11.

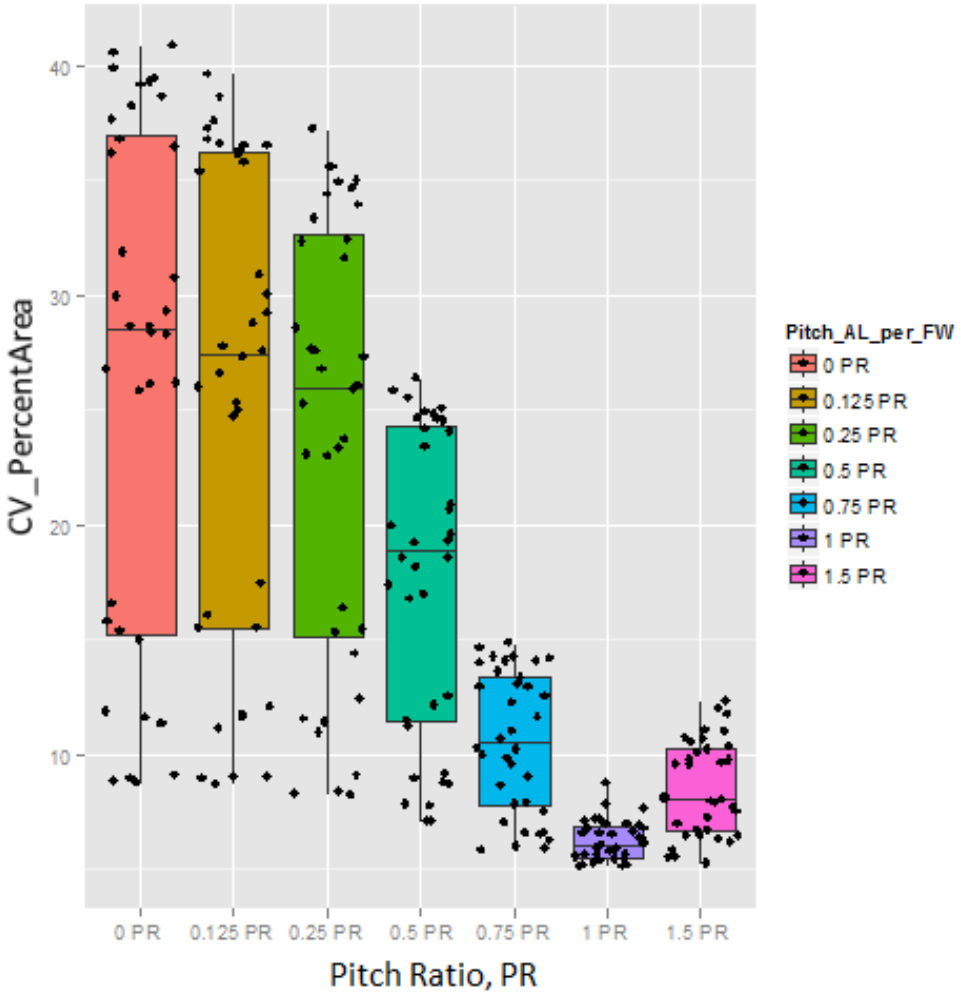

Figure 5-11: Results of the extra pitch rollers tested to fill the missing gap between 0 and 1 pitch ratio. Note that the x-axis is categorical and therefore not scaled by PR value.

Figure 5-11 shows how the product flow evenness varies with pitch ratio for all the extra pitch rollers. It is clear that the product flow CV does decrease as PR increases, at least up to around PR=1. The extra pitch roller data also give better insight as to how quickly the product flow CV decreases as a function of pitch ratio.

5.4.1.2 Number of Flutes (*F*)

Figure 5-12 shows how the product flow evenness varies with the number of flutes on a meter roller. It is important to note that the repetitions of roller data displayed are from all of the rollers but Figure 5-12 only examines the effect of the number of flutes.

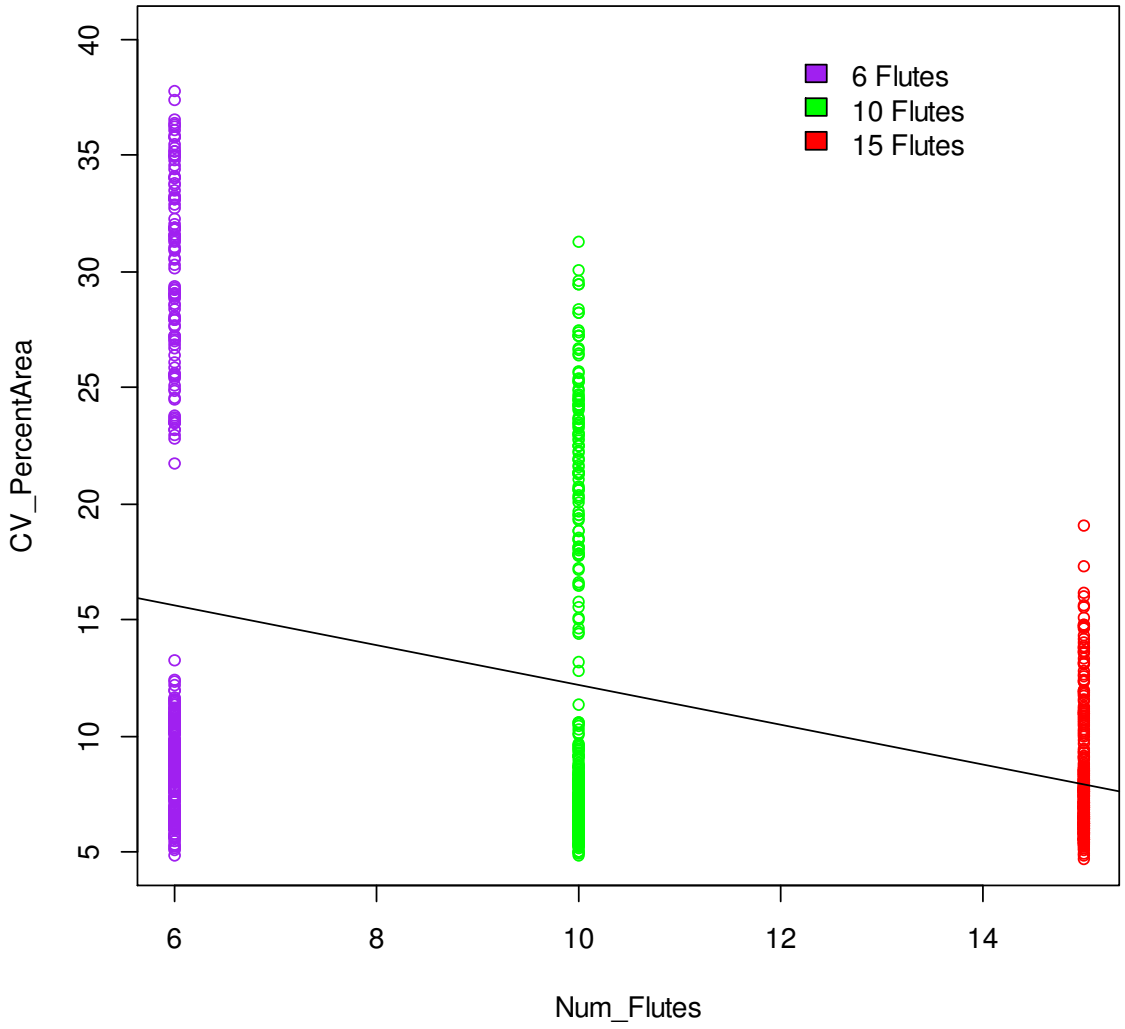

Figure 5-12: Variation of product flow (CV_PercentArea) versus the number of flutes (F) and the general linear trend of the product flow variation as the number of flutes on a roller is increased (note: not including the extra pitch rollers).

The first and most important trend to note here is the consistent improvement in product flow evenness (lower CV) as the number of flutes increases. While the number of flutes increases the volume of individual flutes gets smaller and the capacity of the roller typically decreases. The second important trend to notice, specifically with the 6-flute rollers and to a lesser extent with the 10-flute rollers, is the gap in the data. This gap is caused by the significant effect of changing the flute pitch of the rollers. The cluster of data with the poorest product flow

evenness (high CV) correlates with all the rollers that have straight flutes (0 PR). The higher CV correlates to a visual pulsating of flow coming off the rollers at operating speeds. The zero pitch ratio data cause the linear trend line to skew higher with the lower number of flutes when in fact the addition of a non-zero pitch can bring the product flow evenness almost equivalent with the 10 and 15-flute rollers. The individual glm completed with the number of flutes versus the product flow evenness also showed that the number of flutes had a significant amount of explanatory power towards the overall model. When considering the form of the empirical model of meter roller performance the number of flutes should be included.

5.4.1.3 Meter Roller Speed

Meter roller speed is referred to as a design parameter in this section when in fact it really is a test parameter, but because each roller is suited for a specific throughput range the roller speed needs to be incorporated as a parameter in the design process. Meter roller speed came out as the third highest rank in terms of statistical significance in terms of explaining product flow evenness.

Figure 5-13 shows a distinct improvement in product flow evenness as meter roller speed increases, which was anticipated going into the study. In practice, decreasing flute volume, increasing the number of flutes, and increasing meter roller speed is a typical strategy to get more even flow off the meter roller. The 6, 10, and 15 flute rollers all followed the same general trend with the 6 and 10 flute rollers having the largest improvement. But, just like the three previous parameters, the data are distinctly split to a cluster in the 20 to 40% CV range that correlate to the 0 pitch ratio rollers and a cluster in the 5 to 15% CV range that have a pitch ratio greater than 0. Figure 5-14 depicts the relationship between meter roller speed and pitch ratio as they correlate to the CV of product flow over all four repetitions.

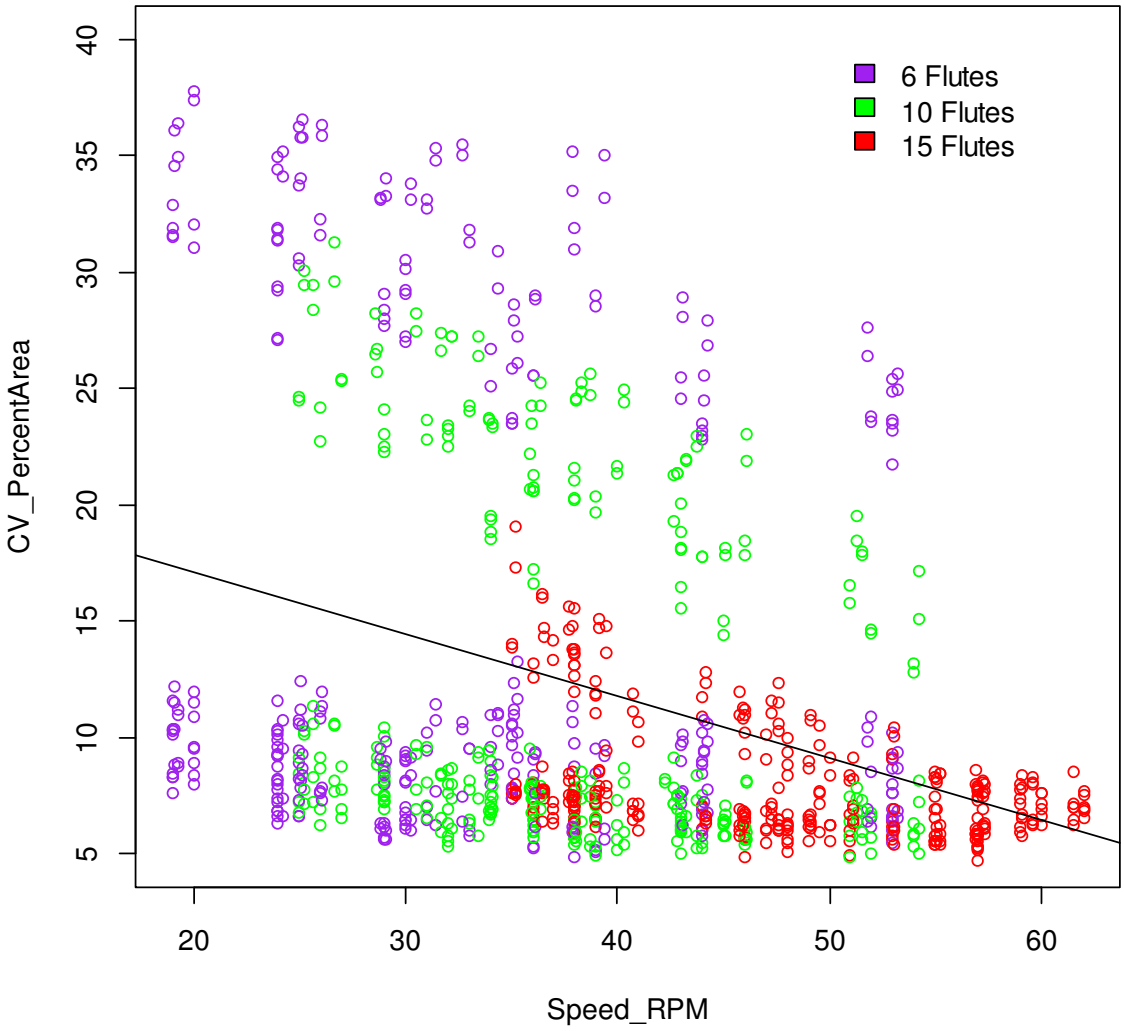

Figure 5-13: Variation of product flow (CV_PercentArea) versus the meter roller speed showing the general linear trend across the entire dataset as meter roller speed is increased.

Figure 5-14: Data spread showing the effect of product flow evenness as meter roller speed and pitch ratio was varied.

It is clear from Figure 5-14 that meter roller speed is very beneficial to product flow evenness when the roller has straight flutes but as soon as a non-zero pitch is added to the roller the benefit of added roller speed, other than controlling throughput, appears to be minimal. If for some reason adding a pitch to meter rollers was too costly, then simply increasing roller speed and increasing the number of flutes would be the cheapest and easiest way to improve roller

performance. However, adding a pitch ratio greater than 0 appears to help push the meter roller performance above what just adding flutes and increasing meter speed can do. Meter roller speed does carry enough weight as shown by the statistical analysis and should be considered as a potential variable in the model development section.

5.4.1.4 Center Distance to Fillets (R_2)

The center distance to the fillets versus the product flow evenness in Figure 5-15 shows a similar trend to that of the number of flutes. The R_2 parameter is fairly reliant on the number of flutes to achieve a certain level because the flute size decreases as more flutes are added to the periphery of a meter roller. The R_2 limitation can be seen with the 15 flute roller data in Figure 5-15 where all three levels fall outside the range of the 6 and 10 flute roller solely because of the decreased flute size to fit 15 flutes on a roller. The separation in the data between straight flutes and flutes with a pitch ratio of 1 and 1.5 is also very apparent in the 6 and 10 flute rollers. The effect of roller speed is evident in the vertical spread of data for each (higher roller speed results in lower CV). Because the trend of the R_2 parameter relies heavily on the number of flutes, the pitch ratio, and roller speed, this would explain why the glm of the total model (Table 5-5) and the residuals from the individual glm show it is insignificant (PR(>|t|) > 0.5) to the overall model determining the product flow evenness. Therefore, it is safe to say that parameter R_2 does not need to be included in the overall empirical model algorithm to be developed from the data.

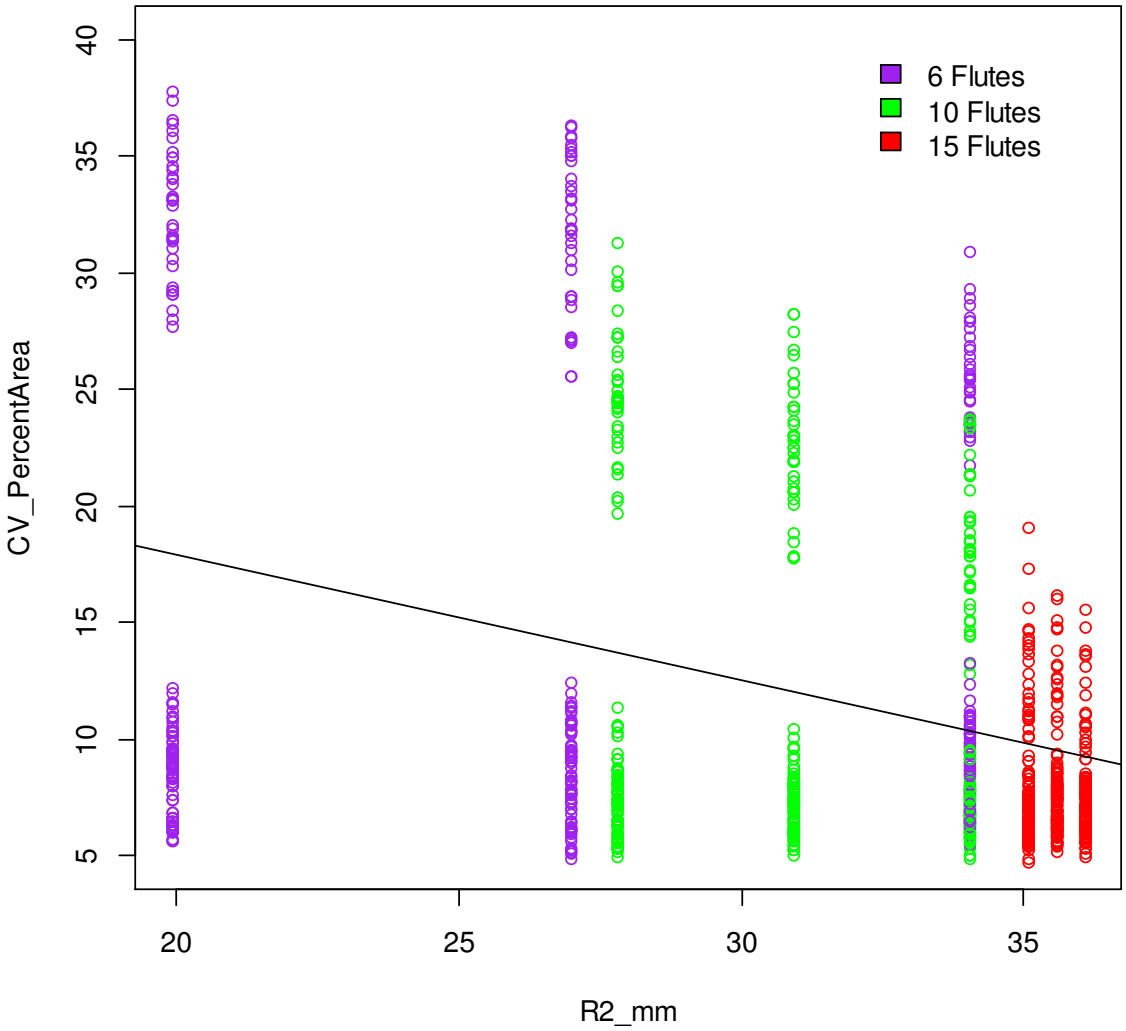

Figure 5-15: Variation of product flow (CV_PercentArea) versus the center distance to fillets (R_2) and the general linear trend in the product flow variation as R_2 increases (effective flute depth decreases as R_2 increases).

5.4.1.5 Flute Profile Shape (PHI)

The flute profile shape parameter, PHI, data presented in Figure 5-16 are segmented similarly to the R_2 parameter, specifically the 6 and 10-flute rollers with and without a pitch ratio form separate clusters, where the zero-pitch rollers occupy the top region (higher CV) of each roller dataset. Overall, there is a very slight decrease in product flow evenness from a minimum PHI (PHI = 0) to a maximum PHI parameter for each of the rollers where the glm p-value infers

that it is slightly insignificant (p-value slightly greater than 0.05) but the residual value from Table 5-6 ranks it as the parameter with the least amount of significance to the total response (change in product flow CV). With this information from the statistical analysis, and residuals that are actually less than the R_2 parameter, it is also safe to say that the flute profile parameter PHI does not need to be included any further in developing an empirical model algorithm.

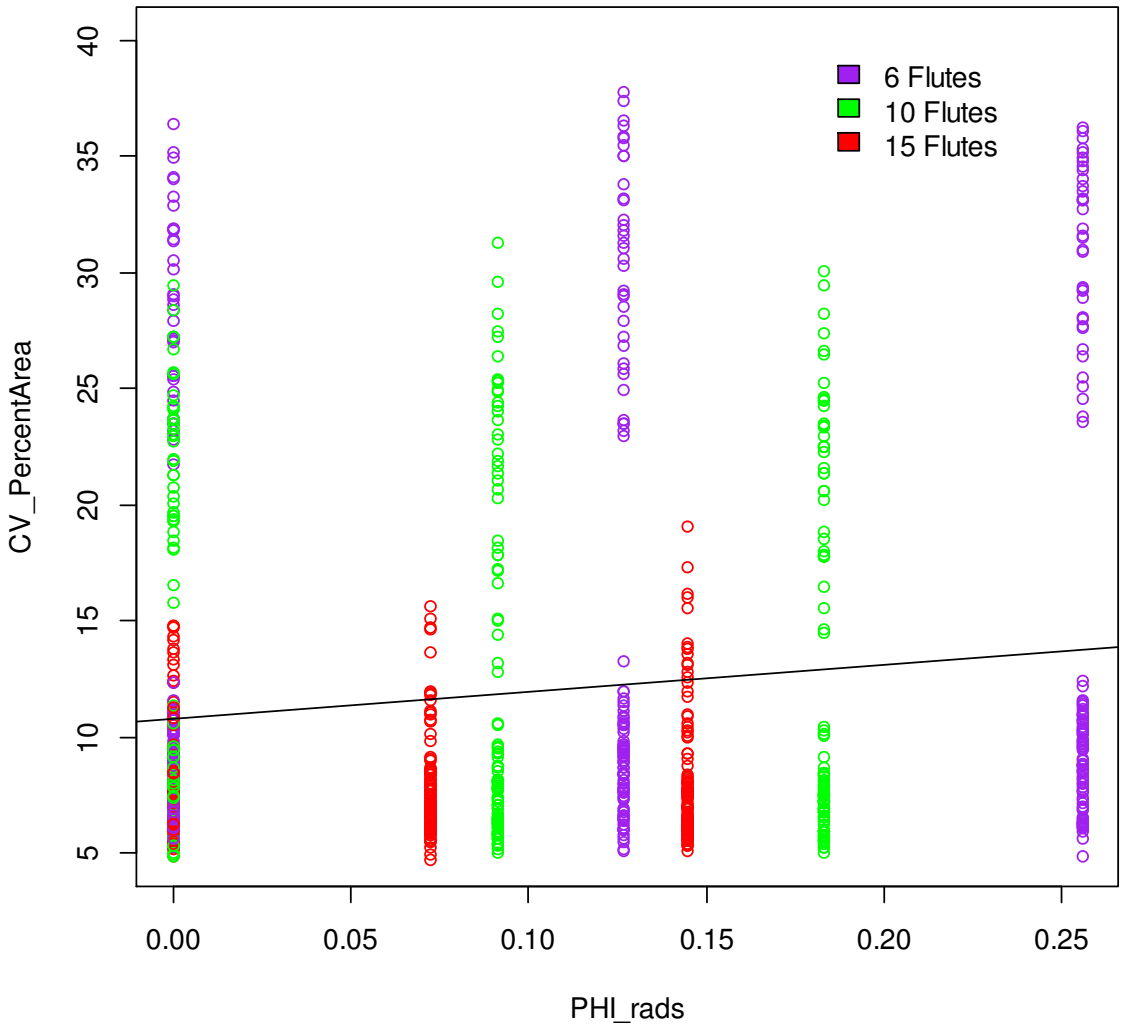

Figure 5-16: Flute profile shape (PHI) versus the variation of product flow (CV_PercentArea) coming off the roller.

5.4.2 Model Development

From the data presented it is clear that the model should include pitch ratio, the number of flutes, and meter roller speed as variables. Moving forward with determining the form of the empirical model one must first know the underlying relationship of each parameter with the output. As discovered in the previous section pitch ratio came out as the dominant variable and the only variable with an apparent non-linear relationship. This non-linear relationship is displayed in Figure 5-17. (more detailed Figure 5-11) with a 3rd order polynomial line fit separately for rollers with 6, 10, and 15 flutes, using the extra-pitch roller data to explain the actual relationship of the pitch ratio (most significant explanatory variable) on product flow CV.

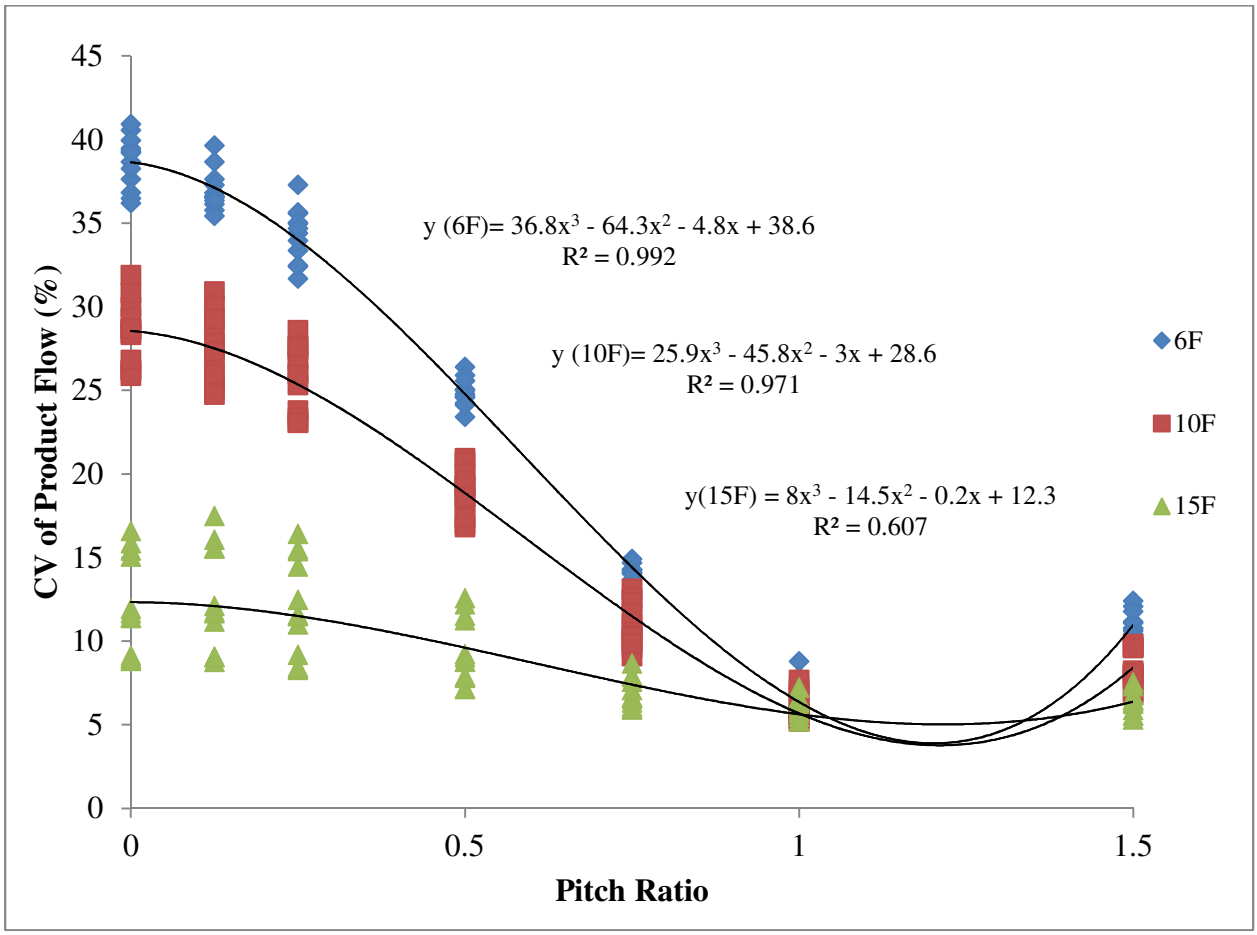

Figure 5-17: Meter roller product flow evenness as a function of pitch ratio with the extra pitch rollers and a trend line fitted for each group of meter rollers showing the overall relationship.

Figure 5-17 suggests that pitch ratio is well described by a third-order relationship with product flow CV. It is intuitive to think a third-order relationship better describes the relationship between pitch ratio and product flow CV over a second-order relationship because of the greater correlation in the range of pitch ratios between 0 and 1. A second-order relationship will dramatically underestimate this empirical relationship between flute pitch and product flow CV. The vertical spread of the data is attributed to the change in meter roller speed during testing. Using the observed 3rd order polynomial trend for pitch ratio (x_1 in eqn. 5-10) and incorporating the known linear relationship of both the number of flutes (x_2 in eqn. 5-10) and meter roller speed (x_3 in eqn. 5-10) with product flow CV, polynomial expansion can be applied to the variables. The polynomial expansion yields the general form of the model in equation 5-10 with the maximum number of coefficients and interactions possible knowing the underlying relationships of each variable. One will notice that the x_1 term is the only variable with a quadratic and cubic term. This is because of the observed 3rd order relationship in Figure 5-17 with pitch ratio (x_1) and the x_2 and x_3 terms only having a linear relationship (hence no squared or cubic terms).

$$\begin{aligned} CV(x_1, x_2, x_3) = {} & x_1^{\,3}\left(b_1 x_2 x_3 + b_2 x_2 + b_3 x_3 + b_4\right) + \\ & x_1^{\,2}\left(b_5 x_2 x_3 + b_6 x_2 + b_7 x_3 + b_8\right) + \\ & x_1\left(b_9 x_2 x_3 + b_{10} x_2 + b_{11} x_3 + b_{12}\right) + \\ & \left(b_{13} x_2 x_3 + b_{14} x_2 + b_{15} x_3 + b_{16}\right) \end{aligned} \qquad 5\text{-}10$$

Where, CV = Coefficient of Variation of Product Flow

x_1 = Pitch Ratio (PR)

x_2 = Number of Flutes (F)

x_3 = Meter Roller Speed (ω_m) and,

b_n = The coefficients to be determined (n=1 to 16)

Equation 5-10 needs to be optimized because not all interactions may be necessary in the model. The model form optimization strategy chosen is a stepwise regression function in Matlab R2014b (MATLAB, Natick, MA). This function is typically used for variable selection to ensure the simplest model is achieved based on a goodness of fit (RMSE) and low model complexity (The MathWorks, Inc., 2014). It is an iterative process that starts with the lowest number of variables and adds variables one at a time and adjusts coefficients to minimize the root mean squared error (RMSE). The root mean squared error is essentially a measure of the standard deviation of the residuals (Measured-Predicted) in the model so it is important to graph the residuals to visually inspect the model performance. An example output of the stepwise regression function can be found in Appendix C.

The stepwise regression for the model form optimization is solely done on the extra pitch roller data to achieve the proper 3rd order polynomial form. The extra pitch roller data were randomly split into a training set (60%) and a testing set (40%) for the stepwise regression. Three different random training/testing splits of the data sets were used for the stepwise regression to compare how coefficients change with each model form. Each testing set should be used to test the model form and compare RMSE values for a goodness of fit measure. The use of three different training and testing (Tr.1, Tr.2, and Tr.3) sets helps ensure overfitting of the data does not happen. Table 5-7 shows the coefficients and variables for the optimized model form from the stepwise regression on the three different training sets.

Table 5-7: Model form optimization results and coefficients from the stepwise regression with the extra pitch roller data split into three different training/testing sets as shown by Tr.1, Tr.2, and Tr.3.

Variable	Coefficient	**Tr.1**	**Tr.2**	**Tr.3**
$x_1^3*x_2*x_3$	b1	-0.054	-0.061	-0.064
$x_1^3*x_2$	b2	0	-0.557	-0.378
$x_1^3*x_3$	b3	0.160	0.561	0.521
x_1^3	b4	40.107	31.521	35.258
$x_1^2*x_2*x_3$	b5	0.083	0.134	0.131
$x_1^2*x_2$	b6	0	0	0
$x_1^2*x_3$	b7	0	-1.385	-1.158
x_1^2	b8	-76.879	-39.912	-53.215
$x_1*x_2*x_3$	b9	0.013	-0.042	-0.038
x_1*x_2	b10	0.805	1.685	1.633
x_1*x_3	b11	-0.416	0.729	0.574
x_1	b12	0	-33.686	-25.569
x_2*x_3	b13	-0.024	-0.020	-0.017
x_2	b14	-1.517	-1.461	-1.659
x_3	b15	0	-0.100	-0.123
Intercept	b16	52.6294	54.8596	55.9296
Training	RMSE	0.693	0.632	0.677
Testing	RMSE	0.834	0.900	0.767

Table 5-7 displays the generated coefficients and optimized model form from the stepwise regression analysis on the extra pitch roller data. The stepwise regression function removes variables from the model based on statistical significance to the output on a 95% confidence interval. Each coefficient has a p-value associated (see Figure C-9) with it. When the p-value computed is less than 0.05 the variable is brought into the model, otherwise it is left out. This procedure continues until the RMSE is optimized. From the results in Table 5-7 the training sets shows two potential model forms, one with 11 coefficients (from Tr.1) and one with 15

coefficients (from Tr.2 & Tr.3). The three training sets Tr.1, Tr.2, and Tr.3 all had similar RMSE values of 0.693, 0.632, and 0.677 respectively for the goodness of fit measure using the 60% training values to test the model. The training RMSE values are expected to be lower than the testing RMSE values seen in Table 5-7 because using the same data that predicted the coefficients will almost certainly have a better fit. Showing that the training set is not a perfect fit also gives confidence that the model is not just memorizing the data. This is the main reason that a separate training set of data that has not been introduced to the model is the best way to test the model performance. So the model form of equation 5-10 needs to be tested with the three training sets correlating to the optimization results in Table 5-7. The three training sets yield the testing RMSE values and give a measure of the model performance.

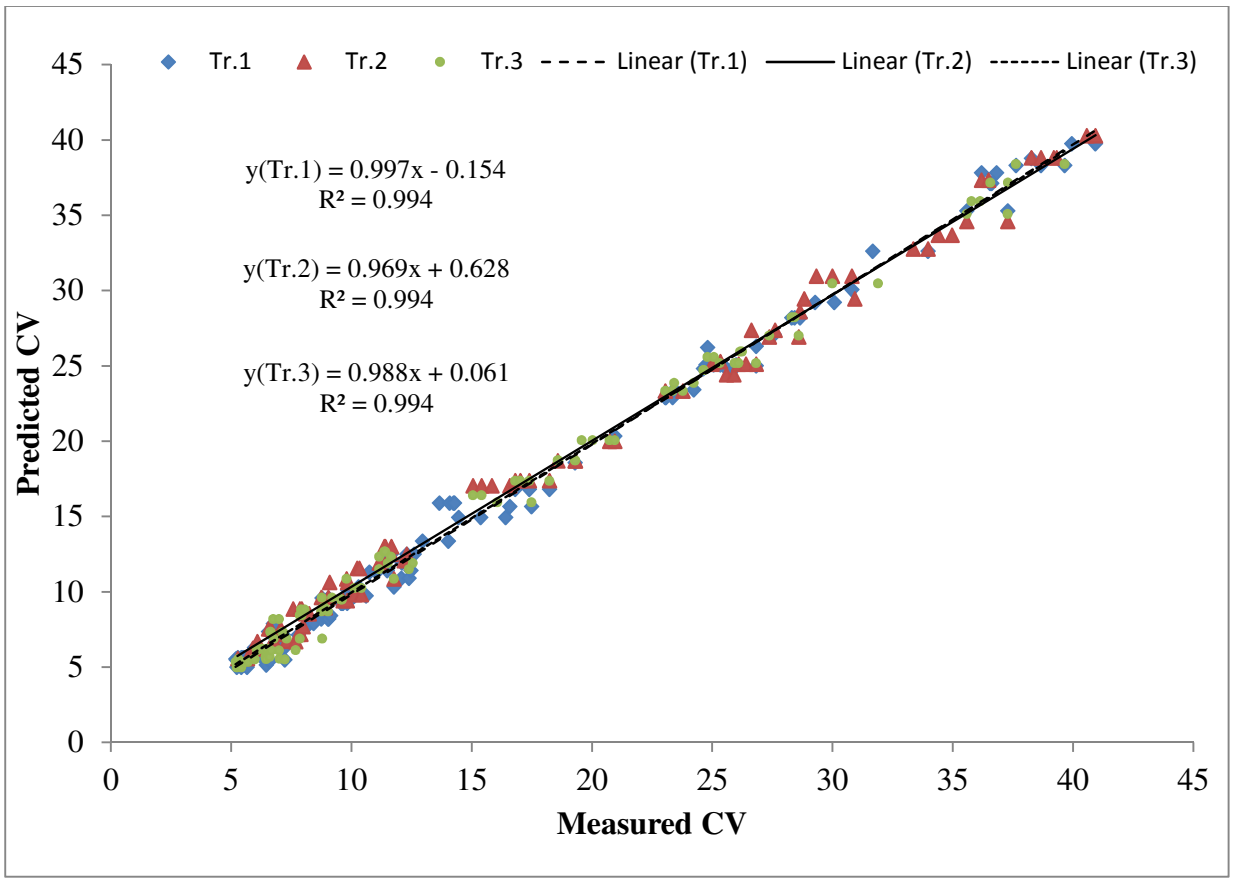

Figure 5-18: Model fit summary of measured CV versus predicted CV output using testing data from the three optimized models Tr.1, Tr.2, and Tr.3 of the general form in equation 5-10.

Figure 5-18 visually displays the correlation of the measured data versus the predicted output using the 40% testing data from the three sets to assess the fit of the models generated from the extra pitch roller data. Each of the three training sets give acceptable R squared values in Figure 5-18 and more importantly the testing RMSE values of 0.834, 0.900, and 0.767 correlating to Tr.1, Tr.2, and Tr.3 respectively. Also, when viewing the residuals (see Figure C-10 for example) of each testing set they appear to be randomly dispersed and not following a distinct trend which is a good visual indication of model fit. When tested, the training set 3 (Tr.3) gave the lowest RMSE to indicate the best model fit, but for model validation both the 11 and 15 coefficient model form will be used to fit the original meter roller data.

5.4.3 Model Validation

The model validation technique used for this study will be a combination of fitting the meter roller data with 70% of the raw data and then testing the model effectiveness with the remaining 30%. The raw data referred to here are the data collected from the original 81 rollers (not including the extra pitch rollers) as displayed in Figure 5-10 (as well as Figure 5-12 to Figure 5-16). Using the general model form shown in equation 5-11 and the results of the model optimization form with the extra pitch roller data in Table 5-7, a set of coefficients will be calculated and, most importantly, the final overall form of the model determined. After the model is trained and tested with the 70/30 split of the raw data, the parameters of the model (PR, *F*, and meter speed) can be solved to find the minimum predicted product flow CV of the model and the meter roller parameters that correspond.

The model optimization done in the previous section revealed two potential forms of the model with lower model complexity than the general form of equation 5-10. The two potential model forms come from the model optimization results in Table 5-7 where an 11-coefficient (from Tr.1) and a 15-coefficient (from Tr.2 and Tr.3) model form and all show a good model fit

in Figure 5-18. Equation 5-11 and 5-12 show the 11 and 15 variable model form of the product flow.

$$CV_{Tr1}(x_1, x_2, x_3) = x_1^{\,3}\left(b_1 x_2 x_3 + b_3 x_3 + b_4\right) + x_1^{\,2}\left(b_5 x_2 x_3 + b_8\right) + x_1\left(b_9 x_2 x_3 + b_{10} x_2 + b_{11} x_3\right) + \left(b_{13} x_2 x_3 + b_{14} x_2\right) + c \quad 5\text{-}11$$

$$CV_{Tr2,3}(x_1, x_2, x_3) = x_1^{\,3}\left(b_1 x_2 x_3 + b_2 x_2 + b_3 x_3 + b_4\right) + x_1^{\,2}\left(b_5 x_2 x_3 + b_7 x_3 + b_8\right) + x_1\left(b_9 x_2 x_3 + b_{10} x_2 + b_{11} x_3 + b_{12}\right) + \left(b_{13} x_2 x_3 + b_{14} x_2 + b_{15} x_3\right) + c \quad 5\text{-}12$$

Where, CV_{TRn} = Coefficient of Variation of Product Flow from specific training (Tr) data

x_1 = Pitch Ratio (PR)

x_2 = Number of Flutes (F)

x_3 = Meter Roller Speed (ω_m) and,

b_n = The coefficients to be determined (n=1 to 16)

While reducing model complexity and maintaining a high correlation is one of the main goals, it is desired to keep both model forms until all the data have been fitted and tested. There is a possibility that further model optimization can occur based on the how the coefficients are calculated. For fitting the data to get the coefficients the raw data were randomly split up into three different training/testing sets denoted by T1a, T2a, and T3a for the 11 coefficient model form and T1b, T2b, and T3b for the 15 coefficient model form. The training/testing set was split so that approximately 70% was used for fitting and training the coefficients, and 30% was used for testing the model. Table 5-8 shows the generated coefficients, the new variables of the empirical model and goodness of fit measurement from testing the model.

Table 5-8: Fitted model coefficients yielding the new optimal model form from training and testing the 11 (T1a – T3a) and 15 (T1b – T3b) coefficient models with a 70/30 split of the raw data.

Variable	Coefficient	From 11 Coefficient Model Form (Tr.1)			From 15 Coefficient Model Form (Tr.2 and Tr.3))		
		T1a	T2a	T3a	T1b	T2b	T3b
$x_1^3*x_2*x_3$	b1	-0.013	-0.014	-0.014	3.37E-04	-1.67E-03	-2.13E-03
$x_1^3*x_2$	b2				-0.5543	-0.517	-0.505
$x_1^3*x_3$	b3	0.049	0.061	0.072	-0.092	-0.069	-0.054
x_1^3	b4	31.399	31.928	30.424	13.740	13.437	12.803
$x_1^2*x_2*x_3$	b5	0	0	0	0	0	0
$x_1^2*x_2$	b6						
$x_1^2*x_3$	b7				0	0	0
x_1^2	b8	-58.002	-59.236	-56.623	0	0	0
$x_1*x_2*x_3$	b9	0.048	0.049	0.049	2.82E-03	7.49E-03	9.42E-03
x_1*x_2	b10	0.152	0.207	0.181	1.998	1.913	1.788
x_1*x_3	b11	-0.162	-0.168	-0.190	0.342	0.288	0.246
x_1	b12				-54.121	-53.326	-50.764
x_2*x_3	b13	-0.028	-0.029	-0.027	-0.001	-0.004	-0.005
x_2	b14	-0.499	-0.475	-0.481	-1.566	-1.447	-1.351
x_3	b15				-0.318	-0.280	-0.261
Intercept	b16	38.098	38.135	37.478	49.917	48.714	47.147
Testing	SSE	1101.767	866.218	940.488	984.189	705.665	759.254
	RMSE	1.956	1.916	1.955	1.849	1.722	1.757

Training and testing the previous model form in equation 5-11 with the raw test data yields the coefficients in columns T1a, T2a, and T3a (T*n*a columns). The coefficients all remain fairly consistent. Based on the fitted model results an additional variable ($x_1^2*x_2*x_3$) can be eliminated from the 11 coefficient model form therefore decreasing the model complexity for this dataset to 10 coefficients. The dataset being fitted only had pitch ratios of 0, 1, and 1.5 which appears to have an underlying quadratic relationship with the product flow CV as seen in Figure

5-10. Because the optimized model form was developed including the extra pitch rollers which had a cubic relationship between PR and product flow CV, the cubic PR values will dominate the squared PR interaction with the linear variables leaving only the pure PR squared value. This is why the variable interaction ($x_1^2*x_2*x_3$) was forced to zero when fitting the raw data to the 11-coefficient model.

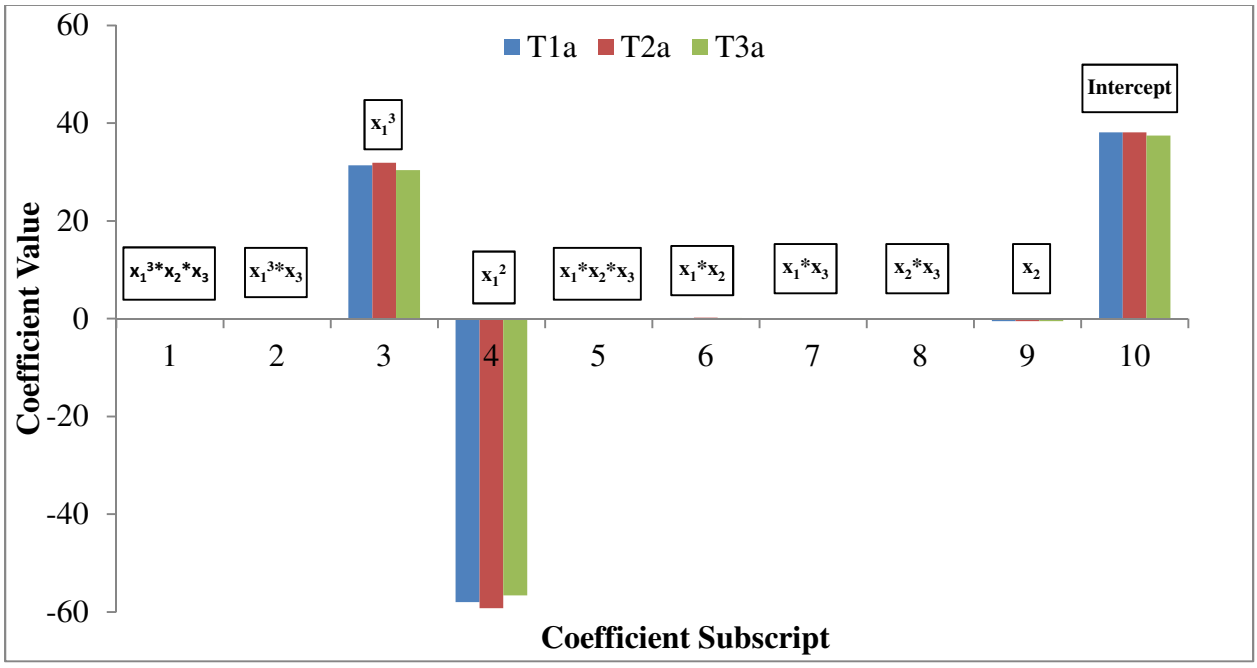

Figure 5-19: Coefficients of the 10-coefficient empirical model after fitting the raw data to the 11-coefficient base model form showing the dominant interactions.

Figure 5-19 shows the dominant interactions of the 10 coefficient model with the cubic and squared PR interactions playing a large factor while all the linear interactions appear small but are all statistically significant. Even though the model was reduced to 10 coefficients when fitting the raw test data, the 11 coefficient model form of equation 5-11 should still be the base model form to start with when fitting to a set of meter roller data. Because equation 5-11 was developed based on the full spectrum of pitch ratios in between 0 and 1 it will yield the most representative trend.

When training and testing the 15-coefficient model formed from equation 5-12 with the same test data yields the coefficients in columns T1b, T2b, and T3b (T*n*b columns). This model was optimized down further to 12 coefficients from 15 for this dataset. Similar to what happened with the 11 coefficient model, the remainder of the squared pitch ratio (x_1^2) variables were all eliminated when fitted to the data. The cubed and linear relationship variables appear to balance out the response as seen in the graph of the coefficients in Figure 5-20.

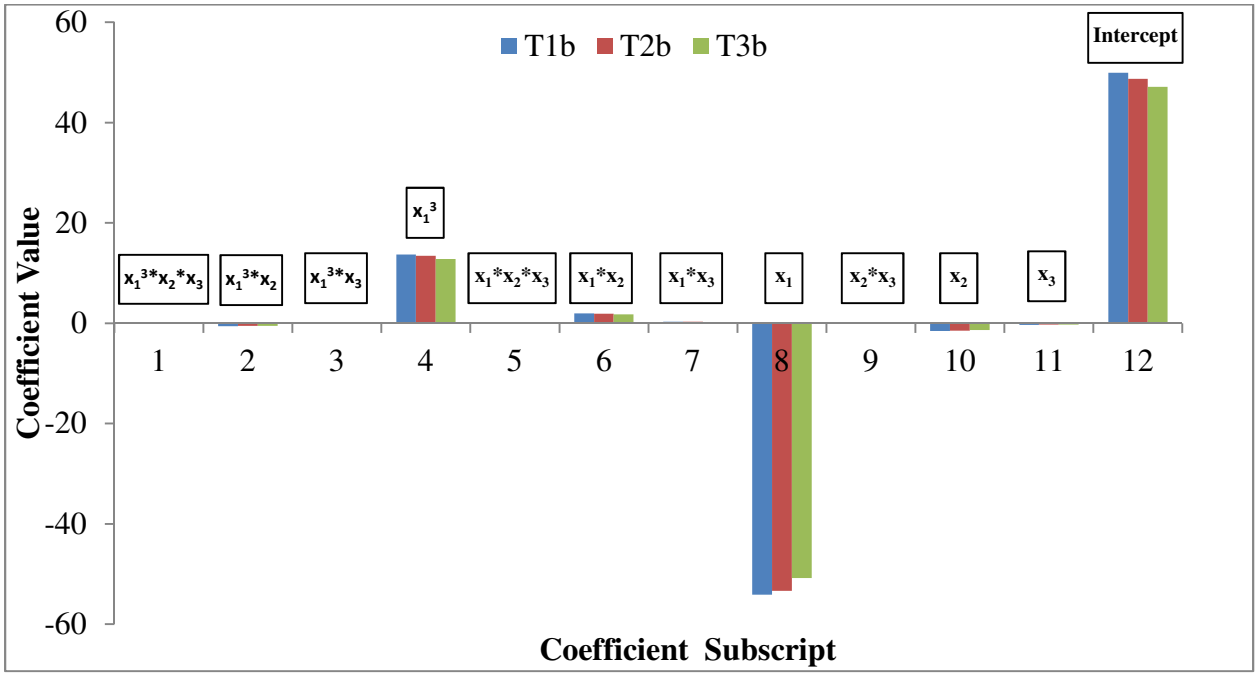

Figure 5-20: Coefficients of the 12-coefficient empirical model after fitting the raw data to the 15-coefficient base model form showing the dominant interactions.

Figure 5-20 shows the distinctly different dominant interactions of the new 12-coefficient model compared to the 10-coefficient model in Figure 5-19. The cubic PR interaction is definitely dominant in both which is consistent but a larger emphasis is put on the linear interaction of PR in the 12-coefficient model. The goodness of fit measure and model complexity will be the determining factor in choosing between the 10 and 12-coefficient model.

When comparing the RMSE of both models from Table 5-8 the 12-coefficient model is slightly lower than the 10-coefficient model but only by about 8.5%. This does not necessarily mean the 12-coefficient model is 8.5% better at predicting the product flow because of the added model complexity. When looking at the average of RMSE from each set (1.94 for the 10-coefficient model and 1.78 for 12-coefficient model), an 8.5% increase in RMSE really equates to a decrease in the dispersion of the product flow CV residuals of 0.16%. A CV of 0.16% is a very small amount of improvement to accept when it requires the addition of two more coefficients in the model. It is safe to say that the 10 and 12-coefficient models perform almost equivalently based on the RMSE and R squared correlation graphs in Appendix C (Figure C-11 and Figure C-15). It then comes down to model complexity as the deciding factor and because the 10-coefficient model has fewer variables while performing equivalently to the 12-coefficient model, the 10-coefficient empirical model should be the preferred model form to predict future meter roller performance with wheat as well as predict the optimal meter roller design. Because the 10-coefficient model is actually built off of the 11-coefficient model in equation 5-11 then the 11-coefficient model should be considered as the base starting point when fitting any new meter roller data in wheat. From here the determined coefficient values will determine if all coefficients are required. For the data presented in this paper for wheat equation 5-14 shows the final form of the 11-coefficient empirical model.

$$CV_{11c}(PR,F,\omega_m) = PR^3\left(b_1F\omega_m + b_2\omega_m + b_3\right) + PR^2\left(b_4F\omega_m + b_5\right) + PR\left(b_6F\omega_m + b_7F + b_8\omega_m\right) + \left(b_9F\omega_m + b_{10}F + b_{11}\right) \quad 5\text{-}13$$

The coefficients *(b_1,…., b_{11})* present in equation 5-13 are numbered according to Table C-15 where a set of coefficients are predicted for the model. The table of predicted coefficients is shown in Appendix C. The coefficients for equation 5-13 were calculated using a 70/30 split of the entire dataset plus the extra pitch roller data to cover the whole spectrum of pitch ratios. The

fitted curve of the empirical model (equation 5-13) as it would follow the 6, 10, and 15-flute rollers using the original data graphed for predicting the product flow CV with equation 5-13 can be seen in Figure 5-21. The extra pitch roller data were not added in this figure as it was used to develop and generate the optimal model form to use with the original roller data.

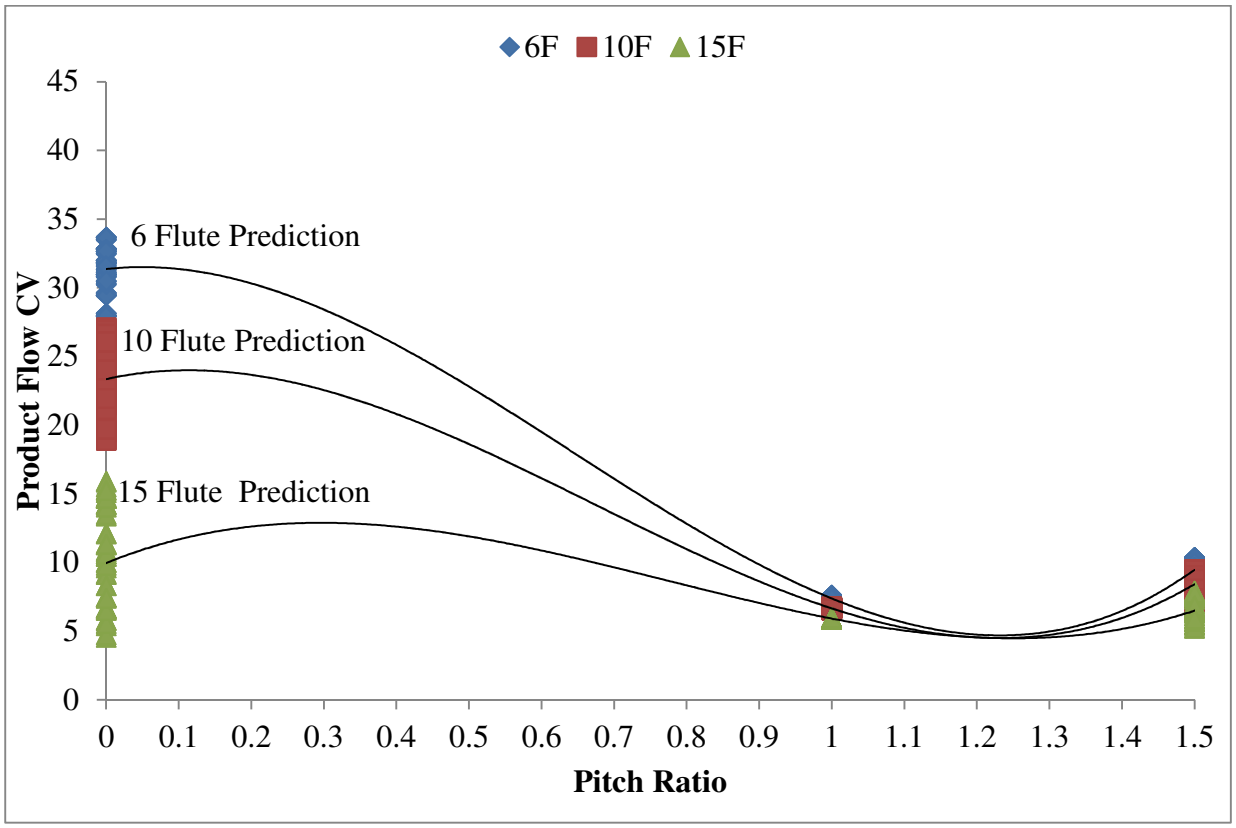

Figure 5-21: Overall correlation model fit of the 11-coefficient empirical model form (CV_{11c}) of the 6, 10, and 15-flute rollers displayed as product flow CV versus pitch ratio with a trend line fitted to show the general trend.

Figure 5-21 incorporates all of the variables of the final empirical model including the pitch ratio (PR), number of flutes (F), and meter roller speed (ω_m) but was only displayed graphically as product flow CV versus pitch ratio to show the overall correlation of the model. With the empirical model form determined and the data fitted to the model, the meter roller parameters can be predicted. Figure 5-17 shows the best possible estimate of the optimal meter

roller where the CV dips to a minimum at a pitch ratio of about 1.2 for the 6 and 10 flute rollers. Of course this estimate is based solely on the trend line of the extra pitch roller but a cubic relationship with pitch ratio will give that same general shape when using the empirical model (equation 5-13) to predict. Therefore, locating the minimum CV predicted by equation 5-13 will yield the meter roller with the optimal parameters PR, F, and ω_m that correspond. Table 5-9 gives the predicted optimal meter roller parameters that would give the most even product flow from the rollers.

Table 5-9: Predicted optimal meter roller parameters to give the most even product flow.

Empirical Model Type	Number of Flutes (F)	Meter Speed, ω_m (RPM)	Pitch Ratio (PR)	Predicted CV
11 Coefficients (Eqn. 5-13)	6	53	1.25	4.30
	10	54	1.25	4.39
	15	62	1.32	4.48

CHAPTER 6. SUMMARY AND CONCLUSIONS

The metering system is the heart of any operation whether it requires precise dispensing of particulate material at specific rates such as in agricultural seeding systems or an industrial bulk conveying operation where product relocation is the main goal rather than precise control of the product rates. A meter roller or rotary air lock is the main component in most of these metering systems. Specifically, in agricultural seeding systems (air seeders) the need to have more precise metering systems is becoming more and more important as seed prices increase and the emphasis on the agronomic benefits of more even seed placement increases. In addition, a more even flow of product being introduced into the distribution system of the seeder will improve the accuracy of other sensors that could be utilized in conjunction with the metering system. With little work done in literature on optimizing the design of meter rollers, the importance of developing a design tool in the form of an empirical model has become apparent.

Building a design tool like an empirical model requires an accurate test method to build and validate the model. A method called the continuous test method was developed to measure the performance of metering systems in a quick, accurate and efficient way. The test method utilizes an imaging system set up to capture images of the product flow as it is metered from the roller on a continuous basis. The images are then passed through an imaging analysis program to calculate the percent area of product occupying each image. For each test the metering system performance is measured as the coefficient of variation (CV) of the percent area of product per image. The lower the CV is, the better the metering performance in terms of product flow evenness. The test method was validated to ensure the data captured were representative and comparable across a range of meter rollers and product, specifically wheat. The test method validation led to three main conclusions relating to the parameters of the continuous test method. First, product should be imaged at or above a minimum rate defined by the frame-per-flute

(fPFL) ratio. The minimum recommended fPFL is 10 for wheat but can be taken as low as 6 if roller speed and camera settings are a limitation. The minimum recommended fPFL is 15 for canola. Second, a constant frame height must be maintained throughout the entire test set for every roller and product being tested to ensure the most consistent data are collected. Third, the oversampling and potential occlusion imposed on the particle flow from a constant fPFL ratio and frame height does not affect the metering system performance measure to a practically significant level.

The next major step was parameterizing the meter roller so the design of specific rollers can easily be controlled and the parameters can effectively be utilized in the developed empirical model. The main parameters that define the shape of a flute on a meter roller of constant diameter and length are split into two categories, two minor characteristics that control small details and four major flute shape characteristics that are visually more distinct. The two minor characteristics are the angular fin width, β, and the radius of the fillet circles, R_1, that give the curvature of a flute. The four major shape characteristics are the number of flutes F, the center distance to the fillet circle, R_2, the fillet circle angular distance, φ, and the pitch ratio PR. All six parameters are potential variables of the empirical model.

Experimental data were collected for 81 prototyped meter rollers with three levels of F, three levels of R_2, three levels of PR, and three levels of φ while the two minor roller parameters were held constant. These rollers were tested over four repetitions, repetition 1 and 2 back-to-back and then repetitions 3 and 4 back-to-back at a later date, at three different meter roller speeds (ω_m) with wheat flows that correspond to a minimum, average, and maximum application rate in Canada. From the results and statistical analysis it was found that the fillet circle angular distance φ and the center distance to the fillet circle R_2 were insignificant variables in explaining

variations in the product flow off the rollers. However, the number of flutes F, the pitch ratio PR, and meter roller speed ω_m have significant correlations with the product flow measure. From the 81 meter rollers tested the product flow CV ranged from 4.7% (lowest non-uniformity of flow) up to 37.7% (highest non-uniformity). Figure 5-10 shows all the experimental data as product flow CV versus PR showing a non-linear relationship where the higher product flow CV's occur at a PR of 0 (straight flutes) and the lowest product flow CV's occur around a PR between 1 and 1.5 (curved flutes).

The raw data and statistical analysis provided valuable insight into the relationship between each parameter and the product flow CV. However, there seemed to be a large gap in the data between the pitch ratios of 0 to 1. To gain a better understanding of how the product flow CV would actually transition from a PR of 0 down to a minimum around 1, a small set of rollers were prototyped with PR's of 0.125, 0.25, 0.5, and 0.75. These new extra pitch rollers were made with 6, 10, and 15 flutes (same as original rollers) and operated at 3 different roller speeds that correlate to the throughput of the roller based on the volume of the flutes. The extra pitch roller testing used 21 rollers over four repetitions (7 levels of PR, 3 levels of F, 3 roller speeds, 1 R_2, and 1 φ). The extra pitch data indicated a cubic relationship between product flow CV and PR. Understanding that the number of flutes, F, and meter roller speed, ω_m, have a linear relationship with product flow CV and pitch ratio PR has a cubic relationship, a polynomial expansion yielded the general base form of the empirical model. This general form was made up of 16 variables, but was reduced using a stepwise regression procedure with Matlab (MATLAB, Natick, MA). Models of this form resulted in RMSE values of 0.767 to 0.900 for the extra roller testing set, and 1.94 using the original data set. The final empirical model form without specific coefficients fit is shown in equation 5-13 with product flow CV as a function of pitch ratio PR,

the number of flute F, and meter roller speed ω_m. Different coefficients could be fit to this model form depending on data; the form of the model is most important

The empirical model developed predicted the optimal roller parameters for a 6, 10, and 15 flute meter roller. The optimal parameters include a pitch ratio of 1.25 for the 6 and 10 flute rollers and a pitch ratio of 1.32 for a 15 flute roller. An optimal meter roller speed of 53, 54, and 62 RPM was also predicted for the 6, 10, and 15 flute roller in wheat and yields a predicted CV of 4.30, 4.39, and 4.48, respectively. Overall, the optimal meter roller predicted for use in wheat would be a roller with 6 flutes, a pitch ratio of 1.25, at a meter speed of 53 RPM with a predicted product flow CV of 4.30. Speed would obviously be dependent on the desired rate of material, but these parameters would give the most even product flow out of the meter roller.

For future work it would be beneficial to prototype a set of predicted rollers and confirm that they match the empirical model prediction. As well, the same procedure could be used for product other than wheat.

LIST OF REFERENCES

Alchanatis, V., Brikman, R., & Kashti, Y. (2002). A Machine vision system for evaluation of planter seed spatial distribution. *CIGR Journal.* 4*:* 11-20*.*

Allied Vision Technologies. (2002). *Products: Cameras: Gigabit Ethernet: Prosilica GE: GE680*.Retrieved from Allied Vision Technologies Website: http://www.alliedvisiontec.com/us/products/cameras/gigabit-ethernet/prosilica-ge/ge680.html.

Basnet, B. B., Murray, J. R., & Tullberg, J. N. (2006). Planter seed metering components. *Planters and Their Components*.: 151.

Borowska, J., Konopka, R., & Zadernowski, R. (1996). Composition of some physical properties of different pea cultivars. Food/Nahrung, 40(2), 74-78.

Boumans, G. (1985). *Grain Handling and Storage*. The Netherlands, Amsterdam: Elsevier Science.

Boydas, M. G., & Turgut, N. (2007). Effect of vibration, roller design, and seed rates on the seed flow evenness of a studded feed roller. *Applied Engineering in Agriculture*, 23(4): 413-418.

Buckmaster, D. R., Goering, C. E., Rohrbach, R. P., & Srivastava, A. K. (2006). Crop Planting. In McCann, P. Ed., *Engineering principles of agricultural machines.* 231-269. St. Joseph, MI: American Society of Agricultural and Biological Engineers.

Chakraverty, A., Mujumdar, A. S., Raghaven, G. S. V., & Ramaswamy, H. S. (2003). *Handbook of Postharvest Technology: Cereals, Fruits, Vegetables, Tea, and Spices.* New York, N.Y.: Marcel Dekker, Inc.

CNH America LLC. (2008). *Meter roller options.* Available at: http://agriculture.newholland.com/us/en/Products/Planting-and-Seeding-Equipment/AirCarts_new/Pages/Performance_details.aspx#feature_content.

Ess, D. R., Hawkins, S. E., & Young, J. C., Christmas, E. P. (2004). Evaluation of the Performance of a Belt Metering System for Soybeans Planted with a Grain Drill. In *The Canadian Society for Engineering in Agricultural, food, and Biological Systems (ASAE/CSAE) Annual International Meeting*, Paper # 041085. Ottawa, Ont., Canada.

Fastec Imaging Corporation. (2015). Overview of TroubleShooter and Ranger Cameras. *TroubleShooter/Ranger Camera Operator's Manual.* San Diego, California, United States.

Flexi-Coil Ltd. (2001). Metric meter rate information. *20 Series Air Cart* [Manual]. (GH-030.1).

Gervais, J. & Schollar, D. (2008). Measuring and defining continuous flow of fluted meter rollers. In *Agriculture and Bioresource Engineering 495.3 Design Report*.

Gervais, J. & Noble, S. (2010). The development of a standard test method for measuring the eveness of flow off meter rollers. In *Commission of Agricultural Engineering 17th Annual Congress Meeting*.

Henry, J., Gervais, J., Schollar, D., Noble, S. D., & Hui, K. P. C. (2012). System and Method for Measuring Flow Rate from a Meter Roller. U.S. Patent No. 8,176,797 B2.

Guler, I. E. (2005). Effects of flute diameter, fluted roll length, and speed on alfalfa seed flow. *Applied Engineering in Agriculture.* 21(1): 5-7.

Hagney, M. (2009, January). *News: Exapta Solutions, Inc*. Retrieved from Exapta Solutions, Inc. Website: http://wwwexapta.com/news/nws_AccuracySeedPlacement_jan09.pdf.

Hart, L. (2008). Meter redesign trims 5.5% off seeding costs. *Grain News*. January, 28 issue, 17.

Igbozulike, A. O., & Aremu, A. K. (2009). Moisture dependent physical properties of Garcinia Kola seeds. *Journal of Agricultural Technology*. 5(2): 239-248.

Jayan, P. R., & Kumar, V. J. F. (2004). Planter design in relation to the physical properties of seeds. *Journal of Tropical Agriculture*. 42(1-2): 69-71.

Jotaki, T., & Tomita, Y. (1970). Performance characteristics of a rotary feeder. *Journal of Res Association of Powder Technology*. 7(6): 58-61.

Karayel, D., Wiesehoff, M., Ozmerzi, J., & Muller, J. (2006). Laboratory measurement of seed drill seed spacing and velocity of fall of seeds using high-speed camera system. *Computers and Electronics in Agriculture.* 50: 89-96.

Kessel, S. R. (1985). The Interaction between Rotary Valves and Pneumatic Conveying Pipelines. PhD Thesis. London, England: School of Engineering Thames Polytechnic.

Kim, K. U. & Ryu, I. H. (1998). Design of roller type metering device for precision planting. *American Society of Agricultural Engineers.* 41(4): 923-930.

Kraus, M. N. (1980). *Pneumatic conveying of bulk materials.* 2nd ed. New York, N. Y.: McGraw-Hill Publications Co.

LabVIEW (Software) (2008). Austin, Texas, United States: National Instruments Corporation.

Maleki, M. R., Jafari, J. F., Raufat, M. H., Mouazen A. M., & De Baerdemaeker, J. (2006a). Evaluation of seed distribution uniformity of a multi-flight auger as a grain drill metering device. *Biosystems Engineering*. 94(4): 535-543.

Maleki, M. R., Mouazen, A. M, De Ketelaere, B, & De Baerdemaeker, J. (2006b). A new index for seed distribution uniformity evaluation of grain drills. *Biosystems Engineering*. 94(3): 471-475.

Masoumi, A. A. & Tabil, L. (2003). Physical properties of chickpea (*C. arietinum*) cultivars. ASAE Paper No. 036058. St. Joseph, Mich.: ASAE.

The MathWorks, Inc. (2014). *Support: Documentation: Statistics and Machine Learning Toolbox*. Retrieved from The MathWorks Inc. Website: http://www.mathworks.com/help/stats/index.html.

MATLAB (Software) (2014). Natick, Massachusetts, United States: The MathWorks Inc.

Mayerle, D. J. (2006). Equalizing meter device. U.S. Patent No. 7,100,522 B2.

MDrive 42 Ethernet TCP/IP Configurator (Software) (2009). Marlborough, Connecticut, United States: Schneider Electric Motion USA Retrieved from the Schneider Electric Motion USA Website: http://motion.schneider-electric.com/lmd/lexium-mdrive-software.php.

Mohsenin, N. N. (1986). *Physical properties of plant and animal material: structure, physical characteristics and mechanical properties*. 2nd ed. Amsterdam, Netherlands: Gordon and Breach Science Publisher Inc.

Navid, H., Ebrahimian, S., Gassemzadeh, H. R., & Mousavi nia, M. J. (2011). Laboratory evaluation of seed metering device using image processing method. *Australian Journal of Agricultural Engineering*, 2 (1), 1-4.

NIST/SEMATECH (2012). *e-Handbook of Statistical Methods*. Retrieved August 2015 from NIST/SEMATECH of the U.S. Department of Commerce Website: http://www.itl.nist.gov/div898/handbook/eda/section3/eda35a.htm..

Point Grey Research Inc. (2012). *Cameras: Legacy Products: Dragonfly: Product Datasheet*. Retrieved from Point Grey Research Inc. Website: http://www.ptgrey.com/products/legacy.asp?product=Discontinued.

Point Grey Research Inc. (2014). *Cameras: IEEE 1394: Dragonfly2*. Retrieved September 2014, from Point Grey Research Inc. Website: http://ww2.ptgrey.com/IEEE-1394/dragonfly-2.

R Development Core Team (2012). *R: A language and environment for statistical computing*. R Foundation for Statistical Computing, Vienna, Austria. ISBN 3-900051-07-0, URL http://www.R-project.org/.

Razavi, S. M. A., Yeganehzad, S., & Sadeghi, A., (2009). Moisture dependent physical properties of canola seeds. *Journal of Agricultural Science and Technol*ogy. 11: 309-322.

Reed, A. R., (1978). The effect of adverse air pressure difference on the performance of a rotary valve used for the flow control of bulk materials. PhD Thesis. London, England: School of Engineering Thames Polytechnic.

Singh, N., Kaur, N., Rana, C. R., Singh, N., & Sharma, S. K., (2010). Diversity in seed and flour properties in field pea (*Pisum sativum*) germplasm. *Food Chemistry.* 122: 518-525.

SolidWorks (Software) (2010). Velizy, France: Dassault Systemes SolidWorks Corp.

Stroshine, R. (1998). *Physical Properties of Agricultural Materials and Food Products.* West Lafayette, IN: Copy Cat.

APPENDIX A . METER ROLLER DESIGN AND TESTING SPECIFICATIONS

During the design of the meter rollers and experimental procedure development there was a number of parameters (critical roller speed, meter roller testing speeds, camera frame rates, etc.) calculated for each roller and populated into lists. This section of the appendix will display the lists of test parameters and necessary equations used for calculation.

Table A-1: Meter roller labels, testing order, and testing speeds.

Roller #	Rep 1 and 2 Testing Order	Roller Speed (RPM)			fPFL Ratio
	Meter Roller Label	min	med	max	
1	6F_medR2_maxPHI_0deg	25.07	31.47	37.86	11
2	10F_maxR2_minPHI_54deg	33.97	42.63	51.29	11
3	15F_minR2_maxPHI_24deg	35.17	44.14	53.10	11
4	6F_minR2_medPHI_90deg	20.05	25.17	30.28	11
5	10F_medR2_maxPHI_36deg	28.98	36.37	43.76	11
6	15F_minR2_minPHI_0deg	36.58	45.91	55.24	11
7	6F_maxR2_minPHI_60deg	35.10	44.05	53.00	11
8	10F_minR2_medPHI_0deg	26.67	33.48	40.28	11
9	15F_maxR2_medPHI_36deg	40.77	51.17	61.56	11
10	6F_minR2_minPHI_0deg	19.27	24.18	29.10	11
11	10F_maxR2_medPHI_54deg	35.91	45.06	54.22	11
12	15F_medR2_medPHI_24deg	39.13	49.11	59.08	11
13	6F_maxR2_maxPHI_60deg	34.33	43.08	51.83	11
14	10F_medR2_minPHI_0deg	28.66	35.97	43.28	11
15	15F_medR2_maxPHI_36deg	36.48	45.78	55.08	11
16	6F_medR2_medPHI_90deg	26.07	32.72	39.36	11
17	10F_minR2_maxPHI_54deg	25.22	31.65	38.08	11
18	15F_maxR2_minPHI_24deg	39.49	49.55	59.62	11
19	6F_medR2_minPHI_60deg	23.93	30.04	36.14	11
20	10F_medR2_medPHI_0deg	30.54	38.32	46.11	11
21	15F_minR2_medPHI_36deg	37.68	47.29	56.90	11
22	6F_minR2_maxPHI_90deg	19.11	23.98	28.85	11
23	10F_minR2_minPHI_54deg	25.63	32.17	38.70	11
24	15F_maxR2_maxPHI_0deg	37.95	47.63	57.31	11
25	6F_maxR2_medPHI_0deg	35.27	44.26	53.25	11
26	10F_maxR2_maxPHI_36deg	34.14	42.85	51.56	11

27	15F_medR2_minPHI_36deg	37.91	47.58	57.25	11
28	6F_medR2_maxPHI_90deg	25.07	31.47	37.86	11
29	10F_maxR2_minPHI_0deg	33.97	42.63	51.29	11
30	15F_minR2_maxPHI_36deg	35.17	44.14	53.10	11
31	6F_minR2_medPHI_60deg	20.05	25.17	30.28	11
32	10F_medR2_maxPHI_54deg	28.98	36.37	43.76	11
33	15F_minR2_minPHI_36deg	36.58	45.91	55.24	11
34	6F_maxR2_minPHI_0deg	35.10	44.05	53.00	11
35	10F_medR2_medPhi_54deg	30.54	38.32	46.11	11
36	15F_maxR2_maxPHI_24deg	37.95	47.63	57.31	11
37	6F_medR2_minPHI_90deg	23.93	30.04	36.14	11
38	10F_minR2_minPHI_0deg	25.63	32.17	38.70	11
39	15F_maxR2_minPHI_0deg	39.49	49.55	59.62	11
40	6F_minR2_maxPHI_60deg	19.11	23.98	28.85	11
41	10F_minR2_maxPHI_36deg	25.22	31.65	38.08	11
42	15F_minR2_medPHI_0deg	37.68	47.29	56.90	11
43	6F_medR2_medPHI_60deg	26.07	32.72	39.36	11
44	10F_minR2_medPHI_54deg	26.67	33.48	40.28	11
45	15F_medR2_medPHI_0deg	39.13	49.11	59.08	11
46	6F_minR2_minPHI_90deg	19.27	24.18	29.10	11
47	10F_medR2_minPHI_36deg	28.66	35.97	43.28	11
48	15F_maxR2_medPHI_24deg	40.77	51.17	61.56	11
49	6F_maxR2_maxPHI_0deg	34.33	43.08	51.83	11
50	10F_maxR2_medPHI_36deg	35.91	45.06	54.22	11
51	15F_medR2_maxPHI_24deg	36.48	45.78	55.08	11
52	6F_maxR2_medPHI_60deg	35.27	44.26	53.25	11
53	10F_maxR2_maxPHI_0deg	34.14	42.85	51.56	11
54	15F_medR2_minPHI_24deg	37.91	47.58	57.25	11
55	6F_maxR2_minPHI_90deg	35.10	44.05	53.00	11
56	10F_medR2_maxPHI_0deg	28.98	36.37	43.76	11
57	15F_medR2_medPHI_36deg	39.13	49.11	59.08	11
58	6F_medR2_minPHI_0deg	23.93	30.04	36.14	11
59	10F_minR2_medPHI_36deg	26.67	33.48	40.28	11
60	15F_maxR2_maxPHI_36deg	37.95	47.63	57.31	11
61	6F_medR2_medPHI_0deg	26.07	32.72	39.36	11
62	10F_maxR2_maxPHI_54deg	34.14	42.85	51.56	11
63	15F_minR2_minPHI_24deg	36.58	45.91	55.24	11
64	6F_medR2_maxPHI_60deg	25.07	31.47	37.86	11
65	10F_medR2_medPHI_36deg	30.54	38.32	46.11	11

66	15F_medR2_maxPHI_0deg	36.48	45.78	55.08	11
67	6F_minR2_maxPHI_0deg	19.11	23.98	28.85	11
68	10F_maxR2_medPHI_0deg	35.91	45.06	54.22	11
69	15F_medR2_minPHI_0deg	37.91	47.58	57.25	11
70	6F_minR2_minPHI_60deg	19.27	24.18	29.10	11
71	10F_maxR2_minPHI_36deg	33.97	42.63	51.29	11
72	15F_maxR2_minPHI_36deg	39.49	49.55	59.62	11
73	6F_maxR2_medPHI_90deg	35.27	44.26	53.25	11
74	10F_minR2_maxPHI_0deg	25.22	31.65	38.08	11
75	15F_maxR2_medPHI_0deg	40.77	51.17	61.56	11
76	6F_maxR2_maxPHI_90deg	34.33	43.08	51.83	11
77	10F_minR2_minPHI_36deg	25.63	32.17	38.70	11
78	15F_minR2_maxPHI_0deg	35.17	44.14	53.10	11
79	6F_minR2_medPHI_0deg	20.05	25.17	30.28	11
80	10F_medR2_minPHI_54deg	28.66	35.97	43.28	11
81	15F_minR2_medPHI_24deg	37.68	47.29	56.90	11

Table A-2 shows the critical roller speed as defined by equation 5-5 (Reed, 1985). The critical meter roller speed was used as an upper level limit of the meter roller speed to test at to ensure that a linear throughput is maintained as roller speed increases.

Table A-2: Critical meter roller speed.

Flutes	**Critical Roller Speed, n_{crit} [RPM] (Reed)**				
	Parameter	***PHI (φ)***			
		Level	*min*	*med*	*max*
6F	***R2***	*min*	***49.6***	***50.7***	***49.4***
		med	***56.9***	***60.9***	***59.0***
		max	***81.3***	***81.7***	***79.4***
10F	***R2***	*min*	***60.0***	***62.1***	***59.2***
		med	***66.2***	***70.4***	***66.9***
		max	***78.5***	***83.3***	***78.9***
15F	***R2***	*min*	***85.0***	***87.7***	***81.5***
		med	***88.3***	***91.3***	***84.7***
		max	***92.2***	***95.4***	***88.4***

After the meter roller nomenclature had been developed, the second step was to sketch the 2D profile of the 6, 10, and 15-flute rollers. The goal of the 3D model template is to develop one single flute that is fully variable as the six main parameters are adjusted. Then this single flute can be mirrored multiple times to create the profile of a roller with the desired number of flutes. Starting with the known diameter of the roller (78.74 mm) and the known angle between each flute around the periphery of the roller (60° for a 6 flute roller, 36° for a 10 flute roller, and 24° for a 15 flute roller), secondary lines can be drawn to set the initial boundary of one flute. Referring back to the sketch of a single flute and its parameters in Figure 5-1 the flute depth is calculated to give the bottom boundary of the flute so another circle can be added of the appropriate diameter as it corresponds to one of the three levels of R_2. Once the bottom boundary of the flute is set then the angled walls of the flute are drawn as the well as fillet circles of a constant diameter that defines the profile of the flute. These fillet circles are constrained by a certain angular distance (φ) according to the parameters specified in Table 5-1. With the fillet circles constrained, the flute walls can also be constrained to never have less than a 10° angle with the vertical centerline separating the flutes on the template. The touch to the flute at this point is to set the fin width of 2.8mm which equates to 0.071 radians (4.08°). After ensuring that the model is fully constrained (lines are all black) then the template will look similar to Figure A-1.

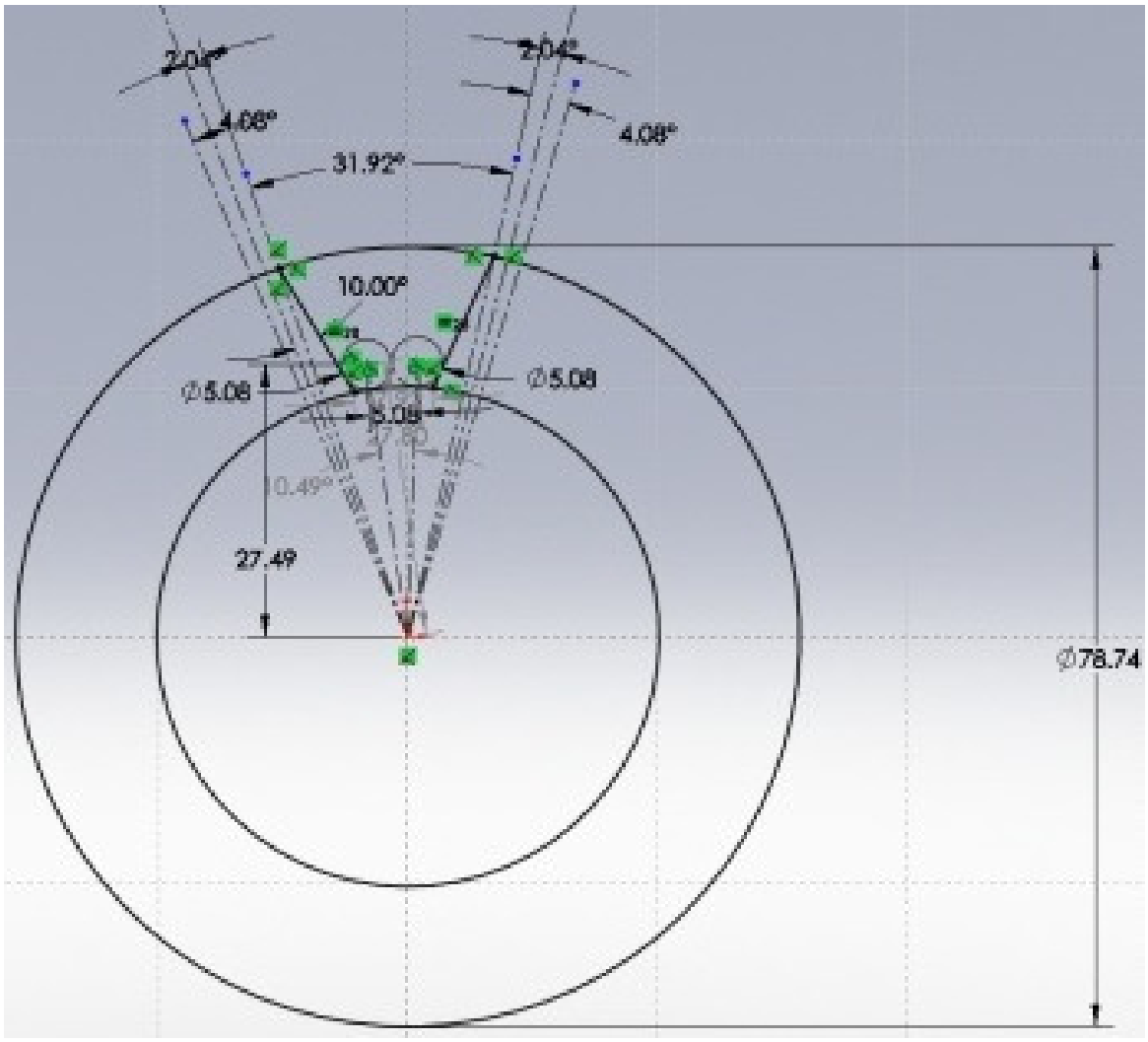

Figure A-1: Model template of the flute design on the rollers (*10F_minR2_maxPHI* shown).

At this point the flute template can be taken and mirrored around the periphery of the roller in the 3D CAD program to create the desired roller profile template. The flute shown above was done specifically for a 10 flute roller. Once the roller profile template is complete then a solid extrusion can be applied to create the 3D roller. At this point in the design a flute pitch can be assigned by incorporating a helical pattern to the extrusion. The final profile of the 10F_minR2_maxPHI_36deg roller after the pitch has been applied can be seen in Figure A-2.

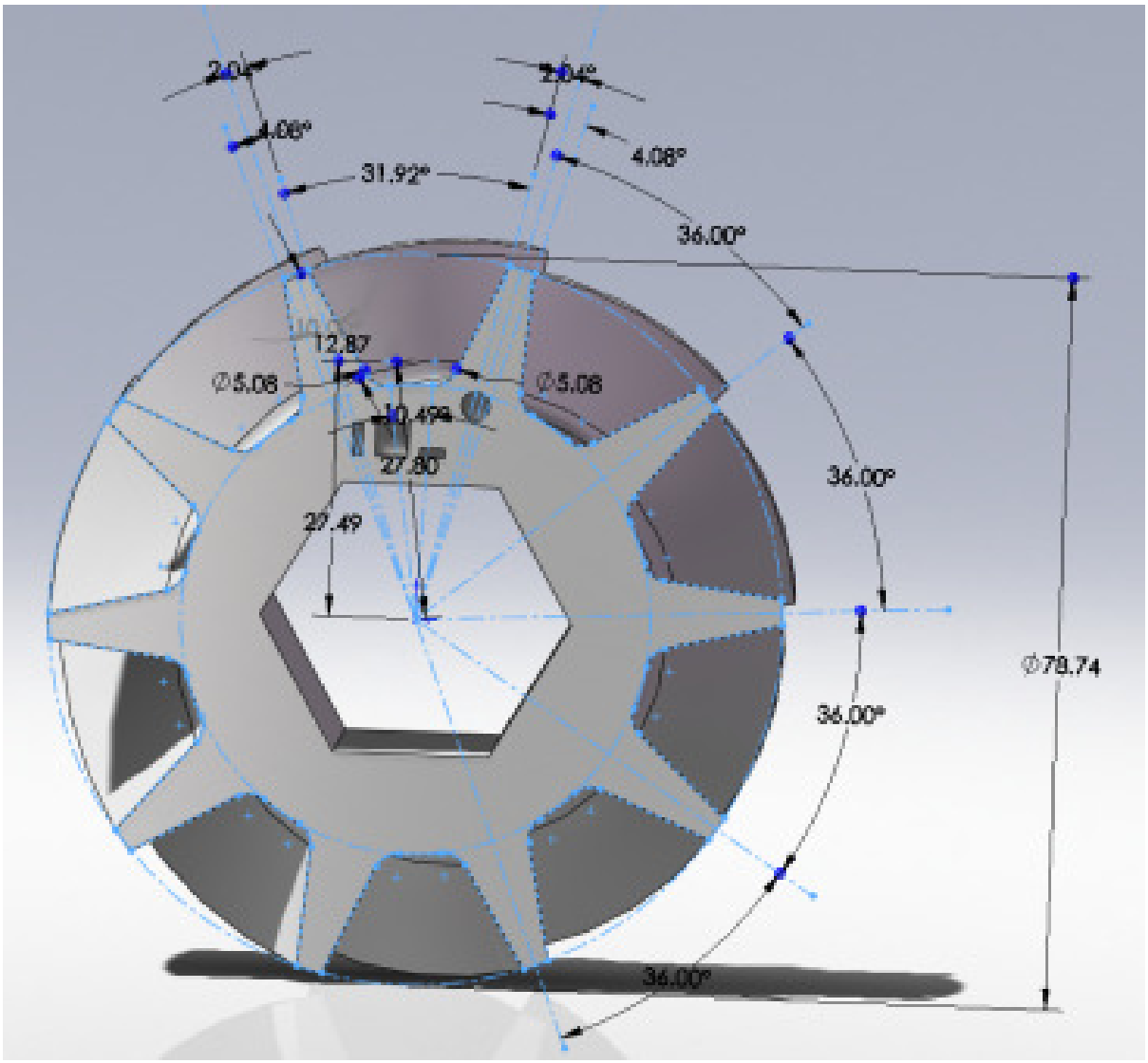

Figure A-2: Meter roller profile template with a flute pitch assigned (*10F_minR2_maxPHI_36deg* roller shown).

This approach can be applied to two thirds of the 81 rollers required. There is one special case that causes the profile of the flute to have a curved shape similar to the sketch in Figure 5-3. In this instance there are no fillet circles defining the shape of the profile and thus the angular distance of the fillets (φ) is effectively zero. Instead, one large circle is created to define the curved profile shape of the flute. The angle between flutes (flute wall boundary) and the flute depth (flute bottom boundary) are the same as the previous design discussed, but now a circle

will be drawn in to fit between the flute wall boundaries and the flute bottom boundary. Figure A-3 shows what the final meter roller profile looks like when a curved flute profile (φ=0) is incorporated.

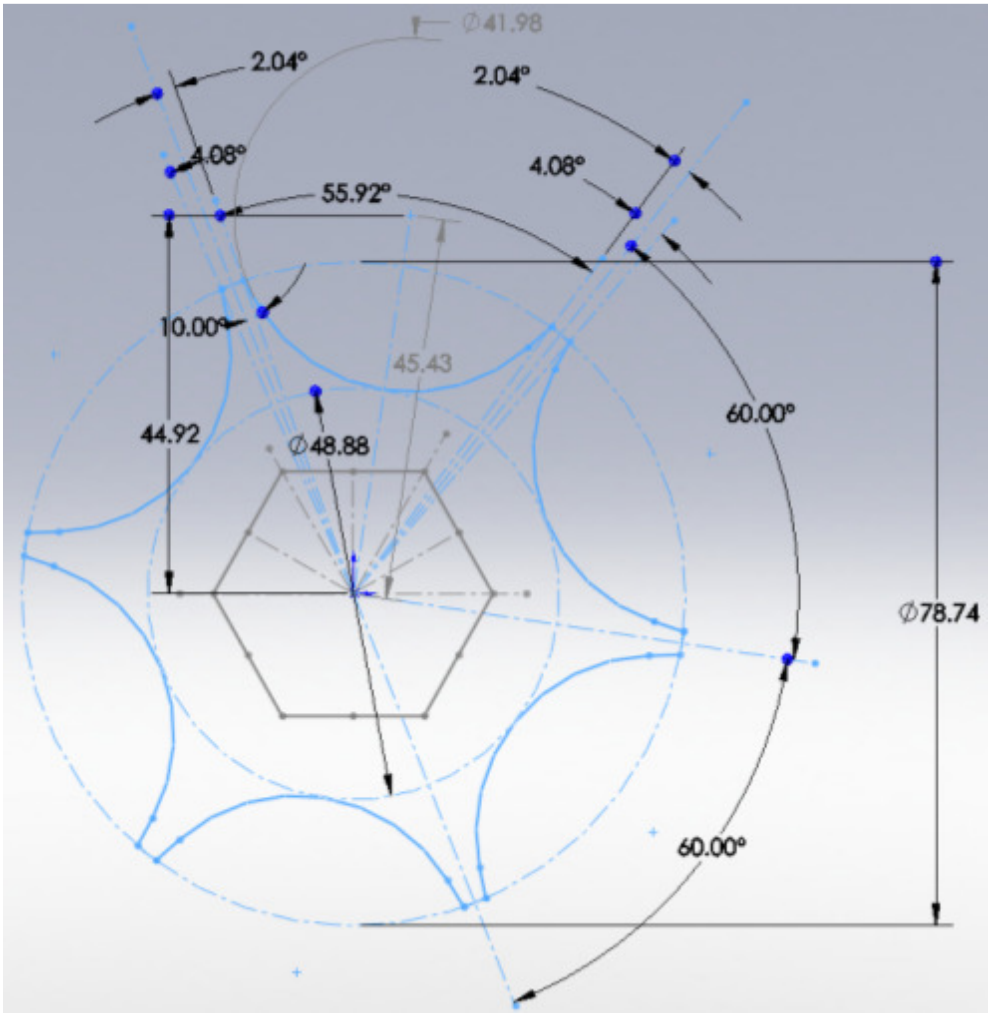

Figure A-3: Meter roller profile template with a curved flute profile (*6F_medR2_minPHI* shown).

Overall, there was a total six flute profile templates created in SolidWorks. One each for the 6, 10, and 15 flute rollers with the regular flute profile and then one each for the curved flute profile. Ensuring that the flute templates were fully constrained and incorporate governing parameters that make up the overall meter roller design was the most important aspect of this

exercise. After the flute templates were created they could be mirrored around the periphery of the roller to generate the meter roller profile template for each of the meter rollers designed.

APPENDIX B . STANDARD OPERATING PROCEDURES

Standard operating procedures for the air cart simulator operation and maintenance in the air handling lab at the University of Saskatchewan are described below.

B.1. Changing Meter Rollers on the Air Cart Simulator

The single run air cart apparatus 1 is the taller of the two tanks located in the air handling laboratory and is labeled as 'Air Cart Simulator". Figure B-1 clearly shows an image of the air cart assembly along with labels pointing out the main features of the setup.

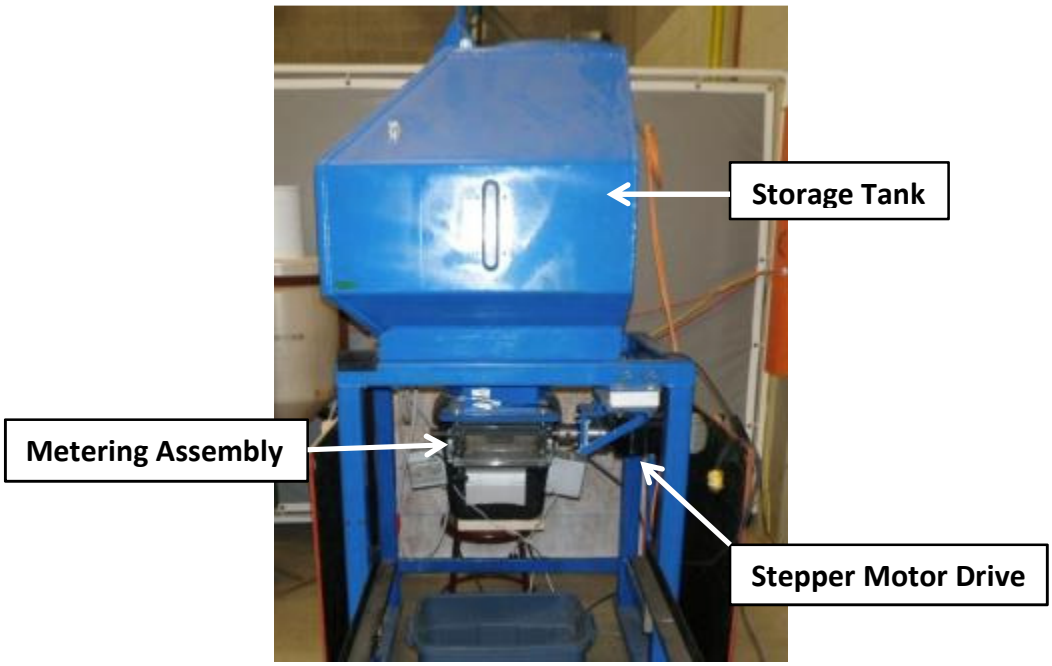

Figure B-1: Air cart simulator.

Changing meter rollers on the metering assembly underneath the tank is a relatively easy operation as it should be because of the frequent changes needed when evaluating various roller designs. The plastic or rubber meter roller profile, as seen in Figure B-2, is mounted on a steel shaft of the appropriate length so it will fit in the assembly. Also on the steel shaft are four bearings, 2 plastic blank sections, 4 plastic moldings that fit the bearings on the hexagonal shaft, 2 steel bearing covers, 2 steel cotter pins to hold everything in place, and 2 rubber end caps to

cover bearings and ensure a snug fit in the meter assembly. Each of these parts can be seen in Figure B-2. In this document, roller profiles refer to the individual roller segments and the meter roller refers to the full assembly of parts seen in Figure B-2.

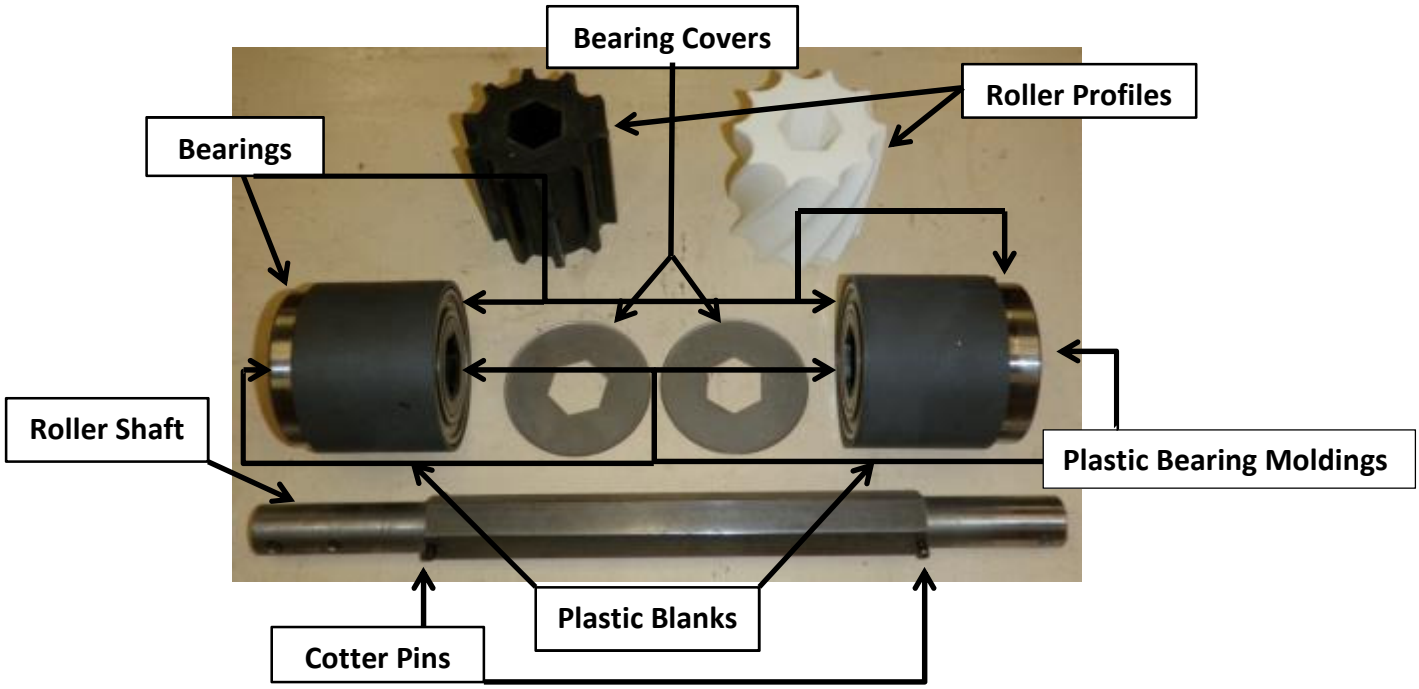

Figure B-2: Breakdown of meter roller parts (rubber end caps not shown).

This document will give step by step process of how to change the meter roller on the air cart simulator. This process assumes only one shaft is being used with multiple roller profiles to be mounted on the shaft for placement in the metering assembly. Therefore this process will also include how to replace the meter roller profiles on the shaft.

1. Ensure power to the stepper motor drive is disconnected either by unplugging the USB connection or unplugging the power cord. This just ensures the motor will not turn on you while your hands are in the metering assembly.

2. Ensure that the tank is either empty of product or the tank shutoff slide is in place. The shutoff slide is slid in the appropriate grooves between the metering assembly and the storage tank opposite the motor drive side of the apparatus. If the slide is not in place then product will come streaming out as soon as you swing open the assembly. See Figure B-5 for placement of the shutoff slide.

3. Undo the two assembly clamps while holding the assembly up in place so it does not come swinging down when the clamps are undone. See Figure B-3 for location of the assembly clamps.

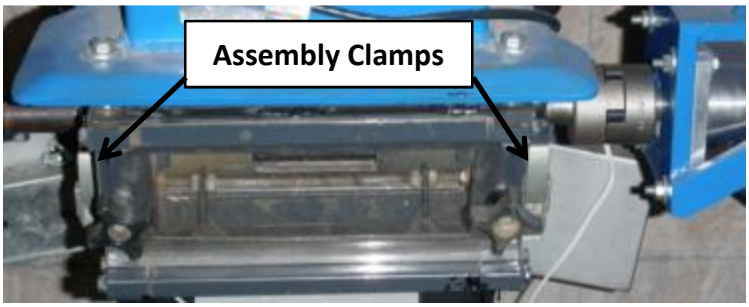

Figure B-3: Metering assembly clamps.

4. After the two clamps are undone and while you are still holding the assembly up, grab the end of the roller shaft with one hand and hold it up into position. Note: This shaft only weighs about 5 pounds. While holding on to one end of the shaft, swing the meter assembly down and out of the way.

5. With the assembly swung out of the way, the roller can be pulled out of the lovejoy coupler that joins it to the stepper motor drive. The easiest way to uncouple the roller is to first lower the far end of the roller enough so it is clearing the grooves of the assembly then pull away gently. Note: Ensure rubber coupler fitting remains on the drive end. Figure B-4 and Figure B-5 show the uncoupling of the lovejoy coupler and a view of the assembly with the roller pulled out of operating position.

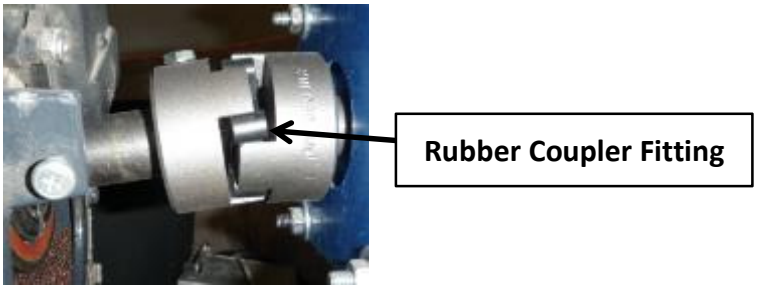

Figure B-4: Coupling and uncoupling the lovejoy coupler from the stepper motor drive when removing and installing a meter roller in the metering assembly.

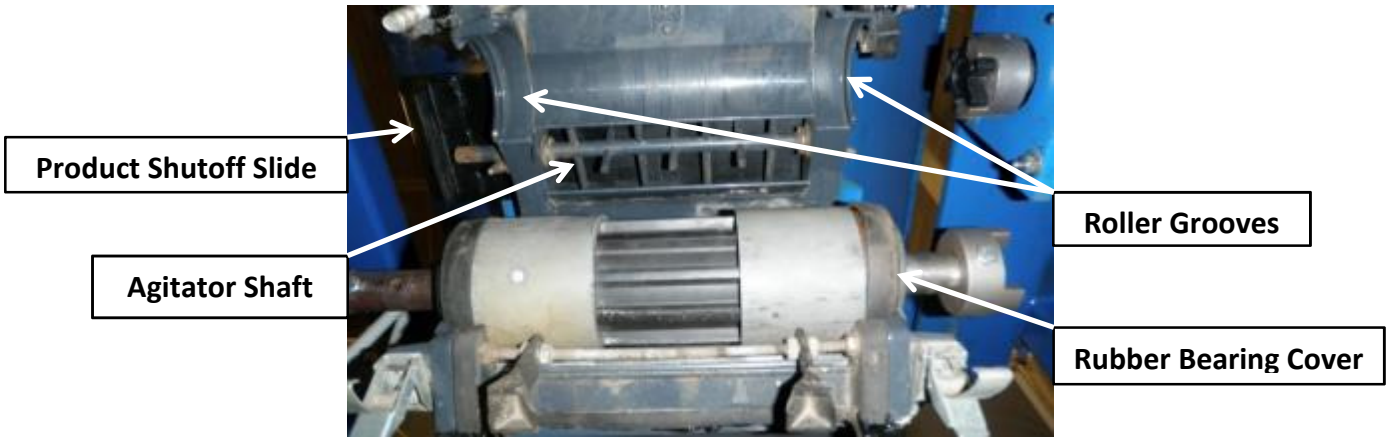

Figure B-5: Bottom view of opened metering assembly with the meter roller pulled out.

6. The meter roller can be pulled away and placed on a sturdy workbench for removal of the roller profile. The following, steps a to f, is the general process to follow when changing the meter roller profile segment.

    a. Using the appropriate size of wrench, unscrew the bolt or allan key out of the lovejoy coupler so you can slide the coupler off of the shaft.

    b. Slide rubber bearing covers off the end of the roller.

    c. Using a punch of the appropriate size and a hammer, tap out the cotter pin on the end the lovejoy coupler was pulled off. Note: It is possible to tap the opposite cotter pin out and slide pieces off the opposite way but typically there will be a plastic lobe bolted on that end of the shaft that triggers an agitator arm when the roller is in operation. The lobe is not pictured in any figures but the agitator shaft can be seen in Figure B-5.

    d. With the cotter pin out, the bearings, plastic bearing mold, plastic blank section, steel bearing cover and roller profile segment can be slid off of the shaft. Ensure the materials are pulled with an evenly distributed force or pieces will jam and feel as if they are stuck. Note: when pulling the plastic blank section off, there will be a bearing stuck in each end of it with the plastic bearing mold inserted in each bearing. Some of the bearings may not fit snug in the blank section so they could be pulled out separately. Figure B-6 shows what the roller will look like after this stage of the changeover. Refer to Figure B-2 for identification of specific parts.

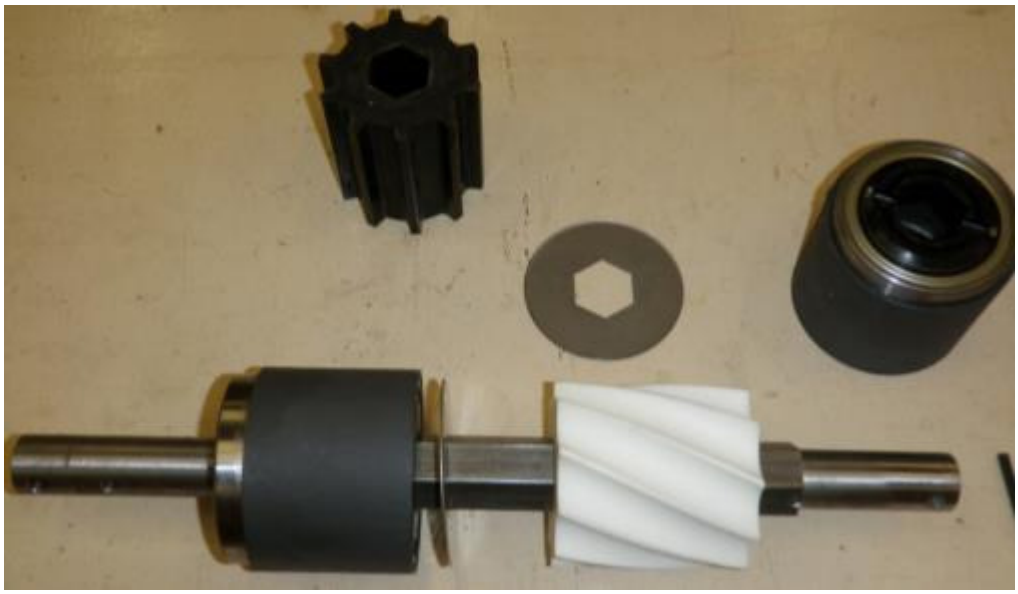

Figure B-6: Disassembling the meter roller to replace the meter roller profile segment on the meter roller shaft.

e. The new roller profile segment can be slid onto the shaft now. Ensure that a bearing cover is in place before sliding the new segment on.

f. Next the plastic blanks with the bearings and bearing moldings can be slid on so that the groove on the bearing molding lines up with the hole on the shaft for the cotter pin to be punched back into place. Once everything is slid onto the shaft, the rubber bearing covers can be slid on each end of the roller so it is ready to be placed back in the metering assembly. Refer to Figure B-5 which shows the roller with rubber bearing covers and the lovejoy coupler fastened to the shaft ready for placement in the metering assembly.

7. The roller is now ready for placement back in to the metering assembly. The best way to do this is to first connect the lovejoy couplers, as seen in Figure B-4, and push the roller up into position so that the rubber bearing covers fit up into the grooves on the top of the metering assembly. Once the roller is in the grooves, the bottom half of the assembly can be swung up into place and clamped shut. One must also ensure that the grooves on the bottom half line up with the roller for a snug and even fit. Refer to Figure B-5 for a general schematic inside the metering assembly.

8. The meter roller is now ready for operation. The product slide that blocks off the hopper outlet into the metering assembly can be pulled open. If no slide is available, then product can be dumped into the hopper for metering. Note: the product slide is not a standard piece of hardware on the test stand. However, it is something was added to for easier roller changeover.

B.2. Running a Test to Measure Meter Roller Performance on the Air Cart Simulator

The air cart simulator test stand is located in the Air Handling Laboratory in the Hardy Lab at the University of Saskatchewan can be seen in Figure B-7 and will be referred to throughout this document. This document is to ensure the apparatus is operated properly for its intended use in the safest manner. A list of safety precautions and step-by-step approach to conducting a single test with the apparatus will be outlined in this document as well as a list of troubleshooting ideas.

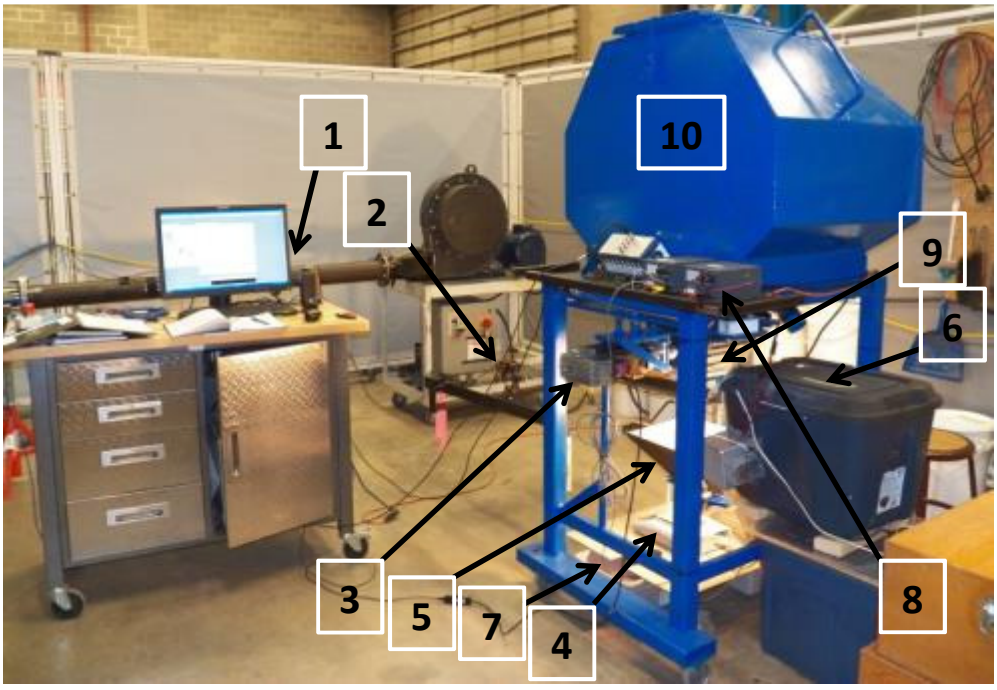

Figure B-7: Air cart simulator test stand.

Table B-1: Components that make up the air cart simulator.

1.	Computer Hub to Control the Test Rig Operation via LabVIEW
2.	High-Speed Camera
3.	Stepper Motor
4.	Precision Balance
5.	Hopper and Servo Assembly
6.	Diffuser Light Box
7.	Bulk Sample Region
8.	External Power Source Hub
9.	Metering Assembly
10.	Storage Tank

B.2.1. Safety Precautions

1. Safety glasses, hearing protection, dust mask, lab coats and gloves are available in the cabinet in the air handling laboratory and should be worn when required.

2. Watch for wires when working around the test rig.

3. Ensure work area is cleaned at the end of each day (vacuumed and swept) to keep any mice, gopher, and any other pests that may be attracted to leftover product.

4. The diffuser box may get very hot because of the lights required to give the uniform light source. Ensure that the cooling fans in the light compartments are on before each day (will hear a light hum).

5. Never look directly at the lights or put your hand inside of the diffuser box when the lights are on.

6. Vacuum inside diffuser box regularly to ensure dust does not collect in or around the light compartments.

7. Use the platform ladder to fill the storage tank and so not carry more than you can manage. As well do not carry more than the platform ladder is meant to handle (300 lbs total). See Figure B-8.

8. When walking around apparatus watch for bumping hazards, specifically the camera frame which has sharper edges that marked with fluorescent flags.

9. Watch for bumping hazards when working around or underneath the apparatus.

10. Hearing protection is only required when the fan is operating in the air handling lab. The fan is not required for these tests but there may be others in the area operating other test stands that require the fan.

11. In an emergency or power outage, disconnect the power to the system (particularly the lamps) before leaving the area in case the power was to come back on.

12. Ensure the power to the test rig is disconnected at the end of each day.

Figure B-8: Platform ladder for adding product to the storage tank.

B.2.2. Operating Procedure

A ‘Test’ in this document refers to one meter roller and one product at three roller speeds for two repetitions which makes up six cycles of the test program. One cycle is one repetition of one roller with one product at one meter roller speed. Therefore a single ‘test’ encompasses six cycles of the program.

1. Open up the test program titled ‘Roller Test Program Final_DEC2011.vi’. The LabVIEW program will appear on the screen as seen in Figure B-9. When the program is opened each block will be empty. Figure B-9 is set up already to run a test for roller 10F_medR2_medPHI_0deg with field peas.

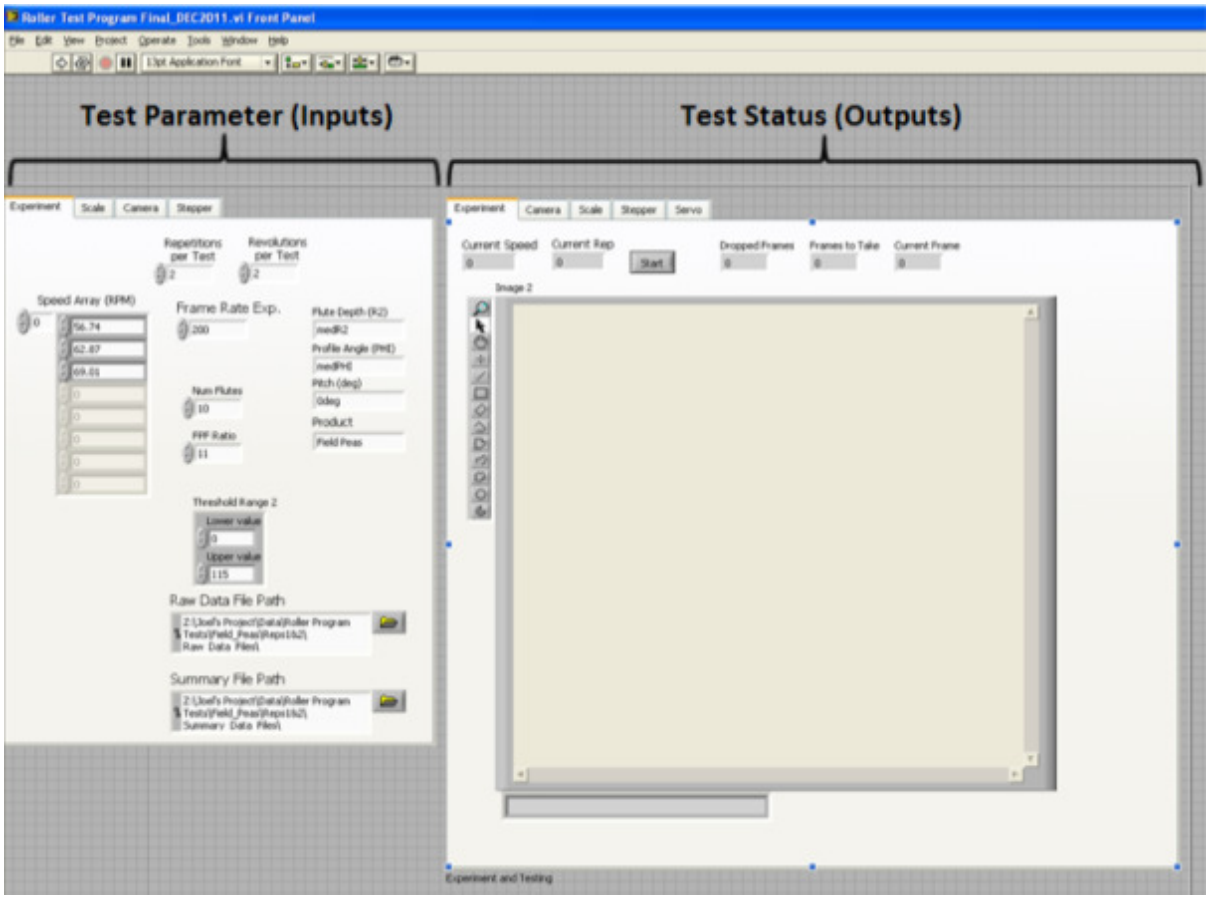

Figure B-9: LabVIEW test program home screen.

2. All of the blanks (blocks) in the test parameter must be set before you can proceed to the next step, especially the “Raw Data File Path” and “Summary File Path”. You must refer to the ‘Meter Roller Test Order’ list in Appendix C to input the proper test parameters. A quick description of each block on the home screen referring to Figure B-9 is as follows:

   Test Parameters (Inputs):

   a. Speed Array (RPM): Three input meter roller speeds to be tested.

   b. Repetitions Per Test: Sets the number of repetitions of each roller speed. Standard is 2.

   c. Revolutions Per Test: Sets the number of revolutions of data to be captured in each repetition. Standard is set at 2.

   d. Frame Rate Exp.: This does not need to be set for each test nor does it actually set anything for the test therefore it can be ignored.

   e. Num Flutes: Describes the number of flutes on the meter roller being tested. It is critical that this is set properly before each test or the data are invalid.

f. fPF Ratio: Describes the number of camera frames to be captured per flute (frame-per-flute ratio) of the meter roller. For each product tested every roller must be tested at the same fPF roller as outlined in the 'Meter Roller Test Order' list in Appendix A.

g. Flute Depth (R_2): Describes the depth of the flute on the roller being tested. There is only three levels of the R_2 value denoted minR_2, medR_2, and maxR_2. The numeric value corresponding to each R_2 value is defined in the 3D model of each roller. R_2 is a measurement from the center of the roller to the bottom of the flute, therefore minR_2 corresponds to the deepest (largest) flutes and maxR_2 corresponds to the shallowest (smallest) flutes. See Figure B-10.

h. Profile Angle (PHI): Describes the profile shape of the flute on each roller. There is only three levels of PHI denoted minPHI, medPHI, and maxPHI. The numeric value corresponding to each PHI value is also defined in the 3D model of each roller. PHI is a measurement of the angular distance between the fillets, R_1, that define the width and angle of each flute. Therefore, minPHI corresponds to 0 radians between the fillets and maxPHI corresponds to a maximum angular distance between fillets (different for rollers with different number of flutes) that defines the U-shape of the flutes. See Figure B-10.

i. Pitch (deg): Describes the pitch or angle of the spiral on the meter roller. There is only three levels pitch variations for each set of rollers. There is a minimum, medium, and maximum value depending on the number of flutes on a roller. 6 flute rollers will have 0, 60 and 90deg values; 10 flute rollers will have 0, 36 and 54deg values; 15 flute rollers will have 0, 24 and 36deg values. The minimum value corresponds to straight flutes, the medium value corresponds to a spiral that ensures when one flute is done emptying the next flute will begin dumping, the maximum value corresponds to a spiral 1.5 times that of the medium value. See Figure B-11 for an example of a 10 flute roller with a medium value (24 degrees) for the pitch.

j. Product: Describes what product is being tested.

k. Threshold Range: Sets the threshold limit on each image so that only the product is observed and specific calculations can be achieved on that image. Every test will have the same threshold range of 115 because the diffuser box will output uniform light in the background.

l. Raw Data File Path: Defines the file path that the raw data from each test is saved too. This must be manually changed before each test so previous data are not overwritten.

m. Summary File Path: Defines the file path that the summary data from each test is saved too.

Test Status (Outputs):

n. Current Speed: Displays what roller speed is being tested at that moment.

o. Current Rep: Displays what repetition the current speed is operating.

p. "START": The button the starts the test (6 cycles of the program).

q. Dropped Frames: Informs the user if any frames were dropped from the test. May suggest an issue with the test (see troubleshooting section).

r. Frame to take: Display the number of frames the camera will take on the specific repetition. The number displayed is determined from the number of flutes, fPFL ratio, and the number of revolutions defined in the test parameters.

s. Current frame: Displays an instantaneous update of exactly what frame is being captured during a test.

t. Image 2: After a repetition is complete all of the images will quickly cycle through as a quick check to make sure the images were captured.

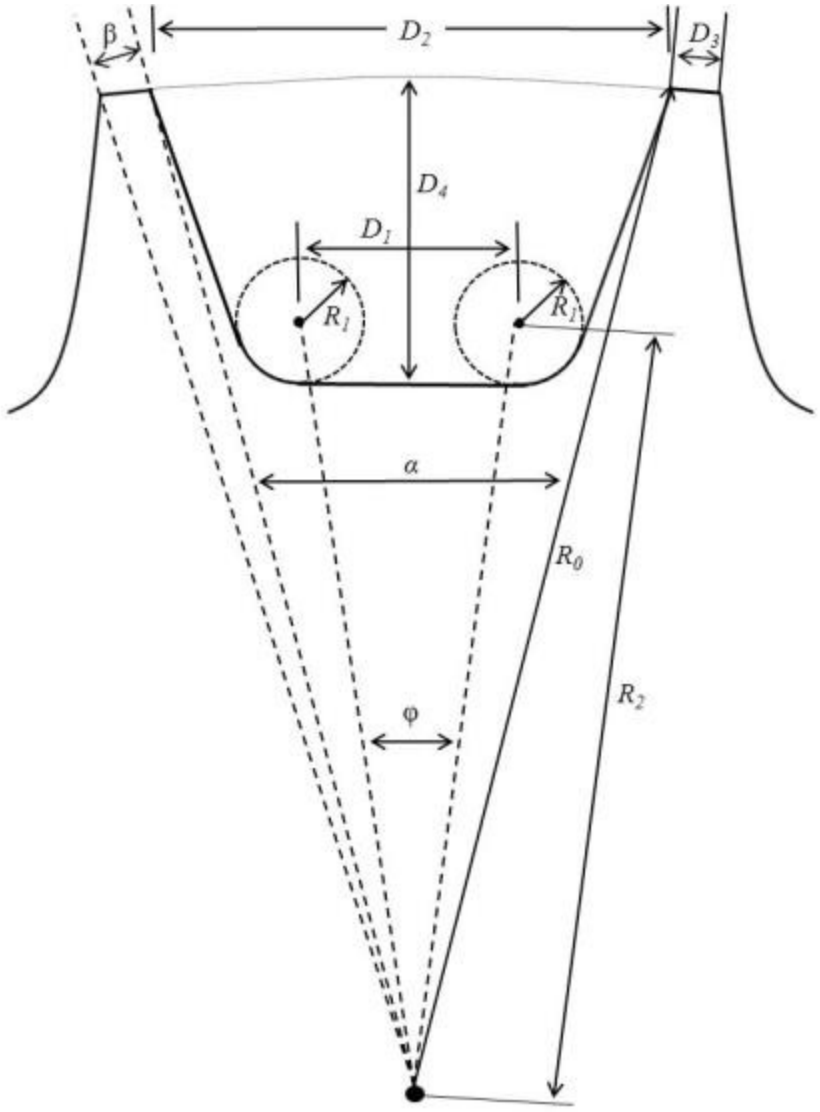

Figure B-10: Schematic of the parameters that describe a flute on a meter roller

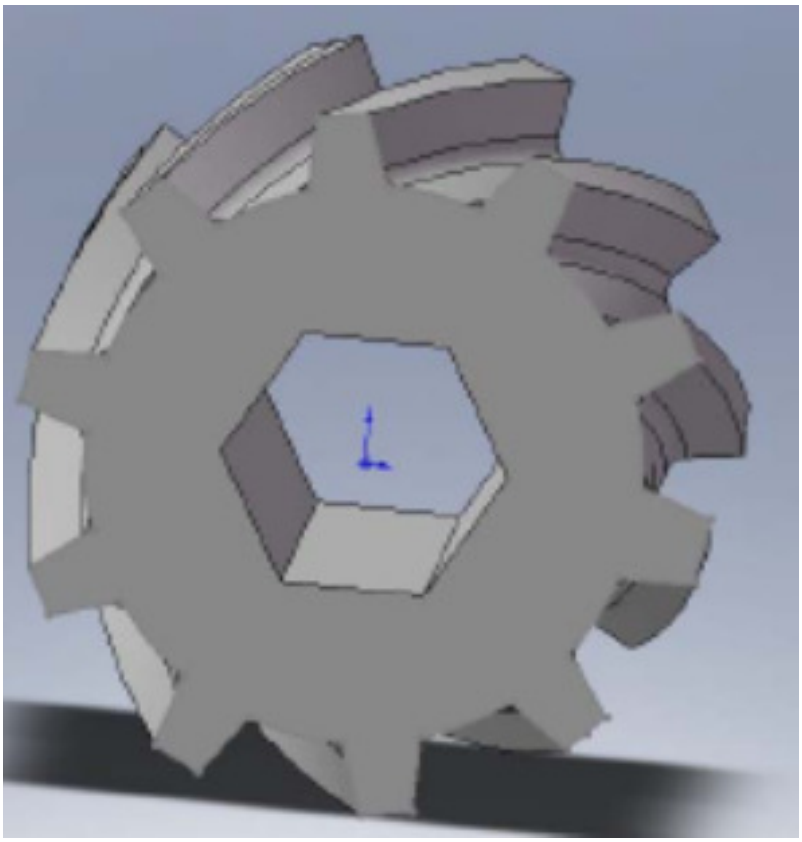

Figure B-11: 10-flute roller with a medium pitch (PR of 1).

3. With the roller in the metering assembly, the hopper placed under the assembly on the precision balance, and product cutoff slide open (see SOP for Changing Meter Rollers) the arrow at the top left of the screen can be clicked to initiate the program. Now you will be able to cycle through each of tabs on the input and output side of the program to check if each function is operating (not necessary each time but is good to do at the start of each day). At this time it is necessary to go to the "Stepper" tab on both sides (Input and Output side). See Figure B-12 to see what will appear when both "Stepper" tabs are selected. Now input a roller speed in RPM. Typically 10 RPM is good enough. Press "START" and leave for 10 seconds. The roller will turn at 10 RPM for 10 seconds to prime the meter roller with product. After about 10 seconds hit "STOP". The meter roller is now primed.

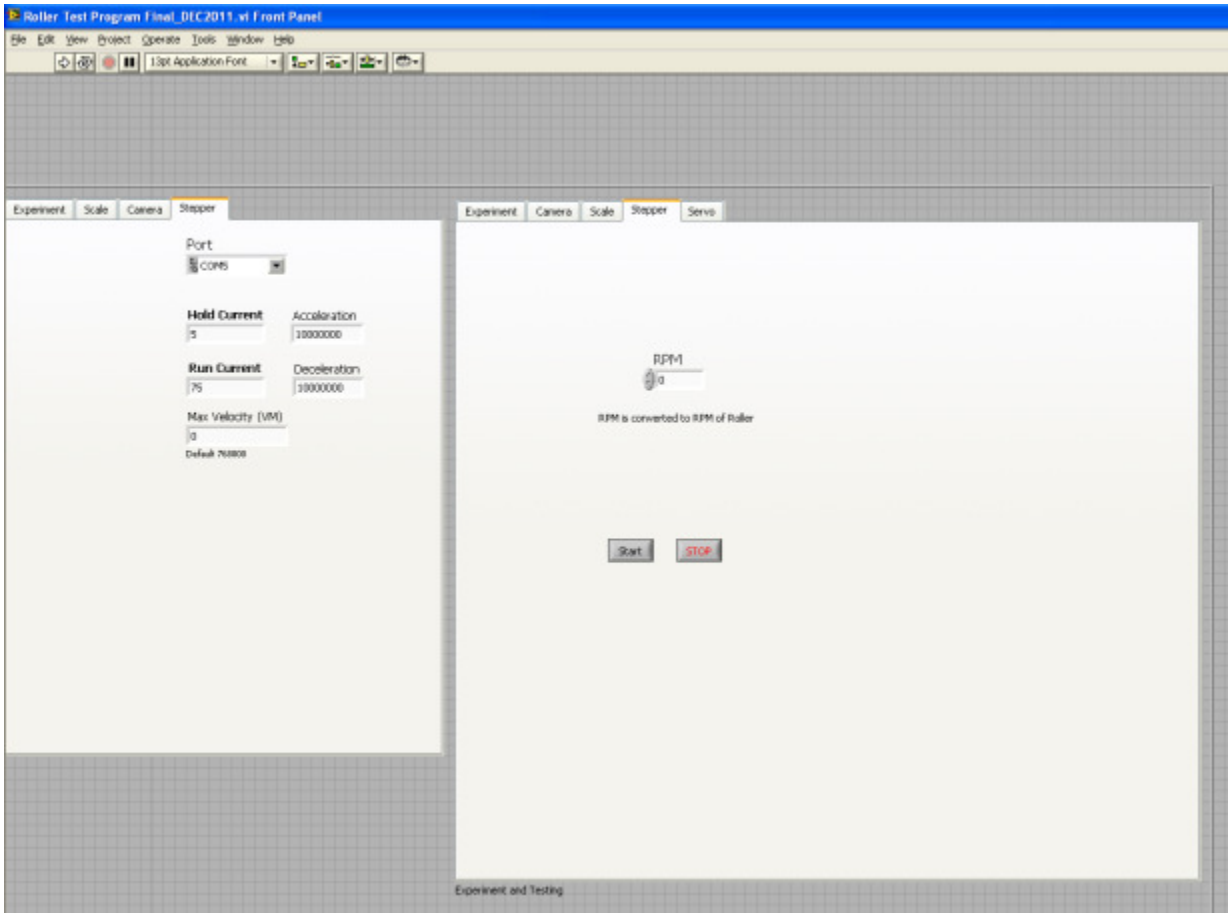

Figure B-12: Home screen when the "Stepper" tab is selected.

4. Now select the “Camera” tab on both sides. See Figure B-13 for a view of the home screen when the “Camera” tabs are selected. No settings have to be adjusted on this screen. Leaving the threshold tab on the bottom right unselected you can hit the “START” button at the bottom. Note: if this is the first time of the day that you are checking the camera you will hit “START” then “STOP” and then “START” again for the camera image to show up on the screen. After you hit “START” the image of the opening on the diffuser will appear on the screen. You should not see any black images encroaching around the edge of the image. If there is any black images observed around the edge of the image you must adjust the diffuser box so it is centered. It may have been bumped (or the test rig was moved slightly) to cause it image not to be centered anymore. If you adjust the diffuser box a quick check to make sure the roller is centered should also be done. Holding a piece of paper underneath the roller that shows where the meter roller boundaries would be so it shows up on the camera. If the image is centered you must hit “STOP” now. This step should be done before each test to ensure the image is centered with the diffuser box opening and the product that will come off the roller.

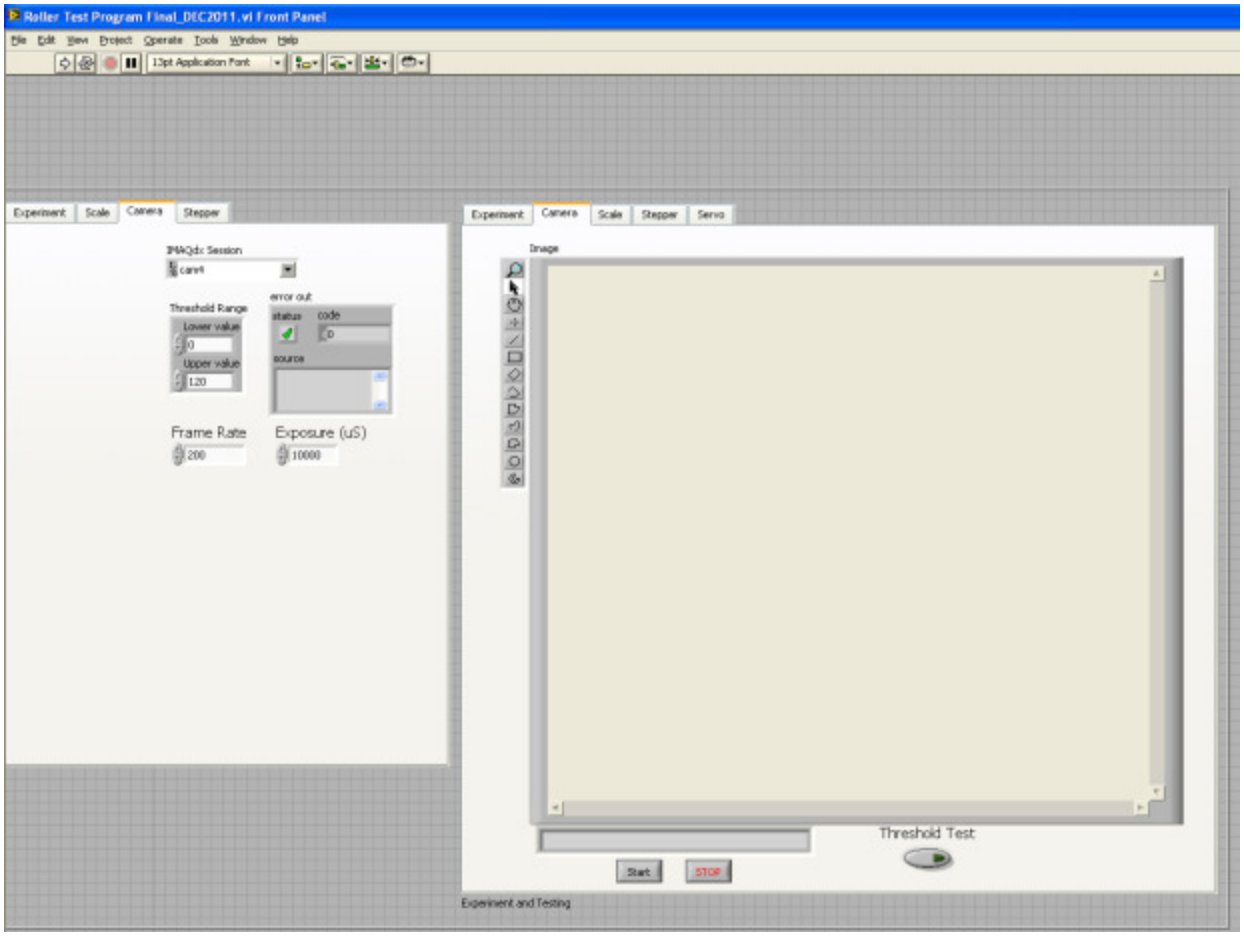

Figure B-13: Home screen when the "Camera" tab is selected.

5. After priming the roller and testing the camera, click the stop button (red stop sign along the top of the home screen). Click on both the “Experiment” tabs and double-check the test parameters for the meter roller and product about to be tested. Once it’s verified the test parameters are correct, the initialization arrow along the top of the screen can be pushed followed by pushing the “START” button. The test has now begun. One test goes through six cycles of the program. One cycle of the program goes through the following steps:

    a. Is the precision balance stable? If "NO" wait 10 seconds, if "YES" continue.

    b. Close shutter at the bottom of hopper.

    c. Tare the balance.

    d. Start the roller, two revolutions at the set roller speed. There is an at least half a revolution before the camera starts to allow for acceleration product to full fall.

    e. The camera starts when the roller is up to speed and grabs a set amount of images set out by the test parameters.

f. As soon as the camera is done grabbing the images the rollers stops turning.

g. Wait 10 seconds for the balance to stabilize then grab the mass.

h. Open the shutter to empty product out of the hopper into the bulk sample region.

i. The program cycles through all the images, analyses and records the data.

j. This is the end of one cycle. The program cycles back up to step (a).

6. While a test is operating, the following roller to be tested can be prepared on the side. Refer to the standard operating procedure for changing meter rollers on the air cart simulator for how to change the roller segment.

7. When the test program is done going through the six cycles you can click the stop button (red stop sign along the top).

8. Go to the "Raw Data File Path" and "Summary Data Path" Tab and change the name of the file to the next roller. This ensures that if you were to accidently hit start again you will not overwrite the data you just collected.

9. Go into the data file saved on the computer, open it up, copy the data (should be 6 rows of data) and paste it into a "Compiled Summary" file where all the data from every roller (81 in total) from that particular product will be saved. The "Compiled Summary" file is one that is created and updated by the user and not by the LabVIEW test program. It is a way for the user to continually check the data after every test and locate it all in one file where the test program saves each test in their own separate files.

10. Walk around to the side (opposite the external power source hub) and close the product cutoff slide. When some of the larger products like field peas or chickpeas are in the metering assembly the slide may be difficult to close so a hammer may be needed to get the slide started. Make sure the slide is closed all of the way. It will feel very solid when closed all the way.

Figure B-14: View of product being metered into the hopper and down the slide into the product catchment during step11.

11. Go back to the computer and hit the start arrow at the top of the screen (NOTE: ensure the file name has been changed from the test you just completed to the name of the next roller you plan to test). Engage both of the "Stepper" tabs on the home screen and press "START" (Figure B-12) to start the meter roller. Set the speed to whatever you want, 10 to 20 RPM works best. Let the roller meter until the product flow is minimal or almost nothing. This step cleans the product out of the metering assembly so there is minimal product spillage on the next steps. See Figure B-14 for a view of product coming out of the roller and out the hopper.

12. When product has stopped flowing out of the assembly hit "Stop" (Figure B-12).

13. Step over the camera frame and sit in front of the metering assembly. Setting the white tray on top of the hopper underneath the metering assembly to catch any excess product, you can continue with changing the meter roller out (See standard operating procedure for changing meter rollers on the air cart simulator). Ensure the when you undo the two clips on the metering assembly to have one hand supporting the assembly and roller so it does not come shooting open and spill product all over the floor.

14. When the next roller is up in place, clear any obstructions from in front of the camera and step out of the frame and pull the product cutoff slide open to let the assembly fill with product for the next test. There is no need to pull the product slide right out of the assembly, just enough to ensure product is reaching the roller.

15. Go back to the computer and press "START" on the stepper scree to turn the roller on for about 10 seconds to prime it. Hit "Stop" after the 10 seconds.

16. Go back to Step 4.

B.2.3. Troubleshooting

This section presents a list of possible issues that may occur during operation as well as a potential fix to get rid of the error and a reason why the error may have occurred.

APPENDIX C . METER TESTING AND STATISTICAL ANALYSIS RESULTS

Analysis of the raw data collected required a lot of coding in R, Matlab, and Excel as well as a lot of figures and graphs generated. The majority of this information is not displayed in the thesis but may be beneficial for further understanding. Anything displayed in this appendix has been noted or referred to in the body of the thesis.

Raw data from test to establish lower sampling limits in Chapter 4:

The data from this test was summarized in the body of the thesis, however it is important to have the raw data results summarized from each camera rate tested. The camera rates tested here were limited by the camera itself but it was sufficient enough to evaluate the lower sampling limit of the test method. The raw data shown here is a summary of each test of the canola and wheat tests captured with a fine and extra coarse roller. The data in tables…..were used to create Figure 4-5 and Figure 4-6 and the raw data used to summarize Table C-1 was used to create Figure 4-7 in explaining the anomaly at 12 fps (14.4 fPFL). The raw data points that make up Tables C-1 to C-4 was not placed in the appendix because with the large amount of data captured it made more sense to summarize.

Table C-1: Canola tested with an extra coarse roller at increasing frame rates to locate a lower sampling limit for the continuous test method. The extra coarse roller with canola showed one anomaly at 12 fps that was discussed in the body of the thesis.

Frame Rate (fps)	Rep 1			Rep 2			Rep 3			Total Avg. CV
	STDV	CV	Avg. Area-per-Frame	STDV	CV	Avg. Area-per-Frame	STDV	CV	Avg. Area-per-Frame	
1	1.90	28.9	6.60	1.71	24.9	6.86	1.87	29.3	6.37	27.7
2	1.79	29.0	6.17	2.16	32.6	6.62	1.79	28.5	6.27	30.1
3	1.82	29.0	6.29	1.95	30.5	6.38	1.87	30.3	6.19	29.9
4	1.81	29.9	6.04	1.85	28.6	6.48	1.87	30.8	6.06	29.8
5	1.99	31.3	6.35	1.74	26.0	6.67	1.75	27.6	6.33	28.3
6	1.95	29.6	6.56	1.95	29.2	6.68	1.88	29.6	6.34	29.5
7	1.89	29.6	6.39	2.01	30.4	6.61	1.93	30.5	6.33	30.2
8	2.10	32.1	6.53	2.01	31.0	6.47	1.82	29.1	6.26	30.8
10	1.94	30.4	6.38	1.88	29.6	6.36	1.91	30.0	6.36	30.0
12	1.93	30.7	***6.30***	1.89	32.0	***5.91***	1.41	27.8	***5.06***	30.2
14	1.94	30.9	6.27	1.97	30.5	6.45	1.88	31.6	5.96	31.0
20	1.92	30.0	6.39	1.93	30.8	6.28	1.88	29.5	6.37	30.1
24	1.85	29.5	6.28	1.85	29.2	6.36	1.90	30.9	6.16	29.8
28	1.89	31.1	6.08	1.94	30.0	6.46	1.92	30.3	6.33	30.4

Table C-2: Canola tested with a fine roller at increasing frame rates to locate a lower sampling limit for the continuous test method. The fine roller with canola showed very consistent data all the way through with an apparent lower sampling limit around 6 fps (7.2 fPFL) but was eventually chosen to be 15 fPFL (greater than 12 fps in this table).

Frame Rate (fps)	Rep 1			Rep 2			Rep 3			Total Avg. CV
	STDV	CV	Avg. Area-per-Frame	STDV	CV	Avg. Area-per-Frame	STDV	CV	Avg. Area-per-Frame	
1	0.62	35.3	1.76	0.57	31.7	1.81	0.65	37.5	1.74	34.8
2	0.70	38.7	1.81	0.69	37.1	1.86	0.59	33.6	1.76	36.5
3	0.66	36.6	1.82	0.77	40.8	1.89	0.70	38.7	1.81	38.7
4	0.64	37.1	1.74	0.69	37.0	1.85	0.70	37.3	1.86	37.1
5	0.68	39.7	1.71	0.68	37.2	1.83	0.60	35.5	1.70	37.5
6	0.65	38.4	1.69	0.71	38.7	1.84	0.65	38.2	1.70	38.4
7	0.66	36.7	1.79	0.70	37.6	1.86	0.65	38.0	1.71	37.4
8	0.65	38.7	1.68	0.70	38.2	1.83	0.67	38.8	1.72	38.6
10	0.68	38.2	1.78	0.68	36.3	1.87	0.65	38.1	1.71	37.5
12	0.66	31.3	2.12	0.70	32.7	2.13	0.61	33.7	1.82	32.6
14	0.69	38.9	1.77	0.71	38.1	1.86	0.66	37.8	1.74	38.3
20	0.65	38.4	1.70	0.67	37.5	1.80	0.67	38.0	1.77	38.0
24	0.67	38.6	1.73	0.67	37.4	1.79	0.67	37.7	1.77	37.9
28	0.68	38.4	1.78	0.68	37.8	1.79	0.66	38.2	1.73	38.1

Table C-3: Wheat tested with an extra coarse roller at increasing frame rates to locate a lower sampling limit for the continuous test method. The extra coarse roller with wheat showed very consistent data all the way through with an apparent lower sampling limit around 6 fps (7.2 fPFL).

Frame Rate (fps)	Rep 1			Rep 2			Rep 3			Total Avg. CV
	STDV	CV	Avg. Area-per-Frame	STDV	CV	Avg. Area-per-Frame	STDV	CV	Avg. Area-per-Frame	
1	0.81	31.7	2.56	0.74	30.1	2.45	0.55	22.6	2.44	28.1
2	0.86	36.5	2.37	0.90	36.2	2.49	0.88	37.1	2.37	36.6
3	0.76	32.2	2.37	0.90	37.3	2.42	0.77	31.0	2.49	33.5
4	0.78	33.0	2.36	0.84	36.0	2.35	0.84	34.5	2.44	34.5
5	0.72	29.1	2.49	0.79	32.7	2.42	0.74	29.7	2.51	30.5
6	0.80	33.4	2.40	0.84	34.4	2.45	0.85	33.4	2.55	33.7
7	0.79	33.2	2.38	0.82	35.7	2.28	0.82	33.4	2.45	34.1
8	0.80	34.2	2.33	0.80	33.6	2.38	0.79	33.8	2.35	33.9
10	0.81	33.8	2.40	0.77	32.9	2.33	0.80	32.9	2.44	33.2
12	0.78	32.9	2.36	0.78	33.1	2.37	0.76	30.7	2.46	32.2
14	0.78	32.0	2.43	0.80	34.6	2.32	0.79	33.5	2.37	33.4
20	0.78	33.8	2.29	0.79	32.9	2.41	0.81	35.7	2.27	34.1
24	0.81	34.0	2.38	0.80	32.4	2.47	0.76	32.1	2.36	32.8
28	0.77	32.1	2.38	0.80	32.8	2.44	0.78	32.6	2.39	32.5

Table C-4: Wheat tested with a fine roller at increasing frame rates to locate a lower sampling limit for the continuous test method. The fine roller with wheat showed very consistent data all the way through with an apparent lower sampling limit around 6 fps (7.2 fPFL).

Frame Rate (fps)	Rep 1			Rep 2			Rep 3			Total Avg. CV
	STDV	CV	Avg. Area-per-Frame	STDV	CV	Avg. Area-per-Frame	STDV	CV	Avg. Area-per-Frame	
1	0.33	40.5	0.81	0.43	44.4	0.96	0.21	25.29	0.84	36.7
2	0.37	41.1	0.91	0.41	43.9	0.93	0.39	46.80	0.83	43.9
3	0.34	39.8	0.85	0.38	43.6	0.88	0.37	42.87	0.87	42.1
4	0.32	39.8	0.81	0.39	42.4	0.91	0.33	39.15	0.84	40.5
5	0.34	41.3	0.83	0.36	40.2	0.90	0.34	40.41	0.85	40.6
6	0.33	41.3	0.80	0.37	41.6	0.88	0.37	41.55	0.89	41.5
7	0.34	42.1	0.81	0.34	40.1	0.84	0.38	42.41	0.89	41.6
8	0.36	42.4	0.86	0.36	41.4	0.86	0.37	41.74	0.88	41.9
10	0.34	41.3	0.82	0.37	40.9	0.92	0.35	40.58	0.87	41.0
12	0.36	40.4	0.89	0.37	43.1	0.85	0.38	42.82	0.89	42.1
14	0.33	39.6	0.84	0.39	44.6	0.87	0.38	42.47	0.89	42.2
20	0.36	41.2	0.87	0.37	41.4	0.90	0.38	40.82	0.92	41.1
24	0.36	42.7	0.85	0.39	43.5	0.89	0.36	41.92	0.87	42.7
28	0.37	42.0	0.88	0.38	42.2	0.90	0.37	41.91	0.87	42.1

Tukey test for product overlap analysis in Chapter 4 computed in R:

A tukey HSD (honest significant difference) test was performed on four sets of data correlating to Figure 4-8, Figure 4-9, Figure C-3 and Figure C-4 to show the significance of the slight trend of product flow CV decreasing as the roller speed increased on a 95% confidence interval. The R code and figures outputted from the analysis are displayed here for reference.

```
>model_1 <- aov(Area_Percent~Speed_RPM, data = WheatDataAll)
>tuk_1 <- glht(model_1, linfct = mcp(Speed_RPM = "Tukey"))
>summary(tuk_1)
>tuk.cld_1 <- cld(tuk_1,level=0.05)
>opar_1 <- par(mai=c(1,1,1.8,1))
>plot(tuk.cld_1,ylim=c(0,30),yaxp = c(0, 30, 5))
```

```
>title("Percent Area Corrected for Speedvs 3 Speeds Tested",
line = 5)

>abline(9.65, 0, untf = FALSE, col="Blue",lwd=2)
```

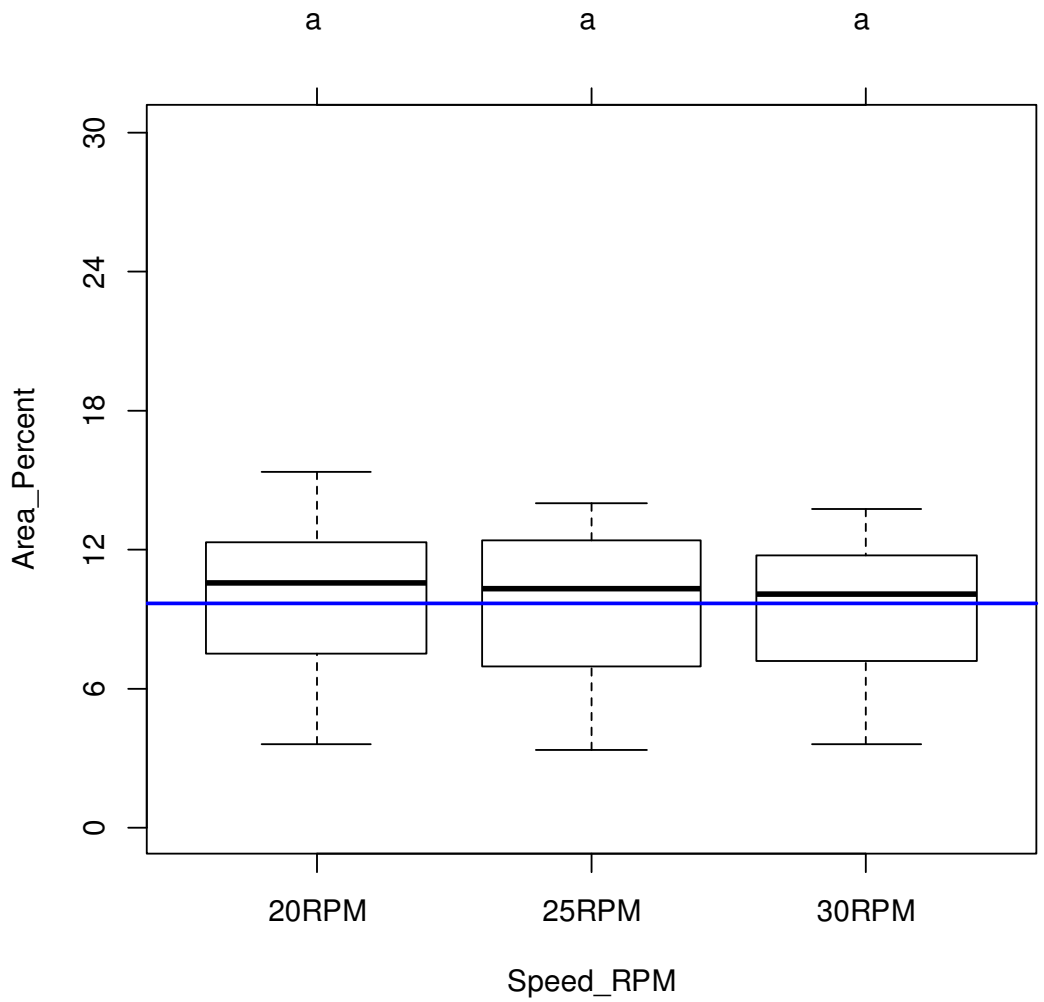

Figure C-1: Tukey HSD test result graphical representation for a 6-flute meter roller in wheat to compare the significance of product overlap as roller speed is increased.

Table C-5: Test statistic output from the Tukey HSD comparison for the product overlap significance with a 6-flute meter roller in wheat.

Mean Comparison	Estimate	Std. Error	t-value	Pr(>|t|)
25RPM - 20RPM == 0	-0.097	0.255	-0.380	0.923
30RPM - 20RPM == 0	-0.420	0.255	1.645	0.227
30RPM - 25RPM == 0	-0.323	0.255	1.265	0.416

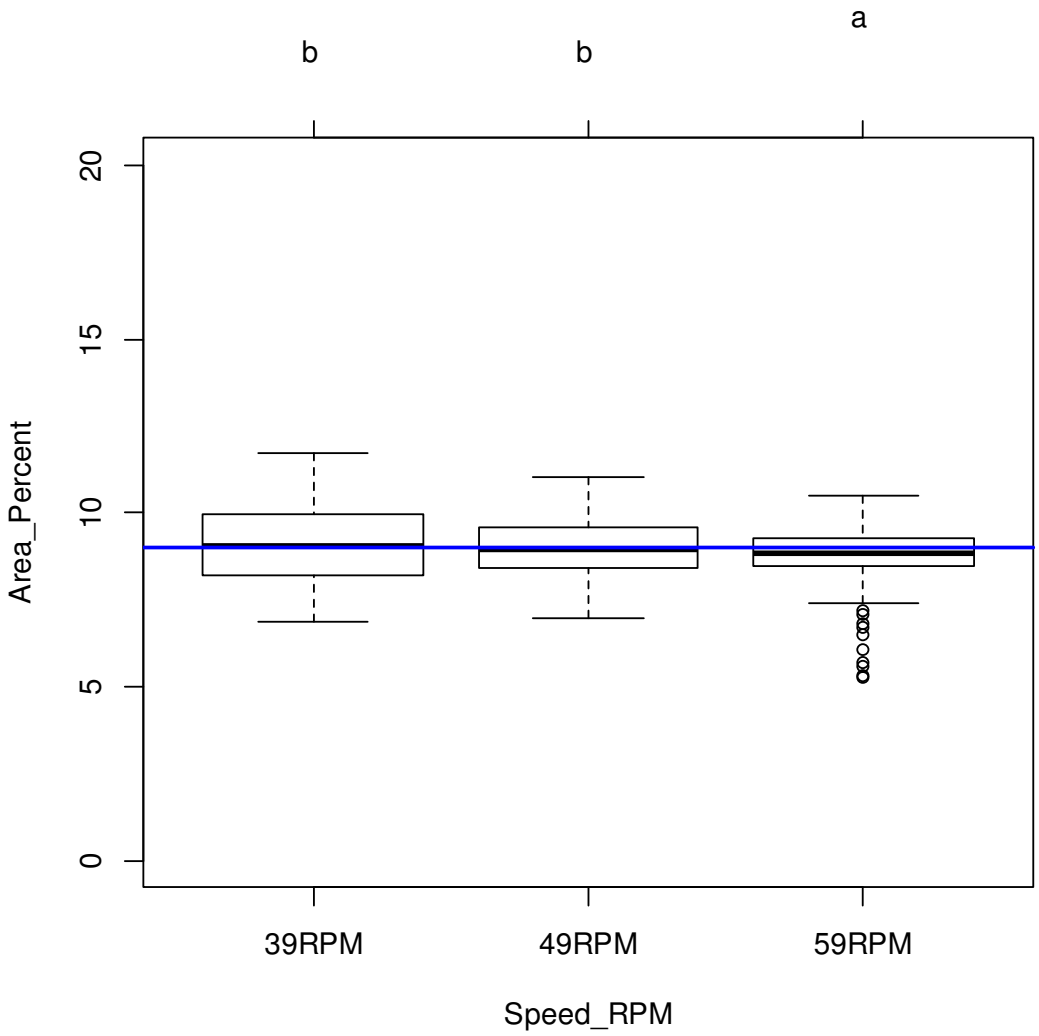

Figure C-2: Tukey HSD test result graphical representation for a 15-flute meter roller in wheat to compare the significance of product overlap as roller speed is increased.

Table C-6: Test statistic output from the Tukey HSD comparison for the product overlap significance with a 15-flute meter roller in wheat.

Mean Comparison	Estimate	Std. Error	t-value	Pr(>|t|)
49RPM - 39RPM == 0	-0.108	0.048	-2.250	0.063
59RPM - 39RPM == 0	-0.281	0.048	-5.878	1e-04
59RPM - 49RPM == 0	-0.173	0.048	-3.628	0.001

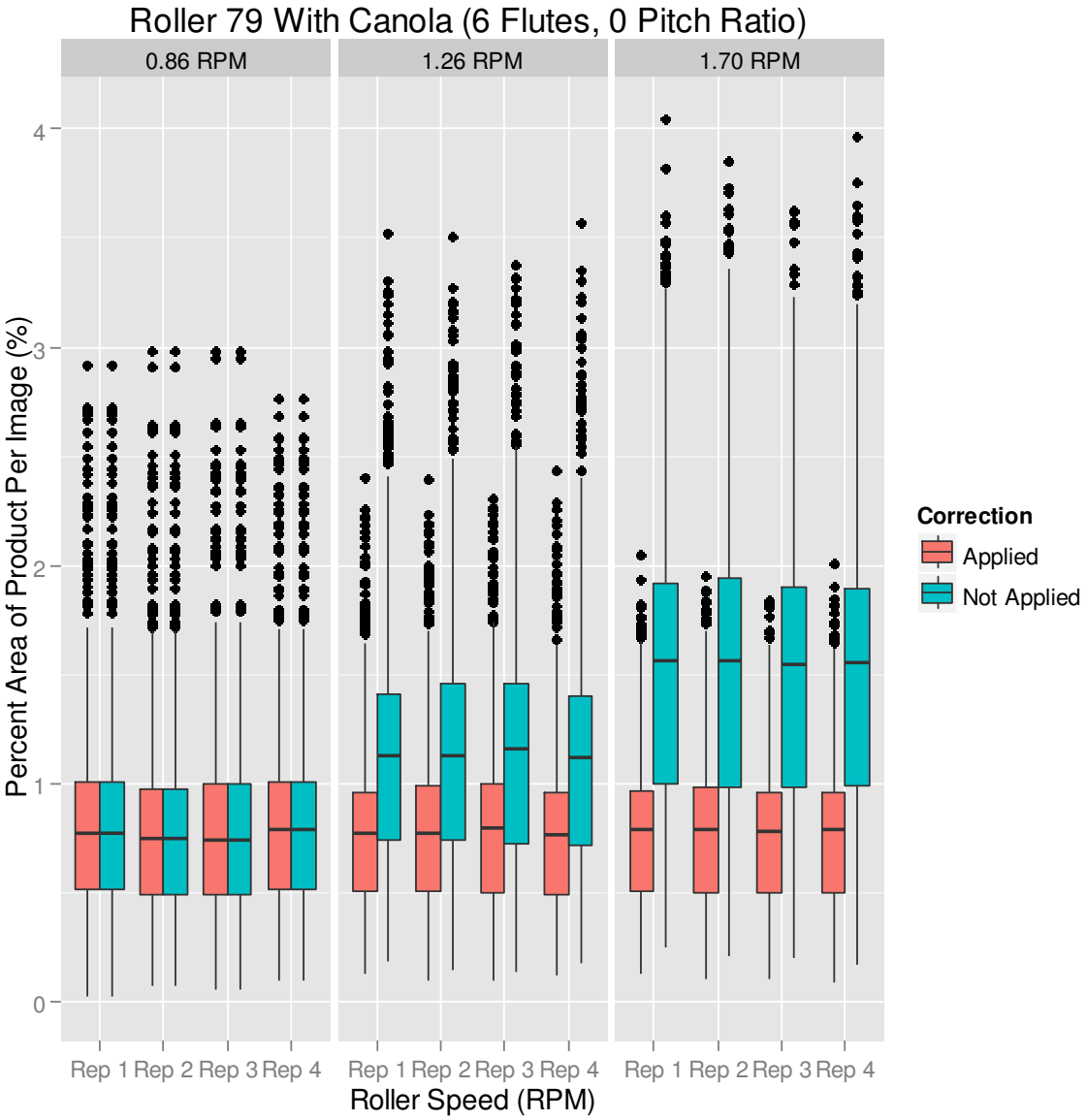

Figure C-3: Percent area of product per image vs roller speed with a 6-flute prototyped roller in canola showing the inconsistency of product flow at low roller speeds where the extreme points (black dots) show the large pulse of product from each flute.

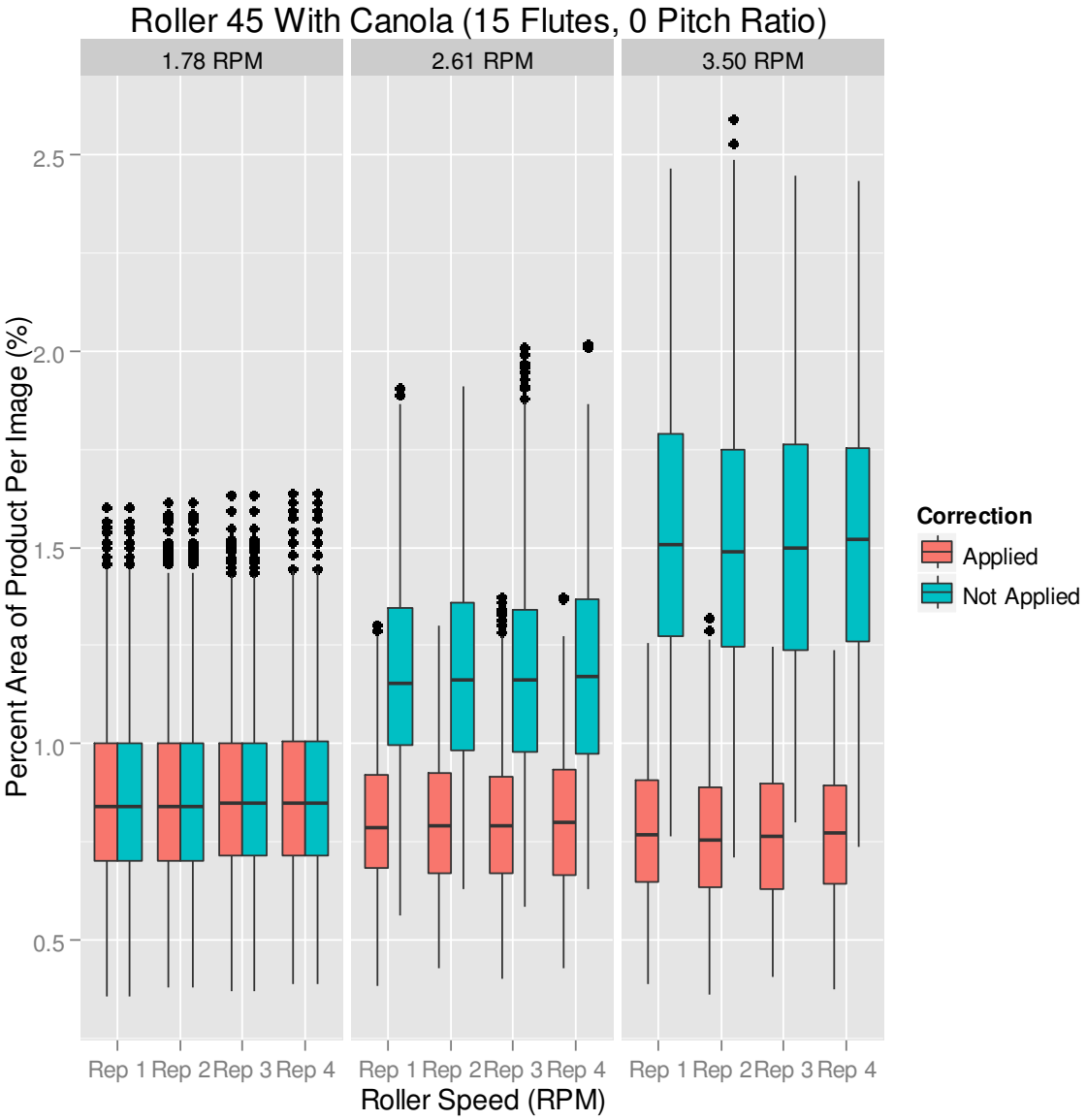

Figure C-4: Percent area of product per image vs roller speed with a 6-flute prototyped roller in canola showing the inconsistency of product flow at low roller speeds where the extreme points (black dots) show the large pulse of product from each flute.

Levene's test for homogeneity of variances computed in R:

```
> leveneTest(Wheat1234ANOVA$CV_PercentArea, Wheat1234ANOVA$Rep)
```

Levene's Test for Homogeneity of Variance (center = median)

	Df	F value	Pr(>F)
group	3	1.2222	0.3004
	968		

General Linear Model (GLM) in R of the entire dataset (total glm) incorporating all five design parameters:

Table 5-5 displays the output of the glm.

```
model_Wheat<-
glm(CV_PercentArea~Num_Flutes+R2_mm+PHI_rads+Pitch_deg+Speed_RPM
)
```

General Linear Model (GLM) and ANOVA in R of each design parameter individually and compared against the total glm to determine the order of significance:

Table 5-6 and Table C-7 displays the output of the glm and ANOVA, specifically the residuals of the model.

```
model1_Flutes<-glm(CV_PercentArea~Num_Flutes)
    model2_R2<-glm(CV_PercentArea~R2_mm)
  model3_PHI<-glm(CV_PercentArea~PHI_rads)
model4_Pitch<-glm(CV_PercentArea~Pitch_deg)
model5_Speed<-glm(CV_PercentArea~Speed_RPM)

anova(model_Wheat,model1_Flutes,test="F")
  anova(model_Wheat,model2_R2,test="F")
 anova(model_Wheat,model3_PHI,test="F")
anova(model_Wheat,model4_Pitch,test="F")
anova(model_Wheat,model5_Speed,test="F")
```

Table C-7: Results of the ANOVA for the GLM's of each parameter versus the summary model GLM of wheat.

Model	Response Var.	Explanatory Var.	DoF	Resid. Dev	Deviance	F	Pr(>F)
model_Wheat1234	CV	all parameters (+)	966	21489			
model1_Flutes	CV	Num_Flutes	970	55612	-34124	383.5	2.2E-16
model2_R2	CV	R2_mm	970	58044	-36555	410.82	2.2E-16
model3_PHI	CV	PHI_rads	970	64313	-42824	481.28	2.2E-16
model4_Pitch	CV	Pitch_AL_per_FW	970	32673	-11184	125.7	2.2E-16
model5_Speed	CV	Speed_RPM	970	57545	-36056	405.22	2.2E-16

Table C-8: Individual GLM summary output for the number of flutes vs the product flow evenness.

GLM Summary (CV_PercentArea ~ Num_Flutes)				
	Estimate	**Std Error**	**t value**	**Pr(>|t|)**
(Intercept)	20.75818	0.72360	28.69	< 2.00E-16
Num_Flutes	-0.85507	0.06596	-12.96	< 2.00E-16

Table C-9: Individual GLM summary output of the R_2 design parameter vs the product flow evenness.

GLM Summary (CV_PercentArea ~ R2_mm)				
	Estimate	**Std Error**	**t value**	**Pr(>|t|)**
(Intercept)	28.66695	1.54630	18.854	< 2.00E-16
R2_mm	-0.004118	0.052033	0.079	0.937

Table C-10: Individual GLM summary output of the PHI design parameter vs the product flow evenness.

GLM Summary (CV_PercentArea ~ PHI_rads)				
	Estimate	**Std Error**	**t value**	**Pr(>|t|)**
(Intercept)	10.7995	0.3973	27.183	< 2.00E-16
PHI_rads	11.5595	3.0818	3.751	0.000187

Table C-11: Individual GLM summary output of the Pitch Ratio (PR) design parameter vs the product flow evenness.

GLM Summary (CV_PercentArea ~ Pitch_AL_per_FW)				
	Estimate	**Std Error**	**t value**	**Pr(>|t|)**
(Intercept)	19.6582	0.3107	63.27	< 2.00E-16
Pitch_AL_per_FW	-9.2829	0.2985	-31.10	< 2.00E-16

Table C-12: Individual GLM summary output of the Roller Speed parameter vs the product flow evenness.

GLM Summary (CV_PercentArea ~ Speed_RPM)				
	Estimate	**Std Error**	**t value**	**Pr(>|t|)**
(Intercept)	22.45699	0.95704	23.46	< 2.00E-16
Speed_RPM	-0.26700	0.02343	-11.39	< 2.00E-16

Figure C-5: Shows each of the design parameters stacked side-by-side with a linear trendline laid out across the data. This is a stacked figure combining Figure 5-12, Figure 5-15, Figure 5-16, Figure 5-13, and Figure 5-10 together as they were outputted from R after the individual glm was computed.

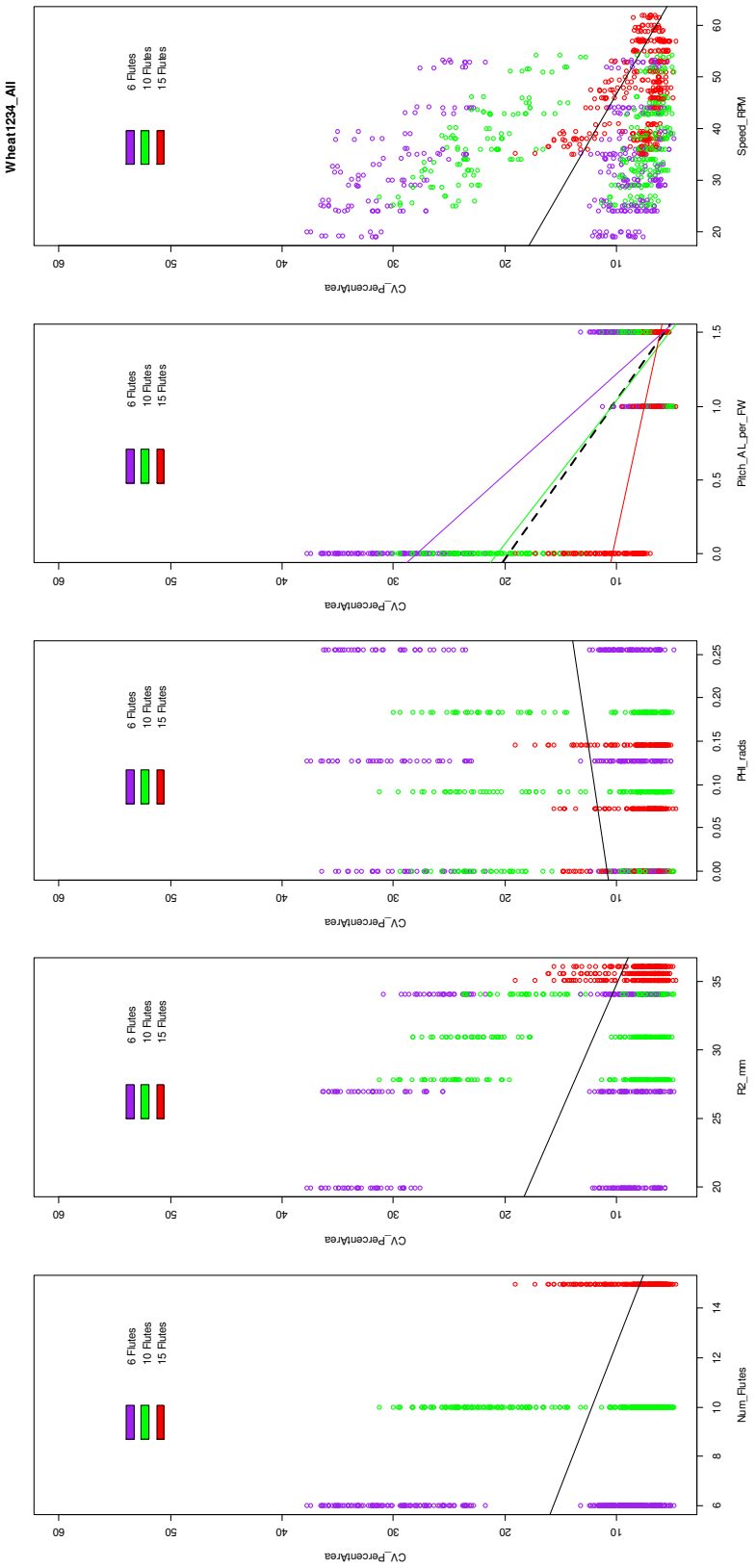

Figure C-5: Individual GLM summary output graph from R of the entire dataset.

Normal Distribution of the Data Collected:

Figure show how the data are normally distributed for roller 15F_medR2_medPHI at the three different pitch ratios (flute pitch) tested.

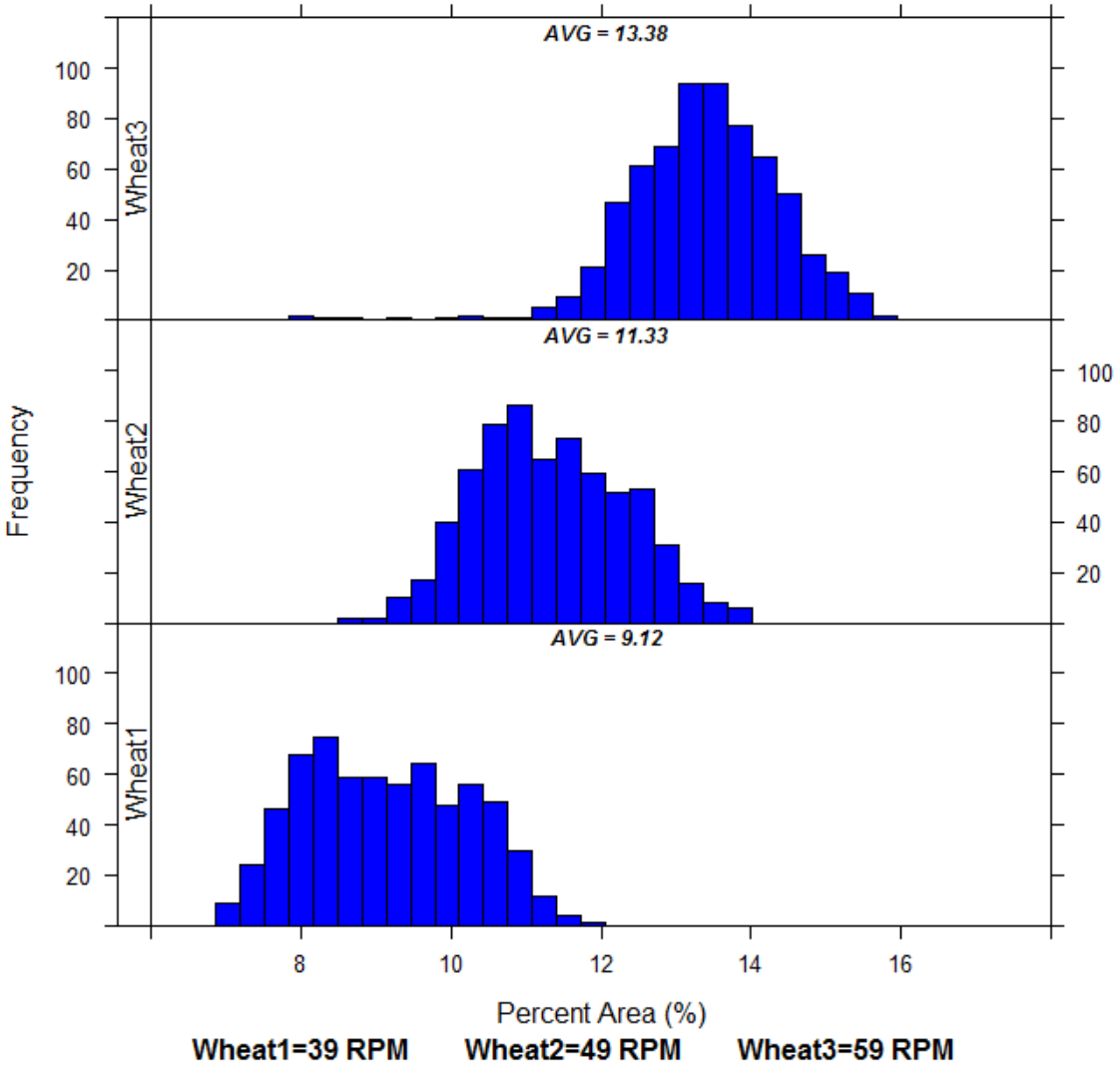

Figure C-6: Normal distribution of the roller data (15F_medR2_medPHI_0deg).

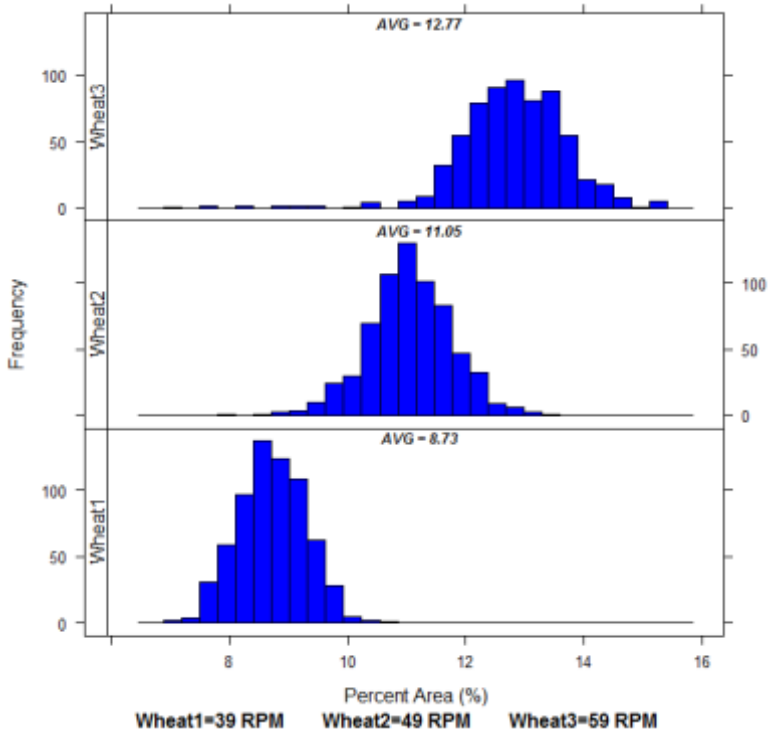

Figure C-7: Normal distribution of the roller data (15F_medR2_medPHI_24deg).

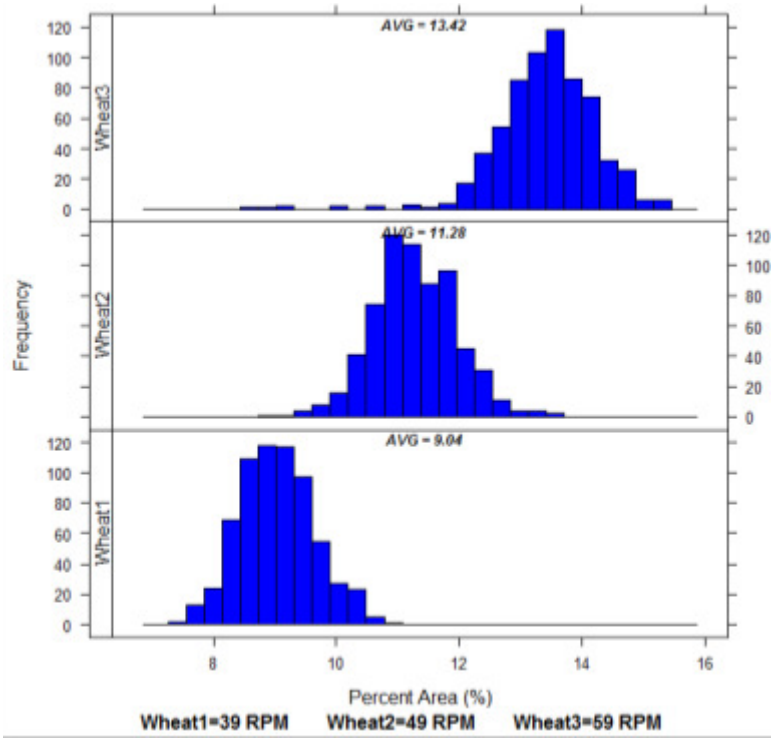

Figure C-8: Normal distribution of the roller data (15F_medR2_medPHI_36deg).

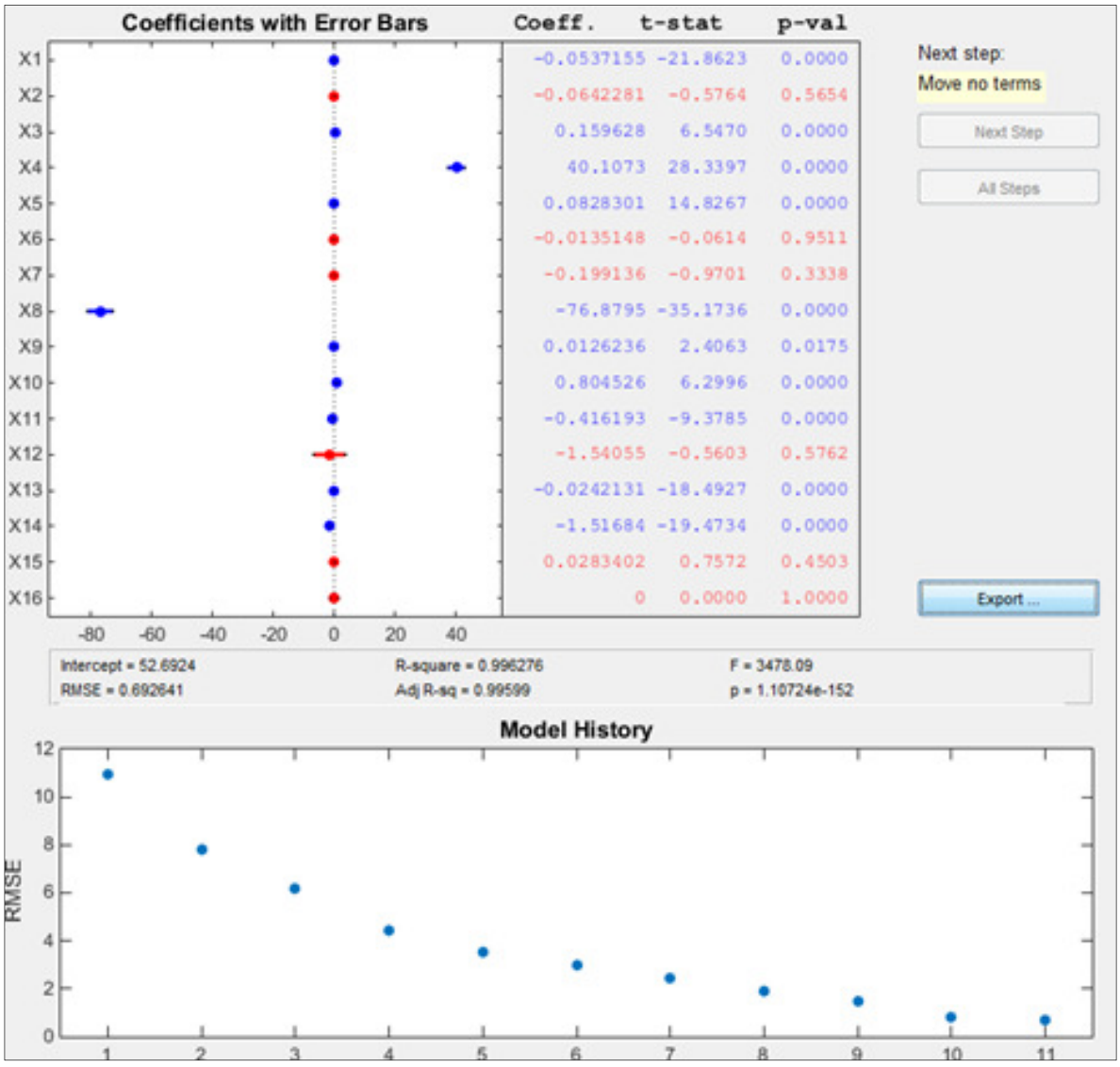

Figure C-9: Matlab output from stepwise regression analysis for training set 1 with extra pitch roller data.

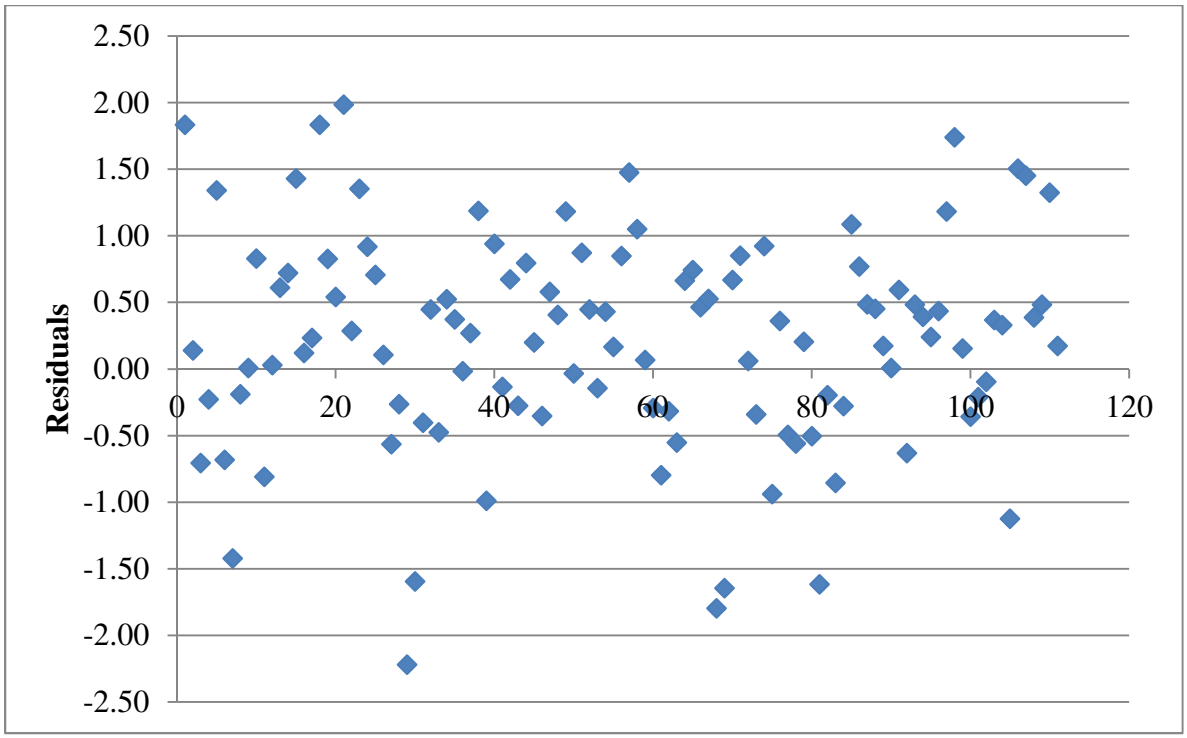

Figure C-10: Residuals comparison of testing model 1 from the model form optimization exercise.

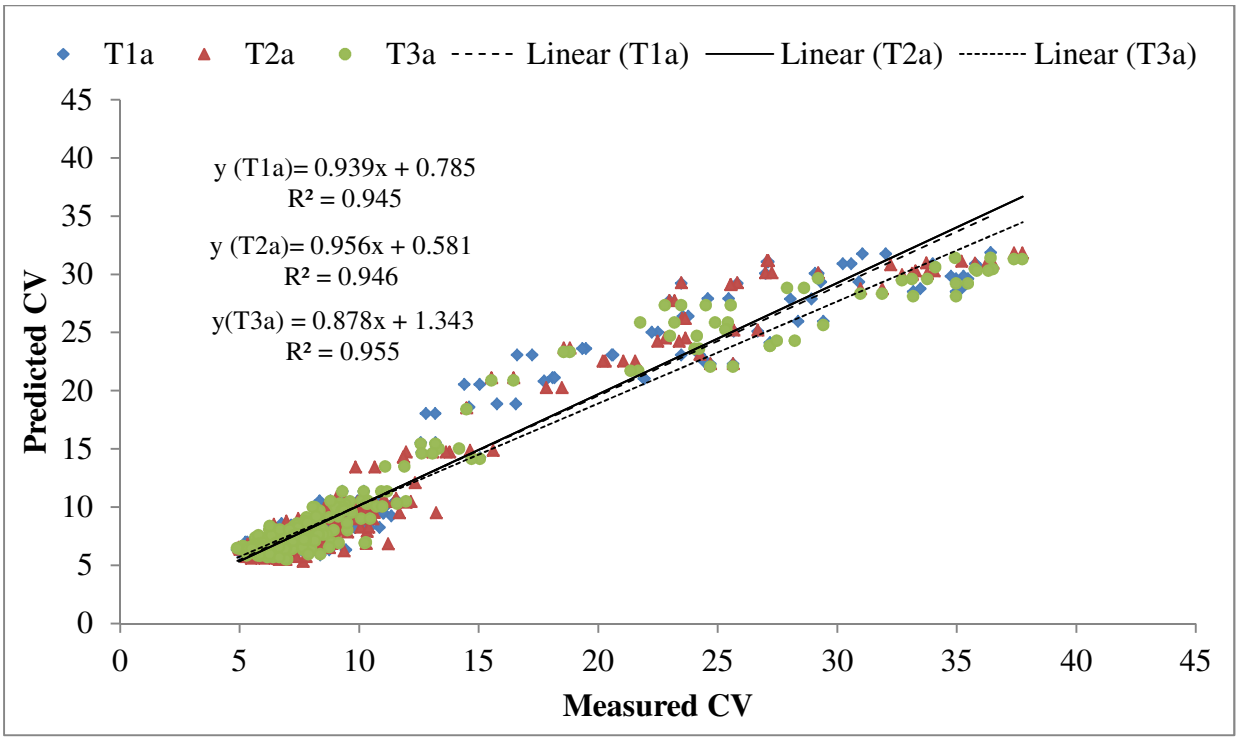

Figure C-11: Model fit with the testing data (30%) on the 10-coefficient empirical model.

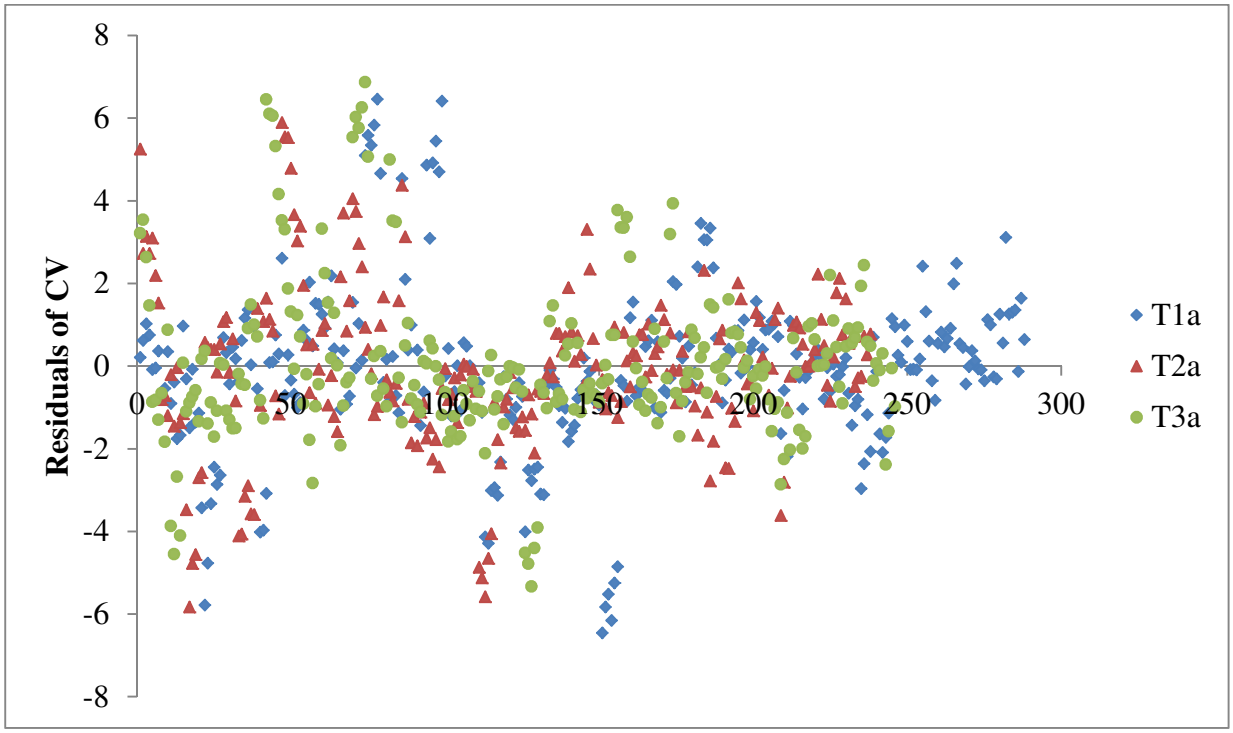

Figure C-12: Residuals from the 10-coefficient empirical model tests showing random error.

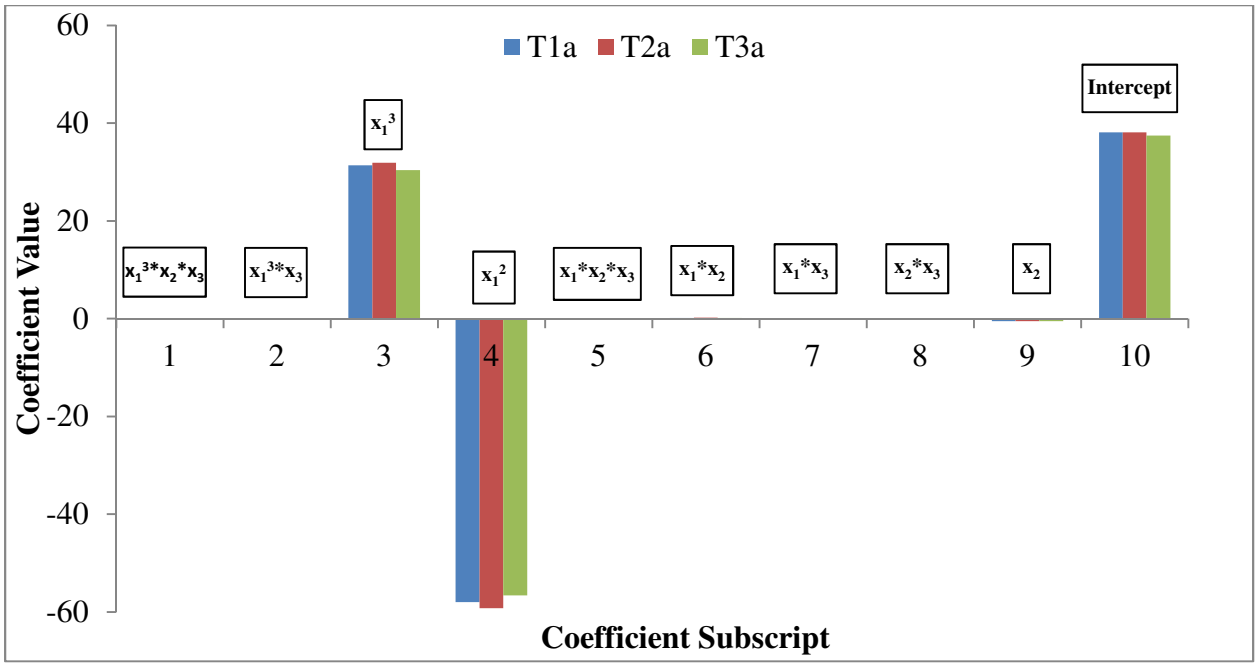

Figure C-13: Coefficients of the 10-coefficient empirical model.

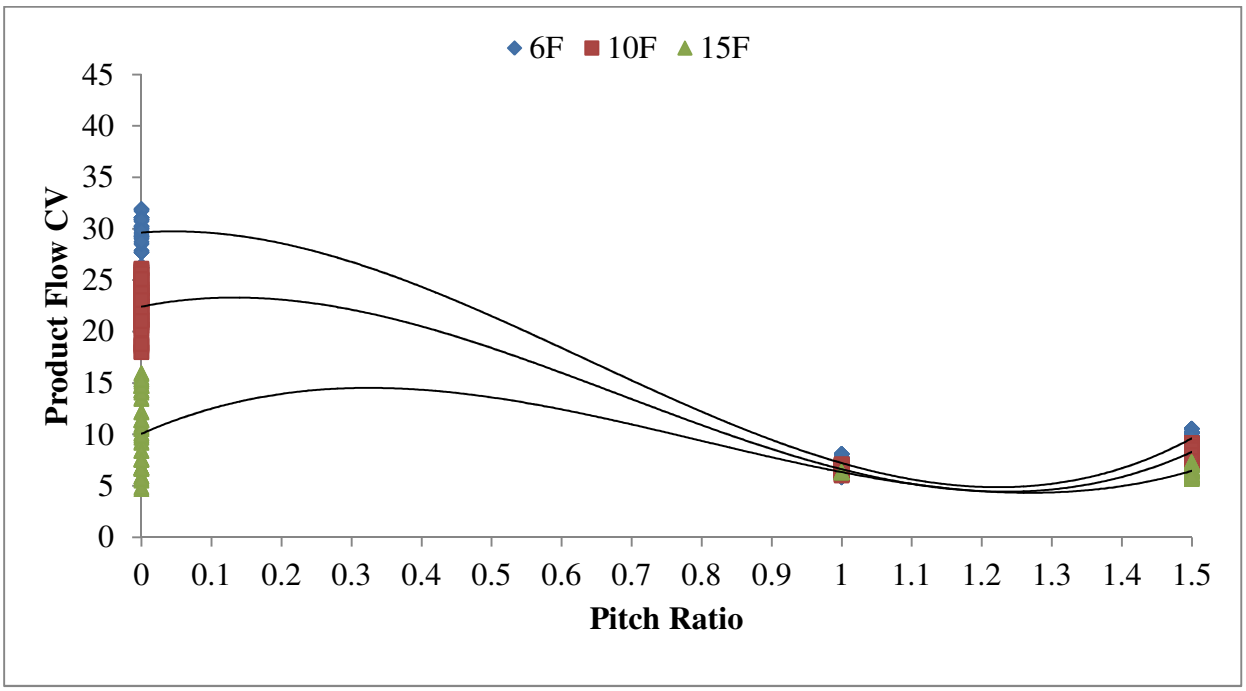

Figure C-14: Correlation fit for 6, 10, and 15-flute rollers with the 10-coefficient model.

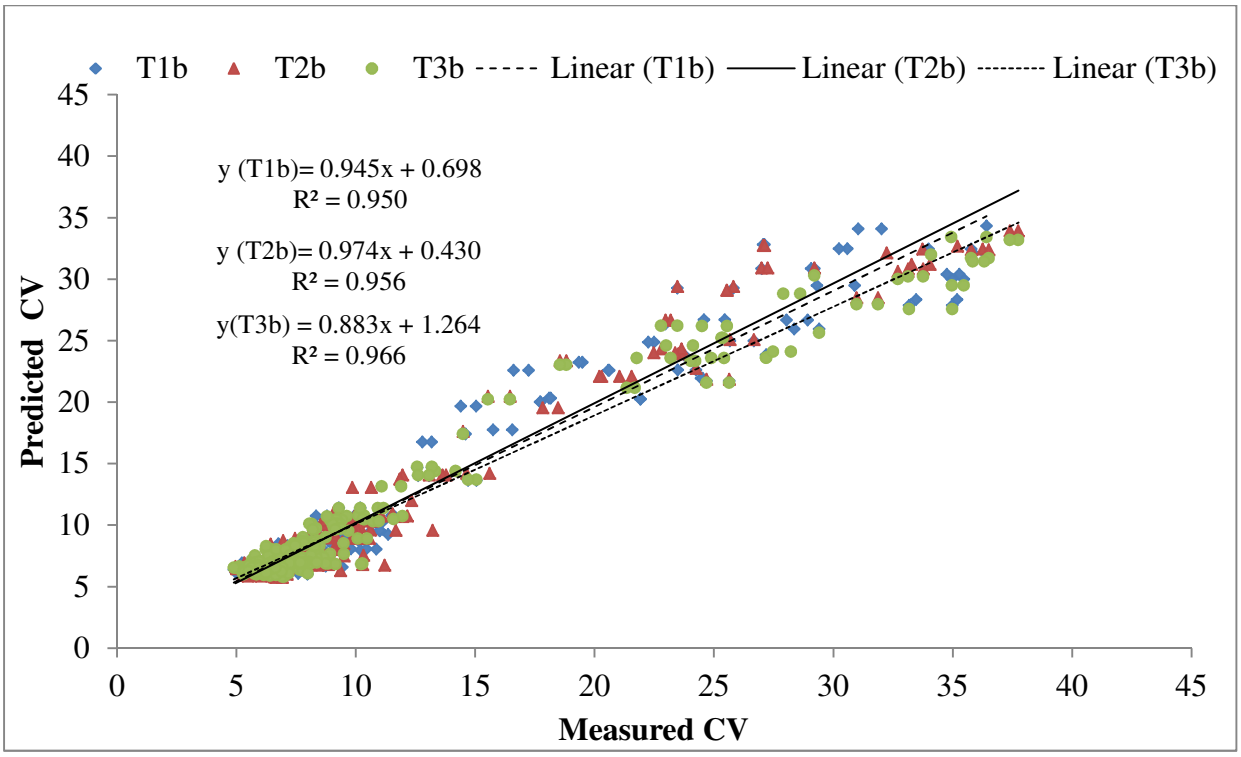

Figure C-15: Model fit with the testing data (30%) on the 12-coefficient empirical model.

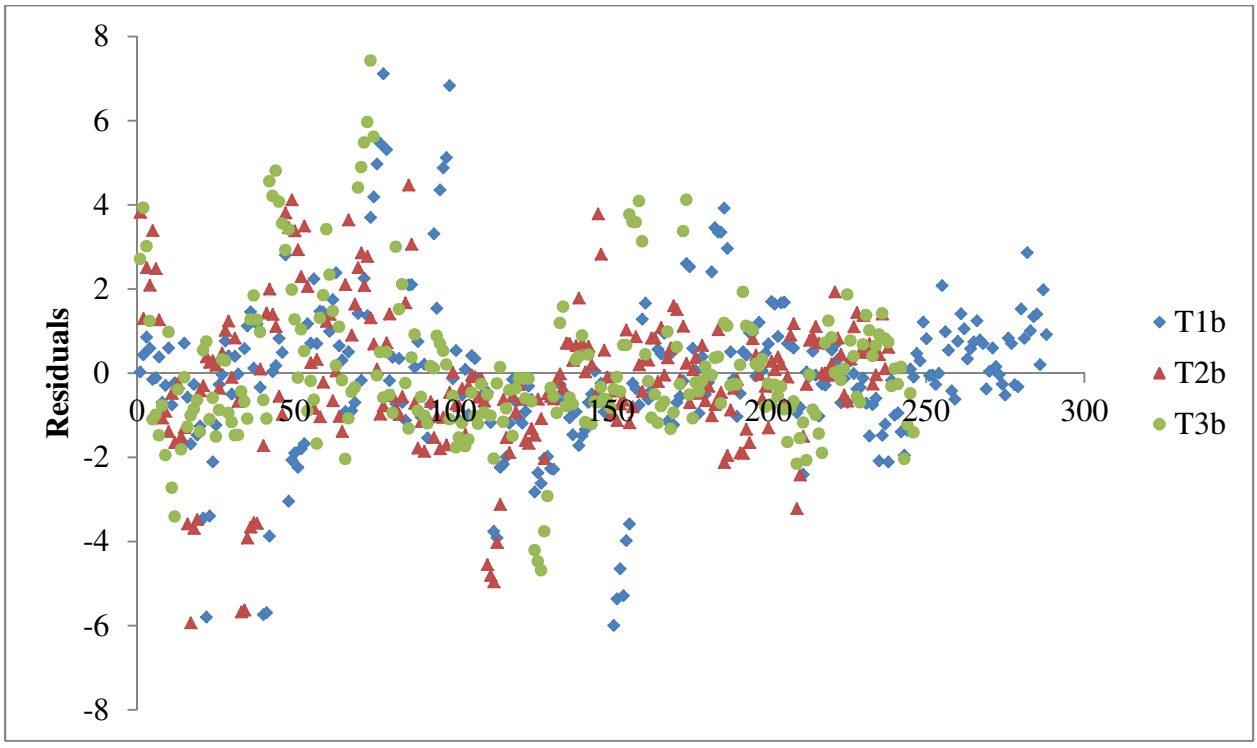

Figure C-16: Residuals from the 12-coefficient empirical model tests showing random error.

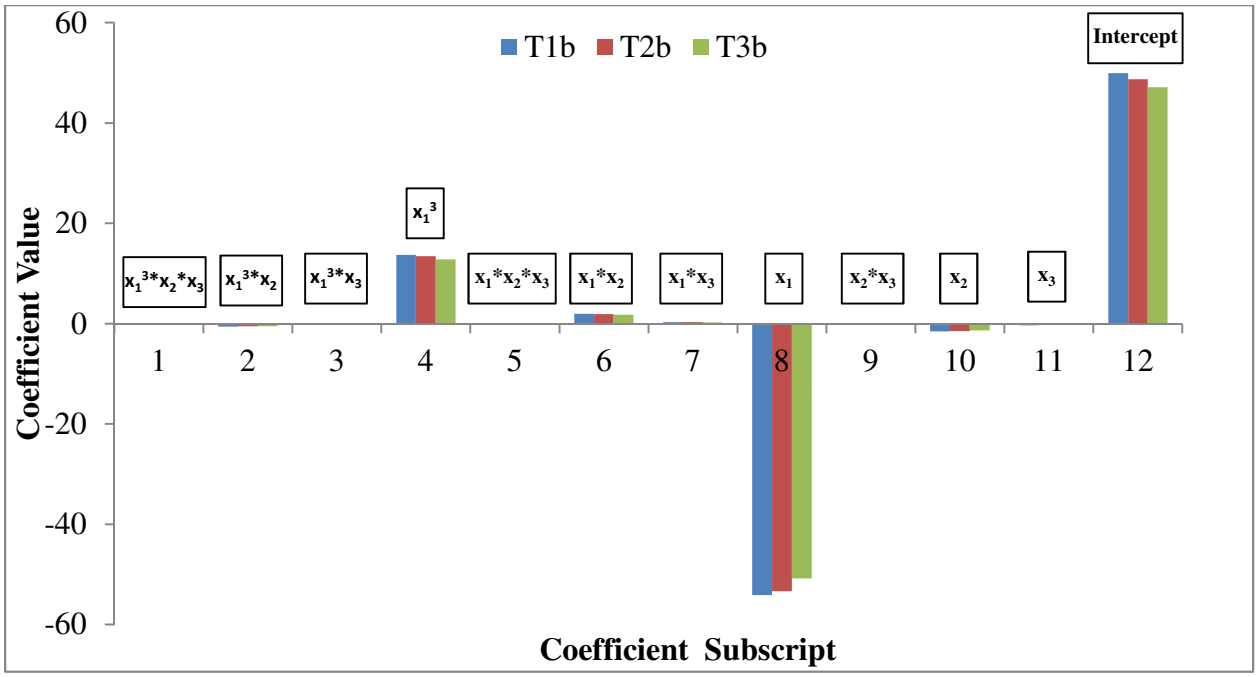

Figure C-17: Coefficients of the 12-coefficient empirical model.

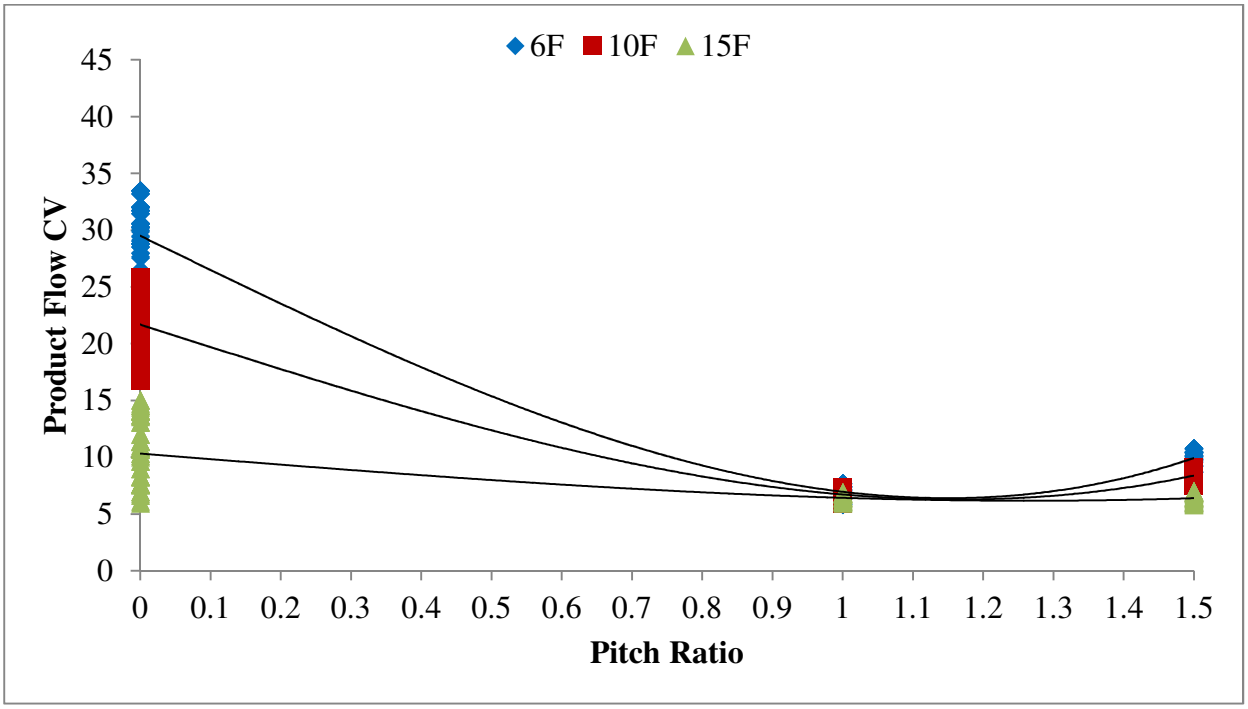

Figure C-18: Correlation fit for 6, 10, and 15-flute rollers with the 12-coefficient model.

Below is the equation for the 11 coefficient model the 10 coefficient empirical model is built off of.

$$CV_{10c}(PR,F,\omega_m) = PR^3\left(b_1F\omega_m + b_2\omega_m + b_3\right) + PR^2\left(b_4\right) + PR\left(b_5F\omega_m + b_6F + b_7\omega_m\right) + \left(b_8F\omega_m + b_9F + b_{10}\right) \quad \text{C-1}$$

Table C-13: Model coefficients of the final empirical model form (10-coefficients model).

Variable	Coefficient	**T1a**	**T2a**	**T3a**
$\mathbf{x_1^3*x_2*x_3}$	b1	-0.013	-0.014	-0.014
$\mathbf{x_1^3*x_3}$	b2	0.049	0.061	0.072
$\mathbf{x_1^3}$	b3	31.399	31.928	30.424
$\mathbf{x_1^2}$	b4	-58.002	-59.236	-56.623
$\mathbf{x_1*x_2*x_3}$	b5	0.048	0.049	0.049
$\mathbf{x_1*x_2}$	b6	0.152	0.207	0.181
$\mathbf{x_1*x_3}$	b7	-0.162	-0.168	-0.190
$\mathbf{x_2*x_3}$	b8	-0.028	-0.029	-0.027
$\mathbf{x_2}$	b9	-0.499	-0.475	-0.481
Intercept	b10	38.098	38.135	37.478
Testing	SSE	1101.77	866.22	940.49
	RMSE	1.96	1.92	1.96

Below is the equation for the 12-coefficient model that fell to the 10 and 11-coefficient empirical model forms.

$$CV_{12c}(PR,F,\omega_m) = PR^3\left(b_1F\omega_m + b_2F + b_3\omega_m + b_4\right) + PR\left(b_5F\omega_m + b_6F + b_7\omega_m + b_8\right) + \left(b_9F\omega_m + b_{10}F + b_{11}\omega_m + b_{12}\right) \quad \text{C-2}$$

Table C-14: Model coefficients of the final empirical model form (12-coefficients model).

Variable	Coefficient	**T1b**	**T2b**	**T3b**
$x_1^3*x_2*x_3$	b1	3.37E-04	-1.67E-03	-2.13E-03
$x_1^3*x_2$	b2	-0.55435	-0.517	-0.505
$x_1^3*x_3$	b3	-0.092	-0.069	-0.054
x_1^3	b4	13.740	13.437	12.803
$x_1*x_2*x_3$	b5	2.82E-03	7.49E-03	9.42E-03
x_1*x_2	b6	1.998	1.913	1.788
x_1*x_3	b7	0.342	0.288	0.246
x_1	b8	-54.121	-53.326	-50.764
x_2*x_3	b9	-0.001	-0.004	-0.005
x_2	b10	-1.566	-1.447	-1.351
x_3	b11	-0.318	-0.280	-0.261
Intercept	b12	49.917	48.714	47.147
Testing	SSE	984.19	705.67	759.25
	RMSE	1.85	1.72	1.76

Table C-15: Model coefficients of the final empirical model form (11-coefficients model).

Variable	Coefficient	**Optimization Values**
$\mathbf{x_1^3*x_2*x_3}$	b1	-0.024
$\mathbf{x_1^3*x_3}$	b2	0.001
$\mathbf{x_1^3}$	b3	37.224
$\mathbf{x_1^2*x_2*x_3}$	b4	0.033
$\mathbf{x_1^2}$	b5	-68.832
$\mathbf{x_1*x_2*x_3}$	b6	0.022
$\mathbf{x_1*x_2}$	b7	0.446
$\mathbf{x_1*x_3}$	b8	-0.032
$\mathbf{x_2*x_3}$	b9	-0.028
$\mathbf{x_2}$	b10	-0.692
Intercept	b11	41.019
Testing	SSE	1923.996
	RMSE	2.196

The final 10 and 12-coefficient empirical models can also be used to predict the optimal meter roller parameters. Although the 10-coefficient model appears to predict a lower optimal CV and the 12-coefficient model predict a higher optimal CV than the 11-coefficient empirical model concluded in the thesis, it is good information to know for future studies. When a new set of meter rollers can be developed and tested against the general model form concluded in this study it will be beneficial to know how each of the potential final model forms actually predict the final meter roller performance.

Table C-16: Predicted optimal meter roller parameters to give the most even product flow

Empirical Model Type	Number of Flutes (F)	Meter Speed, ω_m (RPM)	Pitch Ratio (PR)	Predicted CV
10 Coefficients (Eqn. C-1)	6	53	1.22	3.34
	10	54	1.24	3.73
	15	62	1.27	4.29
12 Coefficients (Eqn. C-2)	6	53	1.15	5.46
	10	54	1.16	5.72
	15	62	1.32	5.79